THE FINITE ELEMENT METHOD FOR NEUTRON DIFFUSION PROBLEMS IN HEXAGONAL GEOMETRY

by

T.Y.C.Wei, K.F. Hansen

June, 1975

Massachusetts Institute of Technology

Department of Nuclear Engineering

Cambridge, Massachusetts 02139

MASSACHUSETTS INSTITUTE OF TECHNOLOGY

DEPARTMENT OF NUCLEAR ENGINEERING

Cambridge, Massachusetts 02139

THE FINITE ELEMENT METHOD FOR NEUTRON DIFFUSION PROBLEMS IN HEXAGONAL GEOMETRY

by

T. Y. C. Wei, K. F. Hansen

June, 1975

COO-2262-7

MITNE-173

THE FINITE ELEMENT METHOD FOR NEUTRON DIFFUSION
PROBLEMS IN HEXAGONAL GEOMETRY

by

Thomas Ying Chung Wei

Submitted to the Department of Nuclear Engineering on June 24,
1975 in partial fulfillment of the requirements for the degree of
Doctor of Philosophy.

ABSTRACT

The use of the finite element method for solving two-dimensional
static neutron diffusion problems in hexagonal reactor configurations is
considered. It is investigated as a possible alternative to the low-order
finite difference method. Various piecewise polynomial spaces are ex-
amined for their use in hexagonal problems. The central questions
which arise in the design of these spaces are the degree of incomplete-
ness permissible and the advantages of using a low-order space fine-
mesh approach over that of a high-order space coarse-mesh one. There
is also the question of the degree of smoothness required. Two schemes
for the construction of spaces are described and a number of specific
spaces, constructed with the questions outlined above in mind, are pre-
sented. They range from a complete non-Lagrangian, non-Hermite quad-
ratic space to an incomplete ninth order space. Results are presented
for two-dimensional problems typical of a small high temperature gas-
cooled reactor. From the results it is concluded that the space used
should at least include the complete linear one. Complete spaces are
to be preferred to totally incomplete ones. Once function continuity is
imposed any additional degree of smoothness is of secondary impor-
tance. For flux shapes typical of the small high temperature gas-cooled
reactor the linear space fine-mesh alternative is to be preferred to the
perturbation quadratic space coarse-mesh one and the low-order finite
difference method is to be preferred over both finite element schemes.

Thesis Supervisor: Kent F. Hansen
Title: Professor of Nuclear Engineering

TABLE OF CONTENTS   Page

LIST OF FIGURES

8

LIST OF TABLES

ACKNOWLEDGMENTS

To Professor Kent F. Hansen, the supervisor of this thesis, goes the author's appreciation not only for the advice he gave and for the manner in which it was communicated but also for his interest in the other aspects of a student's progress through graduate school.

Professor Allan F. Henry, the reader of this thesis, is to be thanked for many constructive and entertaining discussions.

The author would also like to express his gratitude to a number of people at General Atomic: to Dr. Wayne Pfeiffer and Bill Davison for giving him the opportunity to continue work on finite element methods during a summer at General Atomic and allowing him to publish the results as part of this thesis; and to Dr. Robert Steinke for the unstinting help he gave in running the reference cases.

The use of the MACSYMA system, a system supported by ARPA, DOD, under Office of Naval Research Contract N00014-70-A-0362-0001, is to be acknowledged, and the author is indebted to Professor Joel Moses of Project MAC for his assistance.

The work was carried out under Energy Research and Development Agency Contract AT(11-1)-2262. The computations were performed on the IBM 370/168 computer at the MIT Information Processing Center.

Finally, thanks are due to Mrs. Esther Grande, who painstakingly organized the typing of this thesis.

BIOGRAPHICAL NOTE

The author, Thomas Ying Chung Wei, was born on 9 May 1950 in Karachi, Pakistan. He attended the Karachi Grammar School and took his O-level examinations from Cambridge University in November, 1965. He then went to the sixth form in preparation for the A-level examination.

In September, 1967, he enrolled at the Massachusetts Institute of Technology where he studied in the Department of Electrical Engineering and received the Bachelor of Science degree in June, 1970.

He continued on at the Massachusetts Institute of Technology as a graduate student in the Department of Nuclear Engineering and received the Master of Science degree in June, 1972.

Chapter 1

INTRODUCTION

We concern ourselves in this thesis with the general area of numerical approximations to solve the analytic formulations of physical problems. To be more specific; the objective of this thesis is to examine the possibility of using the finite element method as an alternative to the low-order finite difference method for static neutron diffusion calculations in hexagonal reactor configurations.

Numerical methods are generally regarded as being of a more powerful nature than analytic techniques owing to the sheer complexity of the physical problem being simulated. Among numerical techniques, the low-order finite difference method[4-5] is the one most widely used. It is relatively simple to implement and leads to coefficient matrices comparatively simple to invert. It also possesses a number of attractive mathematical properties, one among which is that of convergence. The technique, however, does lead to a large number of unknowns and with computer storage space a finite quantity, this does indeed become a constraint on the use of the method. There is also the accompanying problem of the associated large amount of computation time required with a large number of unknowns.

Much work has been done to try to develop alternate techniques which would give comparable accuracy and require comparable or less computation times with a fewer number of unknowns. We shall only mention one of them, namely the finite element method.[1,7] As with the finite difference

method this method also lends itself to mathematical analysis.

Recent work[1-3, 6] applying the finite element method to rectangular configurations has shown that results comparable in accuracy to those of the low-order finite difference method can be obtained with a fewer number of unknowns. Even though the question of computation time is still to be settled, that observation in itself was considered significant enough to justify examination of the possibility of applying the technique to non-rectangular reactor configurations.

With the advent of the HTGR and the fast breeder reactors the hexagonal reactor configuration has come to assume a position of increasing importance. It was then natural to consider the feasibility of using the finite element method in conjunction with the hexagonal geometry representative of these particular reactor types.

We have attempted to present in the preceding paragraphs a brief description of, and the accompanying rationale for, the objective of this thesis. The remaining portion of this chapter is divided into two sections. Section 1.1 restates the problem in a more detailed manner while section 1.2 presents a description of the finite method.

The remainder of the thesis is arranged as follows. We discuss in Chapter 2 the overall problem of constructing piecewise polynomial spaces for use in the finite element method. Chapter 3 is concerned mainly with the introduction of a number of specific piecewise polynomial spaces. A rationale is given for the specific choices. The numerical results obtained with these specific spaces are examined in the first half of Chapter 4 and the conclusions drawn are presented in the latter half of the chapter along with recommendations for future work.

1.1 Introduction

Diffusion theory calculations in Nuclear Reactor Physics can be divided into three general problem areas. These are namely

(i)   The time independent neutron diffusion problem

(ii)   Depletion calculations

(iii) Kinetics.

This classification is a natural division of the spectrum of possible temporal behavior. Continuing in this vein area (i) can be regarded as being the static case and area (ii) as the quasistatic one. From a calculational standpoint the class of static problems can be regarded as the area on which the calculations of the other classes are built. It is the spatial portion of the overall problem. In this sense it is then quite important to understand the problems associated with this class of calculations, for conclusions about them can be extrapolated to the other areas. This is the area the thesis is concerned with.

Consider a reactor configuration defined by an open region Ω and its boundary $\partial\Omega$. Ω consists of disjoint open subregions Ω_ℓ, $\ell = 1, 2, \ldots, L$ each of which is bounded by $\partial\Omega_\ell$. Figure 1.1 shows the reactor configuration.

Let $\underline{r}$ represent the spatial point and E the energy variable. We also have that $E \in \xi$ where $\xi = [E_{min}, E_{max}]$. The time independent neutron diffusion equation[4] can be written as

$$-\underline{\nabla} \cdot D(\underline{r}, E) \underline{\nabla}\phi(\underline{r}, E) + \Sigma_T(\underline{r}, E) \phi(\underline{r}, E) - \int_\xi dE' \Sigma_s(\underline{r}, E' \rightarrow E) \phi(\underline{r}, E')$$

$$-\frac{1}{\lambda}\chi(E) \int_\xi dE' \nu\Sigma_f(\underline{r}, E') \phi(\underline{r}, E') = Q(\underline{r}, E) \tag{1.1}$$
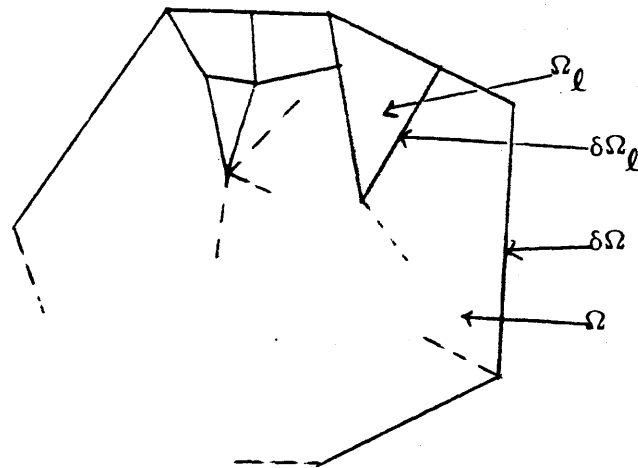
Fig. 1.1. General reactor configuration.

where

$\phi(\underline{r}, E)$ = neutron flux $(n/cm^2 \; sec)$

$D(\underline{r}, E)$ = neutron diffusion coefficient (cm)

$\Sigma_T(\underline{r}, E)$ = total macroscopic removal cross section (cm^{-1})

$\Sigma_s(\underline{r}, E' \rightarrow E)$ = macroscopic scattering cross section from
$\qquad\qquad$ E' to E (cm^{-1})

$\Sigma_f(\underline{r}, E)$ = macroscopic fission cross section (cm^{-1})

v = average number of neutrons produced per fission

$\chi(E)$ = fission spectrum

$Q(\underline{r}, E)$ = neutron source$/cm^3$ sec

λ = system multiplication constant.

The nuclear constants in equation (1.1), D, Σ_T, Σ_s and Σ_f are continuous in each Ω_ℓ and may be discontinuous on $\partial\Omega_\ell$. On $\partial\Omega_\ell$ the following set of interface conditions are used:

$$\phi(\underline{r}, E) \quad \text{and} \quad D(\underline{r}, E) \frac{\partial}{\partial n_\ell} \phi(\underline{r}, E) \text{ are continuous.} \tag{1.2}$$

where $\frac{\partial}{\partial n_\ell}$ is the outward normal derivative along the interface $\partial\Omega_\ell$.
On $\partial\Omega$, the exterior boundary, the boundary condition prescribed is:

$$\phi(\underline{r}, E) = 0 \quad \text{or} \quad \frac{\partial}{\partial n}\phi(\underline{r}, E) = 0 \tag{1.3}$$

Equation (1.1) together with the interface and boundary conditions described above constitute the time independent neutron diffusion problem.

A word is in order here regarding the intersections of two or more material interfaces. Diffusion theory does not hold at these singular points.[1] Experience, however, has shown that the effect of these singularities on reaction rates and integral properties in reactor problems is negligible and the approach taken in this thesis is to simply ignore the fact that the use of diffusion theory is suspect at these points. We do not attempt to introduce singular functions[7] to improve the rate of convergence of the numerical solution.

With the advent of the HTGR and the fast breeder reactors the case where $\partial\Omega_\ell$ is hexagonal in shape has assumed increasing importance vis a vis $\partial\Omega_\ell$ a rectangular shape. Figure 1.2 is a top view of a typical commercial HTGR. As can be seen from the figure each fuel block has a hexagonal cross-section which is in contrast to the LWRs where the cross-section is rectangular. Hence, the increasing importance of hexagonal $\partial\Omega_\ell$'s. This thesis will be concerned with solving the static neutron diffusion problem in such a hexagonal geometry.

An analytical calculation for so complex a problem is out of the question and one must resort to numerical techniques. In dealing with numerical

PERIODICALLY REPLACED
REFLECTOR ZONE
(74 COLUMNS TOTAL)

RODDED
REGION

NOZZLE IDENTIFICATION
NUMBER

49 CONTROL ROD
FUEL COLUMNS

294 FUEL COLUMNS

FUEL REGION
BOUNDARIES

SEGMENT
IDENTIFICATION
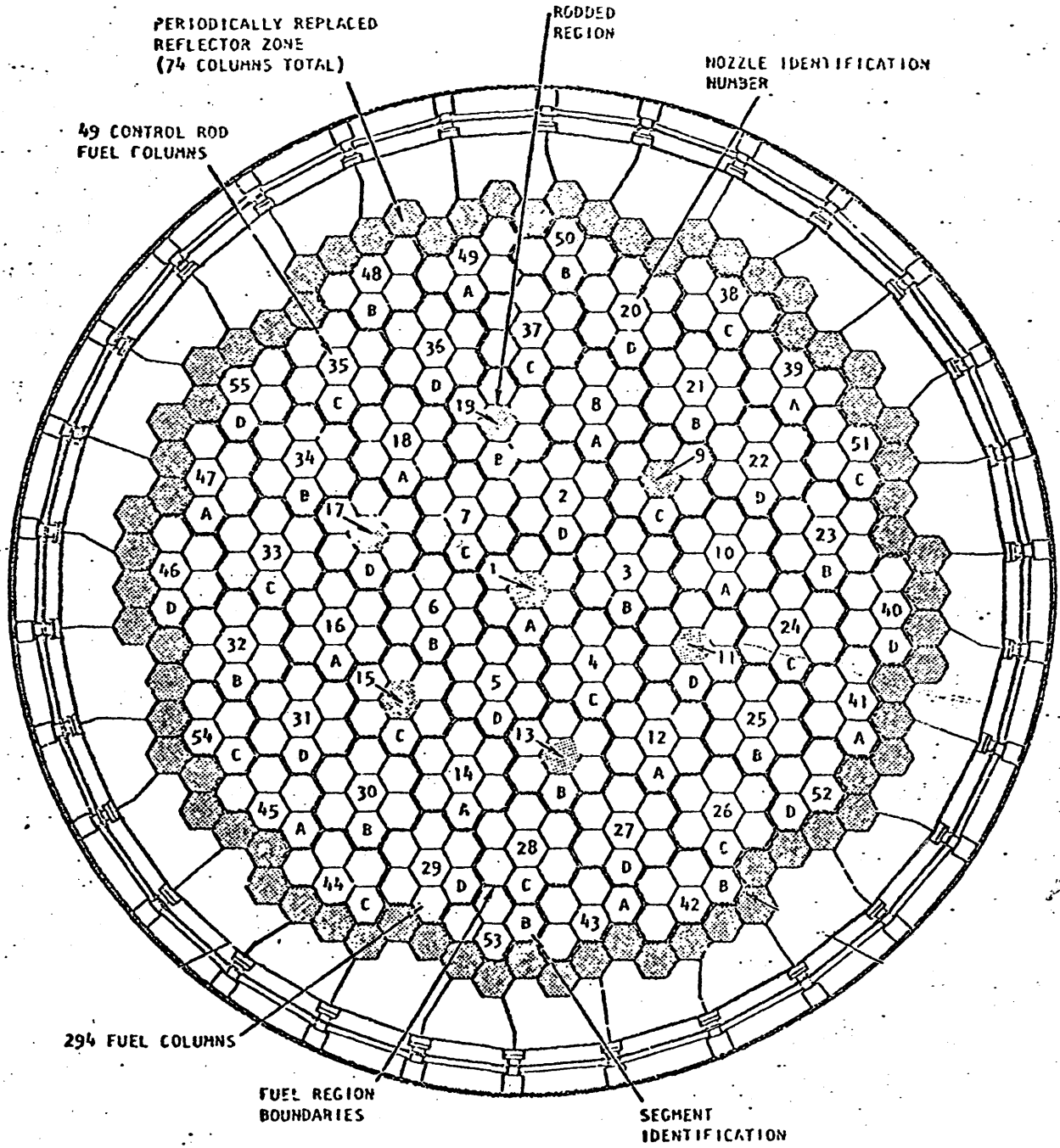
Fig. 1.2. Core layout — typical commercial HTGR. [From Delmarva
Power and Light Co., Summit Power Station PSAR.]

methods the two parameters of importance are the accuracy attainable and the corresponding computation time required to attain that accuracy. To compare two methods a figure of merit such as the accuracy per unit computation time would be needed. In practice, however, such fine tuning is not required and simple comparisons of absolute errors and absolute computation times are used. Consider figure 1.3.

The regions I-IV shown in the figure are intended to be graphical depictions of the classifications involved when numerical methods are grouped on the basis of accuracy attained and computation time required.

One would prefer to work in region I and avoid region IV, but most methods fall into either region II or region III. As most preliminary core design and fuel management calculations fall into region III it was decided to concentrate on this particular region.

The General Atomic company has a two-dimensional code, GAUGE[14] which is a computer implementation of a method which falls in region III. It is a low-order finite difference code and as such exemplifies the method most frequently used to carry out low-accuracy, low-computation time calculations. The low-order finite difference method is the method which provides the standard for comparison by virtue of it being the one which is most frequently used in production codes and it is the one which this thesis proposes to provide a viable alternative to. The point relation used in GAUGE is the one shown in figure 1.4.

The unknowns to be solved for are the flux values at the center of a hexagonal block and at the six corners. This leads to approximately three variables per hexagonal block. As computation time is related to

23
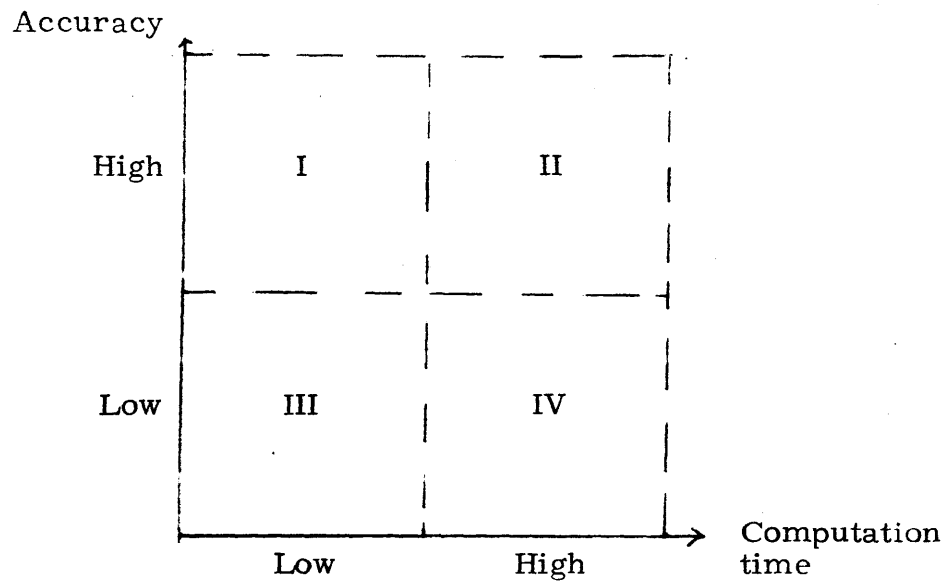
Fig. 1.3. Methods classification scheme.
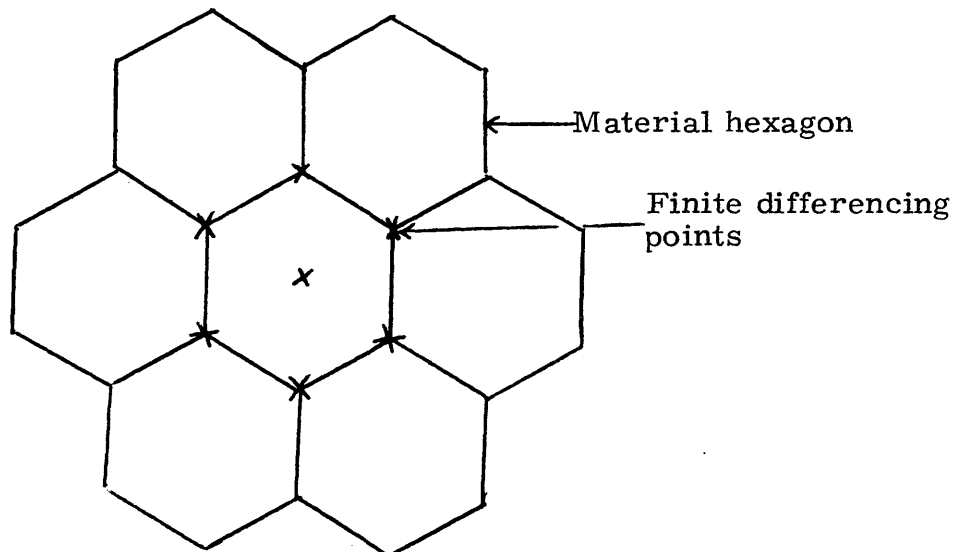
Fig. 1.4. Mesh scheme — low order finite difference method — GAUGE code.

the number of unknowns, a coarse upper bound on the number of variables
which can be used is three unknowns per hexagonal block. It will be shown
later that this is a very coarse upper bound as the complexity of the equa-
tions to be solved enters in a very direct way into the computation time
required.

Turning to the question of accuracy errors typical for GAUGE are
$\epsilon(k_{eff}) \sim 0.7\%$ and ϵ(peaking factors) $\sim 7\%$. In summary any alternative
to the low-order finite difference method in region III should have the
following characteristics:

$\epsilon(k_{eff}) < 0.7\%$

ϵ(peaking factors) $< 7\%$

unknowns per hexagonal block ≤ 3,

where it should be noted that 3 unknowns per hexagonal block is a coarse
upper bound as it assumes that the computation time required per unknown
for the finite element method is roughly equal to that for the finite differ-
ence method. To derive a more precise bound we would have to examine
the structure of the matrices involved in more detail. Figure 1.4 shows
that the low-order finite difference method as implemented in GAUGE has
a 7-point coupling relation in its diffusion term. The finite element
schemes considered in this thesis have, typically, a 7-point block coupling
relation in the diffusion term. In addition, this coupling relation is also
present in the removal and in the source terms. Low order finite differ-
ence leads to diagonal matrices for the removal and source terms. This
brief discussion indicates that the figure of 3 unknowns per hexagonal
block is indeed quite a coarse upper bound as the finite element equations

have more coupling and therefore will necessarily require more computation time per unknown.

Work[1-3] done over the past few years has shown that the finite element method is a viable alternative to the low order finite difference method in the solution of the static neutron diffusion problem for two-dimensional reactor configurations typical of light water reactors. $\partial\Omega_\ell$ in this case is rectangular. The results obtained show that with higher-order coarse-mesh finite element methods, a substantial decrease in the number of variables used can be obtained without a significant degeneration in the accuracy attainable. It still remains to be shown that the increase in complexity of the equations to be solved does not compensate for the reduction in number of variables. This however, does not detract from the significance of the results and this thesis will examine the possibility of using the finite element method in hexagonal geometry.

A fair synopsis of the objective of the thesis would then be that it is to examine the possibility of using the finite element method as an alternative to the low-order finite difference method in region III of figure 1.3 for static neutron diffusion calculations in hexagonal geometry. This implies a concentration on the construction of piecewise polynomial spaces for the approximation of the flux. The next section, §1.2, which describes the finite element method, will point this out in a more emphatic manner.

1.2 The Finite Element Method

We present in this section a discussion of the finite element method. Our treatment is to divide the presentation into two parts. Section 1.2.1 will give a general idea of the relative place of the finite element method[7-9, 11] in the area of numerical approximation schemes while section 1.2.2 will concentrate on describing the body of the method[10] in a more detailed fashion.

1.2.1 Galerkin Scheme

Our purpose in this section is to discuss the finite element method in a broad context and at the same time not lose sight of the fact that our final aim is to apply it to solve the static neutron diffusion problem expressed by the system of equations (1.1)-(1.3).

We begin by rewriting the integro-differential equation (1.1) in the operational form

$$H\phi(\underline{r}, E) = Q(\underline{r}, E) \tag{1.4}$$

where the corresponding boundary and interface conditions are

$$\phi(\underline{r}, E)\Big|_{\partial\Omega} = 0 \quad \text{or} \quad D\frac{\partial\phi(\underline{r}, E)}{\partial n}\Big|_{\partial\Omega} = 0 \tag{1.5}$$

$$\phi(\underline{r}, E) \quad \text{and} \quad D\frac{\partial\phi(\underline{r}, E)}{\partial n_\ell} \quad \text{are continuous across } \partial\Omega_\ell \tag{1.6}$$

and

$$H = -\underline{\nabla} \cdot D(\underline{r}, E)\,\underline{\nabla} + \Sigma_T(\underline{r}, E) - \int_\xi dE' \, \Sigma_s(\underline{r}, E' \to E)$$

$$-\frac{1}{\lambda}\chi(E) \int_\xi dE' \, \nu \, \Sigma_f(\underline{r}, E')$$

There are two general approaches to solving this problem numerically. The first is to approximate the operator H and finite difference falls into this category. The second is to approximate the solution. The finite element method is an example of the second approach. What is done is to write

$$\phi(\underline{r}, E) \approx \hat{\phi}(\underline{r}, E) = \sum_{i=1}^{m} a_k \psi_k(\underline{r}, E) \tag{1.7}$$

where $\{\psi_k(\underline{r}, E)\}$ are known functions and the coefficients $\{a_k\}$ are the unknowns. The set $\{\psi_k(\underline{r}, E)\}$ will be referred to as the superelement set and the finite dimensional approximation space it spans will be denoted by the symbol M_m. One now has to obtain a set of equations to solve for the $\{a_k\}$ and this is where the second approach can be further subdivided. The finite element method obtains its equations by utilizing the weak form of the operator equation (1.4). We now proceed to expound upon the weak form.[1,6]

Let $W^1(\Omega)$ be the class of functions which are continuous and have square integrable first derivatives, that is,

$$u \in W^1(\Omega) \quad \text{if } [\int_\Omega (\nabla u \cdot \nabla u + u^2) \, d^3r]^{1/2} < \infty$$

The weak form of the problem then is to find a function $\phi \in W^1(\Omega)$ such that

$$a(\phi(\underline{r}, E), v(\underline{r}, E)) = (Q(\underline{r}, E), v(\underline{r}, E)) \quad \text{for all } v \in W^1(\Omega) \tag{1.8}$$

where

$$(u(\underline{r}, E), v(\underline{r}, E)) = \int_\xi dE \int_{\Omega'} d^3r \, u(\underline{r}, E) v(\underline{r}, E)$$

$$\Omega' = \Omega \cup \partial\Omega \tag{1.9}$$

and the bilinear form $a(\phi(\underline{r}, E), v(\underline{r}, E))$ is given by,

$$a(\phi(\underline{r}, E), v(\underline{r}, E)) \equiv \sum_\ell \left\{ \int_{\Omega_\ell} d^3r \, (D(\underline{r}, E) \nabla \phi(\underline{r}, E), \nabla v(\underline{r}, E))_\xi \right\}$$

$$+ (R\phi(\underline{r}, E), v(\underline{r}, E)) \tag{1.10}$$

where

$$H = -\nabla \cdot D(\underline{r}, E) \nabla + R \tag{1.11}$$

and

$$(u(\underline{r}, E), v(\underline{r}, E))_\xi = \int_\xi dE \, u(\underline{r}, E) v(\underline{r}, E)$$

To show that a solution to the weak form is a solution of the original problem, we integrate $a(\phi(\underline{r}, E), v(\underline{r}, E))$ in eq. (1.8) by parts and use Gauss's theorem to obtain,

$$\sum_\ell \int_{\Omega_\ell} d^3r (H\phi(\underline{r}, E), v(\underline{r}, E))_\xi + \sum_\ell \int_{\partial\Omega_\ell} \left\{ ds \left(v(\underline{r}, E), D(\underline{r}, E) \frac{\partial \phi(\underline{r}, E)}{\partial n_\ell} \right)_\xi \right\}$$

$$= (Q(\underline{r}, E), v(\underline{r}, E)) \qquad \phi, v \in W^1(\Omega) \tag{1.12}$$

It has been shown that eq. (1.12) leads to the following Euler equations,

$$H\phi(\underline{r}, E) = Q(\underline{r}, E) \qquad \underline{r} \epsilon \Omega_\ell \tag{1.13}$$

and

$$\sum_{\ell} \int_{\partial\Omega_\ell} ds \, D \, \frac{\partial\phi(\underline{r}, E)}{\partial n_\ell} = 0 \tag{1.14}$$

A solution of the weak problem is therefore a solution of the original differential equation. The original formulation of the problem, eq. (1.4), requires $\phi(\underline{r}, E)$ to be twice continuously differentiable in Ω_ℓ and hence restricts it to a class of functions $C^2(\Omega)$ smaller than $W^1(\Omega)$. The weak form is therefore preferred in the actual calculation of the approximate solution as it allows us to look for an approximation in a wider class of functions.

The finite element method belongs to that group of methods which solves an approximation of the weak form of the original problem. It looks for a $\hat{\phi}(\underline{r}, E) \in M_m$ such that

$$a(\hat{\phi}(\underline{r}, E), \psi_k(\underline{r}, E)) = (Q(\underline{r}, E), \psi_k(\underline{r}, E)) \qquad \text{for all } \psi_k(\underline{r}, E) \in M_m$$

$$\tag{1.15}$$

with M_m a finite dimensional space of functions. Using eq. (1.7) we have that eq (1.15) leads to the following matrix system of equations for the expansion constants $\{a_k\}$.

$$\left[(D(\underline{r}, E) \nabla \psi_i(\underline{r}, E), \nabla \psi_j(\underline{r}, E)) + (R\psi_i(\underline{r}, E), \psi_j(\underline{r}, E)) \right] [a_i]$$

$$= \left[(Q(\underline{r}, E), \psi_j(\underline{r}, E)) \right] \qquad i, j = 1, \ldots, m$$

$$\tag{1.16}$$

This is the system of equations the finite element method uses to solve for the expansion coefficients $\{a_k\}$. They shall be referred to as the Galerkin equations as the approximation procedure implied by the

use of eq. (1.15) is a scheme of the Galerkin type. With the use of the weak form, M_m is no longer restricted to $C^2(\Omega)$ but is allowed to become a subset of the larger space $W^1(\Omega)$. This enlarges the set of possible trial functions $\psi_k(\underline{r}, E)$.

The Euler equation, eq. (1.13) indicates that the Galerkin set of equations eq. (1.16) is an equivalent restatement of the differential neutron static diffusion equation, eq. (1.4) in some approximate integral sense. We have up till now, neglected the question of the satisfaction of the boundary and interface conditions, eqs. (1.5)-(1.6), as part of the complete problem. We now address ourselves to this matter.

The Euler equation, eq. (1.14), shows that the Neumann boundary condition of zero current and the normal current continuity condition across a material interface are 'natural' conditions.[1] The Dirichlet boundary condition, $\phi(\underline{r}, E)\big|_{\partial\Omega} = 0$, on the other hand, is an essential boundary condition and many methods have been devised to ensure its satisfaction. The one most frequently used is to restrict M_m to the subspace $W_o^1(\Omega)$ of $W^1(\Omega)$ where the o subscript indicates that for $\psi_i \in W_o^1(\Omega)$ we must have,

$$\psi_i \in W^1(\Omega)$$

and

$$\psi_i\big|_{\partial\Omega} = 0$$

There are other possibilities[12,13] and the use of Lagrangian multipliers is a classical one. The deletion of certain superelement functions

to satisfy the Dirichlet condition certainly leads to fewer coefficients $\{a_{kg}\}$ in eq. (1.16) to solve for. This implies a reduction in computation time. It is however not quite certain what this deletion of trial functions will do to the accuracy of the answer. One can, after all, certainly construct spaces in $W^1(\Omega)$ with the property that certain linear combinations of the elements satisfy the Dirichlet condition without having the elements themselves satisfy the Dirichlet condition. An example of a space of this type is given in chapter 3. We choose to satisfy the Dirichlet condition by working in $W_o^1(\Omega)$.

We have attempted to present in this section a general formulation of the finite element method concentrating on those overall aspects which allow one to obtain an idea of its relative place in the field of approximation schemes. We have also been able to indicate what the constraints on the approximation space M_m are. In summary, for the Neumann problem $M_m \subset W^1(\Omega)$ and for the Dirichlet problem $M_m \subset W_o^1(\Omega)$.

In the next section we present a more detailed and a more mechanistic description of the method itself.

1.2.2 Equation Assemblage

Our objective in this section is to give an algorithmic treatment of the various steps required to arrive at the form of the Galerkin equations, eq. (1.16), preparatory to the actual inversion process. For this reason we shall refer to this section as the section on equation assemblage.

We begin by introducing the multigroup formulation[4] of eq. (1.1) as this is the form which is actually numerically solved by using the finite element method.

The integro-differential eq. (1.1) can be reduced by the use of the conventional multigroup formalism to a set of coupled differential equations

$$-\nabla \cdot D_g(\underline{r}) \, \nabla\phi_g(\underline{r}) + \Sigma_{Rg}(\underline{r}) \, \phi_g(\underline{r}) = \sum_{\substack{g'=1 \\ g'\neq g}}^{G} \Sigma_{sg'g}(\underline{r}) \, \phi_{g'}(\underline{r})$$

$$+ \sum_{g'=1}^{G} \frac{\chi_g(\underline{r})}{\lambda} \left(\nu\Sigma_{fg'}(\underline{r}) \, \phi_{g'}(\underline{r}) \right) + Q_g(\underline{r}) \qquad g = 1, \ldots, G \qquad (1.17)$$

where

$$\Sigma_{Rg}(\underline{r}) = \Sigma_{rg}(\underline{r}) - \Sigma_{sgg}(\underline{r}) \text{ is the group removal cross section.}$$

In the multigroup formulation the corresponding boundary and interface conditions are

$$\phi_g(\underline{r})\big|_{\partial\Omega} = 0 \quad \text{or} \quad D_g \frac{\partial\phi_g(\underline{r})}{\partial n} \bigg|_{\partial\Omega} = 0 \qquad (1.18)$$

$$\phi_g(\underline{r}) \quad \text{and} \quad D_g \frac{\partial\phi_g(\underline{r})}{\partial n} \text{ are continuous across } \partial\Omega_\ell \qquad (1.19)$$

The multigroup formulation has allowed us to effectively remove the energy variable from the problem and we will consider eq. (1.17) as the starting point for our application of the finite element method.

Let us for the moment concentrate on giving a mechanistic outline of the steps involved in solving eq. (1.17) by the finite element method.

One lays down a mesh composed of a set of straight line polygons $\{\theta_j \mid j=1, \ldots L\}$ on Ω as shown in Fig. 1.5.
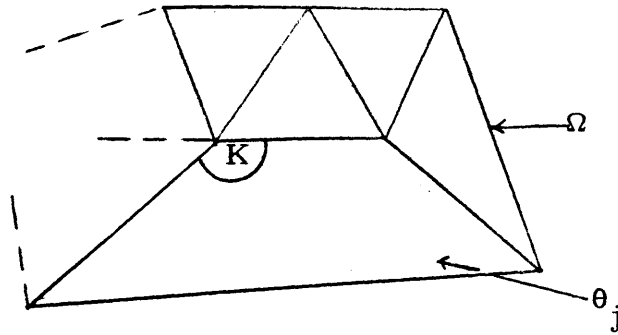
Fig. 1.5. General mesh.

We define a line segment to be the straight line lying between two intersection points. The one restriction on the mesh is that the angle between line segments should not be equal to 180°. The angle K in Fig. 1.5 is an example of what is meant by the angle between line segments. The logic behind this restriction will be appreciated after the discussion in chapter 2 is presented. The polygon θ_j shall be referred to as the basic patch.

We now select a finite dimensional space of functions $M_{m_j}^j$ to approximate the analytic solution of the problem over each of the basic patches $\{\theta_j\}$. That is to say each basic patch θ_j, has a corresponding space of functions $M_{m_j}^j$ which will be used to approximate the analytic solution in that particular region θ_j. $M_{m_j}^j$, in accordance with past work, is chosen to be P_{N_j}, a space of polynomials of maximum order N_j. This means that in a θ_j,

$$\hat{\phi}_g(\underline{r}) = \widetilde{P}_{N_j g}(\underline{r}) \qquad \underline{r} \in \theta_j \qquad (1.20)$$

where $\widetilde{P}_{N_j g}(\underline{r}) \in P_{N_j}$ is some polynomial of maximum order N_j, the

coefficients of which have to be determined.

The next step is to choose a set of functions $\{\Psi^j_{ig}(\underline{r})\,|\,i=1..m\}$ which form a spanning set[*] for the space P_{N_j}. It should be noted that to be consistent with the definition of P_{N_j} each set $\{\Psi^j_{ig}(\underline{r})\,\forall\,i\}$[†] has support only over the corresponding basic patch θ_j. We shall refer to the set $\{\Psi^j_{ig}(\underline{r})\,\forall\,i,j\}$ as the basic element set. Since the set $\{\Psi^j_{ig}(\underline{r})\,\forall\,i\}$ is a spanning set for P_{N_j} we have that,

$$\widetilde{P}_{N_j}g(\underline{r}) = \sum_{i=1}^{m_j} b^j_{ig}\,\Psi^j_{ig}(\underline{r}) \tag{1.21}$$

As the functional forms of the $\{\Psi^j_{ig}(\underline{r})\,\forall\,i\}$ are known, the problem of determining the coefficients of $P_{N_j}g(\underline{r})$, and hence the approximate solution $\hat{\phi}_g(\underline{r})$ in θ_j, becomes one of calculating the set of coefficients $\{b^j_{ig}\,\forall\,i\}$.

If the set $\{\Psi^j_i(\underline{r})\,\forall\,i\}$ forms a basis for P_{N_j} then the number of unknowns $\{b^j_{ig}\,\forall\,i\}$ will be a minimum and in addition one will not have to worry about the significance of such questions as the possibility of having piecewise linear dependence.

We now come to the major step; the problem of relating the basic element set $\{\Psi^j_{ig}(\underline{r})\,\forall\,i,j\}$ of eqs. (1.20)-(1.21) with the super element set $\{\psi_{kg}(\underline{r})\,\forall\,k\}$ of eq. (1.7) where we have converted $\psi_k(\underline{r},E)$ to its

---

[*]A spanning set for a function space is a set of functions which spans that space.

[†]Whenever there is a possible ambiguity we shall use the symbol $\forall$ to denote that the accompanying indices are to vary over their respective ranges. The indices not specified with $\forall$ are fixed in value.

multigroup form. This is the question of determining the approximation space M_m for $\hat{\phi}(\underline{r})$ given that for $\underline{r} \in \theta_j$, $\hat{\phi}(\underline{r}) \in M_{m_j}^j$. We shall only attempt to give a brief discussion of this problem here. The detailed presentation is left to chapter 2.

We begin by introducing the concept of a superpatch, Θ_J. The superpatch is the polygon composed of a number of contiguous basic patches θ_j. It is the region of support of the superelement function $\psi_{kg}(\underline{r})$. $\psi_{kg}(\underline{r})$ is then composed of a set of basic element functions $\{\Psi_{ig}^j(\underline{r}) \,|\, (i, j) \in \overline{G}_J\}$ where $\overline{G}_J$ is a set of ordered indices $\{(s, n)\}$ such that $\theta_n \subset \Theta_J$ and

$$\psi_{kg}(\underline{r}) = \Psi_{sg}^j(\underline{r}) \qquad \underline{r} \in \theta_n \qquad (1.22)$$

We shall refer to the set of indices $\{n\}$ for each superpatch Θ_J as G_J.

The process can be thought of as joining a set of shapes represented by the function set $\{\Psi_{ig}^j(\underline{r}) \,|\, (i, j) \in \overline{G}_J\}$ across the patch boundaries of the $\{\theta_j \,|\, j \in G_J\}$ which form the superpatch Θ_J.

Possible conditions of join are the analytic conditions of the exact problem. These are equations (1.18)-(1.19). Another condition derivable from eq. (1.17) and which could be of use in providing conditions of join is that

$$\phi(\underline{r}, E) \quad \text{and} \quad \frac{\partial^q}{\partial r^q} \phi(\underline{r}, E) \text{ are continuous for all } q \text{ in } \Omega_\ell \qquad (1.23)$$

where

$$\frac{\partial^q}{\partial r^q} = \frac{\partial^q}{\partial x_1^i \partial x_2^j \partial x_3^k} \qquad i + j + k = q$$

Once we have the set $\{\psi_{kg}(\underline{r})\}$ we apply the procedure outlined in § 1.2.1 to obtain the Galerkin equations, eq. (1.16), for the set of coefficients $\{a_{kg}\}$. In the two group external source free case where the assumption is made that there is no upscattering and that no fission neutrons are born in the thermal group, we have as an example of the Galerkin equations,

$$A_1 \underline{a}_1 = \frac{1}{\lambda} \left[F_1 \underline{a}_1 + F_2 \underline{a}_2 \right]$$

$$A_2 \underline{a}_2 = S_1 \underline{a}_1 \qquad\qquad\qquad (1.24)$$

where

$$(A_g)_{ii'} = (D_g(\underline{r}) \underline{\nabla} \psi_{i'}(\underline{r}), \underline{\nabla} \psi_i(\underline{r}))_\Omega + (\Sigma_{rg}(\underline{r}) \, \psi_{i'}(\underline{r}), \psi_i(\underline{r}))_\Omega$$

$$(\underline{F}_g)_{ii'} = (\nu \Sigma_{fg}(\underline{r}) \psi_{i'}(\underline{r}), \psi_i(\underline{r}))_\Omega$$

$$(S_1)_{ii'} = (\Sigma_{s21}(\underline{r}) \psi_{i'}(\underline{r}), \psi_i(\underline{r}))_\Omega \qquad i,\ i' = 1, \ldots, m$$

$$\hat{\phi}_g(\underline{r}) = \sum_{i=1}^{m} a_{ig} \, \psi_i(\underline{r})$$

$$\underline{a}_g = \text{col}\{a_{1g}, a_{2g}, \ldots, a_{mg}\} \qquad g = 1, 2 \qquad\qquad (1.25)$$

To solve this eigenvalue problem for the system multiplication constant λ we adopt the usual power iteration scheme.[4] The power iteration scheme can be written as

$$A_1 \underline{a}_1^{(t)} = F_1 \underline{\Phi}_1^{(t-1)} + F_2 \underline{\Phi}_2^{(t-1)}$$

$$A_2 \underline{a}_2^{(t)} = S_1 \underline{a}_1^{(t)}$$

$$\hat{\lambda}^{(t)} = \frac{\langle \underline{a}_1^{(t)}, \underline{a}_1^{(t)} \rangle + \langle \underline{a}_2^{(t)}, \underline{a}_2^{(t)} \rangle}{\langle \underline{a}_1^{(t)}, \underline{\Phi}_1^{(t-1)} \rangle + \langle \underline{a}_2^{(t)}, \underline{\Phi}_2^{(t-1)} \rangle}$$

$$\underline{\Phi}_1^{(t)} = \frac{\underline{a}_1^{(t)}}{\hat{\lambda}^{(t)}}$$

$$\underline{\Phi}_2^{(t)} = \frac{\underline{a}_2^{(t)}}{\hat{\lambda}^{(t)}}$$

where $\langle , \rangle$ denotes an inner product $\hfill (1.26)$

The power method converges to the eigenvalue λ, of the largest magnitude and therefore gives us the dominant characteristic mode.

We have presented in this chapter a discussion of the specific problem area this thesis will be concerned with in terms of accuracy and computation time. In addition, we have given an idea of the general nature of the finite element method and have described in an algorithmic fashion the steps required in using the method. It was pointed out that the major step involved was in going from the $\{M_m^j \ \forall \ j\}$ to the space M_m. In essence this is the area of the pre-Galerkin calculation phase where we use conditions of join to reduce the basic coefficient set $\{b_{ig}^j \forall \ i, j\}$ of eqs. (1.20)-(1.21) to the super coefficient set $\{a_{ig} \forall \ i\}$ of eq. (1.7). It is the question of the construction of piecewise polynomial spaces and we address ourselves to it in the next chapter.

Chapter 2

CONSTRUCTION OF SPACES

We concern ourselves in this chapter with the step in the assemblage of the Galerkin equations, eq. (1.16), where we go from the basic element set $\{\Psi_{ig}^j \ \forall \ i,j\}$ of eqs. (1.20)-(1.21) to the superelement set $\{\psi_{kg} \ \forall \ k\}$ of eq. (1.7) where we have used the multigroup form of $\psi_k(\underline{r}, E)$.

Section 2.1 discusses the general problems involved in this phase of the finite element method; a phase which we shall refer to as the pre-Galerkin phase as its net effect is to reduce the set of expansion coefficients of eqs. (1.20)-(1.21), the basic coefficient set $\{b_{ig}^j \ \forall \ i,j\}$, to a smaller set of unknowns, the supercoefficient set $\{a_{kg} \ \forall \ k\}$ of eq. (1.7). What is done is to apply conditions to relate the members of $\{b_{ig}^j \ \forall \ i,j\}$ in equations, different from the Galerkin equations, of the form

$$\sum_i \sum_j A_{ig}^j b_{ig}^j = 0 \tag{2.1}$$

This allows us to eliminate a set of variables V, $\{b_{sg}^r\}$, where we will denote the set of ordered pairs (r, s) by L,

$$b_{sg}^r = \sum_{\substack{(i,j) \\ (i,j) \notin L}} B_{sg}^{jr} b_{ig}^j \qquad (r,s) \in L. \tag{2.2}$$

With this result we can rewrite eqs. (1.20)-(1.21) as

$$\hat{\phi}_g(\underline{r}) = \sum_{\substack{(i,j) \\ (i,j) \notin L}} b_{ig}^j \{\Psi_{ig}^j(\underline{r}) + \sum_{(r,s) \in L} B_{is}^{jr} \Psi_{sg}^r(\underline{r})\}$$

$$= \sum_k a_{kg} \psi_{kg}(\underline{r}) \tag{2.3}$$

which means that $\{a_{kg} \ \forall \ k\}$ is the set of remaining b_{ig}^j, V' and

$$\psi_{kg}(\underline{r}) = \Psi_{ig}^j(\underline{r}) + \sum_{(r,s)\in L} B_{is}^{jr} \Psi_{sg}^r(\underline{r}) \qquad (2.4)$$

giving us the approximation space M_m for $\hat{\phi}_g(\underline{r})$.

This is the general scheme for the pre-Galerkin phase. We then use the Galerkin equations to solve for the remaining unknowns; namely those of the set V'. The use of the Galerkin equations implies certain restrictions on the coefficients B_{is}^{jr} because of essential constraints on the superelement functions ψ_{kg}. But in any case, it can be seen that the crux of the matter is that eq. (2.1) should be simple enough to solve algebraically. If simple enough equations can be developed, it can be said that we can reduce the basic coefficient set $\{b_{ig}^j \ \forall \ i,j\}$ to a smaller set of unknowns, the supercoefficient set $\{a_{kg} \ \forall \ k\}$ through a series of mathematical manipulations which once carried out do not have to be repeated for different problems using the same approximation space M_m. Section 2.1 mentions a number of possible conditions which could be applied to affect this reduction in the number of unknowns.

In section 2.2 we discuss the various mesh schemes or, in other words, the different sets of $\{\theta_j \ \forall \ j\}$ which can be used in the case of the hexagonal reactor configuration and in the final section, §2.3, we present methods for constructing approximation spaces M_m.

2.1 Overall Problems

This section concerns itself with the questions which arise when we attempt to go from the basic element set $\{\Psi_{ig} \ \forall \ i,j\}$ to the superelement

set $\{\psi_{kg} \ \forall \ k\}$ which is to be used in the Galerkin formulation, eq. (1.16), to find the unknowns $\{a_{ig}\}$.

The whole issue revolves around the feasibility and desirability of determining an appropriate set of additional constraints which when applied to $\{\psi_{ig}^j \ \forall \ i,j\}$ yield equations for the pre-Galerkin phase which allow us to reduce the set $\{b_{ig}^j \ \forall \ i,j\}$ to the set of fewer unknowns, $\{a_{ig} \ \forall \ i\}$.

The essential constraints are the ones given to us by our use of the weak form, namely $\psi_{kg} \in W_o^1(\Omega)$ for the Dirichlet problem and $\psi_{kg} \in W^1(\Omega)$ for the Neumann problem. These are examples of how the final step in the equation assemblage influences the construction of the approximation space M_m. As will be seen later all the steps in the assemblage have an effect on the construction of the approximation space. Returning to the question of constraints, it was seen that the mathematics dictates the two essential constraints. There are also constraints, which could possibly be used, dictated to us by the physics of the problem. As noted in section 1.2.2 and reiterated here, these are (i) flux continuity; (ii) current continuity; (iii) in the interior homogeneous region, all the derivatives of the flux are continuous; (iv) satisfaction of the diffusion equation within a particular homogeneous region. All of these 'constraints' can be used to further reduce the number of variables which have to be solved for in the Galerkin phase. There are, however, trade-offs involved.

Let us consider constraint (iv). This has already been used in the Galerkin equations. Further usage of it leads to Galerkin coefficient

matrices radically different from ones obtained by the conventional approach. For example, suppose we force neutron conservation for each θ_j by integrating the multigroup diffusion equation, eq. (1.17), over θ_j. This gives us an equation which we can use to eliminate b^j_{1g},

$$b^j_{1g} = \sum_{i=2}^{m_j} A_i(\lambda) \, b^j_{ig}.$$
(2.5)

The coefficients $\{A_i(\lambda)\}$ are also functions of the material properties but it is the λ-dependence which gives the unique character of this approach; for then we can write

$$\hat{\phi}_g(\underline{r}) = \sum_{i=2}^{m_j} b^j_{ig}\{\Psi^j_{ig} + A_i(\lambda)\, \Psi^j_{1g}\} = \sum_{i=2}^{m_j} b^j_{ig} \Lambda^j_{ig}(\lambda) \qquad r \in \theta_j.$$
(2.6)

With this λ-dependence in the trial functions, the coefficient matrices of the Galerkin matrix will become λ-dependent and new iterative processes will have to be devised. Reusage of condition (iv) does not therefore appear to be a viable proposition.

Conditions (i), (ii) and (iii) belong to the generic problem of joining the $\{\Psi^j_{ig} \ \forall \ i,j\}$ across the boundaries of the $\{\theta_j \ \forall \ j\}$. We shall refer to these boundaries as the patch boundaries. It may seem quite attractive to impose as many of these conditions as possible to minimize the number of unknowns remaining. However, when one uses piecewise polynomial functions it turns out that the greater the number of constraints one wants to impose the higher the order N_j of the polynomial space P_{N_j} one has to work in. The dimension of P_{N_j} is depen-

dent on N_j and so if the constraint on the computation time, namely less than 3 variables/fuel hexagon is not to be violated, one has to work with a $M_{m_j}^j$ of increasingly large a defect.[*] This then brings in the question of the effect of incompleteness on accuracy. It must be noted that condition (i) is a restatement of an essential condition, $\psi_{kg} \in W^1(\Omega)$, and therefore must be imposed. Imposition of conditions (i)-(iii) can be considered a viable possibility.

Let us make one final comment before we delve into the various problem areas. When we apply constraints of join we are actually demanding that each and every member of the set $\{\psi_{kg} \; \forall \; k\}$ satisfy the conditions required by the constraints. This is therefore more exacting than asking that the approximation $\hat{\phi}_g(\underline{r})$ satisfy the constraints. It also means that in joining the members of the set $\{\Psi_{ig}^j \; \forall \; i,j\}$, the condition of join applied has to be applied across all the patch boundaries of Θ_J, otherwise $\hat{\phi}_g(\underline{r})$ will not satisfy the condition required.

As can be seen the general problem of constructing a set $\{\psi_{kg} \; \forall \; k\}$ from a set $\{\Psi_{ig}^j \; \forall \; i,j\}$ to generate solutions comparable in accuracy and computation time with the finite difference method, knowing only that we are restricted to spaces $\{P_{N_j} \; \forall \; j\}$ and a mesh of general polygons

---

[*]Let the dimension of $P_{N_j} = d_p$ and the dimension of $M_{m_j}^j = d_M$. Then the defect of $M_{m_j}^j$ with respect to $P_{N_j} = d_p - d_M$. It is a measure of the incompleteness of $M_{m_j}^j$ relative to P_{N_j}. Whenever we use the word "incomplete" in this thesis, it is to be understood that it is used relative to the complete polynomial space, $\overline{P}_{N_j}$.

$\{\theta_j \ \forall j\}$ with the constraint $\psi_{kg} \in W^1(\Omega)$ or $W_o^1(\Omega)$, is not trivial.[16,19] To lend some order to the presentation we shall, accepting the constraints outlined in the previous statement as given, discuss the problem areas in an algorithmic fashion with respect to the questions of feasibility and desirability, always keeping in mind the fact that the different steps, in the final analysis, are implicitly interrelated.

(a) Basic Patch. The basic patch is the polygon θ_j. In our hexagonal problem there appear to be three basic patches:

(i) Triangle; (ii) Quadrilateral; (iii) Hexagon.

Figure 2.1 illustrates some of the possibilities.

(b) Superpatch. We certainly do not want to use a space P_{N_j} with a spanning set $\{\Psi_{ig}^j \ \forall i\}$ such that all the Ψ_{ig}^j are zero on the boundary $\partial\theta_j$ of the basic patch θ_j. With a set $\{\Psi_{ig}^j \ \forall i\}$ which has members with nonzero function values along the patch boundary $\partial\theta_j$ one has to join $\{\Psi_{ig}^j \ \forall i\}$ with the sets corresponding to the contiguous patches so that $\{\psi_{kg} \ \forall k\}$ has function continuity. Let Γ_j refer to the set of basic patches contiguous to θ_j. One could then repeat the process for each $\theta_k \in \Gamma_j$. The process ends when there is a closed boundary with the function value equal to zero along it. We shall refer to this polygon as the superpatch Θ_J.[*] Each basic element function Ψ_{ig}^j is part of a superelement function ψ_{Jg} which has support Θ_J. One should then ask the question of how large Θ_J can be and how large it should be. Intuitively one would expect that a large Θ_J would decrease accuracy as one

---

[*]The concept of the superpatch was introduced in section 1.2.2.

Legend

Hatched area indicates
basic patch

Material
hexagon
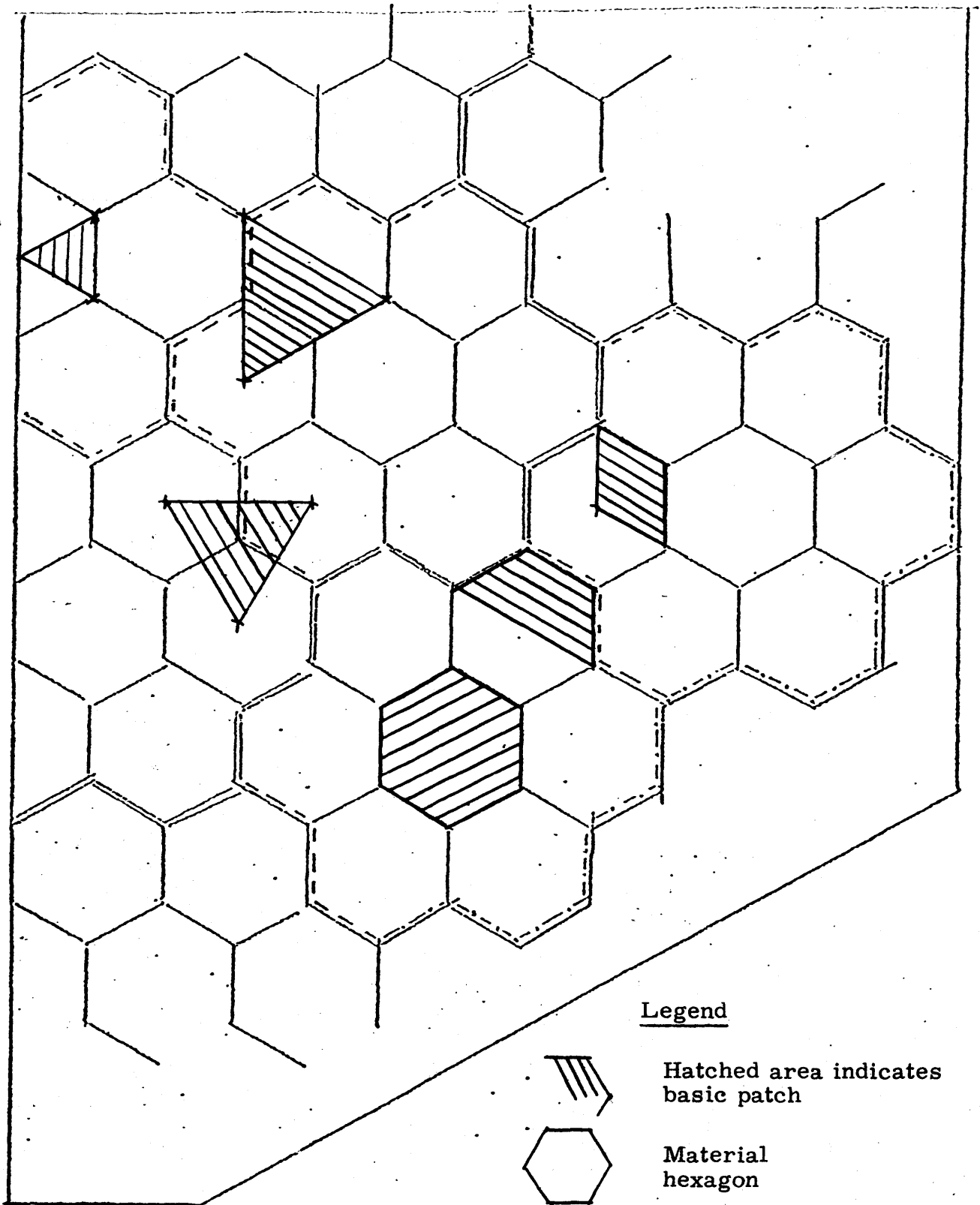
Fig. 2.1. Possible basic patches.

would then have fewer degrees of freedom in the approximation. As for feasibility, apart from the question of size, there is the question of whether or not mixtures of the basic patches are permissible.

To provide an illustration of possible superpatches let us consider the use of the Lagrangian cubics[6] for the basic element set $\{\Psi_{ig}^j \; \forall \; i, j\}$ with θ_j a triangle. We define the vector $\underline{K}_{ig}^j$

$$\left(\underline{K}_{ig}^j\right)_{k'} = \Psi_{ig}^j(\underline{r}_{k'}) \qquad \underline{r}_{k'} \in \theta_j, \qquad k' = 1, \ldots, 10. \qquad (2.7)$$

where the points $\underline{r}_{k'}$ are as shown in Fig. 2.2.
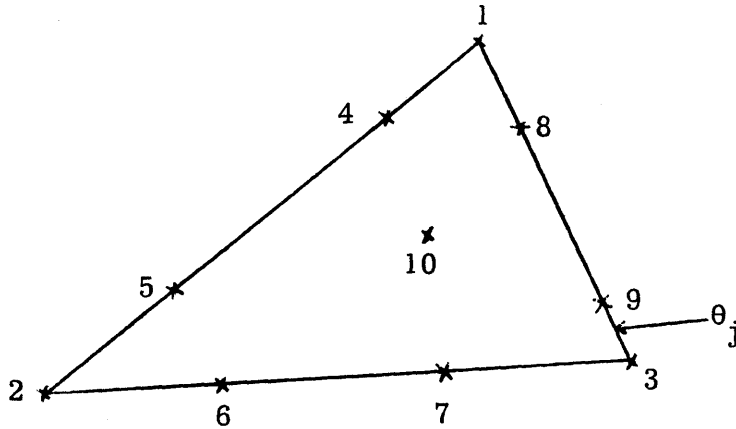
Fig. 2.2.
The points $\underline{r}_{k'}$ for the definition of the cubic Lagrangians.

The Lagrangian cubics are cubic polynomials each of which are determined by the following condition on the corresponding $\underline{K}_{ig}^j$ vector

$$\left(\underline{K}_{ig}^j\right)_{k'} = \delta_{ik'} \qquad k' = 1, \ldots, 10, \qquad i = 1, \ldots, 10. \qquad (2.8)$$

We can classify the Lagrangian cubic set $\{\Psi_{ig}^j \; \forall \; i\}$ into three groups according to the number of sides of θ_j, k_L on which each Ψ_{ig}^j is identically zero. One such set is the group $\{\Psi_{ig}^j \mid i = 1,.3\}$ which has $k_L = 1$.

The set $\{\Psi_{ig}^{j}\,|\,i = 4,\ldots,9\}$ has $k_L = 2$. The members of the last set $\{\Psi_{ig}^{j}\,|\,i = 10\}$ are identically zero on all three sides of θ_j.

Now suppose we apply the constraint of function continuity in going from the basic element set $\{\Psi_{ig}^{j}\;\forall\;i,j\}$ to the superelement set $\{\psi_{kg}\;\forall\;k\}$. In order to obtain function continuity of the set $\{\psi_{kg}\;\forall\;i\}$, certain elements of $\{\Psi_{ig}^{j}\;\forall\;i,j\}$ have to be joined across the interpatch boundaries. For the Lagrangian cubics, the set $\{\Psi_{10g}^{j}\;\forall\;j\}$ does not have to be joined. The set $\{\Psi_{ig}^{j}\;\forall\,j\,|\,i = 4,\ldots,9\}$ has to be joined on one side of θ_j while the set $\{\Psi_{ig}^{j}\;\forall\,j\,|\,i = 1,3\}$ has to be joined on two sides. The superpatches so formed can also be classified into three groups. These are shown in Fig. 2.3. We shall explain the notation used in the figure in the next paragraph where we generalize the

s^1 $\qquad\qquad$ s^2 $\qquad\qquad$ s^3
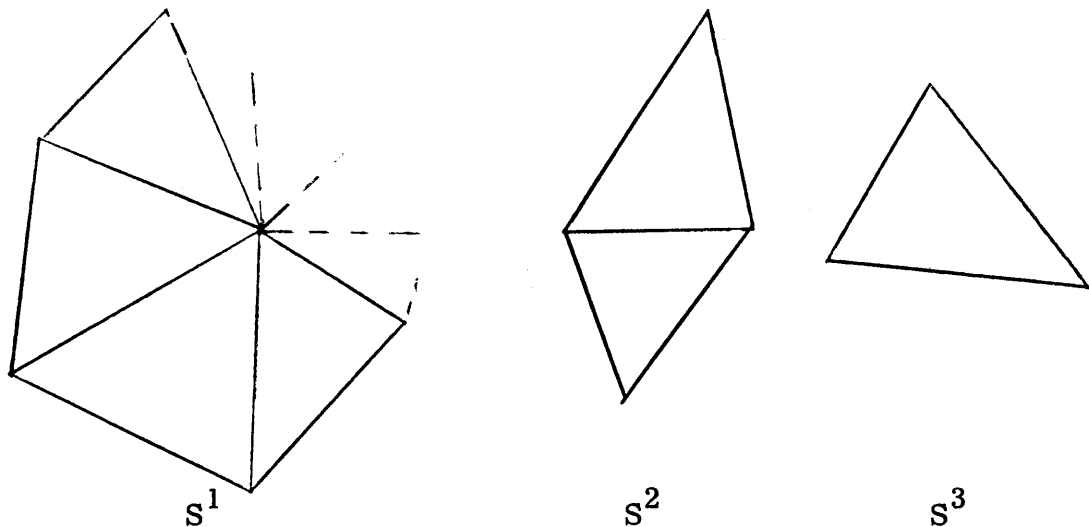
Fig. 2.3. Classes of superpatches — cubic Lagrangian set.

discussion . For this thesis we shall concentrate on the superpatch sets which evolve out of this examination of the Lagrangian cubics. In concluding it should be noted that the superpatches are not all of one pattern.

To generalize the approach let us start by classifying the $\{\Psi_{ig}^{j} \forall \; i\}$ in the case of θ_j = a triangle. This grouping, a mixture of geometrical conditions and function conditions, illustrates the close relation between the geometry of the basic patch and the approximation space. We define T^{k_L} as the set of those Ψ_{ig}^{j} which are zero on exactly k_L number of sides of θ_j.

Assuming that function continuity across patch boundaries can be imposed we arrive at the conclusion that if T^0 is not used there are three classes of superpatches, S^{k_L}, each of which forms the support for a ψ_k composed of basic element functions Ψ_i^j only from T^{k_L}. These superpatch classes are depicted in Fig. 2.3. We shall refer to S^1 as the 1-ring superpatch.

If T^0 is used, then there are other classes of superpatches which are essentially concentric 'rings'. We shall refer to them by the number of 'rings' in the configuration.

Figure 2.3 shows that the use of the complete cubic Lagrangian set for $M_{m_j}^{j}$ means that all three classes S^1, S^2 and S^3 will have to be used. For the complete linear Lagrangian set only S^1 has to be used and only S^1 can be used. The choice of a S^{k_L} definitely implies a constraint in the choice of a $M_{m_j}^{j}$.

As far as the reduction of number of variables is concerned, there

is a real incentive to use only S^1. If we exclude T^0 from the discussion, then the use of S^1 minimizes the number of variables $\{a_{kg} \forall\, k\}$. This is because the ψ_{kg} formed in this manner is composed of the greatest number of basic element functions, Ψ_{ig}^j, possible, thus reducing the number of independent variables in $\{b_{ig}^j\}$ the most. We shall therefore concentrate on S^1 in this thesis.

Let us conclude this segment of the discussion by emphasizing a point which this section brings out. This is that by applying the conditions of join to $\{\psi_{kg} \forall\, k\}$ and not to $\hat{\phi}_g(r)$, we have, in essence, shifted the burden to the determination of the appropriate $\{\Psi_{ig}^j \forall\, i\}$ set. One has to anticipate the constraints which will be used to determine the $\{\psi_{kg} \forall\, k\}$ in finding $\{\Psi_{ig}^j \forall\, i\}$. This implies that the conditions used to determine $\{\Psi_{ig}^j \forall\, i\}$ should be concentrated on the perimeter $\partial\theta_j$ of θ_j.

It should be noted that the classification of $\{\Psi_{ig}^j \forall\, i\}$ into groups $T^{k}L$ can be logically extended to include subclasses based on the number of sides of θ_j on which the gradient and the higher derivatives are zero. We shall not proceed any farther in this thesis with this particular concept.

We now address ourselves to the question of polynomial spaces.

(c) Polynomial Space. To every basic polygonal patch there apparently is a corresponding canonical form for $\widetilde{P}_N(\underline{r})$.

For a triangle[6]

$$\widetilde{P}_N(x,y) = \sum_{i=0}^{N} \sum_{j=0}^{N-i} a_{ij} x^i y^j \qquad (2.9)$$

$$K_N = \text{number of coefficients} = \frac{N}{2}(N+3) + 1. \tag{2.10}$$

For a rectangle[1]

$$P_N(x,y) = \sum_{i=0}^{N} \sum_{j=0}^{N} a_{ij} x^i y^j \tag{2.11}$$

$$K = \text{number of coefficients} = (N+1)^2. \tag{2.12}$$

These canonical forms appear to be forms which, allowing for the constraints of continuity at the corner points of the polygon, permit the determination of the function shape along each of the piecewise linear edges of the polygon to be entirely independent processes. Imposition of function continuity conditions across patch boundaries then becomes 'natural'.

It is possible to obtain the canonical form for the quadrilateral by isoparametrically transforming the rectangle into the quadrilateral.[7] A canonical form for the hexagon is still lacking.

The assumption shall be made that the use of the canonical forms is still appropriate when we try to impose conditions in addition to that of function continuity across the interpatch boundaries.

Even with the general form of $\widetilde{P}_{N_j}$ prescribed we still have a great deal of flexibility. We are faced with the choice of which subspace of $\overline{P}_{N_j}$ to work in and with the determination of the spanning set $\{\Psi^j_{ig} \forall\ i\}$. We could choose to determine the superelement set $\{\psi_{kg} \forall\ i\}$ first and accept the space spanned by the resulting basic element set $\{\Psi^j_{ig} \forall\ i\}$ as our particular subspace $M^j_{m_j}$. This approach, however, does make

questions of completeness and piecewise linear dependence harder to resolve. The possibility that the $\{M_{m_j}^j \,\forall\, i\}$ are not identical can also arise. From this point of view it is more systematic to choose the subspace first and then find the superelement set. We shall refer to the second approach as the mathematical construction and to the first as the physical construction. To determine the set $\{\Psi_{ig}^j \,\forall\, i\}$ one has to specify conditions satisfied by each member of the set in order to find the coefficients of the functional form. The problem of what these conditions should be is closely tied in with the problem of joining the sets across patch boundaries. We shall divide the conditions imposed in the definition of the basic element functions into two classes. One class is termed interpolation conditions and the other class, for the lack of a better name, the noninterpolatory conditions. The set $\{\Psi_{ig}^j \,\forall\, i,j\}$ can be defined by the imposition of conditions from either class but it is much easier to see linear independence and completeness with conditions from the interpolation class. This class contains conditions such as the point specification of a value of the function or its derivative, the specification of $\int \underline{ds} \cdot \nabla \Psi_{ig}^j$ along a line, in other words, conditions which specify a value.

(d) Conditions of Join. The noninterpolatory class is the class of conditions which relate the basic element sets $\{\Psi_{ig}^j \,\forall\, i\}$ of contiguous basic patches across patch boundaries. These conditions are therefore primarily oriented towards the determination of the superelement set $\{\psi_{kg} \,\forall\, k\}$.

Function continuity definitely has to be imposed but there are other

conditions, discussed in preceding sections, such as current continuity, which could be imposed. Variations such as integrated current continuity also fall into this class. Care must be taken not to impose function and current continuity at a singular point as this can lead to $\{\psi_{kg} \ \forall \ k\}$ with zero gradients at these points.[*]

Conceptually it should be possible to combine all the problem areas (a)-(d) into a general formula relating the order of the polynomial N, the number and type of conditions imposed, and the number of sides which θ_j possesses for feasible sets $\{\psi_{kg}\}$. To resolve questions about completeness and piecewise linear dependence one would still have to break ψ_{ig} down into its basic element functions ψ_{ig}^j, but even so, such a general formula would still be very valuable as a synthesis tool.[19] However, it has apparently never been done.[16] This thesis had to resort to a case by case approach. We can not, therefore, claim to have treated the general problem comprehensively but we can say that the sets we come up with for our specific problem do provide answers to some of the fundamental questions outlined in the preceding pages.

We have in the preceding section attempted to outline and discuss, in a general manner, the questions which arise when the various steps involved in trying to assemble the Galerkin equations, eq. (1.16), are examined. We now turn our attention to specific areas beginning in the next section, §2.2, with the different $\{\Theta_J \ \forall \ J\}$ schemes possible.

---

[*]Refer to Appendix D for a more detailed discussion.

2.2 Specific Superpatch Schemes

Let us begin by considering the 'coarsest' meshes possible with the hexagonal reactor configuration which could potentially give us the accuracy and computation time required. We will then construct 'finer' versions by a further subdivision of the basic patches θ_j. The inquiry shall be restricted to regular meshes as it is only in the vicinity of the outer boundary $\partial\Omega$ that the use of an irregular mesh becomes essential. Figures 2.4 and 2.5 show the possibilities. They are

    (a) a fuel hexagon center – fuel hexagon corner mesh

    (b) a fuel hexagon center – fuel hexagon center mesh

    (c) a fuel hexagon center – adjoining fuel hexagon corner mesh

    (d) the fuel hexagon map itself.

If we restrict ourselves to 'simple' superpatches Θ_J, then the largest superpatches possible for each of the meshes (a)-(d) are those depicted in Fig. 2.6. Before we discuss the various superpatches let us keep in mind that the lowest order complete polynomial space, $\overline{P}_1$, has 3 unknowns in the triangular form and 4 in the rectangular cum quadrilateral case. This means that the use of complete P_N spaces requires the use of at least 3 variables per θ_j. This does not necessarily translate into a constraint of at least 3 variables per fuel hexagon because θ_j could encompass more than one fuel hexagon. There is also a reduction in the number of total variables when basic patches, θ_j, are joined to form a superpatch Θ_J as variables are then equated.

It should be reemphasized that the superpatches of Fig. 2.6 will be considered the largest Θ_J possible for the corresponding $\{\theta_j \; \forall \; j\}$ set.

Mesh
(a)

Mesh
(b)

Legend

Mesh lines

Material
hexagon

Fig. 2.4. 'Coarsest' possible meshes.

Mesh (c)

Mesh (d)

Legend

⟵×—————×⟶   Mesh lines

Material hexagon
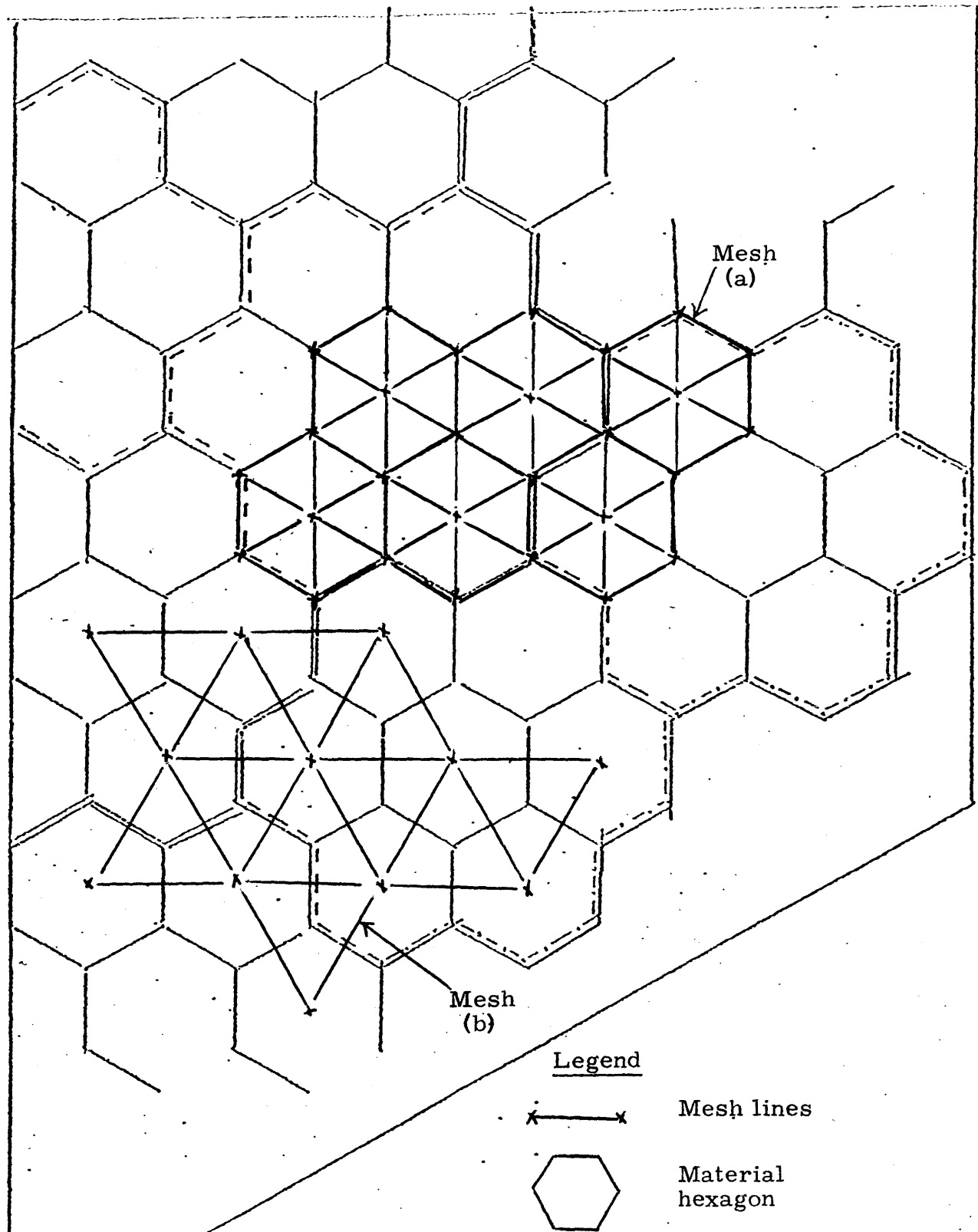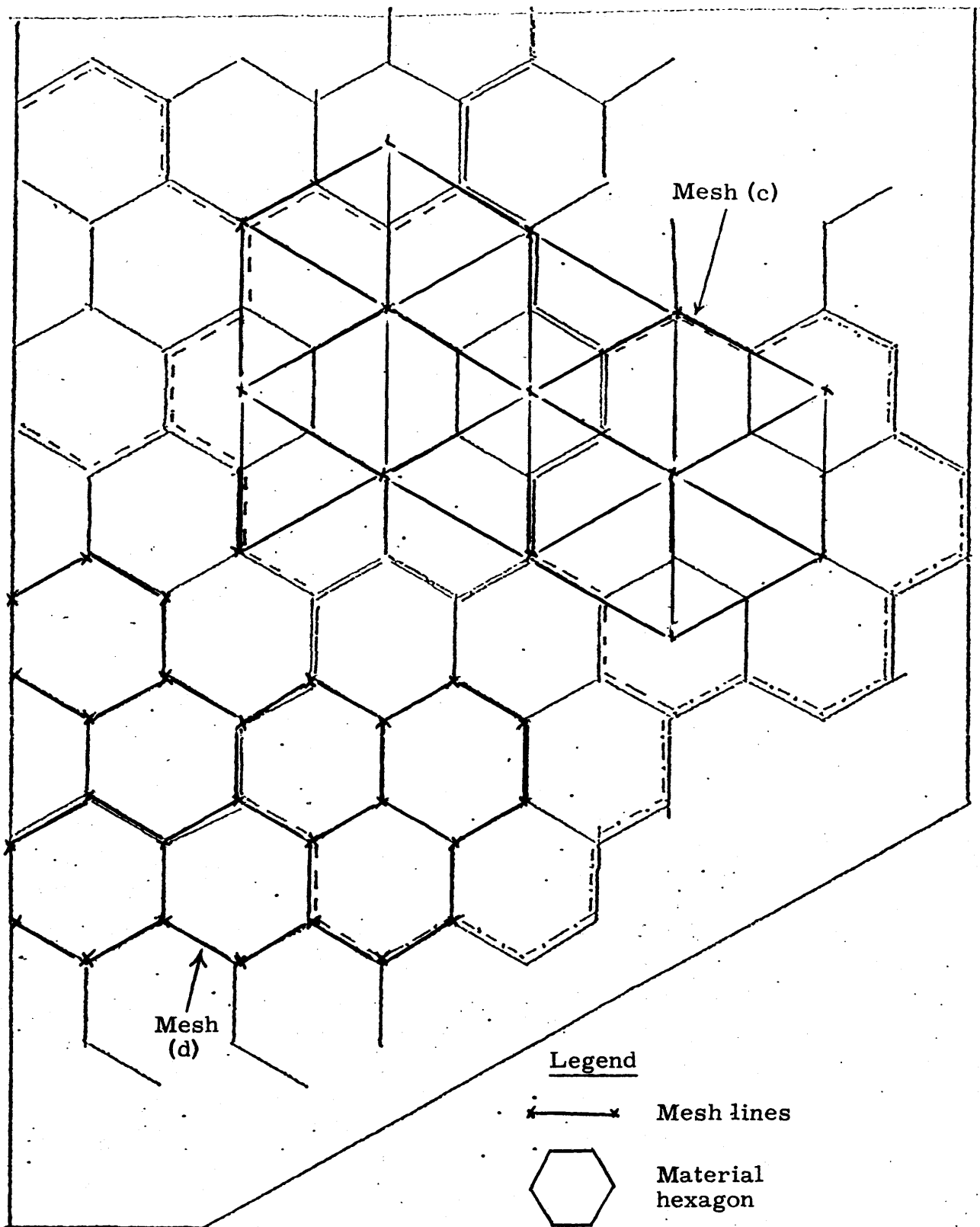
Fig. 2.5. 'Coarsest' possible meshes.
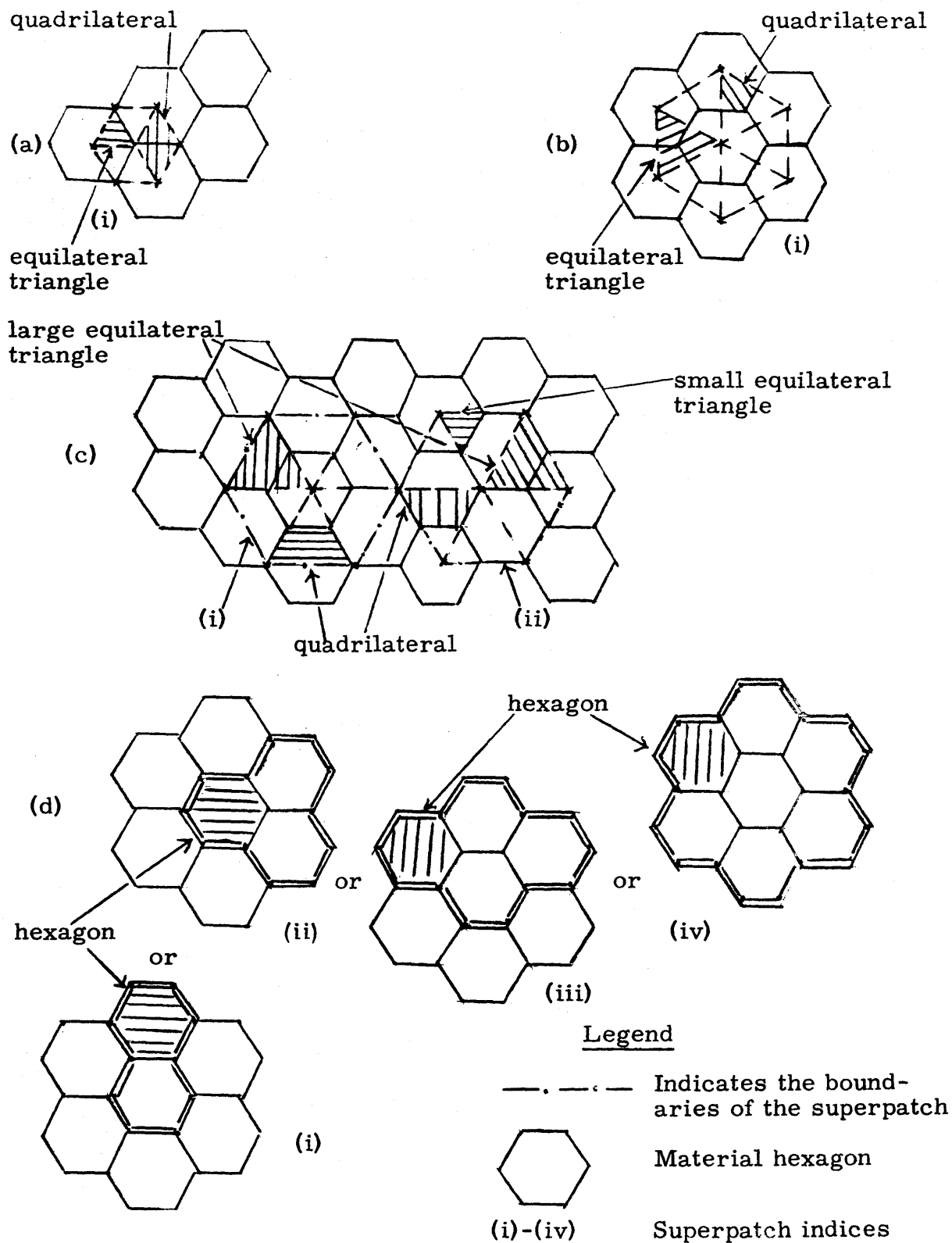
Fig. 2.6. Possible superpatches for each mesh scheme.

It is entirely conceivable that the manner in which the space $M_{m_j}^j$ is broken up into a set $\{\Psi_{ig}^j \,\forall\, i\}$ will lead to a range of superpatches. Consider the Lagrangian cubic example of Fig. 2.3. We shall restrict ourselves to those spaces $M_{m_j}^j$ which can be split up such that there is only one superpatch possible for each mesh $\{\theta_j \,\forall\, j\}$; namely the types depicted in Fig. 2.6. If we ignore mesh (d), the Θ_J depicted in Fig. 2.6 are all of the ring type. As noted in section 2.1 this will minimize the number of unknowns $\{a_{kg} \,\forall\, k\}$.

We now consider each of the meshes (a)-(d) separately and examine the different possible subdivisions of the internal structure of the super-patches, θ_j.

(a) Mesh (a) has a superpatch which can either be divided into $\{\theta_j =$ equilateral triangle$\}$ or $\{\theta_j =$ a $120°$ parallelogram$\}$. Both cases give three unknowns per fuel hexagon for the space $\overline{P}_1$. The quadrilateral option requires a transformation from the rectangular form and leads to complicated square roots. For this reason and also for the reason that the other meshes lead towards the triangular form we shall not consider the quadrilateral possibility. Any complete P_{N_j} space of order higher than one, combined with this superpatch, will violate the constraint on the number of unknowns. Usage of this mesh scheme thus restricts us to the linear Lagrangian functions[6] for $\{\Psi_{ig}^j \,\forall\, i\}$.

(b) For mesh (b) there is again one superpatch. It can be thought of as being composed of either $\{\theta_j =$ equilateral triangle$\}$, or $\{\theta_j =$ a quadrilateral, as shown in Fig. 2.6$\}$. In constructing the 'finer' sub-divisions we restrict ourselves to basic patches which lie entirely

within homogeneous material regions. We then have that within the basic patches the analytic solution for the flux will have as much smoothness as the polynomial approximation.

If we use $\{\theta_j = \text{equilateral triangle}\}$, then $\hat{\phi}_g$ will have derivative continuity instead of current continuity across fuel block interfaces. For the triangular P_{N_j} space it can be seen that the highest complete space which can possibly be used is the space $\overline{P}_2$. Any higher order incomplete space can have at the most 9 degrees of freedom; that is, three superelement functions/fuel hexagon center.

The use of $\{\theta_j = \text{quadrilateral}\}$ brings up many questions. First of all, as has been noted earlier, the quadrilateral P_{N_j} space has complicated functions. But even if we choose to work with the triangular P_{N_j} space there is the question of geometry. We essentially have two rings of quadrilaterals. The conditions applied in the inner ring will be different from the conditions applied in the outer ring. This makes this particular configuration radically different and the question of feasibility quite real. The advantage of the scheme is that the possibility of imposing current continuity across fuel block interfaces is there.

(c) This is an interesting case. Once again we have the option of using $\{\theta_j = \text{large equilateral triangle}\}$. The second option is $\{\theta_j = \text{either}$ a small equilateral triangle or a quadrilateral$\}$. The same points which came up in the discussion of (b) arise here but there is one additional feature to the second option. We now have a mixture of θ_j's. This leads to the coexistence of two superpatches which have different internal structure. Consider superpatch (i). Here the outer boundary is part of

the quadrilateral only. In superpatch (ii) it is split up between the quad-rilateral and the triangle. Imposition of identical conditions in the two cases may lead to sets $\{\Psi_{ig}^{j}\}$ which are of different orders N. This will be shown to be the case in the next section.

It would seem, then, that for the simplest case there should be considerable symmetry in our choice of a superpatch. The $\{\theta_{j} | j \in G_{J}\}$ which makes up the Θ_{J} should be identical and, moreover, should be placed in a geometric configuration such that an interchange in the basic patches, θ_{j}, of the superpatch can be made without having to change the conditions imposed at patch boundaries. In other words, the Θ_{J} should consist only of one ring of similar basic patches.

The next order of difficulty would then occur when the basic patches are not all identical. After that we would have to consider the class of two-ring superpatches.

The order of difficulty is the order of difficulty associated with trying to split the spaces $M_{m_{j}}^{j}$ into the set $\{\Psi_{ig}^{j} \ \forall \ i\}$ which have to sat-isfy the number of joins specified by the geometrical configuration of the superpatch. This question will be examined in section 2.3.

We shall in this thesis concentrate on the one-ring superpatch, that is, class S^{1}, with $\{\theta_{j} = \text{equilateral triangle}\}$. The questions coupled with the usage of this class of Θ_{J} are fundamental enough that clarifi-cations here could be useful in the construction of the more complex rings.

(d) We shall conclude this section by conjecturing on the possibility of constructing superpatches using hexagons as basic patches. The use

of $\{\theta_j = \text{fuel hexagon}\}$ is attractive to the physical intuition as the solution ϕ_g in the fuel block has as much smoothness as a polynomial. Flux continuity and current continuity conditions can then be applied across fuel block interfaces. Applying the principles outlined in the previous section, we see that superpatch (i) of Fig. 2.6(d) is where the space M_N^j has been split into functions which are nonzero only on one side. The next two superpatches (ii) and (iii) split the space into functions which are nonzero on two sides and three sides, respectively. The corresponding cases of more than three sides lead to higher rings. Case (iv) of Fig. 2.6(d) is the case of the six sides. Basic element functions, Ψ_{ig}^j, of two classes T^0 and T^3 have to be combined.

2.3 Construction Methods

Given the superpatch configuration we have now to produce a set $\{\psi_{kg} \forall\ k\}$. There are two approaches to the problem and there are two corresponding methods for constructing the approximation space M_m. We introduced the two approaches in section 2.1 and termed them as

    (i)   the physical construction

    (ii) the mathematical construction.

As the names imply, there is a basic difference in the attitude behind the two approaches. In the case of (i), we appeal to physical intuition to construct superelement functions ψ_{kg} and accept the space spanned by $\{\psi_{kg} \forall\ k\}$ as our approximation space. The conditions used to find the superelement functions are a mixture of the interpolatory and the noninterpolatory sets. We shall refer to this method of construction

as the hybrid method.

The second approach is much more mathematical in nature. Here we start with a known space $E_{N_j}^j$, known in the sense that we have or can derive a basis, $\{e_i^j\}$, in terms of an interpolatory set of conditions. We then apply the noninterpolatory conditions across the patch boundaries to the $\{e_i^j\}$ to obtain the $\{\psi_{kg}\}$ which will be expressed in terms of linear combinations of the $\{e_i^j\}$. This method will be termed the generic scheme.

The relative advantages and disadvantages of the two methods are examined in the following sections but before we discuss them let us examine another possibility for constructing spaces. This is the possibility of using a variational functional to determine the superelement functions ψ_{kg} given that $M_{m_j}^j \subset P_{N_j}$. The functional to be used would have to be one which involved the diffusion equation, eq. (1.1). It can be seen that the method would then suffer from the same liability which use of eq. (1.1) as a constraint has. As pointed out in section 2.1, this is the problem of the introduction of λ into the Galerkin coefficient matrices.

We now move on to a description of the hybrid method and the generic scheme.

2.3.1 Hybrid Method

Here one uses one's physical intuition in determining a set of conditions to apply to the superpatch in order to find the coefficients of ψ_{kg}. If a set of constraints is to produce a feasible superelement set

$\{\psi_{ig}\}$ in conjunction with a given superpatch, it is necessary that the group of constraints satisfy the following test; the number of equations as represented by the constraints must be equal to the number of coefficients of ψ_{kg} which have to be solved for. This, however, is only a necessary condition. For sufficiency we must also ensure that the constraints do not lead to a system of improper or redundant equations. By an improper system we mean that the system is either inconsistent or that the only solution is the trivial solution. Redundancy, on the other hand, leads to a nonunique solution.

Conversely, these tests should enable us to determine the conditions required to produce a feasible set $\{\psi_{kg}\}$ given the superpatch configuration.

Let us demonstrate the procedure by considering mesh (c) of Fig. 2.6. Even though this mesh will not be considered in the remainder of the thesis, this is an interesting case and will illustrate several points. Figure 2.7 is a more detailed illustration of the superpatches in question and we shall refer to it.

Superpatch (i)   Superpatch (ii)
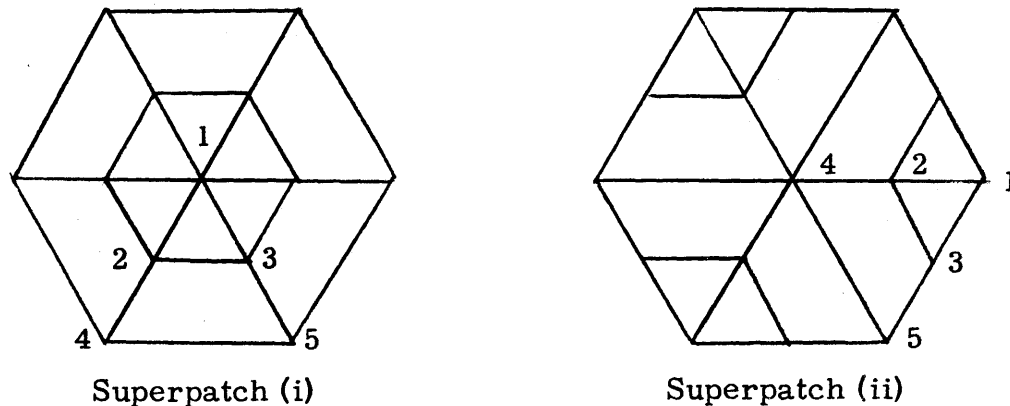
Fig. 2.7. Superpatches of mesh (c) of Fig. 2.3.

Concentrating on triangle 145 of superpatch (i) we have, since we are using the triangular $\widetilde{P}_{N_j}(\underline{r})$, for the superelement function ψ_{kg} which has superpatch (i) for support, in triangle 145,

$$\psi_{kg} = \phi = \begin{cases} \displaystyle\sum_{i=0}^{N} \sum_{j=0}^{N-i} a_{ij} x^i y^j & \text{triangle 123} \\[4mm] \displaystyle\sum_{i=0}^{N} \sum_{j=0}^{N-i} b_{ij} x^i y^j & \text{quadrilateral 2354} \end{cases} \qquad (2.13)$$

Condition		Number of Equations
$\phi_1 = 1$		1
ϕ_{1-2}	continuous across patch boundary 1-2 (point 1 is already prescribed)	$N/2$
ϕ_{1-3}	continuous across patch boundary 1-3	$N/2$
$\phi_{4-5} = 0$		$N+1$
ϕ_{2-3}	continuous across patch boundary 2-3	$N+1$
ϕ_{2-4}	continuous across patch boundary 2-4 (points 2 and 4 function value already continuous across patch boundary)	$N-1/2$
ϕ_{3-5}	continuous across patch boundary 3-5 (points 3 and 5 function value already continuous across patch boundary)	$N-1/2$

Total number of equations for triangle 145 = 4N + 2

$$(2.14)$$

Total number of equations for superpatch = 6(4N+2) $\qquad$ (2.15)

Total number of coefficients

using eq. (2.10) = 12 K_N = 6N(N+3) + 12. $\qquad$ (2.16)

We then have

N	Number of Equations	Number of Coefficients
1	36	36
2	60	72
3	84	120
4	108	180

Only at $N = 1$ do we have agreement. The other values of N lead to infeasible sets. Now supposing we want to impose additional constraints across the patch boundaries, namely those of current continuity. One possibility is to add the following conditions.

Condition		Number of Equations
$\int ds\, D\, \dfrac{\partial \phi_{1-2}}{\partial n}$	integrated normal current continuity across patch boundary 1-2 plus	
$D\, \dfrac{\partial \phi}{\partial n}$	normal current continuity across patch boundary 1-2 at N-2 points	$N-1/2$
$\int ds\, D\, \dfrac{\partial \phi_{1-3}}{\partial n}$	integrated normal current continuity across patch boundary 1-3 plus	
$D\, \dfrac{\partial \phi}{\partial n}$	normal current continuity across patch boundary 1-3 at N-2 points	$N-1/2$
$\int ds\, D\, \dfrac{\partial \phi_{2-4}}{\partial n}$	integrated normal current continuity across patch boundary 2-4	$1/2$
$\int ds\, D\, \dfrac{\partial \phi_{3-5}}{\partial n}$	integrated normal current continuity across patch boundary 3-5	$1/2$
$D\, \dfrac{\partial \phi_{2-3}}{\partial n}$	normal current continuity across patch boundary 2-3	N

Additional number of equations for triangle 145 = 2N

(2.17)

$$\text{Additional number of equations for superpatch} = 12 \, N \qquad (2.18)$$

Now we have

N	Number of Equations	Number of Coefficients
1	48	36
2	84	72
3	120	120
4	156	180

A feasible set now occurs at $N = 3$.

It will be noticed that the interpolation and noninterpolatory conditions imposed lead to an expression of the form $(AN + B)$ for the total number of equations. This holds true in the general case and it leads to a technique for eliminating conditions which would produce infeasible sets. For example, let us suppose that we wanted to add conditions to our original set containing function constraints only. We would then require that

$$6(4N+2) + 6(AN + B) = 6N(N+3) + 12 \qquad (2.19)$$

where

$(AN + B)$ = additional equations introduced for triangle 145 by new conditions.

We can rewrite this as

$$AN + B = N^2 - N \qquad N = 1, 2, 3, \dots . \qquad (2.20)$$

For each N we obtain an indeterminate equation for A and B. These unknowns, however, have to be integer values and sets of A and B can be found. However, one still has to resort to trial and error to obtain

additional constraints consistent with these sets. In any case, eq. (2.20) is a simplified version of what was referred to in section 2.1 as a general formula[16] relating the order of the polynomial N, the number and type of conditions imposed, and the number of sides which θ_j possesses, for feasible sets $\{\psi_{kg}\}$.

Let us now consider superpatch (ii) of mesh (c) which must coexist with superpatch (i). Applying the function conditions to this superpatch and concentrating again on triangle 145 we have

Condition		Number of Equations
$\phi_4 = 1$		1
$\phi_{1-3} = 0$		N+1
$\phi_{3-5} = 0$		N+1
ϕ_{2-3}	continuous across patch boundary 2-3	N
ϕ_{2-1}	continuous across patch boundary 2-1	N/2
ϕ_{4-5}	continuous across patch boundary 4-5	N-1/2
ϕ_{4-2}	continuous across patch boundary 4-2	N-1/2

$$\text{Total number of equations for triangle 145} = \frac{9}{2}N + 2 \tag{2.21}$$

$$\text{Total number of equations for superpatch} = 6\left(\frac{9N}{2} + 2\right) \tag{2.22}$$

Total number of coefficients
$$\text{using eq. (2.10)} = 12\,K_N = 6N(N+3) + 12. \tag{2.23}$$

One can see the problem of using mixtures of $\{\theta_j\}$. Equation (2.15)

and eq. (2.22) are different. This means that in general one will arrive at different values of N for feasible sets with the same conditions.

There are a number of other points which can be brought up:

(i) The greater the number of constraints imposed, the higher the polynomial order of the feasible set. Given the constraint on the number of variables, this means that there is a direct trade-off between the defect of the approximation space and the physical conditions which can be imposed in its definition.

(ii) Unless the physical noninterpolatory condition is imposed on all the patch boundaries, the approximation $\hat{\phi}$ will not satisfy that condition.

As far as a critique of the method goes it becomes evident that the choice of the proper conditions to impose can become quite complicated when one desires more than one function 'centered' on the center of the superpatch. There is always the question of whether the conditions lead to a system of equations which are either improper or redundant. It may not be possible to complete the space without bringing in all the $\{S^{k}{}_{L}\}$, and it is difficult to see when the need does occur. One may also obtain piecewise-linear dependence without realizing it.

We now turn our attention to the more mathematical approach, the generic scheme.

2.3.2 The Generic Scheme

It was seen in the last section that the major disadvantage of the hybrid method is its comparative lack of systematization. There is no algorithmic procedure for a step-by-step examination of the question of

redundant or improper equations. The generic method is much more methodical in nature and gives us precisely that systematization which the hybrid method lacks. It allows us to build up, step by step, a set of conditions which do not lead to redundant or improper equations and is essentially an exercise in Representation.[6] We first concentrate on the basic patch θ_j to find a representation for the approximation space $M_{m_j}^j$. We then use these representations in the joining of the basic element functions across the patch boundaries to find the approximation space M_m for the superelement functions ψ_{kg}. In the process of carrying out these steps one can not only resolve the questions of redundant or improper conditions methodically but can also redefine conditions to eliminate these problems in a systematic manner.

Let us begin by examining the triangular $\widetilde{P}_N(\underline{r})$ form. We have from eq. (2.9) that a function $\xi(\underline{r})$ in this P_N space can be written as

$$\xi(\underline{r}) = \sum_{i=0}^{N} \sum_{j=0}^{N-i} a_{ij} x^i y^j$$

$$= [1][a_{00}][1] + [1 \quad x] \begin{bmatrix} 0 & a_{01} \\ a_{10} & 0 \end{bmatrix} \begin{bmatrix} 1 \\ y \end{bmatrix}$$

$$+ [1 \quad x \quad x^2] \begin{bmatrix} 0 & 0 & a_{02} \\ 0 & a_{11} & 0 \\ a_{20} & 0 & 0 \end{bmatrix} \begin{bmatrix} 1 \\ y \\ y^2 \end{bmatrix} + \dots \qquad (2.24)$$

Equation (2.24) emphasizes the shell nature of the functional form of $\xi(\underline{r})$. Each term in the matrix form represents the shell $\left(\sum_{i=0}^{k} a_{ik-i} x^i y^{k-i} \right)$ quite like the shells present in a Taylor expansion in two independent variables.

Now suppose we can write

$$\xi(\underline{r}) = \sum_{i=1}^{K_N} a_i \zeta_i(x, y) \tag{2.25}$$

where

$$K_N = \text{dimension of } P_N.$$

Then

$$\xi(\underline{r}) = [\zeta_1 \quad \zeta_{K_N}] \begin{bmatrix} a_1 \\ \vdots \\ a_{K_N} \end{bmatrix} = \underline{H}^T(x, y) \cdot \underline{A}. \tag{2.26}$$

Let us introduce an operator J,

$$J = \begin{bmatrix} L_1 \\ \vdots \\ L_{K_N} \end{bmatrix} \tag{2.27}$$

where the L_i are taken from the group of operators used in the set of interpolatory conditions. For illustrative purposes let us choose J such that

$$J\xi(\underline{r}) = \begin{bmatrix} \xi(\underline{r}_o) \\ \vdots \\ \frac{d}{dx} \xi(\underline{r}_a) \\ \vdots \\ \int_{ab} ds \, \hat{n}_{ab} \cdot \nabla \xi(\underline{r}) \end{bmatrix} = J\underline{\xi} \tag{2.28}$$

where we consider θ_j to be a triangle abc and $\hat{n}_{ab}$ = outward normal on ab

We then have from eq. (2.26)

$$
_J\underline{\xi} = [J\zeta_1 \ \cdots \ J\zeta_{K_N}] \begin{bmatrix} a_1 \\ \vdots \\ a_{K_N} \end{bmatrix} \tag{2.29}
$$

If $\quad J\zeta_i(x,y) = \begin{bmatrix} 0 \\ \vdots \\ (1)_i \\ 0 \\ \vdots \\ 0 \end{bmatrix}$, $\quad$ then $\quad \begin{bmatrix} a_1 \\ \vdots \\ a_{K_N} \end{bmatrix} = {}_J\underline{\xi} = {}_J\begin{bmatrix} \xi(0,0) \\ \vdots \\ \cdot \\ \cdot \end{bmatrix}.$

If the above is not true, then suppose that there is a J_1 such that

$$
J_1 \zeta_i(x,y) = \begin{bmatrix} 0 \\ \vdots \\ (1)_i \\ \cdot \\ 0 \end{bmatrix}.
$$

We refer to ζ_i as a standard function of J_1.

Equation (2.29) can be rewritten as

$$
_J\underline{\xi} = Q_{JJ_1} {}_{J_1}\underline{\xi}. \tag{2.30}
$$

It can be shown then that

$$
Q_{JJ_1} = Q_{J_1 J}^{-1} \tag{2.31}
$$

where

$$Q_{JJ_1} = [J\zeta_1 \quad \cdots \quad J\zeta_{K_N}].$$
(2.32)

To aid us in this approach we have two tools at our disposal. The first is that we know of a simple set $\{\zeta_1(x,y), \ldots, \zeta_{K_N}(x,y)\}$. This is the set $B_o \equiv \{1, x, y, \ldots\}$. We do not know the corresponding operator J_o. However, we do know the operators corresponding to the Lagrangian basis sets. These are J_{ℓ_N} where $(J_{\ell_N} \xi(\underline{r}))_i = \xi(\underline{r}_i)$.

Then the question whether a set of interpolation conditions is proper and nonredundant reduces to a question about the corresponding operator J; namely does $(Q_{JJ_o})^{-1}$ exist, which means that

$$\begin{vmatrix} J1 & Jx & \cdots \end{vmatrix} \neq 0.$$
(2.33)

If it is true, then we know that a basis for J is $\{_J\underline{\zeta}_1, \ldots, \, _J\underline{\zeta}_{K_N}\}$, where

$$_J\underline{\zeta}_i = \begin{bmatrix} 0 \\ \cdot \\ (1)_i \\ \cdot \\ 0 \\ 0 \\ 0 \end{bmatrix}.$$
(2.34)

To find the functional form for the $\{\zeta_i\}$ is a matter of transforming to the basis B_o, that is, find $_{J_o}\underline{\zeta}_i$.

$$_{J_o}\underline{\zeta}_i = [Q_{JJ_o}]^{-1} \, _J\underline{\zeta}_i.$$
(2.35)

Then using (2.26) we have

$$\zeta_i(x,y) = [1 \quad x \quad y \quad \cdots] \, _{J_o}\underline{\zeta}_i.$$
(2.36)

Once we have a consistent and nonredundant set of interpolation conditions, we can go on to look at the imposition of noninterpolatory conditions.

To simplify matters, let us consider applying noninterpolatory conditions to the triangle abc only. Suppose we require a function $\xi(\underline{r}) \in P_N$ such that

$$\int_{ab} ds \, \hat{n}_{ab} \cdot \nabla \xi(\underline{r}) = \int_{ac} ds \, \hat{n}_{ac} \cdot \nabla \xi(\underline{r}). \tag{2.37}$$

Let us define two K_N row operators J_A and J_B such that

$$J_A \xi(\underline{r}) = \begin{bmatrix} \xi(r_o) \\ \vdots \\ \int_{ab} ds \, \hat{n}_{ab} \cdot \nabla \xi \end{bmatrix} \tag{2.38}$$

and

$$J_B \xi(\underline{r}) = \begin{bmatrix} \xi(r_o) \\ \vdots \\ \int_{ac} ds \, \hat{n}_{ac} \cdot \nabla \xi \end{bmatrix}. \tag{2.39}$$

That is to say, the only difference between the operators J_A and J_B is that in one row, J_A has $\int_{ab} ds \, \hat{n}_{ab} \cdot \nabla \xi$ while J_B has $\int_{ac} ds \, \hat{n}_{ac} \cdot \nabla \xi$. Equation (2.37) then becomes

$$J_A \xi(\underline{r}) = J_B \xi(\underline{r}) \tag{2.40}$$

which is

$$Q_{J_A J_B J_B} \underline{\xi} = J_B \underline{\xi}, \tag{2.41}$$

an eigenvalue problem with eigenvalue 1. It must be noted that we

must first be certain that J_A and J_B are proper and nonredundant before we examine (2.41).

Now suppose we have a mixture of interpolation conditions and noninterpolatory conditions,

$$
\begin{bmatrix} \xi(\underline{r}_o) \\ \vdots \\ \int_{ab} ds\ n_{ab} \cdot \nabla\xi \end{bmatrix} = \begin{bmatrix} 1 \\ 0 \\ \int_{ac} ds\ n_{ac} \cdot \nabla\xi \end{bmatrix} . \tag{2.42}
$$

Once again we define operatore J_A and J_B given by eqs. (2.38)-(2.39). Then we divide the problem into two parts

$$J_A \xi(\underline{r}) = J_B \xi(\underline{r})$$

$$
J_A \underline{\xi} = \begin{bmatrix} 1 \\ \cdot \\ 0 \\ \cdot \\ K \end{bmatrix} \qquad \text{where} \quad K = \text{some constant.} \tag{2.43}
$$

One can then obtain conditions for a proper and nonredundant set of constraints once again in terms of the elements of $Q_{J_A J_B}$.

It can be seen that the generic scheme rapidly becomes very involved but it does provide a systematic procedure for generating basic element functions Ψ_{ig}^j and superelement functions ψ_{kg}. It is more a tool of analysis than of synthesis but it does point out that a proper choice of J_A and J_B can mean much simplification. A general rule is to try to concentrate the elements of J_A and J_B symmetrically on the corners of the triangle abc. This then simplifies the process of joining across patch boundaries and as a by-product maximizes the number of super-

patches which are of class S^1. After the corners, the sides of the triangle should be used for the elements of these operators. The body of the triangle should be left to the last.

We shall present in the next chapter a number of sets $\{\psi_{kg}\}$ derived by these methods.

Our main concern in this chapter was the discussion of the problems involved in the various steps required to arrive at the form of the Galerkin equations, eq. (1.16), preparatory to the actual inversion process. It can be seen that the central issue is the construction of the approximation space M_m. One has to arrive at a set of conditions which will give rise to a system of proper and nonredundant equations equal in number to the number of coefficients of the required ψ_{kg} and which will lead to M_m with certain desired overall properties such as a specified defect. This is in a sense similar to the task faced by nodal methods where the situation is mitigated by the fact that the conditions are applied to the approximate solution $\hat{\phi}_g(\underline{r})$ instead of to superelement functions. The work presented in this thesis could therefore be of use in constructing nodal schemes.

We have presented two methods of constructing M_m and in the next chapter, Chapter 3, we will introduce a few specific spaces derived by using these techniques.

Chapter 3

SPECIFIC SPACES

We concern ourselves in this chapter with the introduction of a number of approximation spaces M_m derived by the techniques discussed in the preceding pages. These spaces have all been constructed so as not to violate the constraint of three or less than three unknowns per fuel hexagon. They have also been constructed with the object of providing answers to some of the questions raised in Chapter 2 regarding the overall problems involved in the various steps required to arrive at the Galerkin equations, eq. (1.16).

As we are only interested in the S^1 class of superpatches we restrict ourselves to the T^1 subspace of the P_{N_j} space. The specific Θ_J we use are the ones presented in §2.2. Given the constraint of three or less than three variables per fuel hexagon we could divide up our set of spaces into 1-element, 2-element or 3-element sets. As there is one element function associated with each variable we shall use the term, an a-element set, to denote a set which has a variables per fuel hexagon. Rather than divide the spaces we have derived according to this scheme, we shall discuss them under the broad classes of complete or incomplete spaces. The a-element division will be made as a finer subdivision.

Section 2.1 brought up the fact that the constraint of three or less than three unknowns per fuel hexagon led to a choice between high order incomplete spaces and low order complete ones. As noted in that section, whenever we use the term incomplete we use it relative to the

space $\overline{P}_{N_j}$. The space $\overline{P}_{N_j}$ is the space of all polynomials of maximum

order N_j. The term, complete space, is used in reference to $\overline{P}_{N_j}$.

Let us now examine the question of the use of complete vis-a-vis incom-

plete ones for the approximation space M_m.

Intuitively one would feel that certain characteristics could be

missing if incomplete spaces are used. But it is not at all clear what

these characteristics are as it could also be said that low order complete

spaces are missing features of the higher order complete ones. From

a geometrical point of view it would seem that incomplete spaces which

do not contain $\overline{P}_1$ would not converge to the analytic solution as they do

not contain plane surfaces. This, however, is a question of convergence.

We are concerned with accuracy and it is not at all certain how the lack

of this attribute would affect accuracy. It is also not clear if a higher

polynomial order would compensate for the defect of the space. We have

constructed incomplete spaces in section 3.1 with these questions in

mind, and in section 3.2 we present their complementary complete

counterparts.

It should be noted before we begin our presentation that the inclu-

sion of the three-element sets is rather academic from the viewpoint of

computation time, but for completeness of argument we shall include

them in the presentation.

The rationale behind the various choices will be discussed in the

final section, §3.3.

3.1 <u>Incomplete Spaces</u>[18]

Once incompleteness is allowed, our set of permissible spaces becomes much larger. There appears to be no fixed rule in making a choice. We therefore have to resort to our physical intuition. In other words, this is where we use the physical construction approach. We apply the hybrid method to find superelement functions ψ_{kg}.

For our 1-element set, we construct a superelement function on Θ_J which at the center of Θ_J will represent the value of the flux. For our 2-element set, in addition to a flux function, we use another superelement function which represents the normal component of the current integrated around the boundary of Θ_J. We should thus be able to monitor the net inflow of neutrons into a particular volume. To keep the functions of the two elements distinct, we require that the integrated current element should have a value zero at the center of Θ_J. In mathematical terms this is similar to asking for linear independence of the two elements.

Continuing in this vein, we require our 3-element set to have one superelement function for the flux at the center of Θ_J, one for the x-component of the current and one for the y-component of the current at the center of Θ_J. The same condition about keeping the functions of the elements distinct required in the case of the 2-element set will be imposed here.

It can be seen that we have three potential a-element sets which have appealing physical characteristics. The conditions used in the preceding paragraph are, however, not sufficient to define the sets.

Most important of all, one still has to decide on the polynomial order N. We choose to examine two possibilities N = 3 and N = 9. In passing let us say that the choice of the cubic space is motivated in part by the encouraging results[1-3] which have been obtained with it for rectangular geometry. The rest of the argument will be left to a later section.

We have some more conditions left to be imposed and these will be detailed with the mathematical formulation of the respective set.

We now turn to a detailed description of the various spaces. Our discussion will be divided into two parts. The first section (3.1.1) will examine the cubic incomplete spaces, that is, the case where N = 3. The second section (3.1.2) will concern itself with the case N = 9, the case of the $9^{\underline{th}}$-order incomplete space.

3.1.1 Cubic Space

As discussed in the opening section of this chapter there are three possible a-element sets. We have constructed three such sets for the cubic incomplete space and will introduce them in the order of increasing a where $a = 1, \ldots, 3$.

(a) 1-element set

Consider the superpatch Θ_J, hexagon abcdef, of Fig. 3.1 composed of the basic patches $\{\theta_1, \ldots, \theta_6\}$, i.e., triangles 1-6. We impose the following conditions on each of the basic element functions
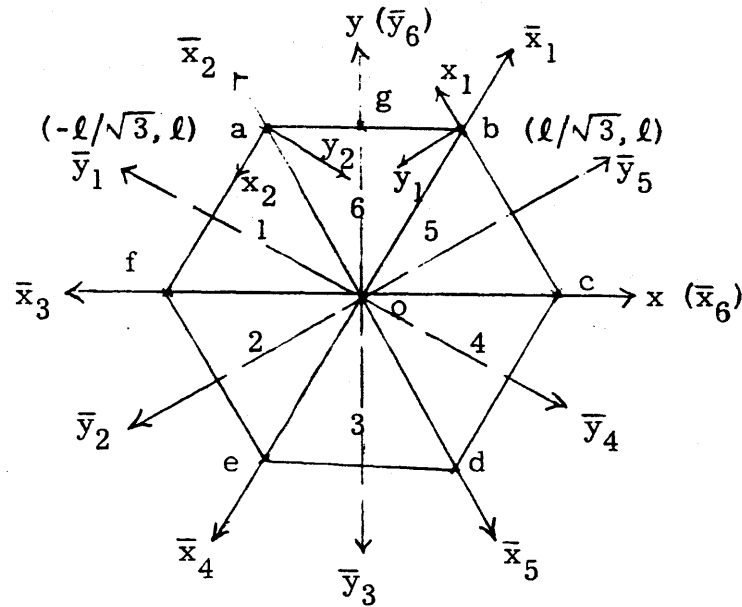
Fig. 3.1. Superpatch — regular mesh.

$\{\Psi_{Jg}^{1f}, \ldots, \Psi_{Jg}^{6f}\}^{*\dagger}$ which define the superelement function $\psi_{kg}^{f}{}^{*\dagger}$,

(i) $\quad \Psi_{Jg}^{jf}(0,0) = 1$

(ii) $\quad \Psi_{Jg}^{jf}(\partial\Theta_J) = 0$

---

*Refer to section 1.2.2, eq. (1.22) for a more detailed statement of the relation between the superelement function ψ_{kg} and the basic element functions Ψ_{ig}^{j}.

†To simplify notation superscript β has been added to the superelement symbol ψ_{Jg} making it ψ_{Jg}^{β}, the $J\underline{th}$ β-type superelement function. The support for this superelement function is the superpatch Θ_J and we shall refer to its 'center' as the $J\underline{th}$ superpatch center. In addition, the basic element function associated with this superelement function over the basic patch θ_j will be denoted by the symbol $\Psi_{Jg}^{j\beta}$, where it is understood j is such that θ_j forms part of the superpatch Θ_J. θ_j is the support of $\Psi_{Jg}^{j\beta}$.

(iii) $\quad \Psi_{Jg}^{jf} = \Psi_{Jg}^{kf} \quad$ at $\quad \theta_j \cap \theta_k$

(iv) $\quad \hat{n}_{jk} \cdot \nabla \Psi_{Jg}^{jf} = \hat{n}_{jk} \cdot \nabla \Psi_{Jg}^{kf} \quad$ at $\quad \theta_j \cap \theta_k \qquad j, k = 1, \ldots, 6,$

where $\hat{n}_{jk}$ normal to $\theta_j \cap \theta_k$ pointing from θ_j to θ_k.

$\quad \partial \Theta_J = $ outer boundary of Θ_J.

In the case of a condition set with $60°$-rotational symmetry, conditions (iii) and (iv) become

(v) $\quad \Psi_{Jg}^{jf} \Big|_{\theta_j \cap \theta_{j-1}} = \Psi_{Jg}^{jf} \Big|_{\theta_j \cap \theta_{j+1}}$

(vi) $\quad \hat{n}_{j-1j} \cdot \nabla \Psi_{Jg}^{jf} \Big|_{\theta_j \cap \theta_{j-1}} = \hat{n}_{jj+1} \cdot \nabla \Psi_{Jg}^{jf} \Big|_{\theta_j \cap \theta_{j+1}}$

where it is understood that $\theta_0 = \theta_6$ and $\theta_7 = \theta_1$. This simplifies matters enormously as we have now decoupled the system of equations for Θ_J into identical subsystems for each θ_j. This means we will only have to concentrate on a single θ_j to solve for Θ_J. Let us concentrate on θ_6, namely the triangle oab. We have that

$$\Psi_{Jg}^{6f}(x, y) = 1 - \frac{9}{4}\left(\frac{y}{\ell}\right)^2 + \frac{5}{4}\left(\frac{y}{\ell}\right)^3 - \frac{9}{4}\left(1 - \frac{y}{\ell}\right)\left(\frac{x}{\ell}\right)^2 \equiv \zeta_1^{1CI}(x, y). \qquad (3.1)$$

In the finite element method it is much more convenient to think in terms of geometrical shapes than in terms of functional notation as the same geometric surface will have different functional notation depending on how θ_j is oriented and translated with respect to the x-y axis. We shall refer to the geometrical shape represented by eq. (3.1) as $\zeta_1^{1CI}(x, y)$. The superscript stands for 1-element cubic incomplete set. We should point out that the corresponding generic approach to obtain

the result represented by eq. (3.1) is presented as a by-product in the discussion of section 3.1.1(c) on the 3-element set.

We then have that the set $\{\Psi_{Jg}^{1f}, \ldots, \Psi_{Jg}^{6f}\}$ which makes up the super-element function ψ_{kg} is $\{\zeta_1^{1CI}(\bar{x}_1, \bar{y}_1), \ldots, \zeta_1^{1CI}(\bar{x}_6, \bar{y}_6)\}$, where the axes $(\bar{x}_6, \bar{y}_6)$ is the set (x, y) and the axes $(\bar{x}_k, \bar{y}_k)$ is the set (x, y) rotated counterclockwise by $k\pi/3$.

(b) 2-element set

We have here two ψ_{Jg}^{β} to define. The conditions common to both are

(i) $\Psi_{Jg}^{j\beta}(\partial\Theta_J) = 0$

(ii) $\Psi_{Jg}^{j\beta} = \Psi_{Jg}^{k\beta}$ at $\theta_j \cap \theta_k$

(iii) $\int ds\, \hat{n}_{jk} \cdot \nabla\Psi_{Jg}^{j\beta} = \int ds\, \hat{n}_{jk} \cdot \nabla\Psi_{Jg}^{k\beta}$ at $\theta_j \cap \theta_k$

(iv) $\hat{n}_{jk} \cdot \nabla\Psi_{Jg}^{j\beta} = \hat{n}_{jk} \cdot \nabla\Psi_{Jg}^{k\beta}$ at a point $\underline{r}_0$ on $\theta_j \cap \theta_k$.

Referring to Fig. 3.1 $\underline{r}_0$ is chosen to be the midpoint of $\theta_j \cap \theta_k$.

The conditions which give the two ψ_{Jg} their distinct physical character are

		ψ_{Jg}^{f} [flux function]	ψ_{Jg}^{c} [integrated current function]
(v)	$\Psi_{Jg}^{j\beta}(0,0)$ =	1	0
(vi)	$\int_{\partial\Theta_J} ds\, \hat{n}_1 \cdot \nabla\Psi_{Jg}^{j\beta} =$	0	6

where

$\hat{n}_1$ = outward pointing normal on outer boundary of Θ_J.

Once again in the case of a set of 60°-rotationally invariant conditions we have that conditions (ii), (iii), and (iv) become

(vii) $\quad \Psi_{Jg}^{j\beta}\Big|_{\theta_j \cap \theta_{j-1}} = \Psi_{Jg}^{j\beta}\Big|_{\theta_j \cap \theta_{j+1}}$

(viii) $\quad \int ds\, \hat{n}_{j-1j} \cdot \nabla\Psi_{Jg}^{j\beta}\Big|_{\theta_j \cap \theta_{j-1}} = \int ds\, \hat{n}_{jj+1} \cdot \nabla\Psi_{Jg}^{j\beta}\Big|_{\theta_j \cap \theta_{j+1}}$

(ix) $\quad \hat{n}_{j-1j} \cdot \nabla\Psi_{Jg}^{j\beta}\Big|_{\substack{\text{midpoint} \\ \theta_j \cap \theta_{j-1}}} = \hat{n}_{jj+1} \cdot \nabla\Psi_{Jg}^{j\beta}\Big|_{\substack{\text{midpoint} \\ \theta_j \cap \theta_{j+1}}}$

We can then again concentrate only on triangle oab, obtaining

$$\Psi_{Jg}^{6f}(x,y) = 1 - \frac{y}{2\ell} - \frac{7}{4}\left(\frac{y}{\ell}\right)^2 + \frac{5}{4}\left(\frac{y}{\ell}\right)^3 - \frac{9}{4}\left(\frac{x}{\ell}\right)^2\left(1 - \frac{y}{\ell}\right) \equiv \zeta_1^{2CI}(x,y)$$

(3.2)

$$\Psi_{Jg}^{6c}(x,y) = -\frac{y\sqrt{3}}{2\ell}\left(1 - \frac{y}{\ell}\right) \equiv \zeta_2^{2CI}(x,y).$$

(3.3)

We refer to the shape represented by eq. (3.2) as $\zeta_1^{2CI}(x,y)$ and that by eq. (3.3) as $\zeta_2^{2CI}(x,y)$. It is interesting to note that $\Psi_{Jg}^{6f}(x,y)$ can be written as

$$\Psi_{Jg}^{6f}(x,y) = \left[1 - \frac{9}{4}\left(\frac{y}{\ell}\right)^2 + \frac{5}{4}\left(\frac{y}{\ell}\right)^3 - \frac{9}{4}\left(1 - \frac{y}{\ell}\right)\left(\frac{x}{\ell}\right)^2\right]$$

$$+ \frac{1}{\sqrt{3}}\left[-\frac{y\sqrt{3}}{2\ell}\left(1 - \frac{y}{\ell}\right)\right]$$

(3.4)

so

$$\zeta_1^{2CI}(x,y) = \zeta_1^{1CI}(x,y) + \frac{1}{\sqrt{3}}\zeta_2^{2CI}(x,y). \tag{3.5}$$

We thus have that the set $\{\Psi_{ig}^{1\beta}, \ldots, \Psi_{ig}^{6\beta}\}$ corresponding to ψ_{Jg}^f is $\{\zeta_1^{2CI}(\bar{x}_1, \bar{y}_1), \ldots, \zeta_1^{2CI}(\bar{x}_6, \bar{y}_6)\}$ and that the one for ψ_{Jg}^c is $\{\zeta_2^{2CI}(\bar{x}_1, \bar{y}_1), \ldots, \zeta_2^{2CI}(\bar{x}_6, \bar{y}_6)\}$.

(c) 3-element set

This set is quite complicated as we lose $60°$-rotational symmetry. It will be easier and will be more informative if we start off by looking for a basis for the complete cubic space $\bar{P}_3$. Consider the triangle oab of Fig. 3.1. Recalling the generic scheme, define

$$J_{3c}\xi(x) = \begin{bmatrix} \xi(o) \\ \partial\xi(o)/\partial x \\ \partial\xi(o)/\partial y \\ \xi(b) \\ \partial\xi(b)/\partial x \\ \partial\xi(b)/\partial y \\ \xi(a) \\ \partial\xi(a)/\partial x \\ \partial\xi(a)/\partial y \\ \partial\xi(g)/\partial y \end{bmatrix}^{*} \tag{3.6}$$

It can be shown that J_{3c} is proper and nonredundant. The operator is also so defined that, allowing for the constraints of continuity at the corners of the triangle, the determination of function shape along the boundaries of the triangle are independent processes. We will therefore

---

*We use the convention that $\xi(a) = \xi(\underline{r}_a)$.

make use of it to find a basis for $\overline{P}_3$. But before we do so let us comment on an interesting point. An operator J'_{3c} defined so that the only difference between J_{3c} and it is the replacement of $\partial \xi(g)/\partial y$ with $\int_{ab} ds\, \hat{n}_1 \cdot \nabla \xi$ would lead to, aside from one normalization factor, the same basis functions. Certain combinations of conditions imply satisfaction of combinations of other conditions. It becomes imperative to use the generic scheme for higher order spaces if errors of redundancy are to be avoided. In any case using the generic scheme we have for $\overline{P}_3$ the basis

$$\Psi^j_{1g}(x,y) = 1 - 3\left(\frac{y}{\ell}\right)^2 + 2\left(\frac{y}{\ell}\right)^3 \equiv \zeta^{3c}_1(x,y) \tag{3.7}$$

$$\Psi^j_{2g}(x,y) = \ell\left(\frac{x}{\ell}\right)\left(1 - \frac{y}{\ell}\right)^2 \equiv \zeta^{3c}_2(x,y) \tag{3.8}$$

$$\Psi^j_{3g}(x,y) = \ell\left(\frac{y}{\ell}\right)\left(1 - \frac{y}{\ell}\right)^2 \equiv \zeta^{3c}_3(x,y) \tag{3.9}$$

$$\Psi^j_{4g}(x,y) = \ell\left(1 - \frac{y}{\ell}\right)\left[3\left(\frac{x}{\ell}\right)^2 - \left(\frac{y}{\ell}\right)^2\right] \equiv \zeta^{3c}_4(x,y) \tag{3.10}$$

and

$$\Psi^j_{kg}(x,y) = \sum_{r=1}^{4} d_{kr}\Psi^j_{rg}(x_1,y_1) \qquad k = 5,\ldots,7$$

$$\tag{3.11}$$

$$\Psi^j_{kg}(x,y) = \sum_{r=1}^{4} d_{kr}\Psi^j_{rg}(x_2,y_2) \qquad k = 8,\ldots,10$$

where the axes (x_1,y_1) and (x_2,y_2) are as shown in Fig. 3.1. With the exception of Ψ^j_{4g}, which $\in T^3$, the set $\{\Psi^j_{ig}\}$ given above $\in T^1$. This is

in marked contrast to the cubic Lagrangian set discussed in section 2.1.
As far as reduction of variables is concerned the cubic Lagrangian set
is less efficient. In passing let us note that Ψ^j_{1g} is identical to the
$u^{o+}(y)^*$ of Kang's 1-D cubic Hermite set.[1] This draws attention to the
possibility of using the three natural axes of hexagonal/triangular geom-
etry to derive element sets. More will be said about this possibility in
the next section.

This basis for $\bar{P}_3$ has four fundamental shapes. These are the ones
given by eqs. (3.7)-(3.10). We shall denote them as $\{\zeta_i^{3c}(x,y)\}$ where
$i = 1,\ldots,4$. To find the three superelement functions, ψ^β_{Jg} of Θ_J we
apply the following set of conditions. The set of common conditions is

(i) $\quad \Psi^{j\beta}_{Jg}(\partial\Theta_J) = 0$

(ii) $\quad \Psi^{j\beta}_{Jg} = \Psi^{k\beta}_{Jg} \qquad$ at $\theta_j \cap \theta_k$

(iii) $\quad \hat{n}_{jk} \cdot \nabla\Psi^{j\beta}_{Jy} = \hat{n}_{jk} \cdot \nabla\Psi^{k\beta}_{Jg} \qquad$ at $\theta_j \cap \theta_k$

The conditions which give the distinct physical character are

		ψ^f_{Jg} [flux function]	ψ^x_{Jg} [x-current]	ψ^y_{Jg} [y-current]
(iv)	$\Psi^{j\beta}_{Jg}(0,0) =$	1	0	0
(v)	$\dfrac{\partial}{\partial x}\,\Psi^{j\beta}_{Jg}(0,0) =$	0	1	0
(vi)	$\dfrac{\partial}{\partial y}\,\Psi^{j\beta}_{Jg}(0,0) =$	0	0	1

---

*See eq. (3.16).

As this set of conditions is not 60°-rotationally symmetrical, we can not in this case just concentrate on triangle oab of Fig. 3.1, but have to solve for the hexagon abcdef as a whole. The ψ^{β}_{Jy} are linear combinations of the $\{\zeta^{3c}_i(x, y)\}$; a different combination for each θ_j.

$$\psi^{\beta}_{Jg}(\underline{r}) = \sum_{k=1}^{4} a^j_{k\beta}\zeta^{3c}_k(x, y) \qquad \underline{r} \in \theta_j. \qquad (3.12)$$

We present the following tableau for the $\{a^j_{k\beta}\}$:

ψ^f_{Jg}

	θ_1	θ_2	θ_3	θ_4	θ_5	θ_6
a^j_{1f}	1	1	1	1	1	1
a^j_{2f}	0	0	0	0	0	0
a^j_{3f}	0	0	0	0	0	0
a^j_{4f}	$-3/4\ell$	$-3/4\ell$	$-3/4\ell$	$-3/4\ell$	$-3/4\ell$	$-3/4\ell$

(3.13)

ψ^x_{Jg}

	θ_1	θ_2	θ_3	θ_4	θ_5	θ_6
a^j_{1x}	0	0	0	0	0	0
a^j_{2x}	$\sqrt{3}/2$	$\sqrt{3}/2$	0	$-\sqrt{3}/2$	$-\sqrt{3}/2$	0
a^j_{3x}	1/2	-1/2	-1	-1/2	1/2	1
a^j_{4x}	0	0	1/2	0	0	-1/2

(3.14)

$$\psi^y_{Jg}$$

	θ_1	θ_2	θ_3	θ_4	θ_5	θ_6
a^j_{1y}	0	0	0	0	0	0
a^j_{2y}	1/2	-1/2	-1	-1/2	1/2	1
a^j_{3y}	$-\sqrt{3}/2$	$-\sqrt{3}/2$	0	$\sqrt{3}/2$	$\sqrt{3}/2$	0
a^j_{4y}	0	$\sqrt{3}/3$	$-\sqrt{3}/6$	0	$-\sqrt{3}/3$	$\sqrt{3}/6$

$$(3.15)$$

It should be noted that the tableaux of eqs. (3.13)-(3.15) are non-unique; specifically $a^j_{4\beta}$ can take on different values. This nonunique-ness is due to the fact that in the space P_3 our set of physical conditions does not lead to sufficient equations to completely define our polyno-mials* and as such is a good example of a case where one should be cautious in applying the physical construction approach. For ψ^f_{Jg} we have chosen a^j_{4f} so that this superelement function is identical to the superelement function of the 1-element cubic incomplete set.

We now address ourselves to the $9^{\underline{th}}$-order incomplete space.

3.1.2 Ninth-Order Space

This is an incomplete polynomial space P_N with N = 9. We concern ourselves here only with the 3-element set possibility.

(a) 3-element set

Consider the superpatch, hexagon abcdef, of Fig. 3.2. In hexago-

---

*Refer to Appendix D.
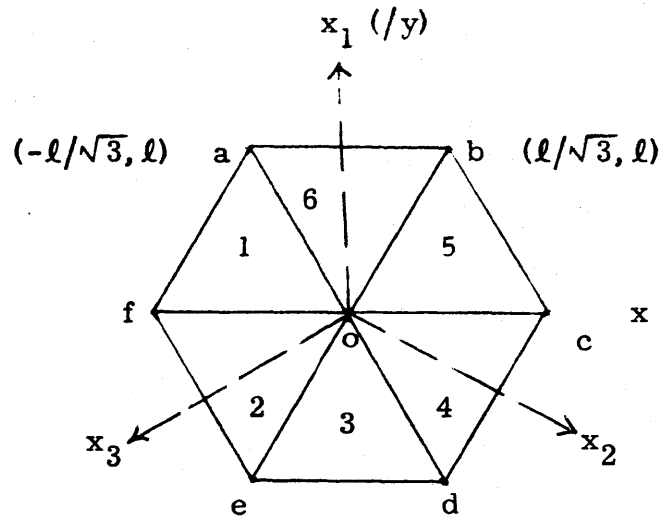
Fig. 3.2. Superpatch — regular mesh. Axes for ninth order incomplete set.

nal/triangular geometry the natural set of axes is a three-axes set.

An example of such a set is the (x_1, x_2, x_3) set shown in Fig. 3.2.

Consider the cubic Hermite set of Kang's[1] in 1-D. These are

$$
u_o(x) = \begin{bmatrix} 3\left(1 + \frac{x}{\ell}\right)^2 - 2\left(1 + \frac{x}{\ell}\right)^3 & -\ell \leq x \leq 0 \\[3mm] 3\left(1 - \frac{x}{\ell}\right)^2 - 2\left(1 - \frac{x}{\ell}\right)^3 & 0 \leq x \leq \ell \\[3mm] 0 & \text{otherwise} \end{bmatrix}
\tag{3.16}
$$

$$
u_1(x) = \begin{bmatrix} \left[-\left(1 + \frac{x}{\ell}\right)^2 + \left(1 + \frac{x}{\ell}\right)^3\right]\ell & -\ell \leq x \leq 0 \\[3mm] \left[\left(1 - \frac{x}{\ell}\right)^2 - \left(1 - \frac{x}{\ell}\right)^3\right]\ell & 0 \leq x \leq \ell \\[3mm] 0 & \text{otherwise} \end{bmatrix}
\tag{3.17}
$$

Using these we can form the following set.

$$\psi_{Jg}^{f} = u_o(x_1)\, u_o(x_2)\, u_o(x_3) \tag{3.18}$$

$$\psi_{Jg}^{y} = u_1(x_1)\, u_o(x_2)\, u_o(x_3) \tag{3.19}$$

$$\psi_{Jg}^{x} = \frac{1}{\sqrt{3}}[u_o(x_1)\, u_1(x_2)\, u_0(x_3) - u_o(x_2)\, u_o(x_1)\, u_1(x_3)] \tag{3.20}$$

It can be shown that this set of ninth-order piecewise polynomials satisfy the following conditions. Conditions common to all three super-element functions are

(i) $\quad \Psi_{Jg}^{j\beta}(\partial\Theta_J) = 0$

(ii) $\quad \hat{n}_1 \cdot \nabla\Psi_{Jg}^{j\beta}(\partial\Theta_J) = 0$

(iii) $\quad \Psi_{Jg}^{j\beta} = \Psi_{Jg}^{k\beta} \qquad$ at $\theta_j \cap \theta_k$

(iv) $\quad \hat{n}_{jk} \cdot \nabla\Psi_{Jg}^{j\beta} = \hat{n}_{jk} \cdot \nabla\Psi_{Jg}^{k\beta} \qquad$ at $\theta_j \cap \theta_k$.

The conditions for the distinct physical character are

		ψ_{Jg}^{f} [flux function]	ψ_{Jg}^{x} [x-current]	ψ_{Jg}^{y} [y-current]
(v)	$\Psi_{Jg}^{j\beta}(0,0) \quad =$	1	0	0
(vi)	$\frac{\partial}{\partial x}\, \Psi_{Jg}^{j\beta}(0,0) =$	0	1	0
(vii)	$\frac{\partial}{\partial y}\, \Psi_{Jg}^{j\beta}(0,0) =$	0	0	1

Condition (ii) is one which was not satisfied by any of the previous

sets. This condition in conjunction with condition (iv) ensures that the approximation, $\hat{\phi}_g$ will have derivative continuity. All the previous sets lead to $\hat{\phi}_g$ with discontinuities in the gradient.

This ninth-order set can in no sense be regarded as having been derived from a set of conditions. There are not enough equations to define it in the set of conditions (i)-(vii). The set was constructed by appealing to the analogy in rectangular geometry and as such illustrates the fact that as we move up to higher order spaces our limited set of physical conditions is insufficient to define our element functions.

We now turn our attention to the complete spaces.

3.2 Complete Spaces[9]

Before we present our various complete sets $\{\Psi_{ig}^j \; \forall \; i\}$, let us dwell on a few features of our approach.

Given that the complete polynomial space $\overline{P}_{N_j}$ is to be used for $M_{m_j}^j$, we still have to decide on the spanning set $\{\Psi_{ig}^j \; \forall \; i\}$. By restricting ourselves to S^1 we have restricted $\{\Psi_{ig}^j \; \forall \; i\}$ to T^1 but even then we still have a latitude of choice. We chose an approach which we shall term the shell idea. The C_1 shell set is the set $\{\Psi_{ig}^j \; \forall \; i\}$ which forms a basis for the space $\overline{P}_1$. The $(C_1 + C_2)$ shell set is the set $\{\Psi_{ig}^j \; \forall \; i\}$ which is a basis for the space $\overline{P}_2$. In general, then, the $(C_1 + C_2 \ldots + C_k)$ shell set is a basis for $\overline{P}_k$. This means that the C_k shell set spans the space $\overline{P}_k \cap \overline{P}_{k-1}^{\,\prime}$.[*] This approach therefore raises the possibility of

---

[*] The $\prime$ symbol indicates the complement.

varying the accuracy attainable by systematically adding or deleting un-knowns. It also offers us the possibility of using a low-order space fine-mesh scheme simultaneously with a high-order space coarse-mesh scheme.   It is made all the more attractive by the fact that we are re-stricted to superpatches Θ_J of the class S^1. From the programming point of view all that is needed is to vary the number of unknowns 'centered' on the centers of the superpatches.

We conclude this discussion by pointing out a difference in attitudes between the construction of the complete shell sets and the construction of the incomplete sets of section 3.2.

Physical intuition played a major part in the construction of the in-complete sets.   We went so far as to associate a 'physical' role with each superelement function.   In the case of the complete shell sets such 'physical' interpretations can be attributed through the interpolation conditions used in defining the $\{\Psi_{ig}^j \ \forall \ i\}$. We choose, however, to think more in terms of geometrical shapes than in terms of physical charac-teristics.   When we join across patch boundaries to form the superele-ment function ψ_{Jg} using the constraint of function continuity, we attempt to use the same basic element function Ψ_{ig}^j in each of the basic patches of Θ_J.   This implies that the basic element function Ψ_{ig}^j should have identical shapes on the sides of θ_j for which it is nonzero; a property which we shall refer to as line median symmetry.[*] In other words, the

---

[*]We shall refer to median symmetry as symmetry of Ψ_{ig}^j about the median bisecting that particular side of θ_j on which Ψ_{ig}^j is identically zero.

θ_j and their corresponding $\{\Psi_{ig}^j \; \forall \; i\}$ are related by linear coordinate transformations. Completeness and linear independence are properties preserved under linear transformations. Function continuity across the patch boundaries is guaranteed if the $\{\Psi_{ig}^j \; \forall \; i\}$ has line median symmetry, a property which is by no means always obtainable. If we were to associate physical attributes, then we would in general have to use different basic element functions Ψ_{ig}^j in the contiguous θ_j of a Θ_J before we would be able to form the ψ_{Jg}. The 3-element incomplete cubic set of section 3.1.1 is an example of such a construction.

Succinctly expressed, we attempt to transform shapes and not interpolation conditions in the construction of $\{\psi_{kg} \; \forall \; k\}$ for our complete shell spaces.

We now turn our attention to describing the complete spaces. The section is divided into 2-D and 1-D spaces. Section 3.2.1 discusses 2-D sets. We gradually build up shell sets starting with C_1 and concluding with $(C_1 + C_2 + C_3)$ and in the process of doing so emphasize various features of the approach. Section 3.2.2 presents a 1-D 'analogue' of the 2-D $(C_1 + C_2)$ shell set. It will enable us to examine in 1-D some of the questions which arise in the construction of the 2-D spaces.

3.2.1 2-D Spaces

Equation (2.24) pointed out the shell nature of the triangular form of $\widetilde{P}_{N_j}(\underline{r})$. One systematic procedure of adding functions to the set $\{\Psi_{ig}^j \; \forall \; i\}$ is to think of the process as the building up of shells. The

C_1 shell is the basis for $\overline{P}_1$ and the sum $C_1 + C_2 \ldots + C_k$ is the basis for $\overline{P}_k$. As one increases the number of variables/fuel hexagon permissible, one can build up to higher and higher order shells. The sum $\sum_{i=1}^{k} C_i$ has an analogue in the Taylor series expansion in two independent variables, and it is conjectured that it is possible to show that the order of the truncation error will be the order of the truncation error of the highest complete shell. If this is so, then there is the possibility of having mixed orders of accuracy without having to alter mesh size by just adding functions to or subtracting functions from $\{\psi_{kg}\}$.

Consider the triangle oab of Fig. 3.1. Let us define an operator J_{1s} such that

$$J_{1s}\xi(x) = \begin{bmatrix} \xi(o) \\ \xi(a) \\ \xi(b) \end{bmatrix} \tag{3.21}$$

The standard functions for this operator is the set

$$\Psi_{og}^{jc1}(x,y) = \zeta_1^{c1}(x,y) \equiv \left(1 - \frac{y}{\ell}\right) \tag{3.22}$$

$$\Psi_{bg}^{jc1}(x,y) = \zeta_1^{c1}(x_1, y_1)$$

$$\Psi_{ag}^{jc1}(x,y) = \zeta_1^{c1}(x_2, y_2) \tag{3.23}$$

This set is the shell C_1 and it is a basis for the space $\overline{P}_1$. As it also belongs to T^1, we only require S^1 superpatches. The corresponding superelement function ψ_{Jg}^{c1}, for the superpatch Θ_J, hexagon abcdef of Fig. 3.1 is composed of the basic element function set $\{\zeta_1^{c1}(\overline{x}_1, \overline{y}_1), \ldots, \zeta_1^{c1}(\overline{x}_6, \overline{y}_6)\}$ where $\zeta_1^{c1}(x,y)$ is the fundamental geometrical shape for

J_{1s}, namely the one represented by eq. (3.22).

We can now add elements to J_{1s} to obtain J_{2s},

$$J_{2s}\xi = \begin{bmatrix} \xi(o) \\ \xi(a) \\ \xi(b) \\ \int_{oa} ds\ \hat{n}_{oa} \cdot \nabla\xi \\ \int_{ob} ds\ \hat{n}_{ob} \cdot \nabla\xi \\ \int_{ab} ds\ \hat{n}_{ab} \cdot \nabla\xi \end{bmatrix} \tag{3.24}$$

where $\hat{n}_{\alpha\beta}$ is the normal to side $\alpha\beta$ of the triangle oab shown in Fig. 3.1 pointing away from the interior of the triangle.

Three standard vectors of J_{2s} are

$$J_{2s}\begin{bmatrix} 0 \\ 0 \\ 0 \\ 1 \\ 0 \\ 0 \end{bmatrix},\quad J_{2s}\begin{bmatrix} 0 \\ 0 \\ 0 \\ 0 \\ 1 \\ 0 \end{bmatrix}\quad \text{and}\quad J_{2s}\begin{bmatrix} 0 \\ 0 \\ 0 \\ 0 \\ 0 \\ 1 \end{bmatrix}.$$

They form the shell C_2 and in functional form are identical to the current superelement function, eq. (3.3), of the 2-element incomplete cubic set. We have

$$\Psi_{og}^{jc2}(x,y) = \zeta_1^{c2}(x,y) \equiv -\frac{y\sqrt{3}}{2\ell}\left(1 - \frac{y}{\ell}\right) \tag{3.25}$$

$$\Psi^{jc2}_{bg}(x, y) = \zeta^{c2}_1(x_1, y_1)$$

$$\Psi^{jc2}_{ag}(x, y) = \zeta^{c2}_1(x_2, y_2). \tag{3.26}$$

(C_1+C_2), the set $\{\Psi^j_{1g}, \ldots, \Psi^j_{6g}\}$ given by eqs. (3.22)-(3.23) and eqs. (3.25)-(3.26), forms a basis for the space $\overline{P}_2$. As $C_2 \in T^1$, S^1 will suffice. It is of interest to note that there is a difference between this basis and the Lagrangian quadratics which are determined with the operator J_{2L}.

$$J_{2L}\xi = \begin{bmatrix} \xi(o) \\ \xi(a) \\ \xi(b) \\ \xi(g) \\ \xi(h) \\ \xi(i) \end{bmatrix} \tag{3.27}$$

where

g = point on oa

h = point on ob

i = point on ab.

As shown in Fig. 3.3* this leads to S^1 and S^2 superpatches. The Lagrangian quadratics are less efficient than our (C_1+C_2) set. We shall also refer to this set as the perturbation quadratic set as one can think of it in terms of the quadratic perturbation C_2 being added to the linear

---

*Refer to section 2.1 which presents a detailed discussion of the Lagrangian cubics and the classification of superpatches.

Lagrangian quadratic functions ξ of class T^1
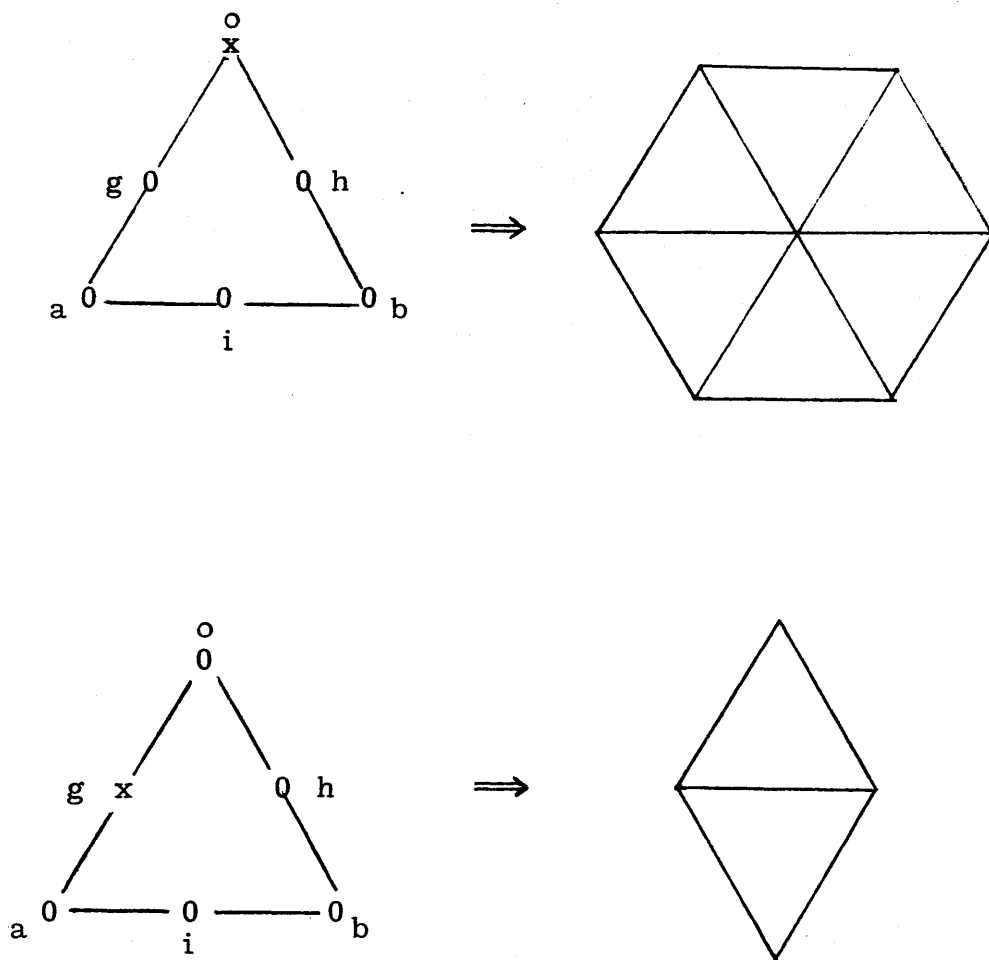
Legend

$0 \equiv \xi = 0$ at this point

$x \equiv \xi = 1$ at this point

$\Longrightarrow$ corresponding superpatch

Fig. 3.3. Superpatches for Lagrangian quadratic set.[†]

[†]Refer to presentation in section 2.1 on Lagrangian cubics for a more detailed discussion.

set C_1. The corresponding superelement set has two functions ψ_{Jg}^{β} with support Θ_J. These are ψ_{Jg}^{c1} which is exactly the superelement function for the C_1 shell set and ψ_{Jg}^{c2}. The corresponding basic element set $\{\Psi_{ig}^1, \ldots, \Psi_{ig}^6\}$ for ψ_{Jg}^{c2} is the set $\{\zeta_1^{c2}(\bar{x}_1, \bar{y}_1), \ldots, \zeta_1^{c2}(\bar{x}_6, \bar{y}_6)\}$ where the axes $(\bar{x}_k, \bar{y}_k)$ are as shown in Fig. 3.1.

The remaining three standard vectors of J_{2s} are the ones

$$
J_{2s}\begin{bmatrix} 1 \\ 0 \\ 0 \\ 0 \\ 0 \\ 0 \end{bmatrix}, \quad
J_{2s}\begin{bmatrix} 0 \\ 1 \\ 0 \\ 0 \\ 0 \\ 0 \end{bmatrix} \quad \text{and} \quad
J_{2s}\begin{bmatrix} 0 \\ 0 \\ 1 \\ 0 \\ 0 \\ 0 \end{bmatrix}.
$$

It should be noted that these are not the J_{2s} vector form of the three linear functions, eqs. (3.22)-(3.23) of C_1. These are

$$
J_{2s}\begin{bmatrix} 1 \\ 0 \\ 0 \\ x \\ x \\ x \end{bmatrix}, \quad
J_{2s}\begin{bmatrix} 0 \\ 1 \\ 0 \\ x \\ x \\ x \end{bmatrix} \quad \text{and} \quad
J_{2s}\begin{bmatrix} 0 \\ 0 \\ 1 \\ x \\ x \\ x \end{bmatrix}
$$

where x represents a nonzero value.

To conclude this section on the space $\bar{P}_2$ we present a set of functions which does not span the space $\bar{P}_1$ but which with the set C_2 spans the space $\bar{P}_2$.

$$
\Psi_{og}^{jRQ}(x,y) \equiv \zeta_1^{RQ}(x,y) = \left(1 - \frac{y}{\ell}\right)^2 \tag{3.28}
$$

$$\Psi_{bg}^{jRQ}(x,y) \equiv \zeta_1^{RQ}(x_1,y_1)$$

$$\Psi_{ag}^{jRQ}(x,y) \equiv \zeta_1^{RQ}(x_2,y_2) \tag{3.29}$$

This set belongs to T^1, so once again only S^1 need be used. It shall be referred to as the regular quadratic set. As with the $(C_1 + C_2)$ set is also has two superelement functions ψ_{Jg}^{β} with support Θ_J. These are ψ_{Jg}^{c2} and ψ_{Jg}^{RQ} where the basic element set for ψ_{Jg}^{RQ} is $\{\zeta_1^{RQ}(\bar{x}_1,\bar{y}_1), \ldots, \zeta_1^{RQ}(\bar{x}_6,\bar{y}_6)\}$. We shall now turn our attention to the space $\bar{P}_3$.

A J_{3s} operator could be constructed by adding elements to J_{2s},

$$J_{3s}\xi = \begin{bmatrix} \xi(o) \\ \xi(a) \\ \xi(b) \\ \int_{oa} ds\, \hat{n}_{oa} \cdot \nabla\xi \\ \int_{ob} ds\, \hat{n}_{ob} \cdot \nabla\xi \\ \int_{ab} ds\, \hat{n}_{ab} \cdot \nabla\xi \\ \hat{m}_1 \cdot \nabla\xi(o) \\ \hat{m}_2 \cdot \nabla\xi(b) \\ \hat{m}_3 \cdot \nabla\xi(a) \\ L\xi(\underline{r}) \end{bmatrix} \tag{3.30}$$

where the unit vectors are as depicted in Fig. 3.4 and the operator L is left undefined. The elements are added in two subshells, one of a group of three and the other of a group of one. The group of three are
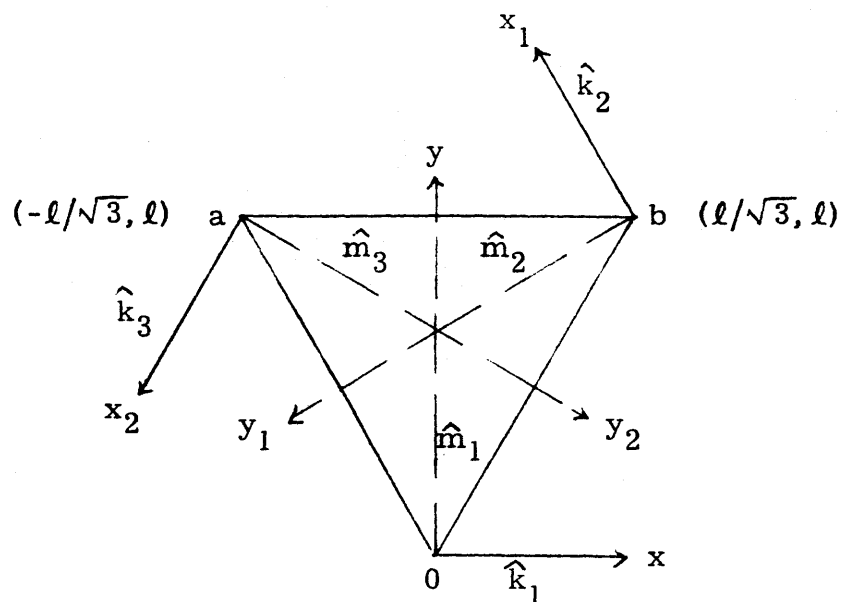
Fig. 3.4. Basic patch for J_{3s} operator of eq. (3.30).

conditions centered on the corners of triangle oab. The group of one is the remaining condition. The C_3^1 subshell is formed by

$$\begin{bmatrix} 0 \\ 0 \\ 0 \\ 0 \\ 0 \\ 0 \\ 1 \\ 0 \\ 0 \\ x \end{bmatrix}, \begin{bmatrix} 0 \\ 0 \\ 0 \\ 0 \\ 0 \\ 0 \\ 0 \\ 1 \\ 0 \\ x \end{bmatrix} \text{ and } \begin{bmatrix} 0 \\ 0 \\ 0 \\ 0 \\ 0 \\ 0 \\ 0 \\ 0 \\ 1 \\ x \end{bmatrix} \text{ while the } C_3^2 \text{ subshell consists of } \begin{bmatrix} 0 \\ 0 \\ 0 \\ 0 \\ 0 \\ 0 \\ 0 \\ 0 \\ 0 \\ 1 \end{bmatrix}.$$

For $C_3^1 \in T^1$ we have that C_3^1 is composed of the set,

$$\Psi_{og}^{jc3}(x, y) = \zeta_3^{3c}(x, y) = \ell\left(\frac{y}{\ell}\right)\left(1 - \frac{y}{\ell}\right)^2$$

$$\Psi_{bg}^{jc3}(x, y) = \zeta_3^{3c}(x_1, y_1)$$

$$\Psi_{ag}^{jc3}(x, y) = \zeta_3^{3c}(x_2, y_2). \qquad (3.31)$$

It should be noted that the shape represented by $\zeta_3^{3c}(x, y)$ is that of eq. (3.9). The remaining subshell C_3^2 consists of

$$\Psi_{10g}^{j}(x, y) = A[\zeta_2^{3c}(x, y) + \zeta_2^{3c}(x_1, y_1) + \zeta_2^{3c}(x_1, y_2) - (\alpha + \beta) \zeta_4^{3c}(x, y)]$$

$$(3.32)$$

where

A = a normalization factor

$$\zeta_2^{3c}(x, y) = \ell\left(\frac{x}{\ell}\right)\left(1 - \frac{y}{\ell}\right)^2$$

$$\zeta_4^{3c}(x, y) = \ell\left(1 - \frac{y}{\ell}\right)\left[3\left(\frac{x}{\ell}\right)^2 - \left(\frac{y}{\ell}\right)^2\right]$$

$$\alpha = \int_{ob} ds\, \hat{n}_{ob} \cdot \nabla \zeta_2^{3c}(x, y)$$

$$\beta = \int_{oa} ds\, \hat{n}_{oa} \cdot \nabla \zeta_2^{3c}(x, y)$$

$\hat{n}_{\gamma\theta}$ = outward normal of corresponding side.

The shapes represented by $\zeta_2^{3c}(x, y)$ and $\zeta_4^{3c}(x, y)$ are those of eqs. (3.8) and (3.10).

The subshell $C_3^1 \in T^1$ but the subshell $C_3^2 \in T^o$. This leads to difficulties as S^1 no longer suffices and S^o will also have to be used.

It would appear from Fig. 3.4 that the 'natural' set of axes to use in defining the operators J for the construction of these shells would

be the set (x, y), (x_1, y_1) and (x_2, y_2). We conclude this section with shell sets constructed by concentrating the interpolatory conditions on the corners of triangle oab of Fig. 3.4 and using this 'natural' set of axes. The corresponding operators J_{2s} and J_{3s} are

$$J_{2s}\xi = \begin{bmatrix} \xi(o) \\ \xi(a) \\ \xi(b) \\ \hat{m}_1 \cdot \nabla\xi(o) \\ \hat{m}_2 \cdot \nabla\xi(b) \\ \hat{m}_3 \cdot \nabla\xi(a) \end{bmatrix} \tag{3.33}$$

$$J_{3s}\xi = \begin{bmatrix} \xi(o) \\ \xi(a) \\ \xi(b) \\ \hat{m}_1 \cdot \nabla\xi(o) \\ \hat{m}_2 \cdot \nabla\xi(b) \\ \hat{m}_3 \cdot \nabla\xi(a) \\ \hat{k}_1 \cdot \nabla\xi(o) \\ \hat{k}_2 \cdot \nabla\xi(b) \\ \hat{k}_3 \cdot \nabla\xi(a) \\ L\xi(\underline{r}) \end{bmatrix} \tag{3.34}$$

C_2 now becomes

$$\Psi_{4g}^{j}(x,y) = -\sqrt{3}\ell\ \zeta_2^{2CI}(x,y) + \frac{\ell}{\sqrt{3}}\ \zeta_2^{2CI}(x_1,y_1) + \frac{\ell}{\sqrt{3}}\ \zeta_2^{2CI}(x_2,y_2)$$

$$= y + \frac{1}{4}\left(3x^2 - 5y^2\right)$$

$$\Psi_{5g}^{j}(x,y) = \frac{\ell}{\sqrt{3}}\ \zeta_2^{2CI}(x,y) - \sqrt{3}\ell\ \zeta_2^{2CI}(x_1,y_1) + \frac{\ell}{\sqrt{3}}\ \zeta_2^{2CI}(x_2,y_2)$$

$$= y_1 + \frac{1}{4\ell}\left(3x_1^2 - 5y_1^2\right)$$

$$\Psi_{6g}^{j}(x,y) = \frac{\ell}{\sqrt{3}}\ \zeta_2^{2CI}(x,y) + \frac{\ell}{\sqrt{3}}\ \zeta_2^{2CI}(x_1,y_1) - \sqrt{3}\ell\ \zeta_2^{2CI}(x_2,y_2)$$

$$= y_2 + \frac{1}{4\ell}\left(3x_2^2 - 5y_2^2\right) \tag{3.35}$$

where

$$\zeta_2^{2CI}(x,y) = -\frac{y\sqrt{3}}{\ell}\left(1 - \frac{y}{\ell}\right).$$

This is the current function of eq. (3.3). For $C_3^1 \in T^1$, we have that C_3^1 is composed of

$$\Psi_{og}^{jc3}(x,y) = \zeta_2^{3c}(x,y) = \ell\left(\frac{x}{\ell}\right)\left(1 - \frac{y}{\ell}\right)^2$$

$$\Psi_{bg}^{jc3}(x,y) = \zeta_2^{3c}(x_1,y_1)$$

$$\Psi_{ag}^{jc3}(x,y) = \zeta_2^{3c}(x_2,y_2) \tag{3.34}$$

and C_3^2 is

$$\Psi_{10g}^{j}(x,y) = A\ell\left(1 - \frac{y}{\ell}\right)\left[3\left(\frac{x}{\ell}\right)^2 - \left(\frac{y}{\ell}\right)^2\right] \tag{3.37}$$

where A = a normalizing factor.

These are the functions of eqs. (3.8) and (3.10). It can be seen from eq. (3.36) that we have lost the property of line median symmetry. C_3^2 is now $\in T^3$ but C_2 has become $\in T^O$. C_3^1 remains $\in T^1$. We have not managed to avoid the use of S^O and have in addition introduced the use of S^3. The operators of eqs. (3.24) and (3.30) are therefore to be preferred to the operators of eqs. (3.33)-(3.34).

3.2.2 1-D Spaces

We present in this section a set of two quadratic functions constructed by the use of the hybrid method. This set shall be referred to as the 1-D hybrid quadratics.

Consider the 1-D 'superpatch' abcde, Θ_J, of Fig. 3.5. It consists
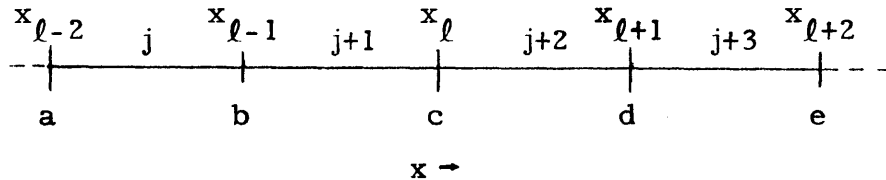
Fig. 3.5. 'Superpatch' for 1-D hybrid quadratics.

of the four 'basic patches' ab, bc, cd and de; $\theta_j, \ldots, \theta_{j+3}$. We define the two functions by imposing the following conditions. Conditions common to both functions are

$$\Psi_{ig}^{j\beta}(a) = \frac{\partial}{\partial x} \Psi_{ig}^{j\beta}(a) = 0$$

$$\Psi_{ig}^{j+3\beta}(e) = \frac{\partial}{\partial x} \Psi_{ig}^{j+3\beta}(e) = 0$$

$$\Psi_{ig}^{j\beta}(b) = \Psi_{ig}^{j+1\beta}(b)$$

$$D^j \frac{\partial}{\partial x} \Psi_{ig}^{j\beta}(b) = D^{j+1} \frac{\partial}{\partial x} \Psi_{ig}^{j+1\beta}(b)$$

$$\Psi_{ig}^{j+2\beta}(d) = \Psi_{ig}^{j+3\beta}(d)$$

$$D^{j+2} \frac{\partial}{\partial x} \Psi_{ig}^{j+2\beta}(d) = D^{j+3} \frac{\partial}{\partial x} \Psi_{ig}^{j+3\beta}(d). \tag{3.38}$$

The conditions which give the functions their unique physical character are

$$\psi_{ig}^f \text{ [flux function]} \qquad \psi_{ig}^c \text{ [current function]}$$

$$\Psi_{ig}^{k\beta}(c) \quad = \qquad 1 \qquad\qquad\qquad 0$$

$$\frac{\partial}{\partial x} \Psi_{ig}^{k\beta}(c) = \qquad 0 \qquad\qquad\qquad 1$$

$$k = j+1, j+2.$$

$$\tag{3.39}$$

These lead to the functions

$$\Psi_{ig}^{j+3f}(x) = \frac{1}{h^2(1+a)} (x-x_{\ell+2})^2 = \zeta_1^f(x)$$

$$\Psi_{ig}^{j+2f}(x) = -\frac{a}{(a+1)h^2} (x-x_\ell)^2 + 1 = \zeta_2^f(x)$$

$$\Psi_{ig}^{j+1}(x) = -\frac{a}{(a+1)h^2} (x-x_\ell)^2 + 1 = \zeta_2^f(x)$$

$$\Psi_{ig}^{jf}(x) = \frac{a}{h^2(1+a)} (x-x_{\ell-2})^2 = \zeta_1^f(x-x_{\ell-2}+x_{\ell+2}) = \zeta_1^f(x+4h) \tag{3.40}$$

for ψ^f_{ig} and

$$\Psi^{j+3c}_{ig}(x) = \frac{1}{2h(1+a)}(x-x_{\ell+2})^2 = \zeta^c_1(x)$$

$$\Psi^{j+2c}_{ig}(x) = -\frac{(2a+1)}{2h(1+a)}(x-x_\ell)^2 + (x-x_\ell) = \zeta^c_2(x)$$

$$\Psi^{j+1c}_{ig}(x) = \frac{(2a+1)}{2h(1+a)}(x-x_\ell)^2 + (x-x_\ell) = \zeta^c_3(x)$$

$$\Psi^{jc}_{ig}(x) = -\frac{1}{2h(1+a)}(x-x_{\ell-2})^2 = -\zeta^c_1(x-x_{\ell-2}+x_{\ell+2}) = -\zeta^c_1(x+4h) \qquad (3.41)$$

for ψ^c_{ig}, where

$$a = \frac{D^{j+3}}{D^{j+2}} = \frac{D^j}{D^{j+1}}$$

$$h = x_{\ell+2} - x_{\ell+1} = x_{\ell+1} - x_\ell = x_\ell - x_{\ell-1} = x_{\ell-2} - x_{\ell-1}.$$

This set is an instructive one and we shall use it here to illustrate one of the questions which arise when one uses the physical construction approach.

The basic ambiguity or flexibility is that there is a choice of where to 'center' ψ^β_{i+g}. We cannot center it at x_ℓ as that leads to linear dependence and we cannot center it at $x_{\ell+4}$ as that will lead to the unphysical condition of forcing the approximation $\hat{\phi}_g$ to be 0 at point e. Even with the elimination of these possibilities we are still left with a number of choices.

Suppose that we center it at $x_{\ell+3}$. This means that the spanning set for $M^{j+4}_{m_{j+4}}$ is $\{\zeta^f_2(x-3h), \zeta^c_2(x-3h)\}$. The spanning set for $M^{j+3}_{m_{j+3}}$ is

$\{\zeta_1^f(x), \zeta_1^c(x), \zeta_1^f(x+h), \zeta_1^c(x+h)\}$. $M_{m_{j+4}}^{j+4}$ and $M_{m_{j+3}}^{j+3}$ are different spaces. This is the difficulty which was alluded to in section 2.1(c) in the discussion on polynomial spaces.

If we center ψ_{i+1g} on $x_{\ell+2}$ we have that the M_N^j are identical. The spanning set for $M_{m_{j+4}}^{j+3}$ is then $\{\Psi_{i+1g}^{fj+4}, \Psi_{i+1g}^{cj+4}, \Psi_{ig}^{fj+4}, \Psi_{ig}^{cj+4}\} \equiv \{\zeta_2^f(x-2h), \zeta_3^c(x-2h), \zeta_1^f(x), \zeta_1^c(x)\}$. This spans the $\bar{P}_2$ space but does not form a basis for it as $\zeta_1^f(x) = \frac{2}{h} \zeta_1^c(x)$. We shall use this 'centering' scheme in all our work with the 1-D hybrid quadratics. This can be regarded as our 1-D analogue of the 2-D P_2 space.

We reserve further discussion of the 'centering' problem to section 3.3.

3.3 Set Choice Rationale

The specific spaces discussed in sections 3.1 and 3.2 were all chosen to illustrate and to resolve certain questions which arise in trying to use the finite element method with our specific constraints.

We give below a discussion of what these questions are and how we intend to answer them. Given the complexity of the problem it must be understood at the start that we can only hope to resolve the questions in numerical terms of accuracy versus computational time.

(1) 'Centering' Scheme — Physical Mesh versus Mathematical Mesh

The 'centering' question touched on in section 3.2.2 is part of the larger problem of using the physical approach to contruct the mesh $\{\theta_j\}$. Up to this point we have only discussed the use of the two approaches,

mathematical and physical, in relation with the construction of the func-
tion spaces. A corresponding distinction can also be made between the
approaches which could be used to construct the mesh $\{\theta_j\}$. In all the
work of the previous sections we started off by choosing the basic
patches θ_j and constructed superpatches Θ_J by 'joining' θ_j in a manner
dictated by the choice of the approximation space M_m. This approach
will be termed the mathematical approach. But, just as we accepted
the $M_{m_j}^j$ as 'given' when we use the hybrid method to construct the
superelement functions ψ_{kg} via the physical approach, we could also
resort to a physical approach in the construction of the mesh by starting
off with the superpatch, Θ_J, appealing to physical intuition in the impo-
sition of superpatches on Ω and accepting the resulting $\{\theta_j\}$ as given.
In 2-D the choice is not only one of 'centering' but also of 'orienting'.
The difficulties, however, are identical to the ones outlined in section
3.2.2 for the 1-D hybrid quadratics. We shall refer to the $\{\theta_j\}$ obtained
in this manner as a physical mesh and reserve the term mathematical
mesh for the mathematical approach.

The physical mesh which will be used in this thesis is shown in
Fig. 3.6.

Two superpatches, the hexagons ABCDEF and abcdef, are depicted
in Fig. 3.6. The basic patches $\{\theta_j\}$ are now the triangles of the osS
type and not the triangles of the obc type which was the case for the
superpatches derived in the previous sections. What we have done is
to allow the superpatch to have a physical identity of its own and imposed
it on the problem in a manner appealing to our physical intuition. In the

Fig. 3. 6.
Physical mesh.

Legend

— · — · — Superpatch boundary
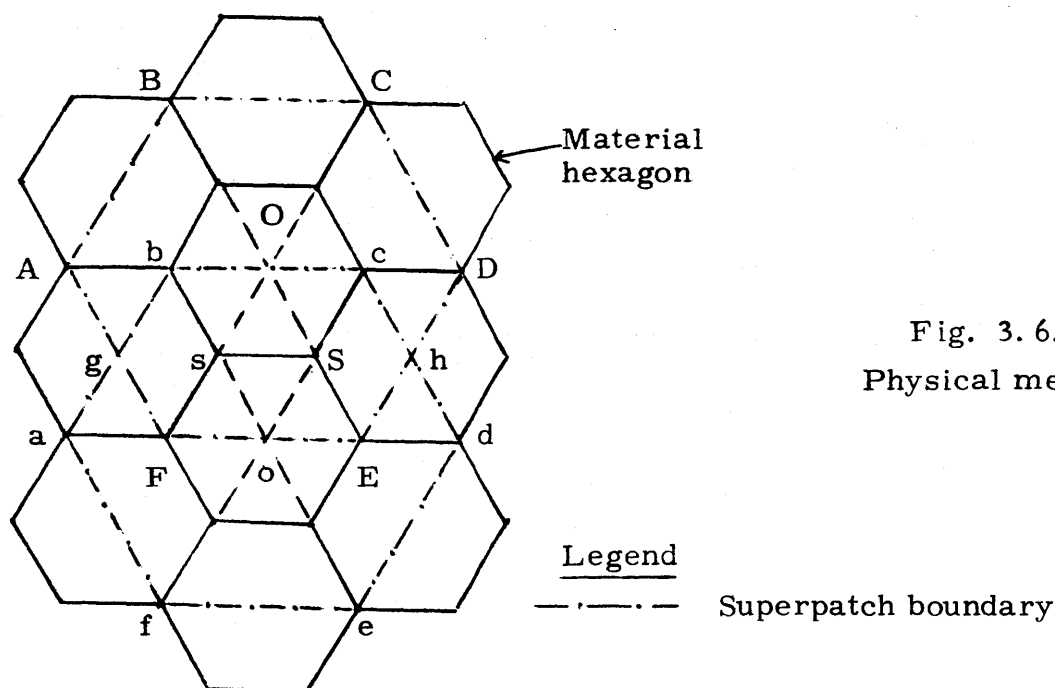
case of Fig. 3.6, we have 'centered' it along with its accompanying superelement function, on the center of a fuel hexagon and interpreted it as representing the region of influence of the fuel hexagon on its neighbours.

We shall use the following superelement sets $\{\psi_{ig}\}$ with the physical mesh.

(i) The shell C_1 defined by eqs. (3.22)-(3.23). With this mesh the use of C_1 can no longer be regarded as merely equating $M_{m_j}^j$ with $\overline{P}_1$. Consider the basic patch triangle osS. The spanning set for it $\{\psi_{og}^{jc1}, \psi_{hg}^{jc1}, \psi_{Og}^{jc1}, \psi_{gy}^{jc1}\}$ does span $\overline{P}_1$ but there is a linear dependence present.

(ii) It appeals to the physical intuition to use the two-element incomplete set eqs. (3.2)-(3.3) with the physical mesh. The integrated current element function of this set will allot a degree of freedom to the net

flow of neutrons into the adjoining fuel hexagons.

Let us conclude this section by pointing to an inherent difficulty of the physical mesh idea. This is the question of boundaries. Consider Fig. 3.6. In order to fit the boundary, we will have to shrink the super-patches associated with the outer ring of fuel hexagons. This means that the $M_{m_j}^j$ will not be identical. What was once a complete space may become an incomplete space. This is the inherent drawback to starting with Θ_J and not θ_j. To fit boundaries one has to devise various Θ_J which aside from the difficulties pointed out in the preceding text may not even be 'physically' appealing.

(2) Incompleteness

As pointed out in section 2.1, given the constraint of less than three variables per fuel hexagon, we have a choice between low order complete spaces and high order incomplete spaces.

The cubic incomplete spaces derived in section 3.1.1 will be used for the class of high order incomplete spaces. Those spaces were so constructed that as we increase the number of ψ_{kg} per fuel hexagon we decrease the defect of the space. It must be noted that these spaces are 'completely' incomplete. They do not span $\overline{P}_3$, $\overline{P}_2$ and $\overline{P}_1$. This is an important point as one could always construct a set of incomplete cubics which does not span $\overline{P}_3$ but spans $\overline{P}_2$ and $\overline{P}_1$.

For the complete spaces we use our shell sets derived in section 3.2.1. They will show the effect of increasing N, the order of the polynomial space.

(3) Condition of Join

As we are working in a piecewise polynomial space, the smoothness of our approximation $\hat{\phi}$ depends upon the degree of continuity we impose in joining the $\{\Psi^j_{lg}\}$ to form the set $\{\psi_{ig}\}$.

We restrict our work to the sets $\{\theta_j\}$ for which $\theta_j \cap \theta_k$ fall in regions of homogeneous material composition. The analytical solution ϕ has all orders of continuity in these regions. Our ninth order set given by eqs. (3.18)-(3.20) leads to a $\hat{\phi}$ with continuity of the first derivative. The incomplete cubic sets lead to a $\hat{\phi}$ with only function continuity. If we compare the results of the two incomplete 3-element sets we will be combining questions of join condition with that of defect of space and order of space. We will, however, obtain an ordering of importance of the various competing effects. It should be noted that the ninth order set is also 'completely' incomplete.

(4) Conditions within θ_j

As material interfaces fall within our basic patches the problem of primary interest is whether or not derivative continuity at these interfaces is an adequate alternative to current continuity. This question has been addressed before.[2-3] We shall endeavor to be slightly more quantitative by presenting 1-D analytic and numerical parametric calculations. The direction of our 2-D work was in part motivated by these results.

(5) Low-Order Space Fine-Mesh versus High-Order Coarse-Mesh

This question is a complex one as the answer is dependent upon

the flux shape being approximated. Nevertheless it is a real question as we do have the choice of using either the fine mesh of Fig. 2.6(a) with the complete linear space or the coarse mesh of Fig. 2.6(b) with the complete quadratic space. The spaces in question are the shell set C_1 or the double shell set $\{C_1 + C_2\}$ derived in section 3.2.1.

Our conclusions using these two sets can only be considered to be valid for a range of flux shapes comparable to the one of our benchmark problem.

(6) Boundary Treatment

The use of regular hexagonal superpatches with the coarse mesh of Fig. 2.6(b) leads to difficulties with alignment of boundaries. One has to resort to other irregular polygons for an exact alignment. This makes it even more important to think initially in terms of θ_j rather than Θ_J. As our sets were actually derived by first finding $\{\Psi_{ig}^j\}$ and then 'joining' using function continuity to form $\{\psi_{kg}\}$ with the regular hexagon as Θ_J, there is no difficulty in extrapolating the logic and joining the $\{\Psi_{ig}^j\}$ to form other polygonal $\Theta_J \in S^1$.

As an initial attempt we restricted Θ_J to the regular hexagon and all the calculations were done with the boundary superpatches overlapping into the region of zero material property adjoining Ω. Calculations were then redone for the more promising alternatives with the use of irregular polygons to fit the boundary exactly.

We conclude this chapter by summarizing, in Fig. 3.7, the alternatives open to us, given the constraints of the problem, in terms of the
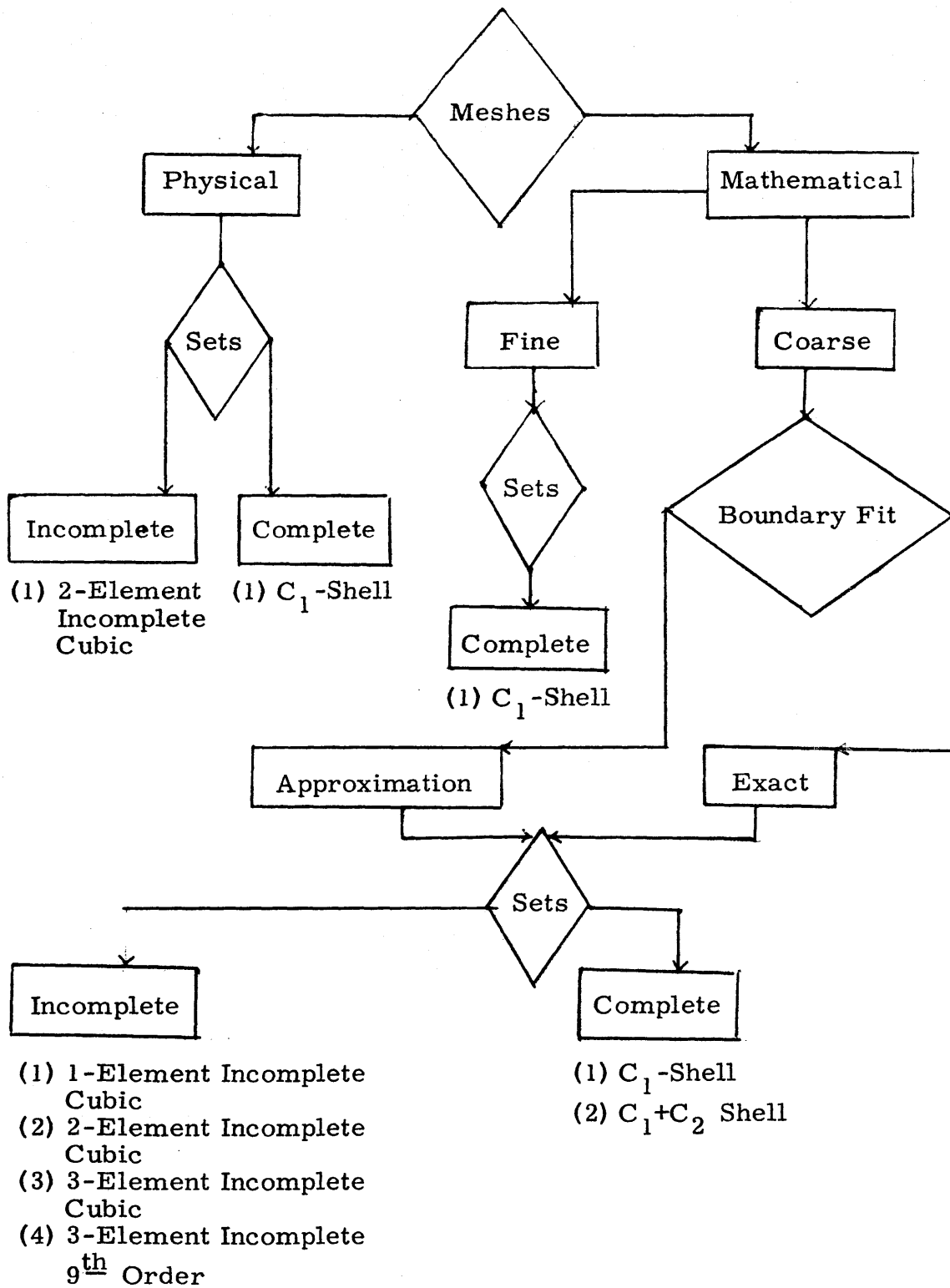
Fig. 3.7. Algorithmic presentation of alternatives — meshes and super-element sets.

meshes and spaces discussed in this chapter and in the previous one.

The term 'Fine' refers to the fine mesh of Fig. 2.6(a). 'Coarse' is the mesh of Fig. 2.6(b). We have chosen to use this mesh as it is the 'finest' of the coarse meshes possible and should therefore lead to the best accuracy.

Chapter 4

RESULTS AND CONCLUSIONS

In this chapter we first present our results and a discussion of the implications. We then draw our conclusions and suggest possible areas for future work.

4.1 Results

The presentation of the results will be divided into two parts, those pertaining to the question of accuracy and those relevant to the discussion of computation time. The results pertaining to accuracy will be further subdivided into analytic, 1-D numerical and 2-D numerical work. The cross sections used were those typical of the HTGR and are tabulated in Appendix A.

4.1.1 Accuracy

As noted and as discussed in the preceding chapters, there are many questions involved in applying the various steps required to arrive at the form of the Galerkin equation, eq. (1.16), preparatory to the actual inversion. In the final analysis, answers to these questions can only be judged on the basis of the accuracy attainable. The questions answered here in terms of accuracy attainable are the ones discussed and summarized in section 3.3. For completeness we shall reiterate them here in the form of a synopsis.

(1) Centering Scheme — Physical Mesh versus Mathematical Mesh

We use the specific physical mesh of Fig. 3.6 to judge the merit of

constructing meshes via the physical approach vis-a-vis construction using the mathematical approach. The mathematical counterpart to the physical mesh used in this investigation is the coarse mesh of Fig. 2.6(b). The results presented are obtained from 2-D numerical calculations using the superelement sets C_1 and the 2-element incomplete cubic set.

(2) Incompleteness

The question of the principle involved in deciding on what degree of incompleteness is to be incorporated into the approximation space $M^j_{m_j}$ is investigated in 2-D as a question of the accuracy of the completely incomplete sets, the sets of section 3.1, and in 1-D as a question of the accuracy of the sets derived from Kang's cubic Hermites and the hybrid quadratic set of section 3.2.2, vis-a-vis the corresponding complete 2-D and 1-D sets of section 3.2.

(3) Conditions of Join

The degree of smoothness to impose when joining the basic element functions Ψ^j_{ig} across patch boundaries to form the superelement function ψ_{kg} is examined both in 1-D and 2-D. In 1-D results are obtained using Kang's cubic Hermites and in 2-D we use the totally incomplete spaces of section 3.1. Results comparing the effect of varying the degree of join, from complete disjointness to continuity of first derivative, for the approximation $\hat{\phi}_g(\underline{r})$ are presented.

(4) Conditions within θ_j

The main question here is the question of derivative continuity

as material interfaces fall within the basic patch θ_j. Analytic and 1-D numerical results using the hybrid quadratic set of section 3.2.2 are presented.

(5) Low-Order Space Fine-Mesh versus High-Order Space Coarse-Mesh

We investigate this problem in 2-D and compare results obtained by using the fine mesh of Fig. 2.6(a) with the set C_1, with those obtained by using the coarse mesh of Fig. 2.6(b) with the set C_2.

(6) Boundary Treatment

As discussed in section 3.3, irregular polygonal superpatches will have to be used for an exact fit with an arbitrary boundary. We first carry out our calculations restricting Θ_J to the regular hexagon. These results are then compared to ones obtained by allowing the use of irregular polygons for Θ_J to fit the boundary exactly.

Given the complexity of the problems, the answers can for the most part only be evaluated in terms of actual computer simulations, that is, in numerical terms. But, as can be seen from the above synopsis, analytic work is not entirely proscribed and we have a mixture of analytic, 1-D and 2-D numerical results. As indicated in the introduction of section 4.1 we present the results according to the classes: analytic, 1-D or 2-D numerical work. To clarify matters, we summarize here the questions considered in each of these groups.

(1) Analytic work: question (4)

(2) 1-D numerical work: questions (2)-(4)

(3) 2-D numerical work: questions (1)-(3) and (5)-(6).

We now consider each of these specific groups in turn.

(1) Analytic

(i) Conditions within θ_j: Derivative Continuity versus Current Continuity

It has been shown in Appendix B that the error in the eigenvalue λ for the 1-D, 1-group, 1-region Dirichlet problem of Fig. 4.1 when

	Region 1	Region 2	
0		L/2	L

x
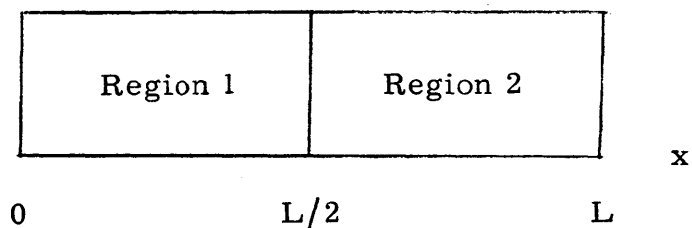
Fig. 4.1. 1-D 2-region problem.

derivative continuity instead of current continuity is imposed at the interface $x = L/2$ is

$$\frac{\Delta\lambda}{\lambda} = \alpha\left(\frac{D_2}{D_1}, \eta\right) = \frac{\beta(D_2/D_1)}{\left\{1 + \left[\dfrac{\eta}{2X_d(D_2/D_1)}\right]^2\right\}} \tag{4.1}$$

where

$$\Delta\lambda = \lambda_c - \lambda_d$$

$$\eta(L_d, L) = \frac{L}{L_d} = \frac{L}{\left(\dfrac{D_2}{\Sigma}\right)^{1/2}}$$

and the functions $\beta(D_2/D_1), X_d(D_2/D_1)$ are graphed in Figs. B. 2 and B.3. For our range of interest, block sizes of about twice the diffusion length, Figs. 4. 2 and 4.3 indicate that for errors in the eigenvalue less than 1%, the difference between D_1 and D_2 should be of the order of less than 25%. Tables 4. 1 and 4. 2 are the tabular counterparts of Figs. 4. 2 and 4. 3.

The corresponding expression for the maximum error in the flux eq. (B. 35) is

$$\max E_1(D_1/D_2) = -\left[1 - \frac{\Phi_c(D_1/D_2)}{\Phi_d(D_1/D_2)} \cdot \frac{\sin X_d(D_2/D_1)}{\sin X_c(D_2/D_1)} \right.$$

$$\left. \cdot \frac{\sin \{X_d(D_1/D_2) \, M(D_1/D_2)\}}{\sin \{X_c(D_1/D_2) \, M(D_1/D_2)\}} \right]$$

$$= -\left[1 - \frac{\mu_c(D_1/D_2)}{\mu_d(D_1/D_2)} \right] \qquad (4. 2)$$

where

$$\mu_j(D_1/D_2) = \frac{\Phi_j(D_1/D_2)}{\sin X_j(D_2/D_1) \, \sin \{X_j(D_1/D_2) \, M(D_1/D_2)\}} \qquad (4. 3)$$

and subscript $j = c$ or d.

The results are summarized in Figs. B. 4-B.6 and Table B. 3. For our range of interest it can be seen from Fig. 4. 4 that for $\max E_1$ less than 10% we must have a $0. 5 < D_2/D_1 < 2$. This leads to an average error ~5% in the flux. Table 4. 3 is the tabular counterpart of Fig. 4. 4.

The results summarized in Figs 4. 3 and 4. 4 have appealing physical
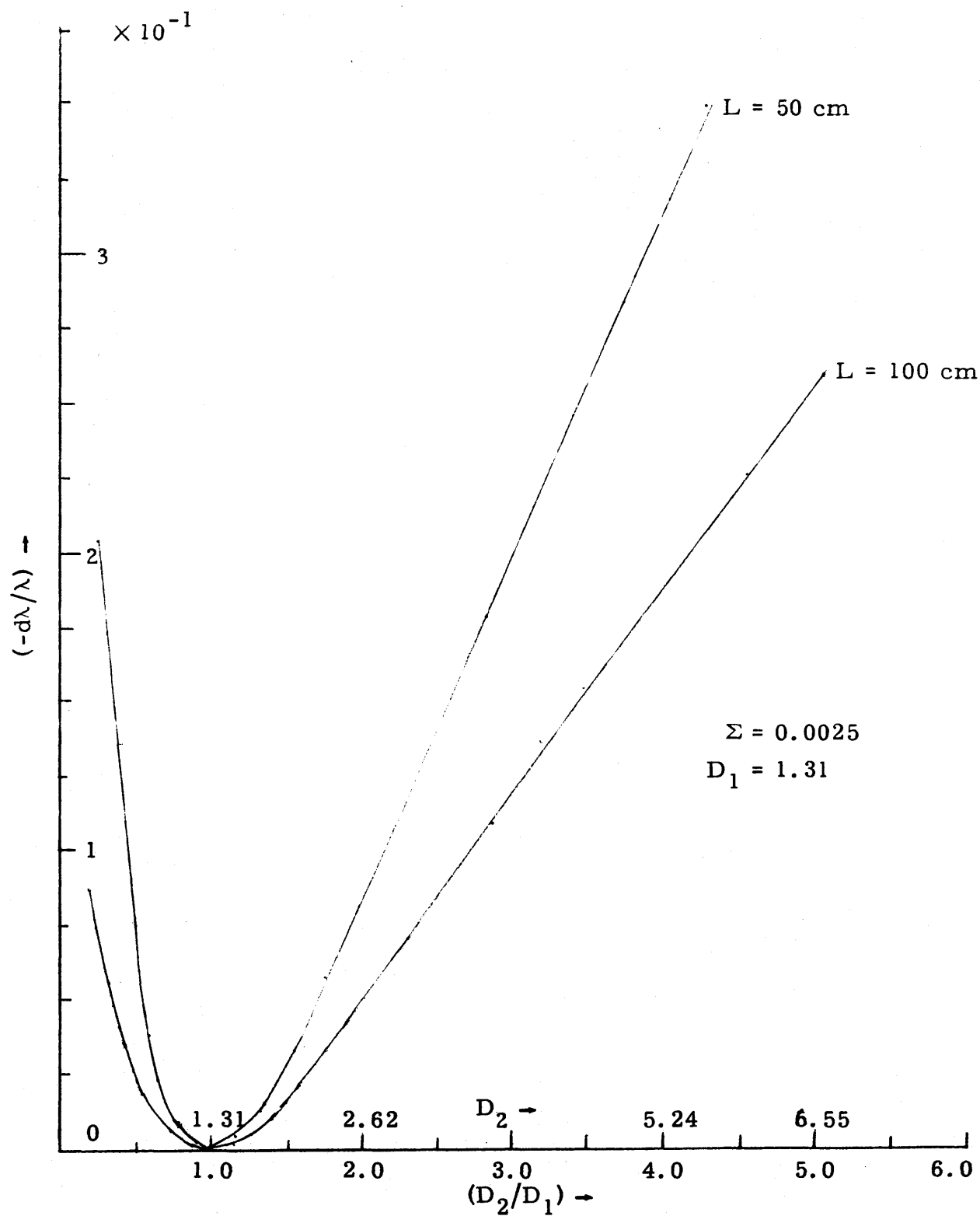
Fig. 4.2. Fraction error in eigenvalue λ. Derivative vs current continuity — 1-group 1-D 2-region problem (Fig. 4.1).
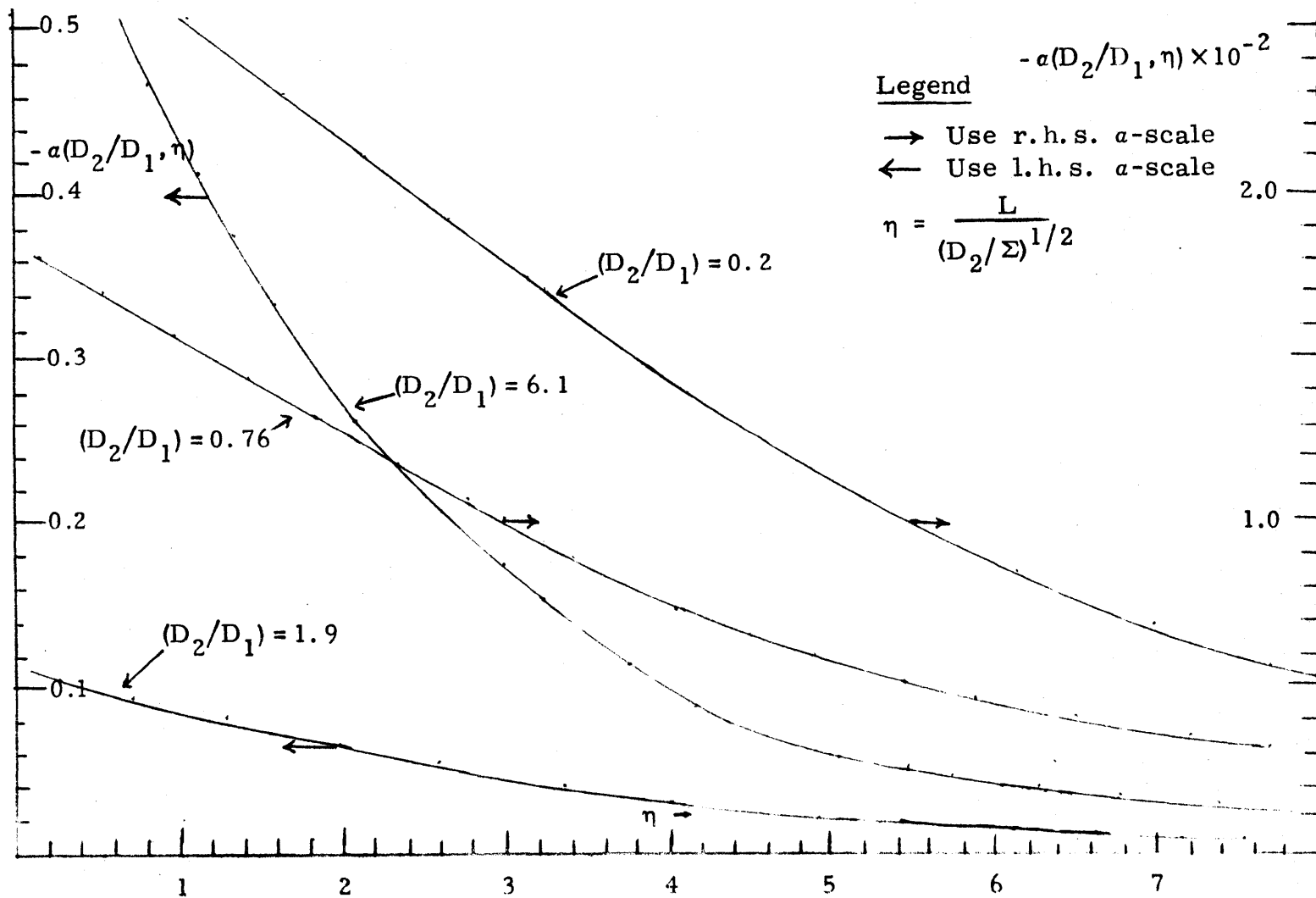
Fig. 4.3. Fraction error in eigenvalue λ. Derivative vs current continuity — 1-group 1-D 2-region problem (Fig. 4.1).

Table 4.1. Conditions within θ_j. Fractional error in eigenvalue λ
for L = 50 cm and L = 100 cm. 1-group 1-D 2-region
problem (Fig. 4.1). $\Sigma = 0.0025$, $D_1 = 1.31$.

$-a(D_2/D_1, \eta)$

D_2/D_1	L = 50 cm	L = 100 cm
0.2	0.22	0.0782
0.305	0.1607	0.0625
0.61	0.0368	0.0169
0.76	0.01	0.0055
1.0	0.0	0.0
1.716	0.0109	0.0066
2.145	0.0435	0.0235
4.29	0.252	0.144
6.55	0.43	0.2537

Table 4.2. Conditions within θ_j. Fractional error in eigenvalue λ
as a function of η and D_2/D_1. 1-group 1-D 2-region
problem (Fig. 4.1).

$-a(D_2/D_1, \eta)$

η \ D_2/D_1	0.2	0.76	1.9	6.1
0	0.577	0.018	0.1017	0.706
2	0.455	0.013	0.063	0.27
4	0.2789	0.007	0.0298	0.095
6	0.1695	0.0042	0.0168	0.045
8	0.109	0.00267	0.009	0.026
10	0.075	0.0018		0.017
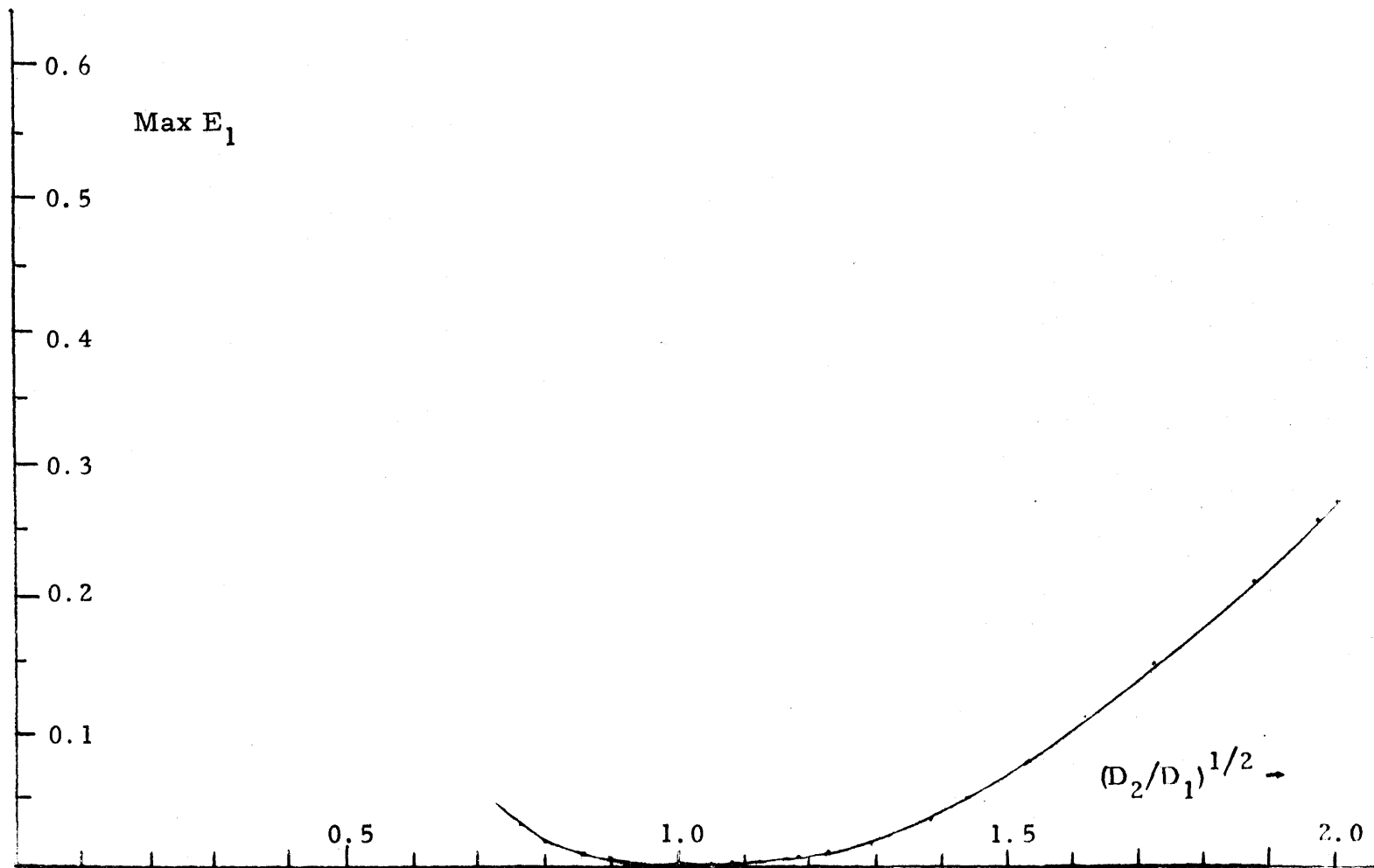
Fig. 4.4. Max $E_1(D_2/D_1)$. Maximum fraction error in flux. Derivative vs current continuity — 1-group 1-D 2-region problem (Fig. 4.1).

Table 4.3. Conditions within θ_j. Maximum error in the flux as a function of D_1/D_2. 1-group 1-D 2-region problem (Fig. 4.1).

D_1/D_2	E_1
1.6375	0.024
1.31	0.0069
1.00	0.0
0.524	0.0339
0.1637	0.5226

interpretations. One would intuitively expect that the error in λ would decrease with increasing problem size as λ is a 'global' property and the interface would play less and less of a role in its determination. In the case of maximum flux error one would not expect the problem size, namely the parameter η, to be important as point flux error is a 'local' property. One would also expect an increasing error for both λ and flux with increases in difference between the diffusion coefficients of the two regions. One would not expect symmetry in the results about the point $D_1/D_2 = 1$ as there is a third medium present, the vacuum. All these expectations are borne out by Figs. 4.3 and 4.4. The parameters η and D_2/D_1 are physically significant dimensionless parameters which can be used to characterize a problem.

(2) 1-D Numerical

(i) Conditions of Join

We investigate here the effect of not imposing flux continuity or current continuity using Kang's Hermite cubic set as our $\{\Psi_{ig}^j\}$. The 1-D 2-region problem, as shown in Fig. 4.1, is now treated in 2-groups with

Table 4.4. Condition of join. Eigenvalue λ — 2-group 1-D 2-region problem.

L = problem size as in Fig. 4.1 (=100 cms)

Case	Description of Calculation		λ
1	Analytic		0.04256
2	Flux continuity-current float	Homogeneous slab — Region 1 material	0.042577
3	Flux float-current float		0.042576
4	Flux continuity-current continuity		0.10854
5	Flux continuity-current float	Region 1 $\neq$ Region 2	0.10854
6	Flux float-current float		0.20707

the material properties taken from the 1-D set of Appendix A. The boundary condition imposed is the Dirichlet condition.

Region 1   Region 2
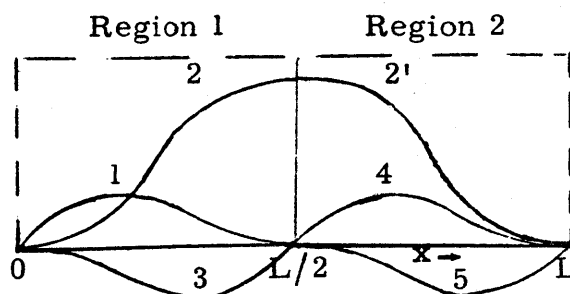
Fig. 4.5. Superelement function set used — Kang's cubic Hermite.

The superelement functions $\{\psi_{2g}, \psi_{2'g}\}$ shown in Fig. 4.5 are the flux functions $u_0(x)$ of Kang's[1] and $\{\psi_{1g}, \psi_{3g}, \psi_{4g}, \psi_{5g}\}$ are the current functions $u_1(x)$. If we impose function continuity by joining ψ_{2g} and $\psi_{2'g}$ across the interface so that $\psi_{2g}(L/2) = \psi_{2'g}(L/2)$, we have our flux continuity-current float case. If, in addition, we impose current continuity by joining ψ_{3g} and ψ_{4g} across the interface so that

$$D_I \frac{d\psi_{3g}(L/2)}{dx} = D_{II} \frac{d\psi_{4g}(L/2)}{dx} ,$$

we have our flux continuity-current continuity case. When none of these conditions are imposed we have our flux float-current float case.

Table 4.4 lists the eigenvalues obtained. Notice the difference in eigenvalue between case (6) and cases (4) and (5). To permit function discontinuities in the set $\{\psi_{ig}\}$ is to violate the 'variational principle.' There is no such difference between the eigenvalues obtained for case (2)

Table 4.5. Condition of join. Supercoefficients $\{a_{kg}\}$ — 2-group 1-D 2-region problem.

L = problem size as in Fig. 4.1 (=100 cms)

Unknowns	Case (2) of Table 4.4		Case (3) of Table 4.4	
	g = 1	g = 2	g = 1	g = 2
a_{1g}	0.24099×10^{-2}	0.376608×10^{-3}	-0.29956×10^{-2}	-0.46818×10^{-4}
a_{2g}	$\lceil 0.75285 \times 10^{-1}$	$\lceil 0.117656 \times 10^{-1}$	-0.93603×10^{-2}	-0.14627×10^{-2}
$a_{2'g}$	$\lfloor 0.75285 \times 10^{-1}$	$\lfloor 0.117656 \times 10^{-1}$	0.264819×10^{-1}	0.41383×10^{-2}
a_{3g}	-0.56455×10^{-4}	-0.88287×10^{-5}	0.70196×10^{-5}	0.10975×10^{-5}
a_{4g}	0.5656×10^{-4}	0.88346×10^{-5}	0.19873×10^{-4}	0.31062×10^{-5}
a_{5g}	-0.24098×10^{-2}	-0.376602×10^{-3}	-0.84764×10^{-3}	-0.13246×10^{-3}

and case (3). However, Table 4.5 shows that there is a difference between a_{2g} and $a_{2'g}$ for case (3). This means that flux continuity will have to be imposed. Table 4.5 also shows that current continuity should be imposed as the coefficients a_{3g} and a_{4g} of case (2) are not equal leading to current discontinuities. It does not make much of a difference in the accuracy as the eigenvalue λ is only off by less than 0.02% from the analytic answer and the coefficients a_{3g}, a_{4g} although not zero, which they should be because of the symmetry, are a factor of 10^{-2} smaller than the other coefficients. But it does reduce the number of unknowns $\{a_{ig}\}$.

(ii) Incompleteness

Tables 4.6 and 4.7 show the convergence behavior of the following $\{\psi_{kg}\}$ sets.

(i) Hermite Flux Set. This set is formed by deleting the current function $u^1(x)$ of Kang's cubic Hermite set.[1] This set is totally incomplete as it does not even span the $\overline{P}_1$ space. Looking at it from another point of view, we have, by retaining only the flux function, forced a fixed relation between the flux and the current at certain points.

(ii) 1-D Hybrid Quadratic Set. This set is discussed in section 3.2.2. The point to note here is that it spans $\overline{P}_2$.

(iii) Hybrid Quadratic Flux Set. Here we only use the flux function of the 1-D hybrid quadratic set. As with the Hermite flux set, this set does not span $\overline{P}_1$.

The problem solved is the 2-group homogeneous case of the bare

Table 4.6. Incompleteness. Eigenvalue λ as a function of mesh size — 2-group 1-D homogeneous slab problem.

L = problem size as in Fig. 4.1 (=100 cm)

λ-analytic answer = 0.1034704

*2h = 'center-to-center' mesh spacing

λ

h (cm) Set	25	16.666	12.5	10.0	8.33	7.14	6.25	5.555
(i) Hermite Flux	0.094491		0.096601	0.09692	0.097094	0.097178	0.097277	0.097319
(ii) 1-D Hybrid Quadratic	0.103449	0.103464	0.103469					
(iii) 1-D Hybrid Quadratic Flux	0.091855	0.092712	0.093170	0.09340	0.093533	0.093589	0.093671	0.093701

*x——x——x——x——x   mesh centers for h = 12.5 cms

0   L/2   L

127

Table 4.7. Incompleteness. Eigenvalue λ as a function of number of unknowns — 2-group 1-D homogeneous slab problem.

L = problem size as in Fig. 4.1 (=100 cm)

λ-analytic answer = 0.1034704

R_n = number of unknowns/group

λ

Set \ R_n	1	2	3	4	5	6	7	8
(i) Hermite Flux	0.094491		0.096601	0.096920	0.097094	0.097178	0.097277	0.097319
(ii) 1-D Hybrid Quadratic				0.103449		0.103464		0.103469
(iii) 1-D Hybrid Quadratic Flux	0.091855	0.092712	0.093170	0.093403	0.093533	0.093589	0.093671	0.093701

slab problem of Fig. 4.1 with the material composition as given in Appendix A. Table 4.6 tabulates the eigenvalue λ as a function of h where 2h is the 'center-to-center' mesh spacing. Table 4.7 presents the same results for λ tabulated against the corresponding number of unknowns per group, R_n. It can be seen from the tables that the two totally incomplete spaces converge to answers different from the analytic result. In contrast, the 1-D hybrid quadratic set does converge to the analytic answer. For mesh sizes roughly comparable to those which will be used in the 2-D sets, λ is off by ~5% for set (i) and ~8% for set (iii), while the error for set (ii) is in the sixth significant figure.

(iii) Conditions within θ_j — Current Continuity versus Derivative Continuity.

Figure 4.6 shows the 2-group problem used. It can be regarded as a 1-D
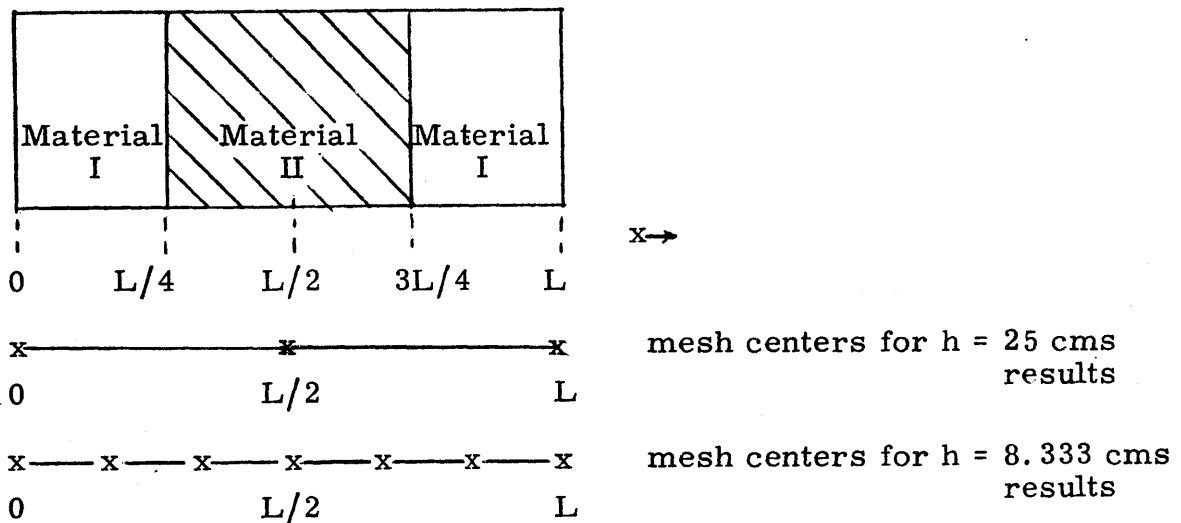
Fig. 4.6. 1-D 3-block section problem.

section through the coarse mesh superpatch we will use in our 2-D work. We center our 1-D hybrid quadratic set on the material block centers 0, L/2

and L. The boundary conditions used are that the flux is zero at x = 0 and x = L. We can, by adjusting the parameter a of this set, impose either derivative continuity or current continuity at the interfaces x = L/4 and x = 3L/4. The results obtained by doing so are presented in Table 4.8 where the eigenvalue λ is tabulated as a function of the ratio of the fast diffusion coefficients of the two materials. This difference in the fast diffusion coefficient is the only difference between material I and material II. The reference values were obtained by using the code CHD with a mesh spacing fine enough to ensure a converged value of λ.

It appears from the table that for a 'center-to-center' spacing, 2h, of 50 cm, derivative continuity gives better accuracy than current continuity. Apparently as far as λ is concerned the analytic solution to the derivative continuity problem is close to the analytic solution to the current continuity problem, that is, the exact problem. But the numerical solution to the derivative continuity problem converges at a rate slower than that of the numerical solution to the current continuity problem. This is borne out by the h = 8.333 cm results of Table 4.8. The decrease in mesh size has resulted in a decrease in λ-error much greater for the current continuity case.

Figure 4.7 shows how the shapes of the 1-D hybrid quadratic set flux and current functions vary with a.

We conclude this section by presenting results for larger 1-D problems composed of alternating material blocks. These problems are as shown in Fig. 4.8.

Table 4.8. Conditions within θ_j. Eigenvalue λ — 2-group
3-block section problem.
L = 100 cms (Refer to Fig. 4.6)

λ h (cm)	$\dfrac{D_1^{II}}{D_1^I}$	1-D Hybrid Quadratic Set		Reference Solution CHD^2
		Derivative Continuity	Current Continuity	
25	0.2	0.10848	0.13772	0.11301
	0.305	0.10757	0.12779	0.11019
	0.61	0.10542	0.11199	0.10587
	0.76	0.10457	0.10782	0.10472
	1.31	0.10226	0.10008	0.10243
	1.9	0.10063	0.096864	0.10150
	6.1	0.096445	0.093401	0.099374
8.333	0.2	0.11179	0.11578	0.11301

$a = 0.2$ ψ_{kg}^{f}

ψ_{kg}^{c}

Region II   Region I   Region II

$a = 5.0$ ψ_{kg}^{f}

ψ_{kg}^{c}

Region II   Region I   Region II

$a = 1.0$ ψ_{kg}^{f}

ψ_{kg}^{c}

Region II   Region I   Region II

$a = 0.76$ ψ_{kg}^{f}

ψ_{kg}^{c}

Region II   Region I   Region II

$a = 1.31$ ψ_{kg}^{f}

ψ_{kg}^{c}

Region II   Region I   Region II
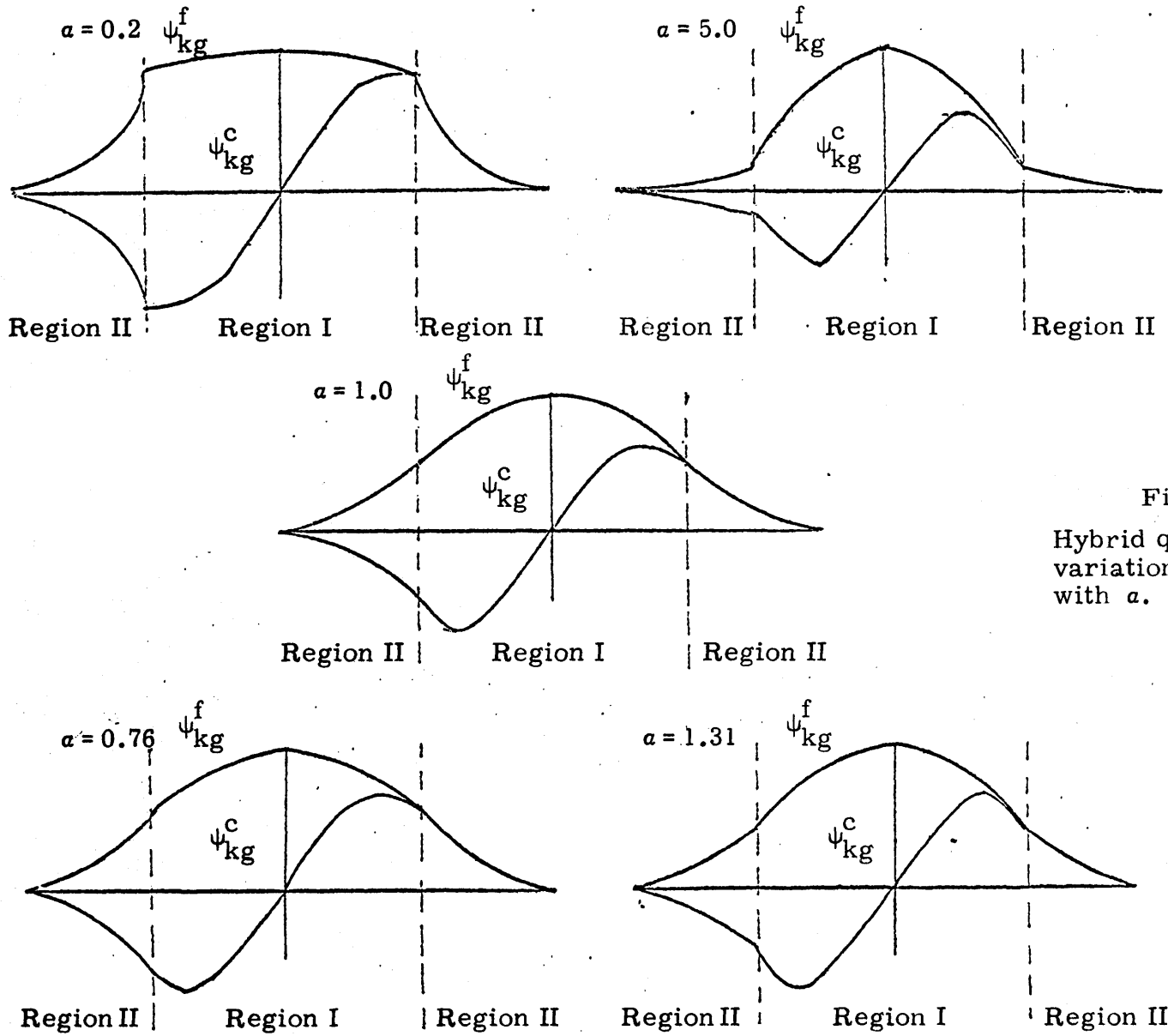
Fig. 4.7.

Hybrid quadratic set —
variation in shape
with a.

Legend

$a = D^{II}/D^{I}$
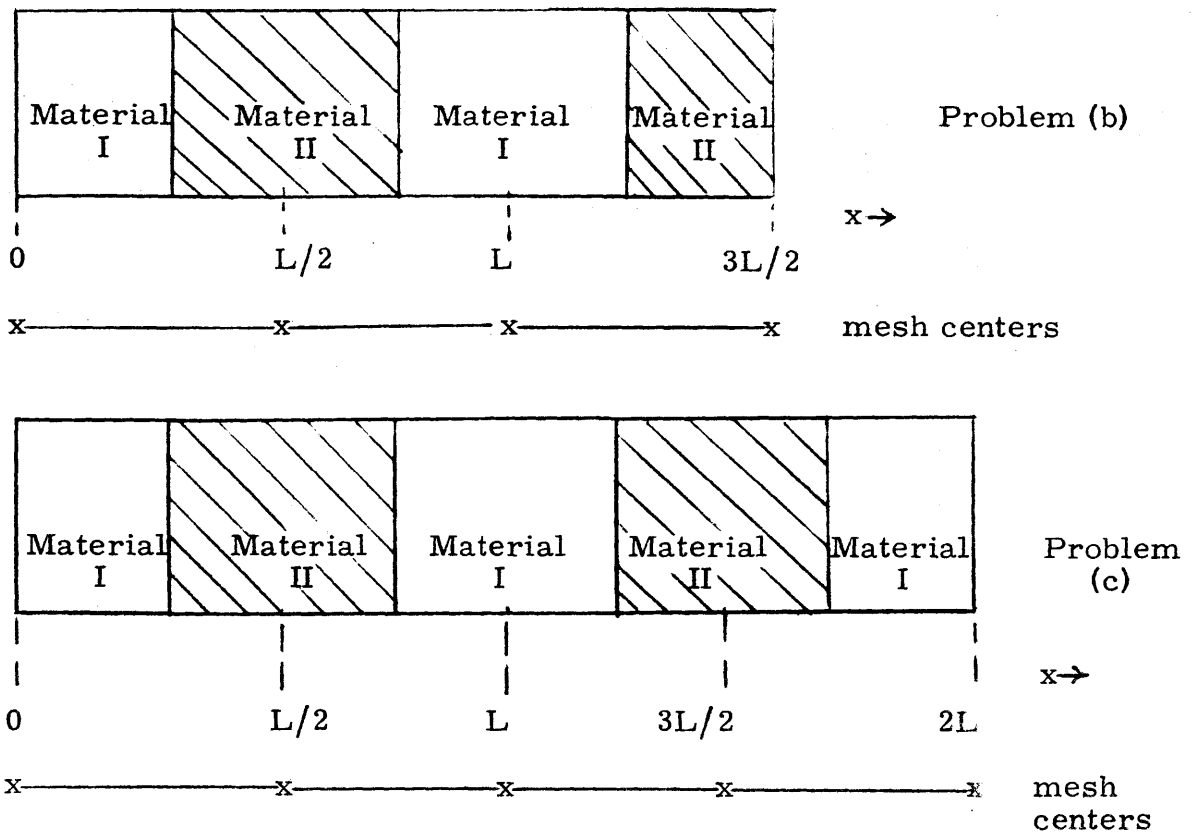
Fig. 4.8. 1-D 4-block section problem — problem (b). 1-D 5-block section problem — problem (c).

Problem (a) is the problem of Fig. 4.7. The same mesh spacing and centering scheme is used for all three problems.

The results are presented in Table 4.9. The error in λ for the 1-D hybrid quadratic set is less than 0.5% for both current and derivative continuity. Use of derivative continuity instead of current continuity within θ_j should therefore give acceptable answers for the range of material properties typical of the HTGR. The possible exception is at the core-reflector interface. It should be noted that for the material compositions used here, $D_1^{II}/D_1^{I} = 0.985$.

Table 4.9. Conditions within θ_j. Eigenvalue λ — 2-group 1-D block section problems of Figs. 4.7-4.8.

L = 100 cms (refer to Fig. 4.7 and Fig. 4.8)

λ

Problem	Hermite Flux	Hybrid Quadratic Flux		1-D Hybrid Quadratic		Reference Solution CHD^2
		Derivative Continuity	Current Continuity	Derivative Continuity	Current Continuity	
(a)	0.34296	0.33456		0.35974	0.36057	0.36150
(b)	0.36764	0.36204	0.36267	0.38054	0.38132	0.38228
(c)	0.39052	0.38793	0.38857	0.40009	0.40083	0.40185

(3) 2-D Numerical

A word is in order here regarding the benchmark problem. This is the small HTGR problem used by G.A. and is shown in Fig. 4.9. The reactor consists of patches of seven hexagonal blocks. The outer ring of patches is the graphite reflector. The central hexagonal block of each of the patches which constitute the core contains a control rod. The remaining blocks of the core patches are of fuel material of the same composition. Cross sections are homogenized over a block and all the calculations will be done in two groups. We restrict ourselves to those rod configurations for which the problem has 60°-rotational symmetry as we shall only solve for a 60° sector of the reactor.

To be considered as a possible alternative our method must at the very least provide an answer of comparable accuracy for the completely unrodded case. This case has the least heterogeneity and the flux should be the smoothest. The imposition of derivative continuity instead of current continuity should, from an approximation point of view, be at its 'best' here.

To be accepted as a potential alternative the method must provide more accurate answers for the fully rodded case. This case has the greatest heterogeneity and the flux shape should vary the most.

To summarize, we have a reflected heterogeneous reactor sector with flux equal to zero at the outer boundary and conditions of rotational symmetry at the edges of the sector. In terms of diffusion lengths the core is about twenty diffusion lengths across and the reflector has a thickness of about two diffusion lengths. We shall consider the fully
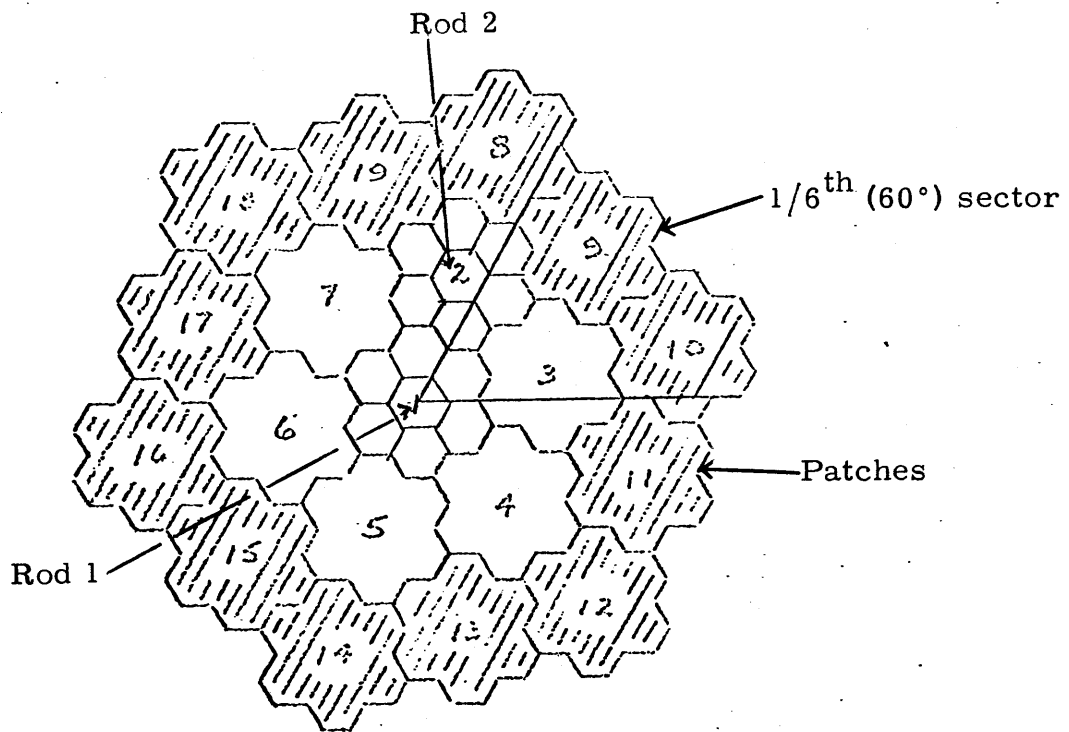
Fig. 4.9. Small HTGR — 2-D benchmark problem.

rodded case to be the deciding benchmark problem.

We conclude this section by elaborating on the questions concerning the boundary referred to in sections 1.2.1 and 3.3.

Section 1.2.1 pointed out that we choose to satisfy the Dirichlet conditions by working in $W_o^1(\Omega)$. If we use $\{C_1 + C_2\}$ for $M_{m_j}^j$ and construct M_m such that $M_m \subset W^1(\Omega)$ but $M_m \not\subset W_o^1(\Omega)$, we arrive at the conclusion that the Dirichlet condition can be satisfied if
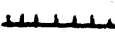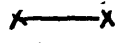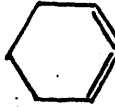
$$a_{ig}^{c2} + a_{jg}^{c2} = 0$$

where $\{a_{ig}^{c2}, a_{jg}^{c2}\}$ are the unknowns in the supercoefficient set $\{a_{kg}\}$ corresponding to the superelement functions $\{\psi_{ig}^{c2}, \psi_{jg}^{c2}\}$, the c2-type superelement functions centered on the θ_j corners lying on $\partial\Omega$. For this particular benchmark problem, there is 60°-rotational symmetry and the number of such corners force the solution $a_{ig}^{c2} = a_{jg}^{c2} = 0$. This means that for this particular problem, we shall obtain the same solution whether or not we delete elements so that $M_m \subset W_o^1(\Omega)$.

Section 3.3 pointed out that for the coarse mesh option, irregular polygons for θ_j would have to be used if the boundary is to be fitted exactly. It is to be noted that Tables 4.12-4.13 are, in the sense of section 3.3, initial calculations; that is, calculations where the boundary has not been fitted exactly. Table 4.14 is a second phase calculation; calculations where the boundary has been fitted exactly. Figure 4.10 shows the initial calculation mesh and Fig. 4.11 the second phase mesh.
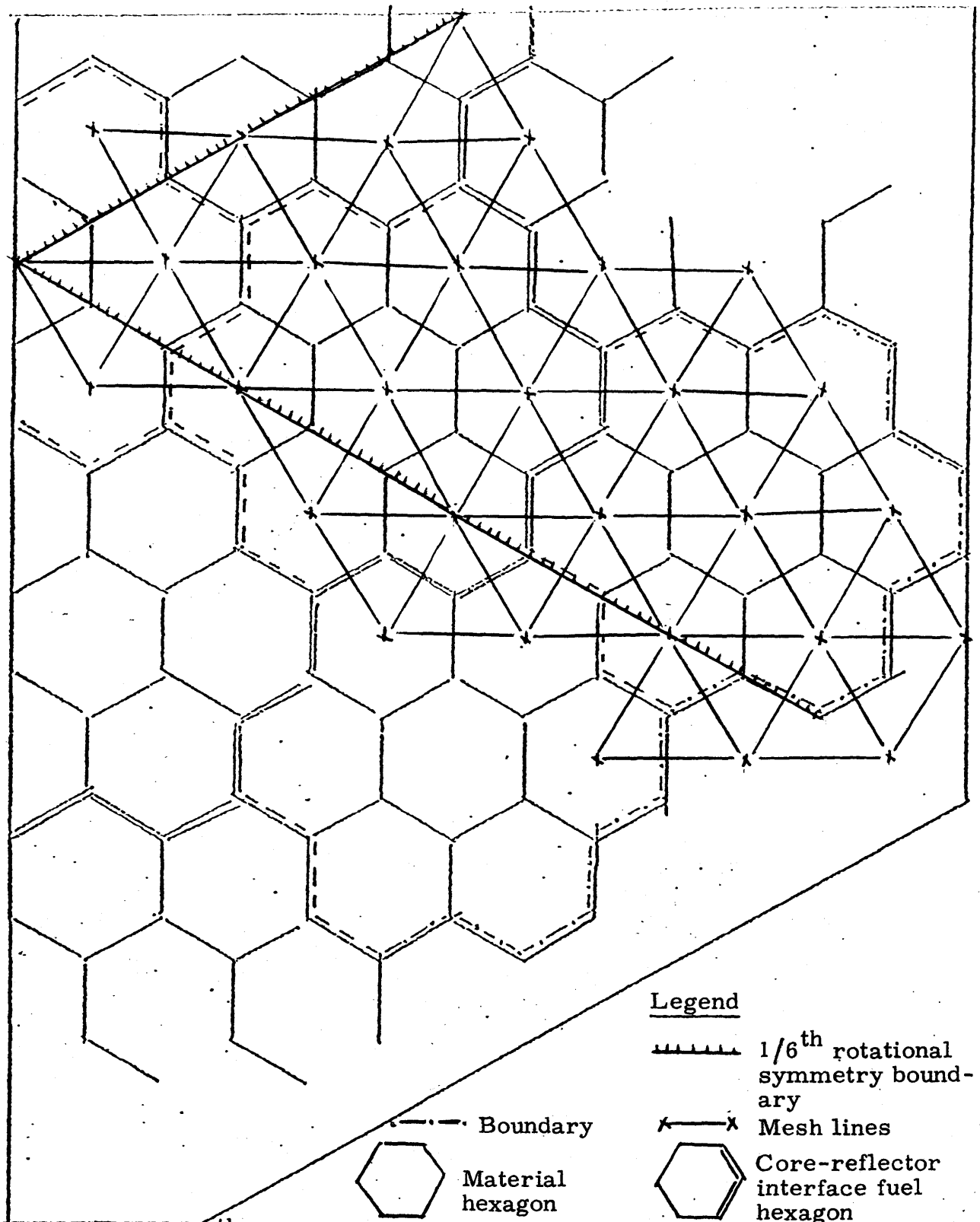
Legend

⊥⊥⊥⊥⊥ 1/6th rotational symmetry boundary

—·—·— Boundary

x——x Mesh lines

⬡ Material hexagon
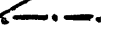
⬡ Core-reflector interface fuel hexagon

Fig. 4.10. 1/6th sector small HTGR — 2-D benchmark problem. Coarse mesh — boundary not fitted exactly.

Legend

ᴧᴧᴧᴧᴧᴧ 1/6th rotational boundary

—·—· Boundary

⊁————⊁ Mesh lines

Material hexagon

Core-reflector interface fuel hexagon
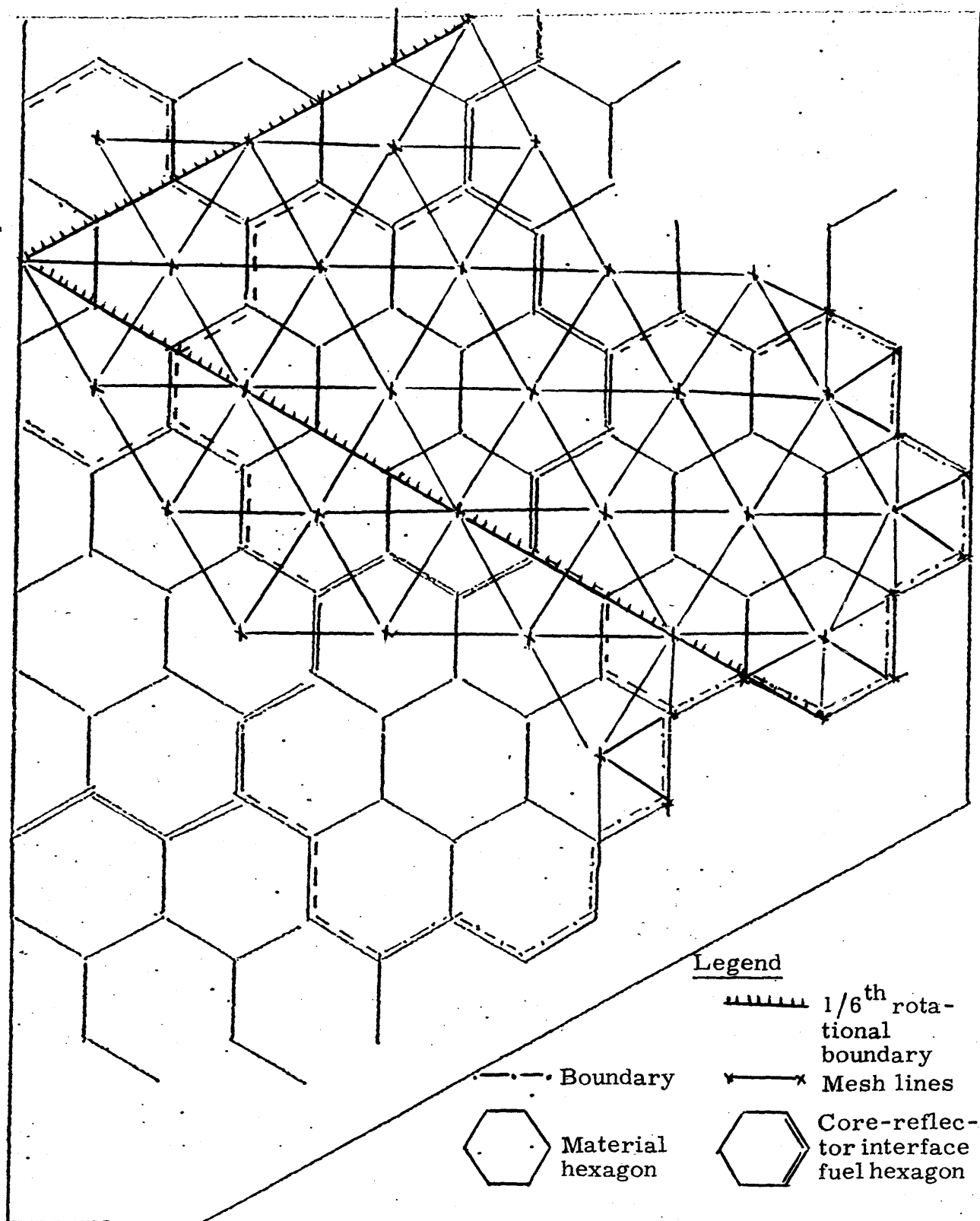
Fig. 4.11. 1/6th sector small HTGR — 2-D benchmark problem. Coarse mesh — boundary exact fit.

(i) Centering Scheme — Physical Mesh versus Mathematical Mesh

We first examine the behavior of the meshes in the case of the Neumann problem. Triangle fgh in Fig. 4.12 is a region of homogeneous material and Neumann conditions are imposed on its boundaries. The problem is therefore a simulation of the infinite medium problem. As we use the C_1 set, 'tent' functions are centered on the points $\{f, g, h, s, p, q, r\}$.

Material hexagon
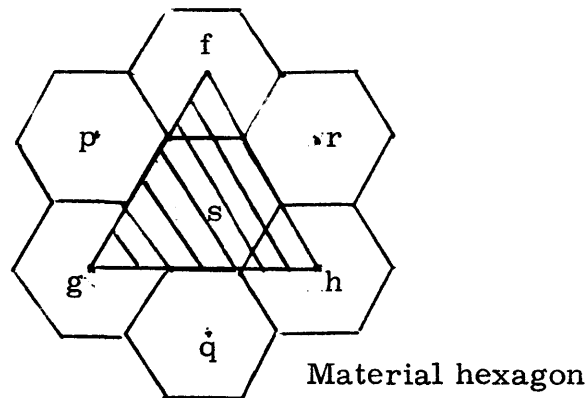
Fig. 4.12. 2-D triangular Neumann problem.

In the case of the physical mesh we rely on the variational principle to force the satisfaction of the natural condition $\frac{\partial\phi}{\partial n} = 0$ along the sides of the triangle. For the mathematical coarse mesh case of Fig. 2.6(b) we impose more conditions: we force $a_{pg} = a_{sg} = a_{qg} = a_{rg}$ and $a_{fg} = a_{hg}$, so the two computational problems are not strictly identical. However, the results do show that for the physical mesh the Neumann problem is unstable. This can be seen from Table 4.10. The error in the eigenvalue λ for $h = 57.73$ cm is due to the positive off-diagonal elements in the $[(D\nabla\psi_i, \nabla\psi_j) + (\Sigma_r\psi_i, \psi_j)]$ matrix. The positive sign

Table 4.10. Centering scheme. Eigenvalue λ and supercoefficients $\{a_{kg}\}$. Physical mesh 2-group 2-D homogeneous triangular Neumann problem (Fig. 4.12).

#	Type of Calculation	λ	a_{gg}*	a_{pg}	a_{sg} $\begin{bmatrix}\text{group 1}\\\text{group 2}\end{bmatrix}$
1	Analytic	0.14507	5.699	0.0	5.699
			1	0	1
2	†$h = 57.73$ cm	1.001314	-0.33106	0.514271	-0.120298
			-0.88094×10^{-1}	0.136844	-0.320105×10^{-1}
3	$h = 10$ cm	0.145068	0.165399	0.838760×10^{-8}	0.165399
			0.290199×10^{-1}	0.147163×10^{-8}	0.290199×10^{-1}
4	$h = 0.1$ cm	0.144688	0.164982	0.836647×10^{-8}	0.164982
			0.289221×10^{-1}	0.146668×10^{-8}	0.289221×10^{-1}
5	$h = 0.0001$ cm	0.184894×10^{-4}	0.184931×10^{-4}	0.937814×10^{-12}	0.184931×10^{-4}
			0.377419×10^{-8}	0.191394×10^{-15}	0.377419×10^{-8}

*As no attempt is made to standardize the normalization of the supercoefficient sets $\{a_{kg}\}$, it is the ratio of the coefficients which is to be considered of significance.

†
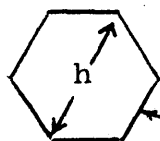
Fuel block

Table 4.11. Centering scheme. Eigenvalue λ and supercoefficients $\{a_{kg}\}$. Mathematical mesh 2-group 2-D homogeneous triangular Neumann problem (Fig. 4.12).

#	Type of Calculation	λ	a_{gg} *	a_{sg}	a_{fg} (group 1, group 2)
1	Analytic	0.14507	5.699	5.699	5.699
			1	1	1
2	$^\dagger h = 46.188$ cm	0.145077	0.165439	0.165439	0.165439
			0.029027	0.029027	0.029027
3	$h = 1.0$ cm	0.145077	0.165439	0.165439	0.165439
			0.029027	0.029027	0.029027
4	$h = 0.1$ cm	0.145077	0.165439	0.165439	0.165439
			0.029027	0.029027	0.029027
5	$h = 0.0001$ cm	0.145080	0.165442	0.165442	0.165442
			0.029028	0.029028	0.029028

*As no attempt is made to standardize the normalization of the supercoefficients $\{a_{kg}\}$, it is the ratio of the coefficients which is to be considered of significance.
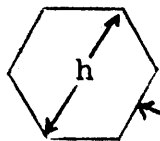
†
Fuel block

Table 4.12. Centering scheme. Eigenvalue λ — 2-group 2-D bench-
mark problem. Fully rodded set I.

Number	Type of Calculation	λ
1	BUG-180[*] — Finest mesh. Finite difference (reference solution)	0.7708[†]
2	Physical mesh — 2-element incomplete cubic set	0.5151[†‡]
3	Mathematical mesh (coarse) — 2-element incomplete cubic set	0.6918

[*]GA code. The mesh scheme used in BUG-180 is shown below in Fig. 4.13. The mesh spacing is half that of the one used in GAUGE. BUG-180 uses a logarithmic boundary condition. To simulate the condition of flux equal to zero on the boundary, a large negative number is input for the logarithm.

[†]Boundary fitted exactly.

[‡]Answer not converged — 50 iterations.
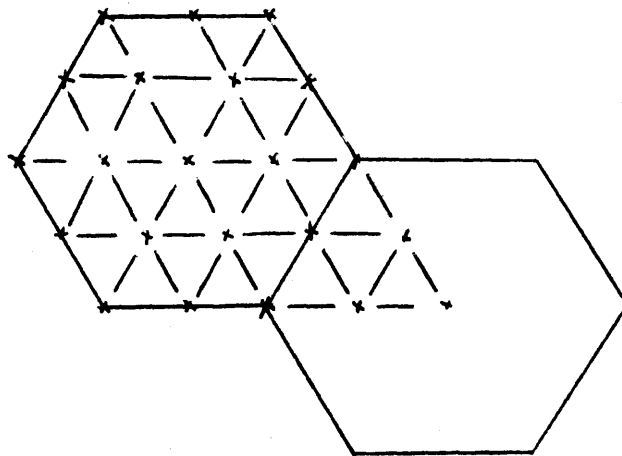
Fig. 4.13. Mesh scheme — BUG-180 code.

occurs when h becomes larger than a critical value. One can no longer

guarantee positive solution vectors a_g,[4] and for this case the flux

solution $\hat{\phi}$ indeed does have negative values. For h very small, round-

off error enters into the solution.[20,21] This, however, does not explain

the drift in the eigenvalue λ which occurs between (3) and (4). The prob-

lem seems to be unstable. Corresponding results for the mathematical

mesh are shown in Table 4.11. Note that the drift does not seem to occur

here. Insofar as the two cases are comparable, the mathematical mesh

appears to be preferable.

Table 4.12 presents results obtained for the benchmark problem

using the 2-element incomplete cubic set. The cross sections used are

those of the fully rodded set I. There again appears to be numerical

problems with the physical mesh. The calculation still had not con-

verged after 50 iterations whereas for the mathematical mesh only

25 iterations were required. In both cases the convergence criterion

was 10^{-6} on λ. Comparison of the first five converged figures shows that

as far as accuracy is concerned the mathematical mesh is again preferred.

Let us examine the physical mesh more closely. In Fig. 4.14 we
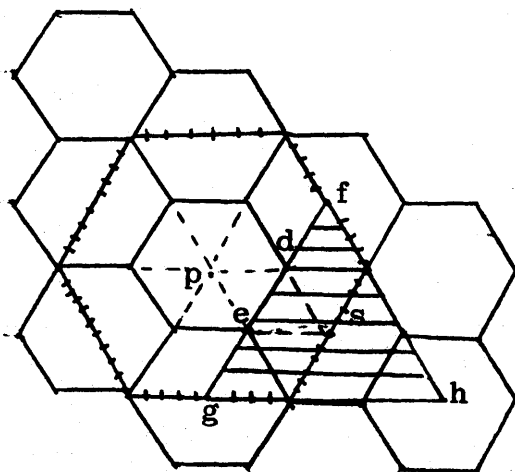
Fig. 4.14.

2-D triangular Neumann problem —
closer examination of physical mesh.

draw in the superpatch Θ_J centered on p. The basic patch is the triangle sde. If we use the C_1 set, it can be seen that there is a piecewise linear dependency over the basic patch, as the basic element function set $\{\Psi_{ig}^{\Delta sde}\}$ consists of four linear functions.

For the 2-element incomplete cubic set, it can be shown that piecewise linear dependency also occurs when the physical mesh is used. The current functions centered on p and s are identical over triangle sde. This is because the current function is a hyperbolic paraboloid and the plane of symmetry for the ones centered on p and s is the plane perpendicular to the paper passing through the line de.

We conjecture that the unstable behavior which occurred with the use of this mesh for the Neumann problem of Fig. 4.12 is attributable to this piecewise linear dependence.

The physical mesh was consequently dropped from further consideration and the results presented in the following sections were all obtained using the mathematical mesh approach.

(ii) Incompleteness

Table 4.13 is a comparison of the totally incomplete sets and the shell sets. These results indicate that one should have at least $\overline{P}_1$ completeness. As variables are added they should be added so that the defect of the space is decreased for the complete sets are to be preferred. The interpretation in terms of physical quantities such as flux and current is of secondary importance to this principle of completeness and the 1-D results of the preceding section should be so construed.

Table 4.13. Eigenvalue λ for various superelement function sets $\{\psi_{kg}\}$. 2-group 2-D benchmark problem. Fully rodded set I.

Number	Type of Calculation	λ
1	BUG-180 — finest mesh. Finite difference (reference solution)[†]	0.7708
2	Coarse mesh — C_1 shell set	0.7695
3	Coarse mesh — $(C_1 + C_2)$ shell set	0.7743
4	Coarse mesh — regular quadratic set	0.7743
5	Coarse mesh — 1-element cubic incomplete set	0.6699
6	Coarse mesh — 2-element cubic incomplete set	0.6918
7	Coarse mesh — 3-element cubic incomplete set	0.6975
8	Coarse mesh — 3-element 9th-order incomplete set	0.2504

[†]Boundary fitted exactly.

It is of interest to note that the two complete quadratic sets, the $(C_1 + C_2)$ shell set and the regular quadratic set, yield identical answers for λ. Table 4.13 shows that both sets give 0.7743 for λ. The two sets lead to the same number of unknowns.

(iii) Conditions of Join

Table 4.13 shows that given a construction which imposes function continuity, additional degrees of continuity in imposing a join are of minor importance compared to reduction of the defect of the space. This

can be seen by comparing the 3-element 9th-order incomplete set result with the 3-element cubic incomplete set result. The 9th-order set leads to a $\hat{\phi}$ with normal current continuity whereas the cubic set does not. As was mentioned in earlier chapters there is a direct trade-off between conditions of join and defect of space. This result points to lower order spaces with smaller defects.

It should be mentioned that the apparent anomaly in Table 4.13, the convergence of the shell set's results to an answer different from that of the reference BUG-180 solution is due to the inexact fit of the boundary.

(iv) High-Order Space Coarse-Mesh versus Low-Order Space Fine-Mesh

Answers to this question have a limited range of extrapolation as it really depends on what flux shape is being approximated. The choice is between using the fine mesh of Fig. 2.6(a) with a complete linear space and the coarse mesh of Fig. 2.6(b) with a complete quadratic space. The results are shown in Table 4.14. A word is in order here regarding the 'interface distortion' qualifier used in Table 4.14. The 'interface distortion' refers to the use of irregular polygons at the core-reflector interface. At the core-reflector interface the difference in diffusion coefficients is a maximum with the ratio being of the order of ~0.67. The use of the irregular polygons precludes the situation of having a smooth polynomial defined across the interface and hence precludes the imposition of derivative continuity at the interface. The mesh used for these 'interface distortion' calculations is shown in Fig. 4.15.

Table 4.14. High order space — coarse mesh versus low order space — fine mesh. Eigenvalue λ — 2-group 2-D benchmark problem.

| # | Type of Calculation | Fully Rodded | | Fully Unrodded |
		Cross Section I	Cross Section II	
1	BUG-180 — finest mesh — finite difference (reference solution)	0.77088	0.77891	0.99869
2	*GAUGE — fine mesh — finite difference	0.76903	0.77643	1.0043
3	*GAUGEFEM — fine mesh — C_1 shell set	0.76382	0.77184	0.99889
4	Coarse mesh — C_1 shell set (without interface distortion)		0.76499[†]	
5	Coarse mesh — C_1 shell set (with interface distortion)	0.7595[†]	0.76805[†]	
6	Coarse mesh — $(C_1{+}C_2)$ shell set (without interface distortion)		0.76745	
7	Coarse mesh — $(C_1{+}C_2)$ shell set (with interface distortion)	0.7598	0.76842	0.99742

*GA codes.
GAUGEFEM is the fine mesh-linear space finite element version of GAUGE. Except for differences in the coarse mesh rebalance section the two codes are algorithmically identical.

[†]Negative fluxes obtained.
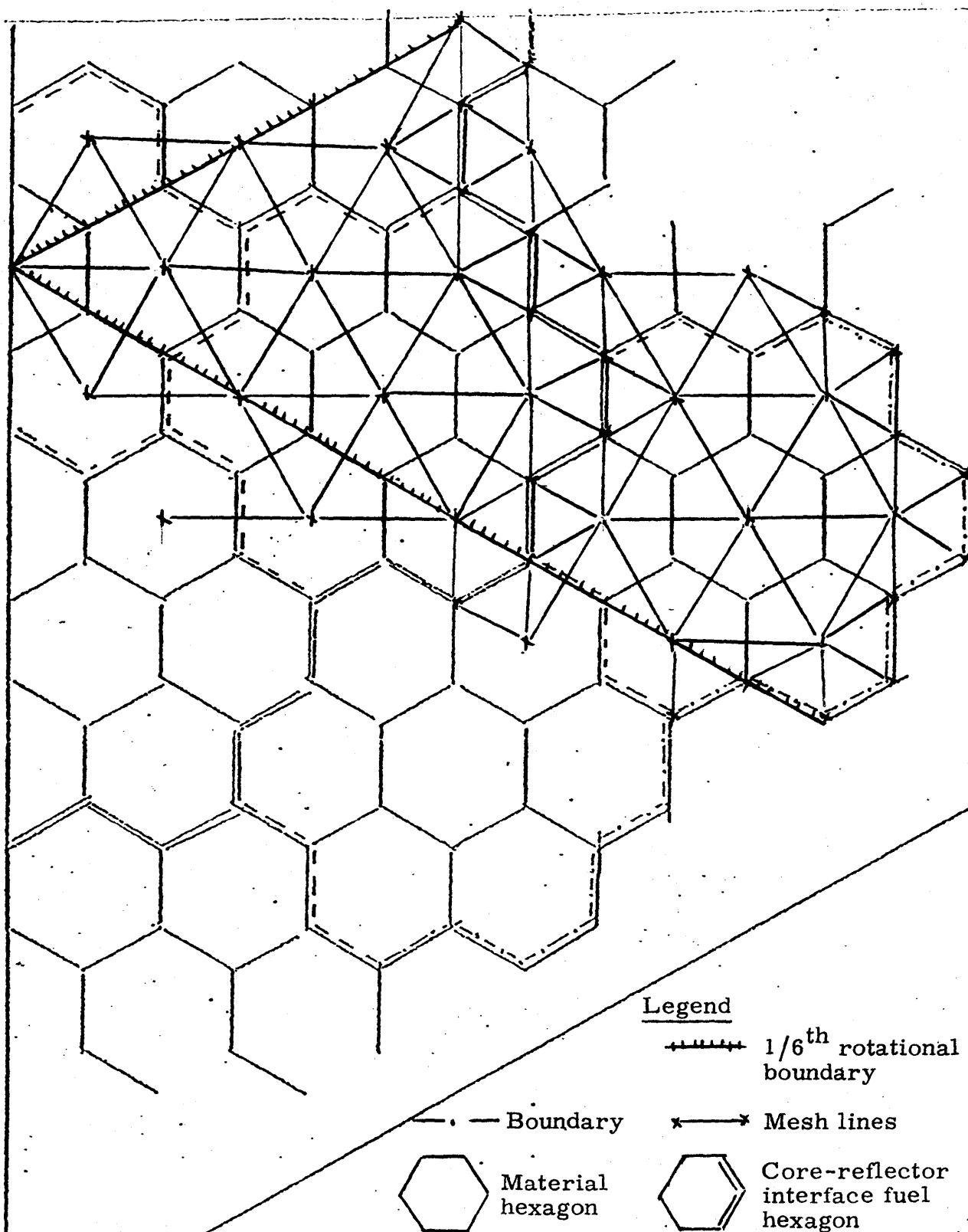
Fig. 4.15. 1/6th sector small HTGR – 2-D benchmark problem. Coarse mesh – boundary exact fit. Interface distortion.

Fig. 4.15. 1/6th sector small HTGR – 2-D benchmark problem. Coarse mesh – boundary exact fit. Interface distortion.

Apparently for flux shapes comparable to the one of the benchmark problem, the fine-mesh linear space approach is to be preferred to the coarse-mesh perturbation quadratic one. For the fully unrodded case all the calculations do well. Comparatively speaking, the fully unrodded case is a less demanding problem.

Figures 4.16 and 4.17 provide an idea of the fast and thermal flux shapes which have to be approximated for the fully rodded case II. The values shown are from the reference BUG-180 solution.

Figure 4.18 is a comparison of power peaking factors for the fully rodded problem II. The perturbation quadratics lead to errors of ~6% for the control rod blocks and less than ~1% for the other core fuel blocks. The fine mesh linear space option GAUGEFEM has an error of ~2% in the control rod blocks and less than 1/2% for the other fuel blocks. GAUGE is in error by ~4% in the central control rod block and less than 1/2% in the outer control block. The average error in the other blocks is ~3%. These power peaking factor results seem to point towards the finite element schemes with the fine-mesh linear space approach favored. The eigenvalue results, however, are in favor of GAUGE. The GAUGE eigenvalue is in error by 0.32%, that of GAUGEFEM by 0.91%. The error with the coarse mesh-perturbation quadratics is 1.34%.

Figure 4.19 is a comparison of power peaking factors for the fully unrodded case. All the approaches do quite well with this problem. It

---

†Power peaking factor ≡ region averaged power density/core average power density.
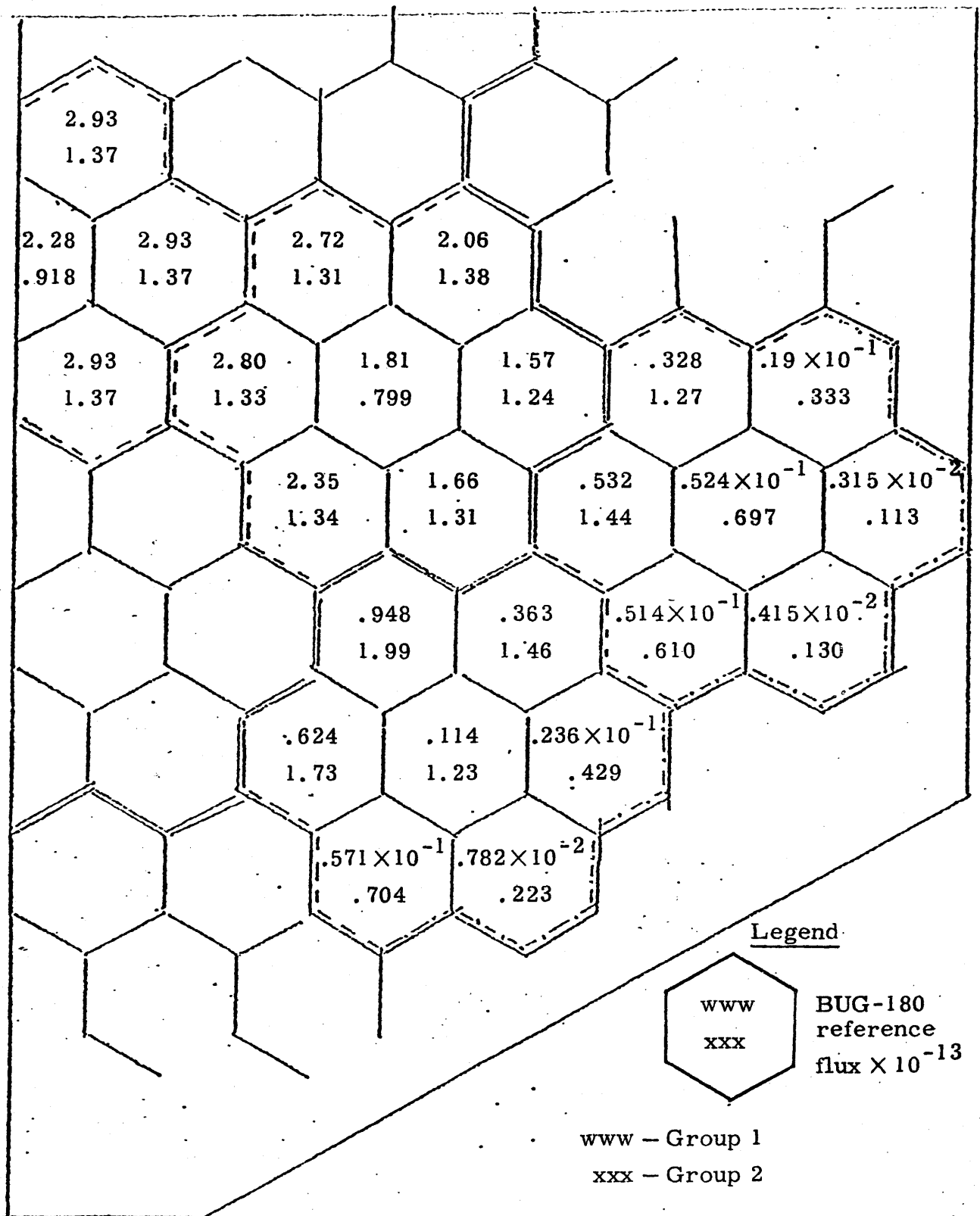
Fig. 4.16. 2-group 2-D benchmark problem — fully rodded set II. Material hexagon averaged flux. Core power = 26.666 MW.

$\times 10^{-13}$

3.08
2.42
1.47
1.01

2.53   3.08   3.06   2.61
2.04   2.47   2.12   1.30
1.09   1.47   1.47   1.94
.758   1.01   .983   .886

3.08   3.08   2.29   1.89   .975
2.42   2.21   1.59   .94 $.623 \times 10^{-1}$ $.662 \times 10^{-1}$
1.47   1.47   1.01   1.57   1.59 $.272 \times 10^{-5}$
1.01   1.00   .652   .833   .781   .809
                                                            $.56 \times 10^{-4}$

        2.82   2.06   1.48   .188 $.139 \times 10^{-1}$
        1.86   .99 $.977 \times 10^{-1}$ $.876 \times 10^{-2}$ $.419 \times 10^{-6}$
        1.79   1.78   1.58   1.23   .374
        .906   .852   1.00   .293 $.178 \times 10^{-4}$

                .206   1.15   .197 $.206 \times 10^{-1}$
                .272 $.67 \times 10^{-1}$ $.168 \times 10^{-4}$ $.536 \times 10^{-6}$
                2.20   1.9   1.28   .459
                1.61   .847 $.293 \times 10^{-3}$ $.201 \times 10^{-4}$

                1.64   3.17 $.815 \times 10^{-1}$
                .126 $.244 \times 10^{-1}$ $.334 \times 10^{-5}$
                2.07   1.87   1.08
                1.32   .611 $.718 \times 10^{-4}$

                        .203 $.314 \times 10^{-1}$
                        $.219 \times 10^{-4}$ $.107 \times 10^{-5}$
                        1.36   .688
                        $.335 \times 10^{-3}$ $.358 \times 10^{-4}$

Legend

| www |
| xxx |
| yyy |
| zzz |

BUG-180 reference flux $\times 10^{-13}$

www – Group 1 maximum
xxx – Group 1 minimum
yyy – Group 2 maximum
zzz – Group 2 minimum

Fig. 4.17. 2-group 2-D benchmark problem – fully rodded set II. Material hexagon maximum and minimum flux. Core power = 26.666 MW.

Legend

www	
xxx	Power
yyy	peaking
zzz	factors

www — GAUGE
xxx — BUG-180
yyy — GAUGEFEM
zzz — Coarse mesh-(C_1+C_2) shell set
(with interface distortion)
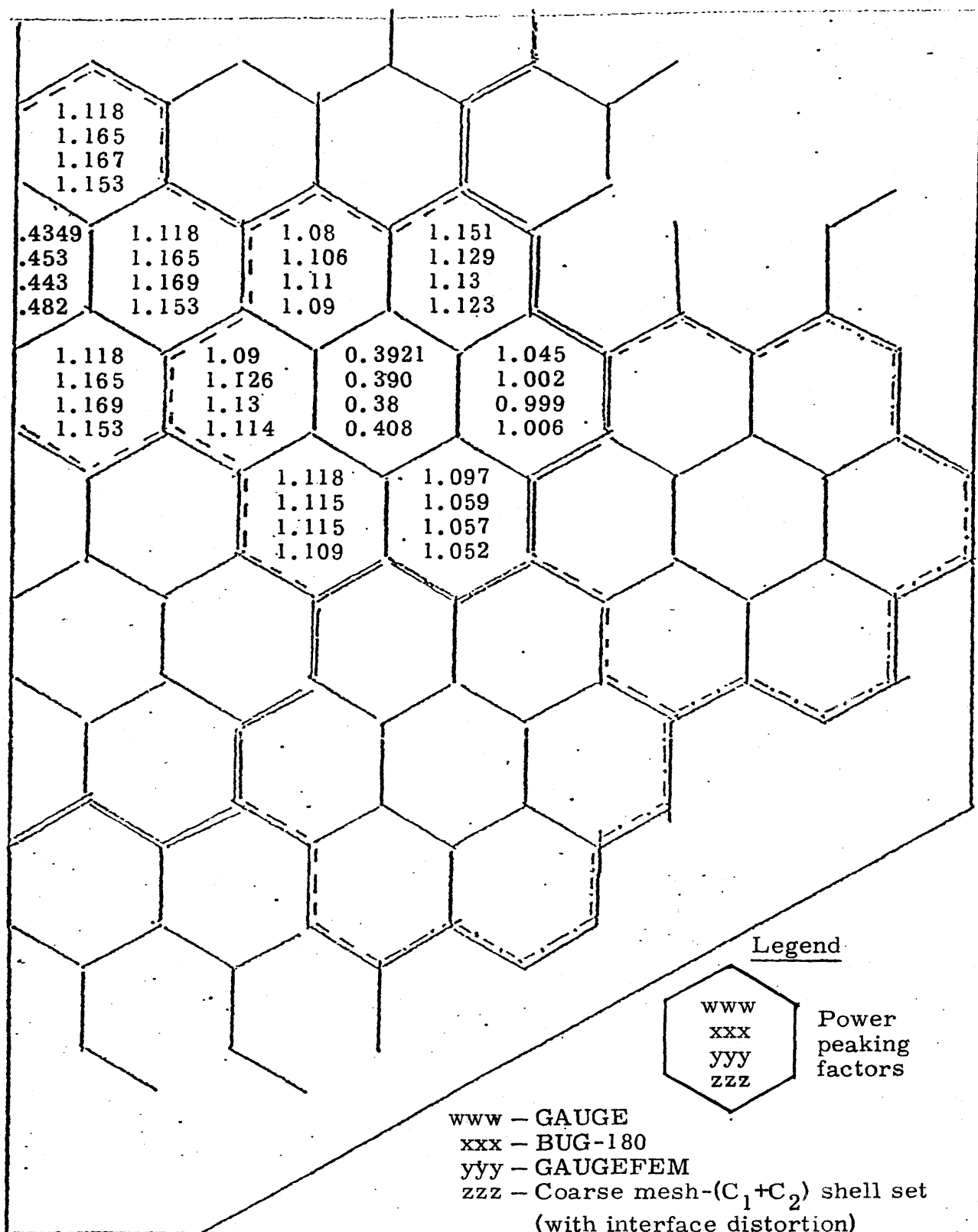
Fig. 4.18. 2-group 2-D benchmark problem — fully rodded set II. Material hexagon power peaking factor.

1.1498	
1.174	
1.1786	
1.182	

.732	1.1498	1.071	1.0686
.752	1.174	1.081	1.058
.758	1.1786	1.085	1.055
.751	1.182	1.083	1.057

1.1498	1.091	0.6199	0.9661
1.174	1.107	0.621	0.945
1.1786	1.1098	0.6228	0.9397
1.182	1.111	0.614	0.942

1.0683	1.0097
1.065	0.991
1.064	0.9868
1.064	0.989

Legend

| www |
| xxx |
| yyy |
| zzz |

Power peaking factors

www — GAUGE
xxx — BUG-180
yyy — GAUGEFEM
zzz — Coarse mesh-(C_1+C_2) shell set
(with interface distortion)
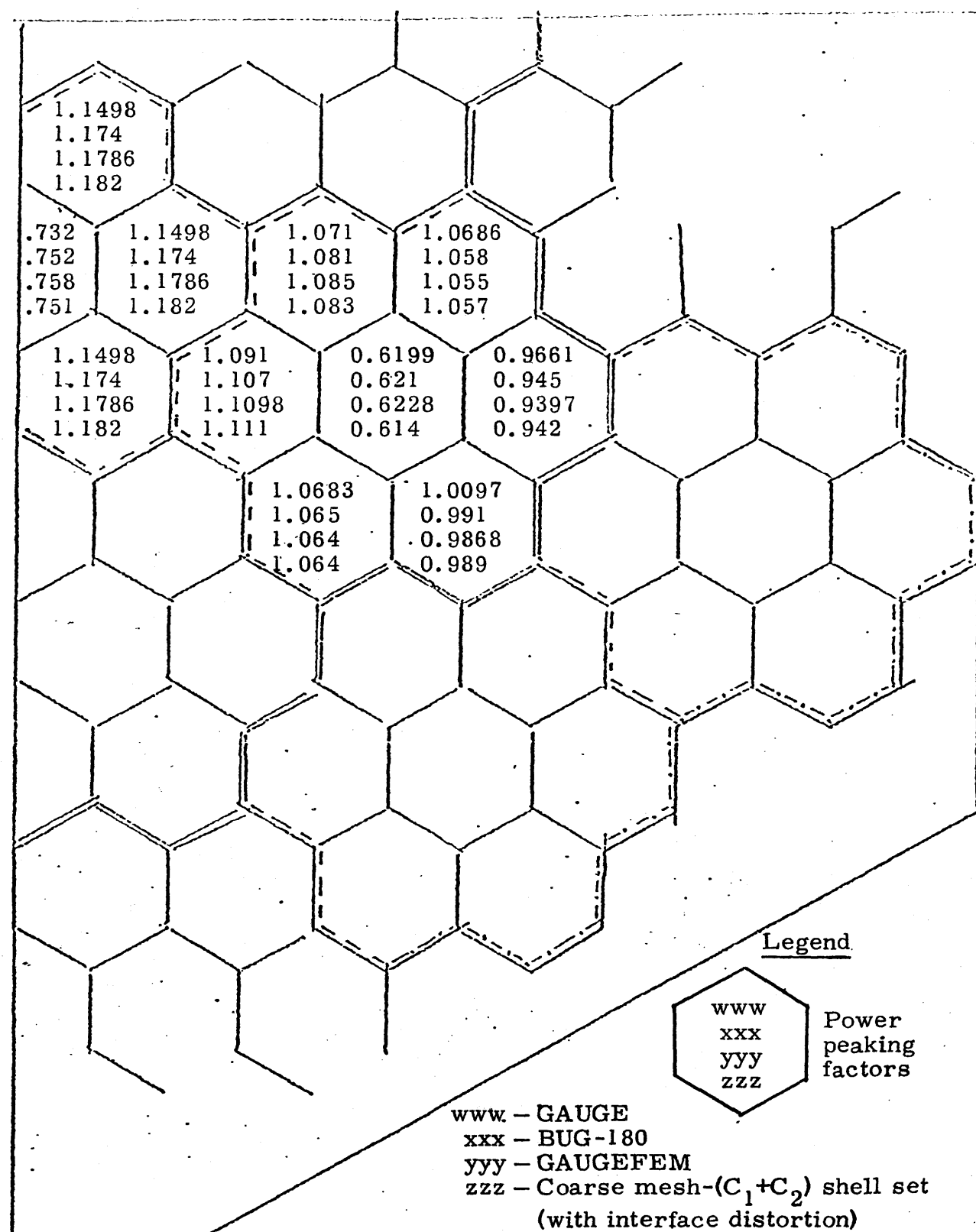
Fig. 4.19. 2-group 2-D benchmark problem — fully unrodded. Material hexagon power peaking factor.

is not as demanding as the fully rodded case. When the power peaking factors are compared GAUGE appears to do the worst. Towards the center of the core the error is ~2%. Elsewhere the error is comparable with the finite element results being of the order of less than 1%. The eigenvalues are also very close. GAUGE is off by 0.56%, GAUGE-FEM by -0.02% and the coarse mesh-perturbation quadratics by 0.12%.

The results indicate that GAUGE is to be preferred over the finite element approaches as the finite element schemes do not give acceptable eigenvalues for the fully rodded case II. It also appears that the fine-mesh linear space is preferable to the coarse-mesh perturbation quadratic approach. Interestingly enough, the finite element technique seems to give better flux results than eigenvalues. Kang[1] has shown that with Hermite elements in rectangular geometry, the error in the flux is of order higher than that of the eigenvalue. These results reinforce the impression that the flux is better approximated in the finite element scheme.

Let us conclude this section by commenting on the negative flux cases of Table 4.14.

The negative fluxes obtained for the coarse mesh-linear set are due to the positive off-diagonal elements in the $[(D \, \nabla \psi_i, \nabla \psi_j) + (\Sigma_r \psi_i, \psi_j)]$ matrix introduced by the use of the irregular polygons to fit the boundary and interface exactly. Consider the isosceles triangle ABC of Fig. 4.15.

$$\nabla \psi_{Ag} \cdot \nabla \psi_{Bg} > 0$$

as the angle between $\nabla \psi_{Ag}$ and $\nabla \psi_{Bg}$ is less than $\pi/2$. This means that

these off-diagonal elements can never be negative as $(\psi_{Ag}, \psi_{Bg}) > 0$. One can not therefore guarantee positive solution vectors a_g.[4]

4.1.2 Computation Time

The computation phases which could lead to significant differences in computation time for the various approaches would be

(i) Assemblage of the equations

(ii) Solution of the equations.

For large problems phase (ii) would dominate and we shall only consider this phase.

Let us assume that phase (i) ends with the assemblage of the matrices A_g and M_g of the following equation,

$$A_g \underline{\phi}_g = \frac{1}{\lambda} M_g \underline{\phi}_g.$$ (4.4)

This is the preparatory form for the power iteration technique.

The mathematical mesh approach and the hexagonal superpatch leads to a 7 'block' point relationship in both A_g and M_g. Each block consists of n elements where n is the number of variables 'centered' on the center of a superpatch. Let

t_m = multiplication time of processing unit

t_a = addition time of processing unit

N_E = total number of variables

K_E = number of inner iterations per source iteration.

Then T_E, the computation time/source iteration for the finite element method, is

$$T_E \cong N_E[7(nt_m + t_a(n-1)) + 6t_a](K_E + 1). \qquad (4.5)$$

For the finite difference scheme implemented in GAUGE, A_g has a 7 point relation but M_g is diagonal. The computation time/source iteration, T_F, in this case is

$$T_F \cong N_F[(7t_m + 6t_a)K_F + t_m] \qquad (4.6)$$

where

N_F = total number of variables for this scheme

K_F = number of inner iterations per source iteration.

When multiplication time dominates we have that

$$\frac{T_E}{T_F} = \frac{N_E}{N_F} \cdot \frac{7n(K_E + 1)}{7K_F + 1} . \qquad (4.7)$$

For the fine mesh-linear space approach of GAUGEFEM, $n = 1$ and we have for $K_E \sim 1$ and $K_F \sim 1$,

$$T_E \sim 1.75 \, T_F. \qquad (4.8)$$

This is a conservative estimate as when K_E and $K_F \gg 1$ we have

$$\frac{T_E}{T_F} \sim n.$$

Equality of T_E and T_F when $n = 1$ is then the lower bound.

Table 4.15 is a tabulation of timing statistics which compare GAUGE and GAUGEFEM for the 1/6th small HTGR problem. They bear out the general features of eq. (4.8). It is of interest to note that the number

Table 4.15. Timing statistics. GAUGE (low-order finite difference) compared with GAUGEFEM (low-order space — fine mesh finite element) — 2-group 2-D benchmark problem.

	Case	Problem Time (sec)	Diffusion Calculation Time (sec)	Number of Source Iterations	Sec/Source Iteration
1	Fully unrodded				
	GAUGE	5.25	1.194	19	0.06
	GAUGEFEM	6.64	2.269	19	0.12
2	Rod 1 in				
	GAUGE	4.78	1.252	21	0.059
	GAUGEFEM	5.44	1.825	18	0.101
3	Rod 2 in†				
	GAUGE	4.95	1.32	22	0.06
	GAUGEFEM	6.88	3.249	23	0.14
4	Fully rodded†				
	GAUGE	5.10	1.453	24	0.06
	GAUGEFEM	6.64	3.119	23	0.135

Convergence criteria 10^{-5} on flux.

†Significant difference in number of rebalance iterations between GAUGE and GAUGEFEM calculations.

of source iterations are roughly equal. This means that T_E/T_F will also be the ratio of the total phase (ii) time. The number of source iterations for the coarse mesh-perturbation quadratic set is comparable ~25 with a convergence criterion of 10^{-6} on the flux and the eigenvalue.

For the perturbation quadratic set when $K_E \sim 1$ and $K_F \sim 1$ we have that

$$\frac{T_E}{T_F} = \frac{N_E}{N_F} \cdot \frac{28}{8} \sim \frac{2}{3} \cdot \frac{28}{8} = 2.3$$

so

$$T_E \sim 2.3 \, T_F. \tag{4.9}$$

This means that as far as computation time is concerned unless the number of source iterations is significantly less, the perturbation quadratic set is inferior to GAUGEFEM and to GAUGE. It should be pointed out that this is a comparatively conservative estimate as when $K_E, K_F \gg 1$ we have $T_E \sim 1.3 \, T_F$. If we assume that we can extrapolate the statistics of Table 4.15, then $T_E/$variable $\sim 1.75 \, T_F/$variable. This means that for the perturbation quadratic set,

$$T_E \sim 1.75 \, T_F \cdot \frac{2}{3} \sim 1.1 \, T_F.$$

GAUGE still takes less time.

4.2 Conclusions

This thesis was concerned with the solution of the static neutron-diffusion equation, eq. (1.1) in hexagonal geometry, using the finite element method. The choice of the finite element method prescribed

the use of the Galerkin equations, eq. (1.16), to calculate the approximation $\hat{\phi}_g(\underline{r})$. With the choice of the equations for the approximation scheme so made, we concentrated on the formulation of the approximation space M_m.

Given the prescribed constraints on accuracy and computation time, the results presented in section 4.1 allow us to draw the following conclusions regarding the construction and application of approximation spaces.

(a) The mathematical mesh is to be preferred over the physical mesh.

(b) It is important to span at least the $\overline{P}_1$ space. One should try for complete spaces over incomplete ones. The order of the highest complete space which can be spanned given the constraint on the number of variables should be maximized.

(c) Function continuity has to be imposed across the join. However, once we have function continuity across the join, it is much more important to reduce the defect of the space than to increase the degree of continuity across the join.

(e) For small HTGR problems, the fine mesh-linear space approach should be chosen over the coarse mesh-perturbation quadratic one.

Given our results comparing the low order finite difference method, as implemented in GAUGE, with our various finite element schemes it is very tempting to draw the conclusion that for hexagonal geometry the finite element method can not be regarded as a viable alternative to

low order finite difference. Our results certainly do point in that direction but a word of caution is necessary here. The small HTGR benchmark problem used here is a relatively exacting problem. For larger problems, problems which would be more frequently met, the flux shape should be more smooth, the system should be less leaky, and the boundary less significant. For LMFBR problems there should be less 'peaking'. In other words, our benchmark problem is probably at the more difficult end of the spectrum. It is recommended, and specific ideas will be proposed in the next section, that further work be done before such a significant statement is made.

4.3 Recommendations

As a direct continuation of the sentiments expressed in the previous paragraph, we suggest the following.

(i) LMFBR problems should be examined and then larger problems should be investigated. To lend some order to the analysis, it would be useful to identify dimensionless parameters which characterize flux shapes: numbers such as the ratio of the diffusion length to the mesh size; the ratio of material properties in adjoining regions. One would then be able to produce a more quantitative analysis of the range for which one approach is to be preferred over another.

(ii) The use of the Lagrangian quadratics should be investigated. The extra '1/2' degree of freedom per triangle may produce greater accuracy than the perturbation quadratic set. It would then remain to be seen if this is compensated by the increase in computation time.

(iii) The shell sets open up the possibility of having variable accu-
racy without changing mesh size by simply changing the number of func-
tions 'centered' at the superpatch centers. Analytical work proving or
refuting the conjecture that the accuracy in θ_j is related to the order of
the highest complete space of M_{m_j} would be welcome.

(iv) A general theory of space construction, as discussed in sec-
tion 2.1 relating the number of sides of Θ_j, the degree of the join, and
the order of the polynomial would be a valuable tool for synthesis.

(v) Finally it appears that more work will have to be done about
techniques to solve the Galerkin equations. As discussed in section 4.1.2,
the possible reduction in the number of variables by using higher order
methods is accompanied by an increase in complexity of the equations
to be solved.

For large problems iterative techniques have to be used and for the
range of interest of this thesis it appears that less computation time
per iteration is required by the low order finite difference method. This
means that the finite element method will have to resolve to iterative
techniques which require fewer iterations.

We suggest one possible iterative technique. This is to tie all the
functions 'centered' at one superpatch center together and solve simul-
taneously for the coefficients of these suprafunctions. The functions at
each center are then untied and solved simultaneously center by center
and the cycle is repeated. This has similarities to the concepts of coarse
mesh rebalance and may aid in reducing the computation time involved.

BIBLIOGRAPHY

1. C. M. Kang and K. F. Hansen, "Finite Element Methods for Space-Time Reactor Analysis," M.I.T. 3903-5, Nov. 1971.

2. L. O. Deppe and K. F. Hansen, "The Finite Element Method Applied to Neutron Diffusion Problems," M.I.T. COO-2262-1, Feb. 1973.

3. J. C. Jacquin, "Application of the Finite Element Method to Heterogeneous Reactor Configurations," S. M. thesis, M.I.T., Sept. 1973.

4. E. L. Wachpress, _Iterative Solution of Elliptic Systems. An Application to the Neutron Diffusion Equations of Reactor Physics_, Prentice-Hall, Inc., Englewood Cliffs, N.J. (1966).

5. M. Clark, Jr. and K. F. Hansen, _Numerical Methods of Reactor Analysis_, Academic Press, N.Y. (1964).

6. H. G. Kaper, G. K. Leaf and A. J. Lindman, "Applications of Finite Element Methods in Reactor Mathematics. Numerical Solution of the Neutron Diffusion Equation," ANL-7925, Feb. 1972.

7. G. J. Fix and G. Strang, _An Analysis of the Finite Element Method_, Prentice-Hall, Inc., Englewood Cliffs, N.J. (1973).

8. S. G. Mikhlin, _Variational Methods in Mathematical Physics_, Pergamon Press, Elmsford, N.Y. (1964).

9. M. Zlamal, "On the Finite Element Method," Numer. Math. _12_, 394-409 (1968).

10. O. C. Zienkiewicz, _The Finite Element Method in Engineering Science_, McGraw-Hill, New York (1971).

11. G. Strang , "The Finite Element Method and Approximation Theory," _SYNSPADE 1970_, Ed. E. Hubbard, Academic Press, New York (1971).

12. I. Babsuka, "The Finite Element Method with Lagrangian Multipliers," Numer. Math. _20_, 179-192 (1973).

13. J. H. Bramble and A. H. Schatz, "Rayleigh-Ritz-Galerkin Methods for Dirichlet's Problem Using Subspaces Without Boundary Conditions," Comm. Pure Appl Math. 23, 653-675 (1970).

14. M. R. Wagner, "GAUGE, A Two Dimensional Few Group Neutron Diffusion-Depletion Program for a uniform triangular Mesh," GA-1307, General Atomic (1968).

15. J. P. Dorsey, et al., BUG-2/BUGTR1, "Two Dimensional Multigroup Burn Up Codes for Rectangular and Hexagonal Geometry," GA-8272, General Atomic (1969).

16. G. Strang, "Piecewise Polynomials and the Finite Element Method," Bulletin of the American Mathematical Society 79, 1128-1137 (1973).

17. A. Birkhofer, S. Langenbuch and W. Werner, "Coarse Mesh Method for Space-Time Kinetics," Trans. Am. Nucl. Soc. 18, 153 (1974).

18. M. Zlamal, "A Finite Element Procedure of the second Order of Accuracy," Numer. Math. 12, 394-402 (1968).

19. J. J. Goel, "Construction of basic functions for numerical utilization of Ritz's Method," Numer. Math. 12, 435-447 (1968).

20. J. H. Wilkinson, The Algebraic Eigenvalue Problem, Oxford Univ. Press, London (1965).

21. J. H. Wilkinson, Rounding Errors in Algebraic Processes, Prentice-Hall, Englewood Cliffs, N.J. (1963).

Appendix A

SETS OF MATERIAL CROSS SECTIONS USED

All the data presented are for two group calculations. The following assumptions are made.

(a) There is no upscattering.

(b) No fission neutrons are born in the thermal group.

The format of the Tables is $\left\{ \begin{array}{l} \text{group 1 value} \\ \text{group 2 value} \end{array} \right.$.

Table A.1. Cross Sections. 1-D numerical work of section 4.1.1(2).

$\nu = 2.43$

Problem	Composition	D (cm)	Σ_r (cm^{-1})	$\nu \Sigma_f$ (cm^{-1})	$\Sigma_{s2\leftarrow1}$ (cm^{-1})
Condition of join	Region 1	1.6835	5.768×10^{-3}	8.82×10^{-5}	1.83×10^{-3}
		1.29702	10.43×10^{-3}	1.46×10^{-3}	
	Region 2	1.65837	2.755×10^{-3}	9.15×10^{-5}	2.07×10^{-3}
		1.29702	2.49×10^{-3}	1.49×10^{-3}	
Incompleteness	Homogeneous slab	1.6835	5.768×10^{-3}	21.43×10^{-5}	1.83×10^{-3}
		1.29702	10.43×10^{-3}	3.547×10^{-3}	
Conditions within θ_j — homogeneous slab	Material I	1.6835	5.768×10^{-3}	21.43×10^{-5}	1.83×10^{-3}
		1.29702	10.43×10^{-3}	3.547×10^{-3}	
	Material II	As in Tbl. 4.8	5.768×10^{-3}	21.43×10^{-5}	1.83×10^{-3}
		1.29702	10.43×10^{-3}	3.547×10^{-3}	
Conditions within θ_j — block section problems	Material I	1.68350	5.678×10^{-3}	21.43×10^{-5}	1.83×10^{-3}
		1.29702	10.43×10^{-3}	3.547×10^{-3}	
	Material II	1.65837	2.755×10^{-3}	22.234×10^{-5}	2.07×10^{-3}
		1.29702	2.49×10^{-3}	3.6207×10^{-3}	

Table A.2. Cross Sections. 2-D numerical work of section 4.1.1(3).

$\nu = 2.43$

Problem	Composition	D (cm)	Σ_r (cm^{-1})	$\nu\,\Sigma_f$ (cm^{-1})	$\Sigma_{s2\leftarrow1}$ (cm^{-1})
Homogeneous triangular Neumann problem	Homogeneous material	1.68350	5.768×10^{-3}	21.43×10^{-5}	1.83×10^{-3}
		1.29702	10.43×10^{-3}	3.547×10^{-3}	
Benchmark problem Fully rodded set I	Core, rod in	1.6835	6.0749×10^{-3}	2.14326×10^{-4}	1.80×10^{-3}
		1.29702	1.01706×10^{-3}	3.54780×10^{-3}	
	Core, regular	1.47493	3.73399×10^{-3}	3.8637×10^{-4}	2.25×10^{-3}
		1.14155	3.96169×10^{-3}	6.1722×10^{-3}	
	Reflector	0.968992	4.98523×10^{-3}	0.0	4.98×10^{-3}
		0.789889	2.9600×10^{-4}	0.0	
Benchmark problem Fully rodded set II	Core, rod in	1.6835	5.9365×10^{-3}	2.14326×10^{-4}	1.83×10^{-3}
		1.29702	1.03×10^{-2}	3.5478×10^{-3}	
	Core, regular	1.47493	3.58649×10^{-3}	3.8637×10^{-4}	2.25×10^{-3}
		1.14155	4.07584×10^{-3}	6.1722×10^{-3}	

$\nu = 2.43$

Problem	Composition	D (cm)	Σ_r (cm^{-1})	$\nu \Sigma_f$ (cm^{-1})	$\Sigma_{s2 \leftarrow 1}$ (cm^{-1})
Benchmark problem Fully unrodded set	Reflector	0.968992	4.98523×10^{-3}	0.0	4.98×10^{-3}
		0.789889	2.9600×10^{-4}	0.0	
	Core, rod out	1.65837	2.92134×10^{-3}	2.22345×10^{-4}	2.07×10^{-3}
		1.29702	2.36030×10^{-3}	3.62070×10^{-3}	
	Core, regular	1.47493	3.58649×10^{-3}	3.86370×10^{-4}	2.25×10^{-3}
		1.14155	4.07584×10^{-3}	6.17220×10^{-3}	
	Reflector	0.968992	4.98523×10^{-3}	0.0	4.98×10^{-3}
		0.789889	2.9600×10^{-4}	0.0	

Appendix B

ANALYTIC EXAMINATION OF CURRENT CONTINUITY

VERSUS DERIVATIVE CONTINUITY

We solve here the two region 1 group 1-D problem shown in Figure B.1 for two cases,

   (a) one when derivative continuity is imposed at the interface L/2

   (b) the other where current continuity is imposed.
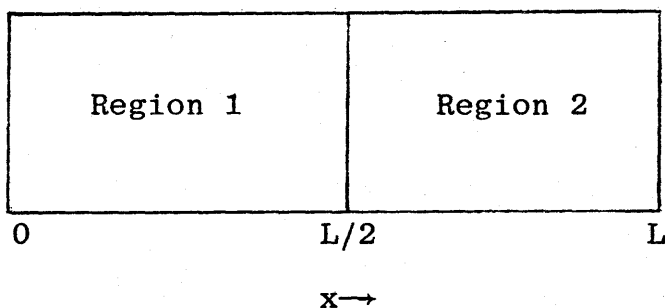
Fig. B.1.   1-D problem for analytic investigation of current continuity versus derivative continuity

Starting with the 1 group 1-D diffusion equation we have,

$$- \frac{d^2\phi}{dx^2} = \left[\nu \, \Sigma_f^j / \lambda - \Sigma^j \right] \frac{\phi}{D_j}$$

$$= k_j^2 \, \phi \qquad\qquad (B.1)$$

where

   j = region index

   $\Sigma = \Sigma_T - \Sigma_s$

and we have dropped the group notation for simplification.

The boundary conditions are

$\phi(0) = 0$

$\phi(L) = 0$.

We then have

$$
\phi = \begin{cases} \phi^1 = B_1 \sin k_1 x & 0 \le x \le L/2 & \text{(B.2)} \\ \phi^2 = B_2 \sin k_2(L-x) & L/2 \le x \le L & \text{(B.3)} \end{cases}
$$

Applying the continuity conditions at the interface,

function continuity: $B_1 \sin k_1 L/2 = B_2 \sin k_2 L/2$ (B.4)

derivative continuity: $B_1 k_1 \cos k_1 L/2 = -B_2 k_L \cos k_2 L/2$
    (B.5)

current continuity: $B_1 k_1 D_1 \cos k_1 L/2 = - B_2 k_2 D_2 \cos k_2 L/2$
    (B.6)

So, for case (a)

$$\frac{1}{k_1} \tan k_1 L/2 = - \frac{1}{k_2} \tan k_2 L/2 \quad , \tag{B.7}$$

for case (b)

$$\frac{1}{k_1 D_1} \tan k_1 L/2 = - \frac{1}{k_2 D_2} \tan k_2 L/2 \quad . \tag{B.8}$$

We shall now restrict ourselves to

$\nu \Sigma_f^1 = \nu \Sigma_f^2$

$\Sigma^1 = \Sigma^2$.

This means from (B.1) that

$$\frac{k_1}{k_2} = \left(\frac{D_2}{D_1}\right)^{1/2} \tag{B.9}$$

Equations (B.7) and (B.8) then reduce to

Case (a)

$$\tan \left(\frac{D_2}{D_1}\right)^{1/2} k_2 \frac{L}{2} = -\left(\frac{D_2}{D_1}\right)^{1/2} \tan k_2 \frac{L}{2} \tag{B.10}$$

Case (b)

$$\tan \left(\frac{D_2}{D_1}\right)^{1/2} k_2 \frac{L}{2} = -\left(\frac{D_1}{D_2}\right)^{1/2} \tan k_2 \frac{L}{2} \tag{B.11}$$

This means

$$k_2^d = d\left(\frac{D_2}{D_1}, L\right) = X_d\left(\frac{D_2}{D_1}\right) \frac{2}{L} \tag{B.12}$$

$$k_2^c = c\left(\frac{D_2}{D_1}, L\right) = X_c\left(\frac{D_2}{D_1}\right) \frac{2}{L} \tag{B.13}$$

$$k_1^d = d\left(\frac{D_1}{D_2}, L\right) = X_d\left(\frac{D_1}{D_2}\right) \frac{2}{L} \tag{B.14}$$

$$k_1^c = c\left(\frac{D_1}{D_2}, L\right) = X_c\left(\frac{D_1}{D_2}\right) \frac{2}{L} \tag{B.15}$$

where the subscripts and superscripts refer to:

d = derivative continuity

c = current continuity .

Now

$$\alpha = \text{fractional error in } \lambda = \frac{\lambda_c - \lambda_d}{\lambda_c}$$

$$= \nu \Sigma_f \left[\frac{1}{\left(c^2\left(\frac{D_2}{D_1}, L\right)D_2 + \Sigma\right)} - \frac{1}{\left(d^2\left(\frac{D_2}{D_1}, L\right)D_2 + \Sigma\right)} \right]$$

$$\left[\frac{c^2(D_2/D_1, L) + \Sigma}{\nu \Sigma_f} \right] \qquad (B.16)$$

So α can be written as,

$$\alpha\left(\frac{D_2}{D_1}, L, D_2\right) = D_2 \frac{(d^2 - c^2)}{(d^2 D_1 + \Sigma)}$$

$$= \frac{D_2 \left[X_d^2\left(\frac{D_2}{D_1}\right) - X_c^2\left(\frac{D_2}{D_1}\right) \right]}{\left[D_2 X_d^2\left(\frac{D_2}{D_1}\right) + \Sigma \frac{L^2}{4} \right]} \qquad . \qquad (B.17)$$

Define

$$\beta\left(\frac{D_2}{D_1}\right) = \left[1 - \left\{ \frac{X_c(D_2/D_1)}{X_d(D_2/D_1)} \right\}^2 \right]$$

$$= 1 - \theta\left(\frac{D_2}{D_1}\right) . \qquad (B.18)$$

Then

$$\alpha\left(\frac{D_2}{D_1}, L, D_2\right) = \alpha\left(\frac{D_2}{D_1}, \eta\right)$$

$$= \frac{\beta(D_2/D_1)}{\left[1 + \left\{ \frac{\eta}{2X_d(D_2/D_1)} \right\}^2 \right]} \qquad (B.19)$$

where

$$\eta(L_d, L) = \frac{1}{\left(\dfrac{D_2}{\Sigma}\right)^{1/2}} = \frac{L}{L_d} \quad . \tag{B.20}$$

It can be shown that the functions $\theta(D_2/D_1)$ and $\beta(D_2/D_1)$ have the following properties

$$\theta(D_2/D_1) = \theta(D_1/D_2)$$

$$\beta(D_2/D_1) = \beta(D_1/D_2) \quad .$$

We have thus identified the two dimensionless parameters of importance. These are D_2/D_1 and L/L_d , both of which appeal to the physical intuition. The functions $\beta(D_2/D_1)$, $X_d(D_2/D_1)$ and $X_c(D_2/D_1)$ are graphed in Figs. B.2 and B.3. Table B.1 is the tabular counterpart of these figures. Numerical results for $\alpha(D_2/D_1, \eta)$ are presented in Section 4.1.1.

We can extend the above calculation to errors in the flux. From equations (B.2) - (B.4) we can write for both (a) and (b),

$$\phi = \begin{cases} B_2 \dfrac{\sin k_2 L/2}{\sin k_1 L/2} \sin k_1 x & 0 \le x \le L/2 \\ \\ B_2 \sin k_2(L-x) & -L/2 \le x \le L \end{cases} \tag{B.21}$$

Normalizing so that
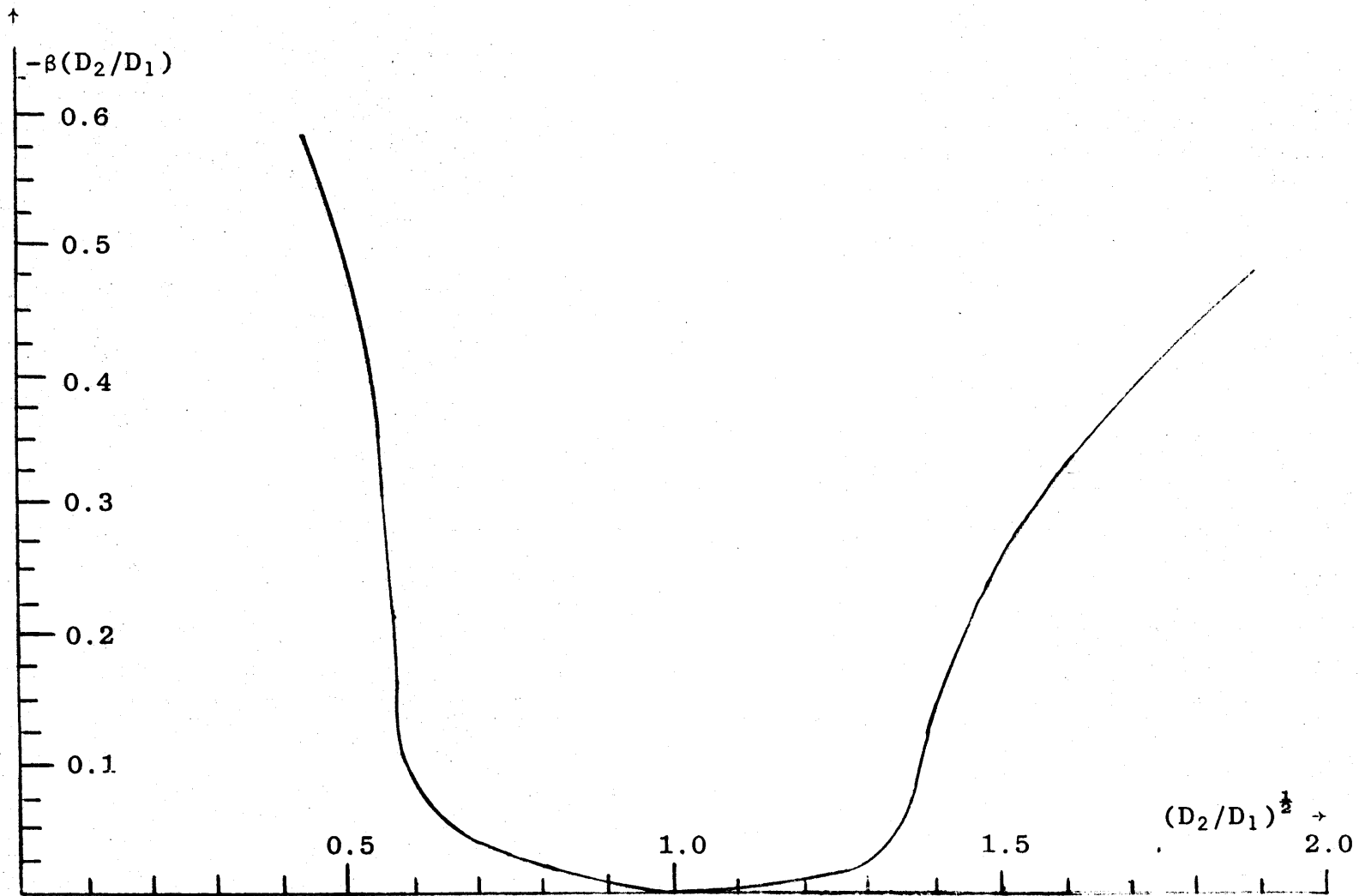
Fig. B.2.   The function $\beta(D_2/D_1)$ – For use in determining eigenvalue error.
1-Group 1-D 2-Region problem (Fig. B.1).
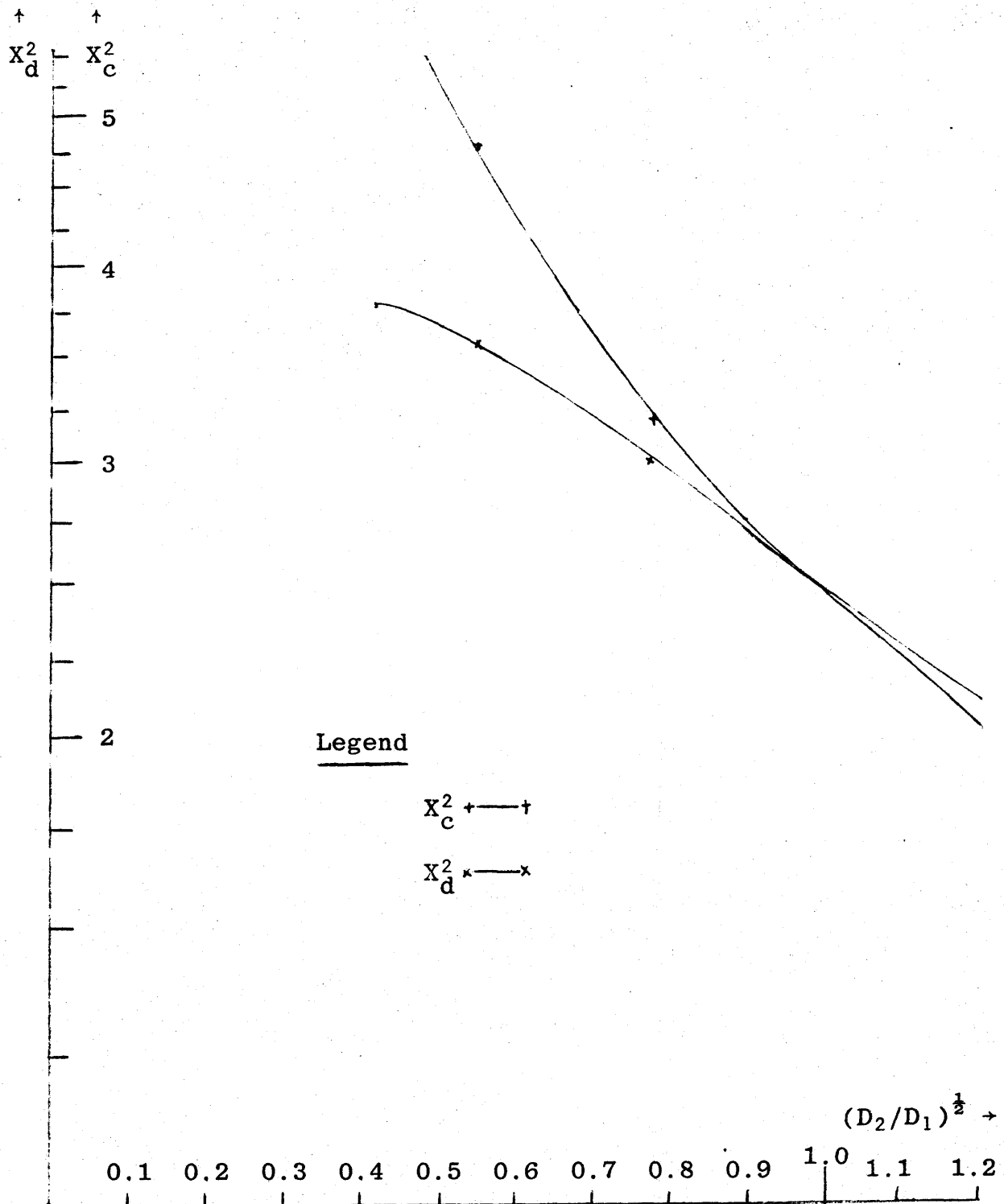
Fig. B.3.   The Functions $X_d^2(D_2/D_1)$; $X_c^2(D_2/D_1)$.   For use in
determining eigenvalue error.
1-Group 1-D 2-Region problem (Fig. B.1).

Table B.1. Tabulated values of the functions $X_d(D_2/D_1)$, $X_c(D_2/D_1)$ and $\beta(D_2/D_1)$ for use in eq. (B.19).

$\dfrac{D_2}{D_1}$	$\left(\dfrac{D_2}{D_1}\right)^{\frac{1}{2}}$	$X_d\left(\dfrac{D_2}{D_1}\right)$	$X_c\left(\dfrac{D_2}{D_1}\right)$	$-\beta\left(\dfrac{D_2}{D_1}\right)$
0.2	0.447	1.935	2.43	0.577
0.305	0.55	1.885	2.18	0.337
0.61	0.78	1.74	1.792	0.06
0.76	0.87	1.672	1.687	0.018
1.0	1.0	1.5709	1.5709	0.0
1.9	1.38	1.289	1.353	0.1017
6.1	2.47	0.79	1.032	0.706

$$\int_0^L \nu \, \Sigma_f \phi \, dx = A$$

we have

$$B_2 = \frac{A'}{\left[-\frac{1}{k} \frac{\sin k_2 \frac{L}{2}}{\sin k_1 \frac{L}{2}} (\cos k_1 \frac{L}{2} - 1) + \frac{1}{k_2} (1 - \cos k_2 \frac{L}{2}) \right]}$$

$$= \frac{A'}{\frac{L}{2} R(D_1/D_2)} \qquad\qquad (B.22)$$

where $A' = \dfrac{A}{\nu \Sigma_f}$.

Then the error in ϕ^1 is,

$$\varepsilon_1 = (B_{2d} \, a_d \, \sin k_1^d \, x - B_{2c} \, a_c \, \sin k_1^c \, x) \qquad\qquad (B.23)$$

where $a_j = \dfrac{\sin k_2^j \frac{L}{2}}{\sin k_1^j \frac{L}{2}}$

and the error in ϕ^2 is,

$$\varepsilon_2 = \left[B_{2d} \, \sin k_2^d (L-x) - B_{2c} \, \sin k_2^c (L-x) \right] \qquad\qquad (B.24)$$

For the fractional error we write,

$$E_1 = \frac{\varepsilon_1}{B_{2c} \, a_c \, \sin k_1^c x}$$

$$= - \left[1 - \frac{B_{2d}}{B_{2c}} \cdot \frac{a_d}{a_c} \cdot \frac{\sin k_1^d x}{\sin k_1^c x} \right] \qquad\qquad (B.25)$$

$$E_2 = \frac{\varepsilon_2}{B_{2c} \; \sin \; k_2^c (L-x)}$$

$$= - \left[1 - \frac{B_{2d}}{B_{2c}} \cdot \frac{\sin \; k_2^d (L-x)}{\sin \; k_2^c (L-x)} \right] \qquad (B.26)$$

Let us define,

$$\Phi_j \left(\frac{D_1}{D_2} \right) = R_j \left(\frac{D_1}{D_2} \right) \cdot \sin \; k_1^j \; \frac{L}{2} = \sin \; X_j \left(\frac{D_1}{D_2} \right) \cdot R_j \left(\frac{D_1}{D_2} \right)$$

$$= \left[\frac{\sin \; X_j \left(\frac{D_2}{D_1} \right)}{X_j \left(\frac{D_1}{D_2} \right)} + \frac{\sin \; X_j \left(\frac{D_1}{D_2} \right)}{X_j \left(\frac{D_2}{D_1} \right)} \right]$$

$$- \left[\frac{\sin \; X_j \left(\frac{D_2}{D_1} \right) \cdot \cos \; X_j \left(\frac{D_1}{D_2} \right)}{X_j \left(\frac{D_1}{D_2} \right)} \right.$$

$$+ \left. \frac{\sin \; X_j \left(\frac{D_1}{D_2} \right) \cdot \cos \; X_j \left(\frac{D_2}{D_1} \right)}{X_j \left(\frac{D_2}{D_1} \right)} \right] \qquad (B.27)$$

where the subscript $j = c$ or d.

We can then write,

$$\frac{B_{2d}}{B_{2c}} \cdot \frac{a_d}{a_c} = \frac{\Phi_c \left(\frac{D_1}{D_2} \right)}{\Phi_d \left(\frac{D_1}{D_2} \right)} \cdot \frac{\sin \; k_2^d \; \frac{L}{2}}{\sin \; k_2^c \; \frac{L}{2}}$$

$$\frac{B_{2d}}{B_{2c}} = \frac{\phi_c\left(\frac{D_1}{D_2}\right)}{\phi_d\left(\frac{D_1}{D_2}\right)} \cdot \frac{\sin k_1^d \frac{L}{2}}{\sin k_1^c \frac{L}{2}} \tag{B.28}$$

Substitution of eq. (B.28) into eqs. (B.25) and (B.26) gives us,

$$E_1\left(\frac{D_1}{D_2}, x\right) = -\left[1 - \frac{\phi_c\left(\frac{D_1}{D_2}\right)}{\phi_d\left(\frac{D_1}{D_2}\right)} \cdot \frac{\sin k_2^d \frac{L}{2}}{\sin k_2^c \frac{L}{2}} \cdot \frac{\sin k_1^d x}{\sin k_1^c x}\right]$$

$$E_2\left(\frac{D_1}{D_2}, x\right) = -\left[1 - \frac{\phi_c\left(\frac{D_1}{D_2}\right)}{\phi_d\left(\frac{D_1}{D_2}\right)} \cdot \frac{\sin k_1^d \frac{L}{2}}{\sin k_1^c \frac{L}{2}} \cdot \frac{\sin k_2^d (L-x)}{\sin k_2^c (L-x)}\right]$$

$$\tag{B.29}$$

To quantify matters, let us only consider the points $x = x_{1\,max}$ amd $x = x_{2\,max}$, where E_1 and E_2 take on their maximum values.

The stationary point of $E_1(D_1/D_2, x)$ occurs at $\partial E_1/\partial x = 0$ which is

$$k_1^c \tan k_1^d x = k_1^d \tan k_1^c x \quad . \tag{B.30}$$

We can therefore write

$$x_{1\,max} = \frac{L}{2} M\left(\frac{D_1}{D_2}\right) \quad . \tag{B.31}$$

The stationary point of $E_2(D_1/D_2, x)$ occurs at

$$k_2^c \tan k_2^d(L-x) = k_2^d \tan k_2^c(L-x) \quad . \tag{B.32}$$

This means

$$\frac{2}{L}(L-x) = M(D_2/D_1)$$

Therefore

$$x_{2\text{ max}} = \frac{L}{2}[2 - M(D_2/D_1)] \qquad (B.33)$$

To find $M(D_1/D_2)$ we have to solve eq. (B.30). Let us rewrite eq. (B.30) as

$$\tan\left(\frac{k_1^d}{k_1^c}\right)(k_1^c x) = \left(\frac{k_1^d}{k_1^c}\right)\tan k_1^c x$$

which is

$$\tan by = b \tan y \qquad (B.34)$$

where

$$b = \frac{k_1^d}{k_1^c} = \frac{X_d}{X_c}$$

Table (B.2) contains the relevant range of values.

Table B.2.   Tabulated values of function $b(D_2/D_1)$
for use in eq. (B.34).

D_1/D_2	b
5.0	0.7963
3.275	0.86467
1.637	0.9709
1.31	0.9911
0.524	0.9526
0.1637	0.7655

For $b > \frac{1}{2}$ eq. (B.34) has only the trivial solution. This corresponds to the boundaries of the block where the minimum occurs. There is no turning point for the maximum and the maximum therefore occurs at the extreme point, $x = L/2$.

We can then write that

$$\max E_1\left(\frac{D_1}{D_2}\right) = -\left\{1 - \frac{\Phi_c\left(\frac{D_1}{D_2}\right)}{\Phi_d\left(\frac{D_1}{D_2}\right)} \cdot \frac{\sin X_d\left(\frac{D_2}{D_1}\right)}{\sin X_c\left(\frac{D_1}{D_1}\right)}\right.$$

$$\cdot \left. \frac{\sin\left[X_d\left(\frac{D_1}{D_2}\right) M\left(\frac{D_1}{D_2}\right)\right]}{\sin\left[X_c\left(\frac{D_1}{D_2}\right) M\left(\frac{D_1}{D_2}\right)\right]}\right\}$$

$$\max E_2\left(\frac{D_2}{D_1}\right) = -\left\{1 - \frac{\Phi_c\left(\frac{D_1}{D_2}\right)}{\Phi_d\left(\frac{D_1}{D_2}\right)} \cdot \frac{\sin X_d\left(\frac{D_1}{D_2}\right)}{\sin X_c\left(\frac{D_1}{D_2}\right)}\right.$$

$$\cdot \left. \frac{\sin\left[X_d\left(\frac{D_2}{D_1}\right) M\left(\frac{D_2}{D_1}\right)\right]}{\sin\left[X_c\left(\frac{D_2}{D_1}\right) M\left(\frac{D_2}{D_1}\right)\right]}\right\} \tag{B.35}$$

The functions $\Phi_c(D_1/D_2)$, $\Phi_d(D_1/D_2)$, $\mu_c(D_1/D_2)$ and $\mu_d(D_1/D_2)$ are graphed in Figs (B.4) and (B.5). We define $\mu_c(D_1/D_2)$ and $\mu_d(D_1/D_2)$ as
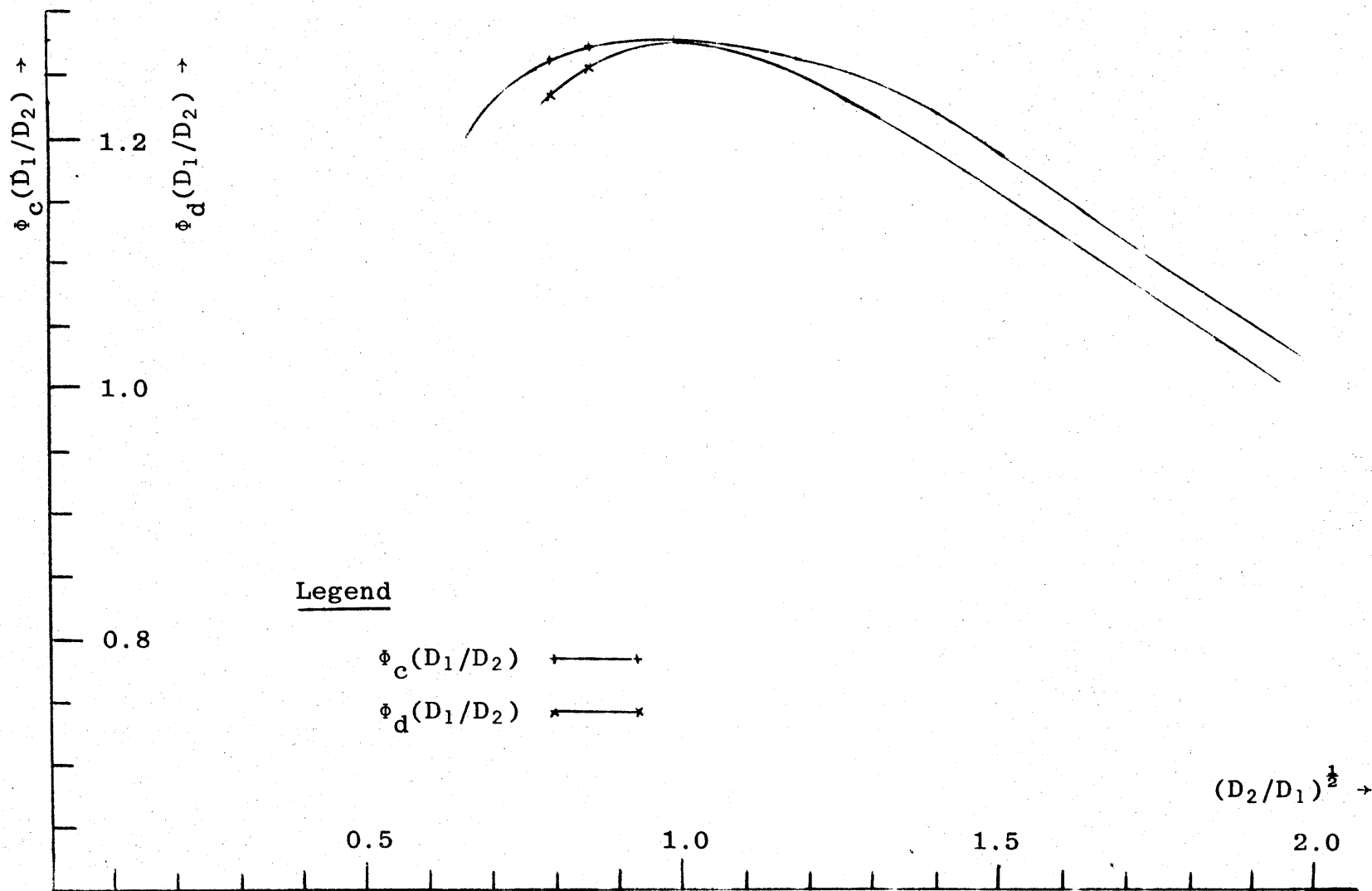
Fig. B.4. The Functions $\Phi_c(D_1/D_2)$ and $\Phi_d(D_1/D_2)$. For use in determining flux error. 1-Group 1-D 2-Region Problem (Fig. B.1).
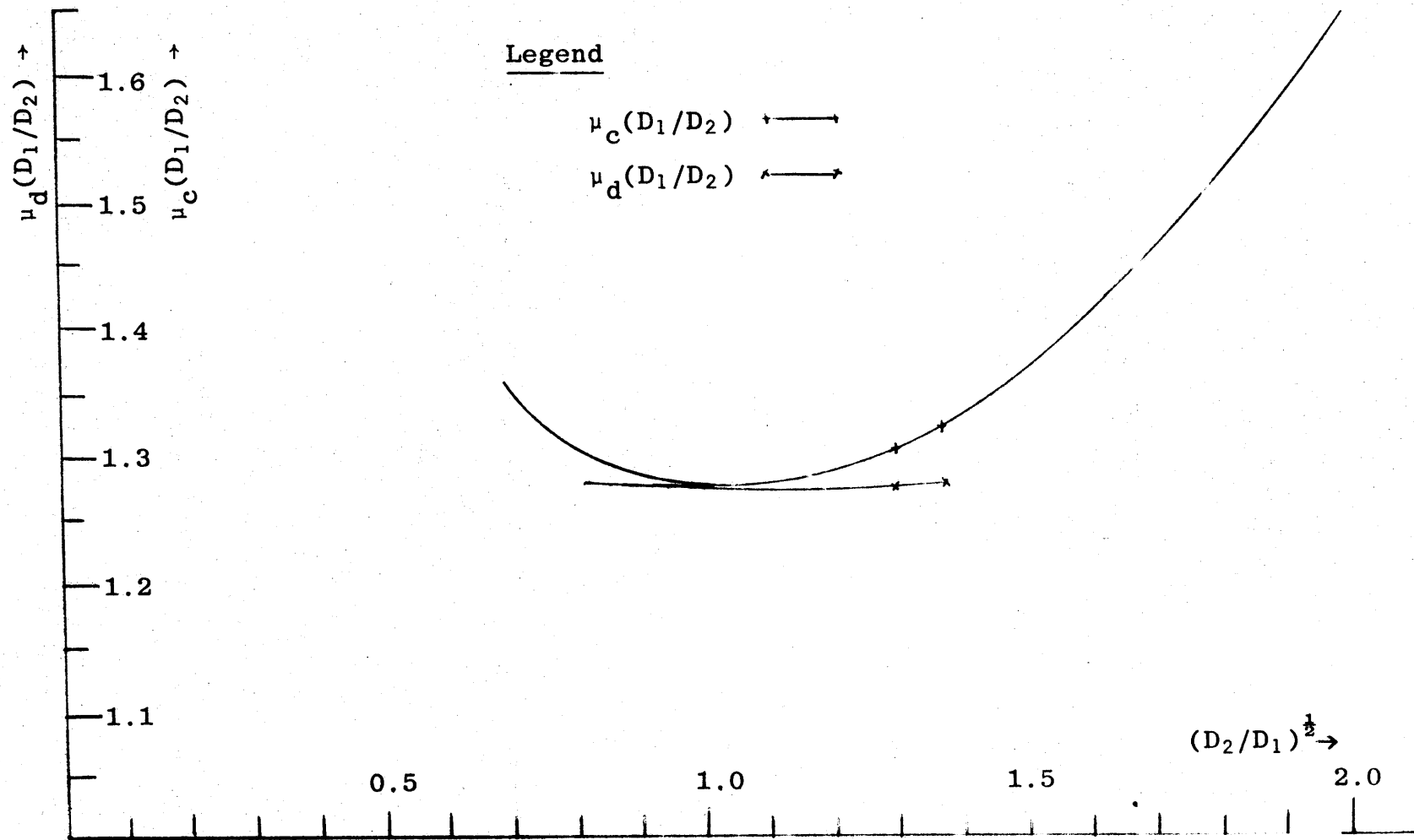
Fig. B.5. The functions $\mu_c(D_1/D_2)$ and $\mu_d(D_1/D_2)$. For use in determining flux error. 1-Group 1-D 2-Region Problem (Fig. B.1).
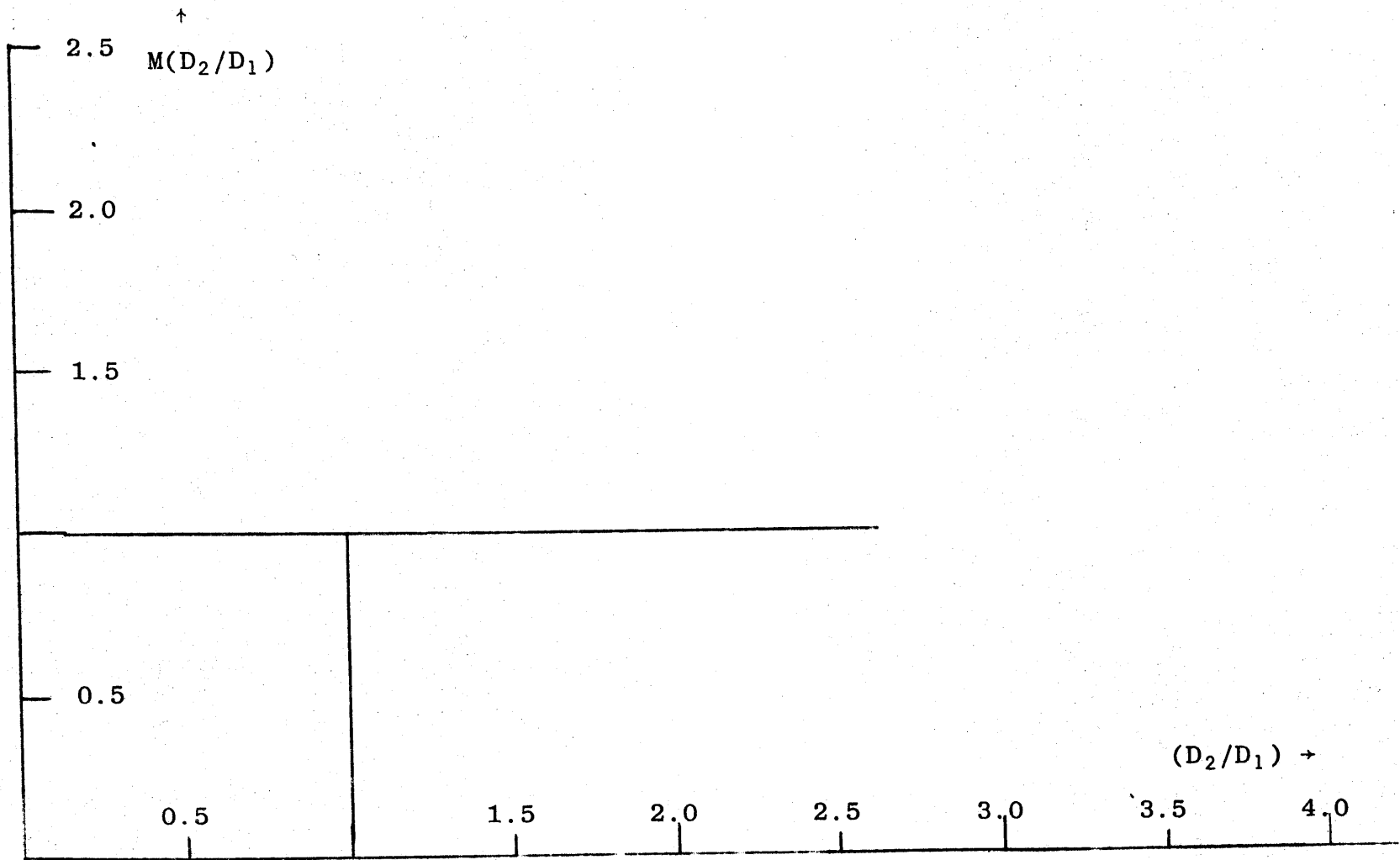
Fig. B.6.   The function $M(D_2/D_1)$.   For use in determining point of Max Flux Error. 1-Group 1-D 2-Region Problem (Fig. B.1).

$$\mu_j\left(\frac{D_1}{D_2}\right) = \frac{\Phi_j\left(\frac{D_1}{D_2}\right)}{\sin X_j\left(\frac{D_2}{D_1}\right) \sin \left\{X_j\left(\frac{D_1}{D_2}\right) M\left(\frac{D_1}{D_2}\right)\right\}} \qquad (B.36)$$

where subscript $j = c$ or d .

The function $M(D_2/D_1)$ is shown in Fig. B.6. Table B.3 is the tabular counterpart of Figs. (B.4) and (B.5). Numerical results for max $E_1(D_1/D_2)$ are presented in Section 4.1.1.

For the range of (D_2/D_1) where $M(D_2/D_1) = 1$, we have that max E_1 = max E_2 .

Table B.3. Tabulated values of the functions $\Phi_d(D_1/D_2)$, $\mu_d(D_1/D_2)$, $\Phi_c(D_1/D_2)$ and $\mu_c(D_1/D_2)$ for use in eq. (B.35).

$\dfrac{D_1}{D_2}$	$\Phi_d\left(\dfrac{D_1}{D_2}\right)$	$\mu_d\left(\dfrac{D_1}{D_2}\right)$	$\Phi_c\left(\dfrac{D_1}{D_2}\right)$	$\mu_c\left(\dfrac{D_1}{D_2}\right)$
1.6375	1.2279	1.2749	1.257	1.306
1.31	1.2577	1.273	1.268	1.282
1.00	1.273	1.273	1.273	1.273
0.524	1.199	1.274	1.2296	1.3176
0.1637	0.8475	1.2809	0.8528	1.9503

Appendix C

INNER PRODUCTS

This appendix presents the inner products required for the 1-D and 2-D Galerkin calculations. We divide the 2-D work into two broad classes: one concerned with the physical mesh and the other with the mathematical mesh. The standard geometrical configuration for the calculation of the inner products is different for the two classes. We further subdivide these classes on the basis of symmetry properties of the $\{\psi_{kg}\}$ sets. These properties enable us to reduce the number of inner products which have to be calculated.

C.1 1-D

The only superelement function set $\{\psi_{kg}\}$ which concerns us here is the 1-D hybrid quadratic set. The inner products for Kang's cubic Hermite set can be found in his thesis.[1] Table C.1 is the list of inner products required for the centering scheme shown in Fig. C.1 and the 1-D hybrid quadratic functions of eqs. (3.40)-(3.41).
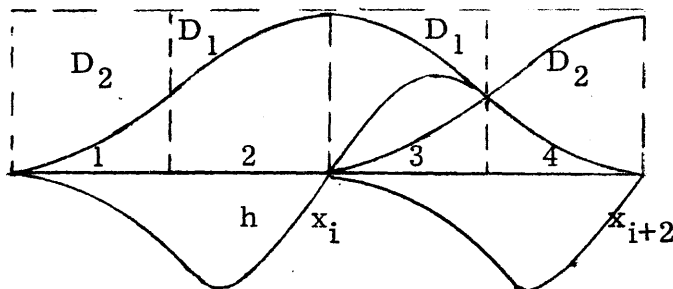
Fig. C.1. Standard 'superpatch' configuration for 1-D hybrid quadratics.

Table C.1. Inner products — standard 'superpatch' configuration of Fig. C.1.

1-D hybrid quadratics.

j	ℓ	k	α	β	$\left(\Psi^{j\alpha}_{\ell g},\ \Psi^{j\beta}_{kg}\right)$	$\left(\nabla\Psi^{j\alpha}_{\ell g},\ \nabla\Psi^{j\beta}_{kg}\right)$
1	i	i	f	f	$\dfrac{h}{5(1+\alpha)^2}$	$\dfrac{4}{3(1+\alpha)^2 h}$
			f	c	$-\dfrac{h^2}{10(1+\alpha)^2}$	$-\dfrac{2}{3(1+\alpha)^2}$
			c	c	$\dfrac{h^3}{20(1+\alpha)^2}$	$\dfrac{h}{3(1+\alpha)^2}$
2	i	i	f	f	$h\left[1-\dfrac{2\alpha}{3(1+\alpha)}+\dfrac{\alpha^2}{(1+\alpha^2)5}\right]$	$\dfrac{4}{3}\dfrac{\alpha^2}{h(1+\alpha)^2}$
			f	c	$-h^2\left[\dfrac{1}{2}-\dfrac{(2+7\alpha)}{(1+\alpha)12}+\dfrac{\alpha(1+2\alpha)}{(1+\alpha)^2 10}\right]$	$\dfrac{2\alpha}{(1+\alpha)}\left[\dfrac{1}{2}-\dfrac{(1+2\alpha)}{3(1+\alpha)}\right]$
			c	c	$h^3\left[\dfrac{1}{3}-\dfrac{(2\alpha+1)}{(\alpha+1)4}+\dfrac{(1+2\alpha)^2}{(1+\alpha)}\dfrac{1}{20}\right]$	$h\left[1-\dfrac{(2\alpha+1)}{(1+\alpha)}+\dfrac{(1+2\alpha)^2}{3(1+\alpha)^2}\right]$

j	ℓ	k	α	β	$\left(\Psi^{j\alpha}_{\ell g},\ \Psi^{j\beta}_{kg}\right)$	$\left(\nabla\Psi^{j\alpha}_{\ell g},\ \nabla\Psi^{j\beta}_{kg}\right)$
3	i	i	f	f	$h\left[1 - \dfrac{2\alpha}{3(1+\alpha)} + \dfrac{\alpha^2}{5(1+\alpha^2)}\right]$	$\dfrac{4}{3}\dfrac{\alpha^2}{h(1+\alpha)^2}$
			f	c	$h^2\left[\dfrac{1}{2} - \dfrac{(2+7\alpha)}{12(1+\alpha)} + \dfrac{\alpha(1+2\alpha)}{(1+\alpha)^2 10}\right]$	$-\dfrac{2\alpha}{(1+\alpha)}\left[\dfrac{1}{2} - \dfrac{(1+2\alpha)}{3(1+\alpha)}\right]$
			c	c	$h^3\left[\dfrac{1}{3} - \dfrac{(2\alpha+1)}{(\alpha+1)4} + \dfrac{(1+2\alpha)^2}{(1+\alpha)^2}\dfrac{1}{20}\right]$	$h\left[1 - \dfrac{(2\alpha+1)}{(1+\alpha)} + \dfrac{(1+2\alpha)^2}{3(1+\alpha)^2}\right]$
	i	$i+2$	f	f	$\dfrac{\alpha h}{(1+\alpha)}\left[\dfrac{1}{3} - \dfrac{\alpha}{5(1+\alpha)}\right]$	$-\dfrac{4}{3}\dfrac{\alpha^2}{h(1+\alpha)^2}$
			f	c	$-\dfrac{\alpha h^2}{2(1+\alpha)}\left[\dfrac{1}{3} - \dfrac{\alpha}{(1+\alpha)5}\right]$	$\dfrac{2\alpha^2}{3(1+\alpha)^2}$
			c	f	$\dfrac{\alpha h^2}{(1+\alpha)}\left[\dfrac{1}{4} - \dfrac{(1+2\alpha)}{10(1+\alpha)}\right]$	$\dfrac{2\alpha}{(1+\alpha)}\left[\dfrac{1}{2} - \dfrac{(2\alpha+1)}{3(1+\alpha)}\right]$
			c	c	$-\dfrac{\alpha h^3}{2(1+\alpha)}\left[\dfrac{1}{4} - \dfrac{(2\alpha+1)}{10(1+\alpha)}\right]$	$-\dfrac{h\alpha}{(1+\alpha)}\left[\dfrac{1}{2} - \dfrac{(2\alpha+1)}{3(1+\alpha)}\right]$

j	ℓ	k	α	β	$\left(\Psi^{j\alpha}_{\ell g},\ \Psi^{j\beta}_{kg}\right)$	$\left(\nabla\Psi^{j\alpha}_{\ell g},\ \nabla\Psi^{j\beta}_{kg}\right)$
4	i	i	f	f	$\dfrac{h}{5(1+\alpha)^2}$	$\dfrac{4}{3(1+\alpha)^2 h}$
			f	c	$\dfrac{h^2}{10(1+\alpha)^2}$	$\dfrac{2}{3(1+\alpha)^2}$
			c	c	$\dfrac{h^3}{20(1+\alpha)^2}$	$\dfrac{h}{3(1+\alpha)^2}$
	i	$i+2$	f	f	$\dfrac{h}{(1+\alpha)}\left[\dfrac{1}{3}-\dfrac{1}{(1+\alpha)5}\right]$	$-\dfrac{4}{3h(1+\alpha)^2}$
			f	c	$-\dfrac{h^2}{(1+\alpha)}\left[\dfrac{1}{4}-\dfrac{(2+\alpha)}{10(1+\alpha)}\right]$	$-\dfrac{2}{(1+\alpha)}\left[\dfrac{1}{2}-\dfrac{(2+\alpha)}{3(1+\alpha)}\right]$
			c	f	$\dfrac{h^2}{2(1+\alpha)}\left[\dfrac{1}{3}-\dfrac{1}{5(1+\alpha)}\right]$	$-\dfrac{2}{3(1+\alpha)^2}$
			c	c	$-\dfrac{h^3}{2(1+\alpha)}\left[\dfrac{1}{4}-\dfrac{(2+\alpha)}{10(1+\alpha)}\right]$	$-\dfrac{h}{(1+\alpha)}\left[\dfrac{1}{2}-\dfrac{(2+\alpha)}{3(1+\alpha)}\right]$

We need only concern ourselves with the set

$$\{\Psi_{ig}^{1f}, \Psi_{ig}^{1c}, \Psi_{ig}^{2f}, \Psi_{ig}^{2c}, \Psi_{ig}^{3f}, \Psi_{ig}^{3c}, \Psi_{i+2g}^{3f}, \Psi_{i+2g}^{3c}, \Psi_{ig}^{4f}, \Psi_{ig}^{4c}, \Psi_{i+2g}^{4f}, \Psi_{i+2g}^{4c}\}.$$

All the inner products can be formulated in terms of the inner products of this set over the standard geometrical configuration of Fig. C.1.

C.2 2-D

In 2-D the meshes we consider lead to two standard geometrical configurations for the calculation of inner products. These two standard configurations correspond to the physical mesh and the mathematical mesh, respectively, and we divide the presentation into two sections: one on the physical mesh and the second on the mathematical mesh.

In the section on the physical mesh we present tables of inner products for the following superelement functions ψ_{kg},

(a) C_1-shell functions

(b) 2-element incomplete cubic functions.

The section on the mathematical mesh is divided into two parts: one on the regular meshes, that is, where the only Θ_J is the regular hexagon; the other on the distorted meshes where we introduce irregular polygons.

In the section on the regular meshes, we further subdivide the presentation into two parts. We first tabulate inner products for the sets $\{\psi_{kg}\}$ which possess the properties of 60°-rotational symmetry and piecewise median symmetry.[*] The sets examined are then

---

[*] The property of piecewise median symmetry is the superelement extension of the property of median symmetry discussed in section 3.2

(a) 1-element incomplete cubic set

(b) 2-element incomplete cubic set

(c) C_1-shell set

(d) $C_1 + C_2$-shell set

(e) regular quadratic set.

We then tabulate the inner products for $\{\psi_{kg}\}$ which do not possess these properties. The sets examined are

(a) 3-element incomplete cubic set

(b) 3-element incomplete 9th-order set.

This completes the section on the regular meshes. For the irregular meshes we present inner products for the following sets:

(a) C_1-shell set

(b) $C_1 + C_2$-shell set.

Both of these sets possess the properties of $60°$-rotational symmetry and piecewise median symmetry.

We now begin by presenting the discussion for the physical mesh.

C.2.1 Physical Mesh

It can be seen from Fig. 3.6 that the standard geometrical configuration is the one of Fig. C.2.

Triangle 4ef is the basic patch θ_j of the physical mesh. All the inner products can be formulated in terms of the inner products over

for the basic element function set $\{\Psi_{ig}^j\}$. A superelement function, ψ_{kg}, is said to possess piecewise median symmetry if the corresponding basic element functions Ψ_{ig}^j possess median symmetry.
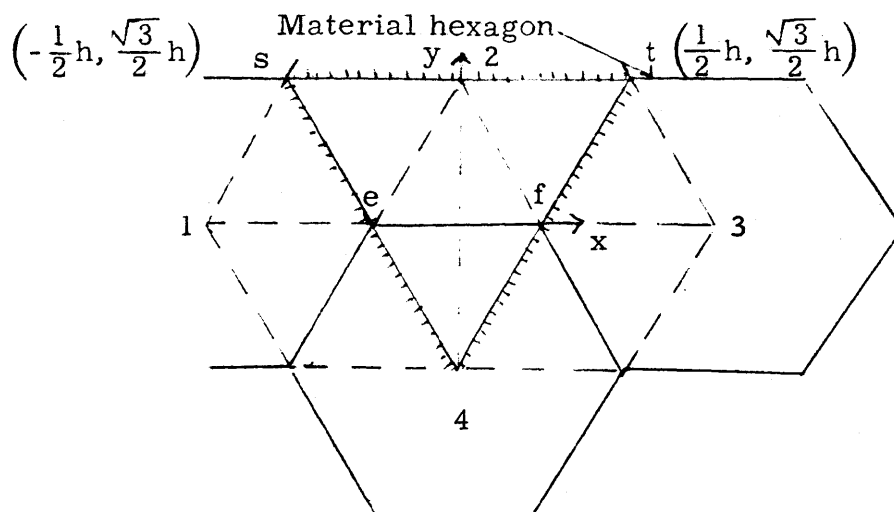
Fig. C.2. Standard basic patch configuration — physical mesh.

triangle 4ef and quadrilateral estf of the set $\{\Psi_{1g}^{\Delta 4ef\alpha}, \Psi_{2g}^{\Delta 4ef\alpha}, \Psi_{3g}^{\Delta 4ef\alpha},$ $\Psi_{4g}^{\Delta 4ef\alpha}, \Psi_{4g}^{quad\ estf\alpha}\}$ by translation and rotation. The 60°-rotational invariance of the inner products of $\{\psi_{kg}\}$ is due to the 60°-rotational symmetry properties of the function sets we use. These sets are the C_1 shell set and the 2-element cubic incomplete set. In addition to this symmetry property these sets also have what we shall refer to as median symmetry. To reiterate, this simply means that $\Psi_{4g}^{\Delta 4st}$, the piecewise function centered on 4 and zero along st, is symmetrical about the median 24. These properties of 60°-rotational symmetry and median symmetry are required in order to conclude that the sets of inner products listed in Tables C.2-C.5 are sufficient sets. The definitions of the function sets used are given in sections 3.2.1 and 3.1.1.

Let us use these standard products to formulate the inner products $(\psi_{ig}^{\alpha}, \psi_{jg}^{\alpha})$.

As can be seen from Fig. C.3, the physical mesh leads to a 13-point

Table C.2. Inner products — physical mesh. Standard basic patch configuration of Fig. C.2.

C_1 shell set.

j	ℓ	k	$\left(\Psi^{jc1}_{\ell g}, \Psi^{jc1}_{kg}\right)h^{-2}$	$\left(\nabla\Psi^{jc1}_{\ell g}, \nabla\Psi^{jc1}_{kg}\right)$
$\Delta 4ef \equiv 1$	4	4	0.049616038	0.144337566
	4	1	0.01127637236	-0.072168783
	4	2	0.058637137	-0.144337566
	1	2	0.0157869214	0.072168783
	1	3	2.2552745 E-3	-0.072168783
Quad estf $\equiv 2$	4	4	0.0225527447	0.4330127

Table C.3. Flux integrals — physical mesh. Standard basic patch configuration of Fig. C.2.

C_1 shell set.

j	ℓ	$\left(\Psi^{jc1}_{\ell g}, 1\right)h^{-2}$
$\Delta 4ef \equiv 1$	4	0.0721687837
Quad estf $\equiv 2$	4	0.072168783

Table C.4. Inner products — physical mesh. Standard basic patch configuration of Fig. C.2.

2-Element cubic incomplete set.

j	ℓ	k	α	β	$\left(\Psi_{\ell g}^{j\alpha},\ \Psi_{kg}^{j\beta}\right)h^{-2}$	$\left(\nabla\Psi_{\ell g}^{j\alpha},\ \nabla\Psi_{kg}^{j\beta}\right)$
$\Delta 4ef$ $\equiv 1$	4	4	f	f	0.0493160067057	0.2144014267
			f	c	-0.012220982	0.044791667
			c	c	0.0037212029	0.018042197
	4	1	f	f	0.0048817295	-0.0288675133
			f	c	-0.007249814	0.0406249988
			c	f	-0.00158575144	-0.0062499978
			c	c	0.0022552745	0.0135316467
	4	2	f	f	0.057698781	-0.1250925625
			f	c	-0.00870535743	-0.101041661
			c	f	-0.0167096816	-0.044791667
			c	c	0.00186060157	-0.0180421963
	1	2	f	f	0.00697691984409	-0.0097728566
			f	c	-0.00070684532	0.0041666627
			c	f	-0.01011672243	-0.049739584
			c	c	0.00107125547	-0.022552745
	1	3	f	f	0.973258336034 E-4	-0.0300703146
			f	c	-0.0005115327	0.0432291664
			c	f	-0.0005115327	0.0432291664
			c	c	0.00107125535	-0.0225527464
Quad estf $\equiv 2$	4	4	f	f	0.0115119680836	0.3244588225
			f	c	-0.0083147314286	-0.1114583333
			c	c	0.00710411464042	0.1262953714

Table C.5. Flux integrals — physical mesh. Standard basic patch
configuration of Fig. C.2.

2-Element cubic incomplete set.

j	ℓ	α	$\left(\Psi_{\ell g}^{j\alpha}, 1 \right) h^{-2}$
$\Delta 4ef \equiv 1$	4	f	0.0712666738532
		c	-0.01953125
Quad estf $\equiv 2$	4	f	0.0442033799848
		c	-0.04296875
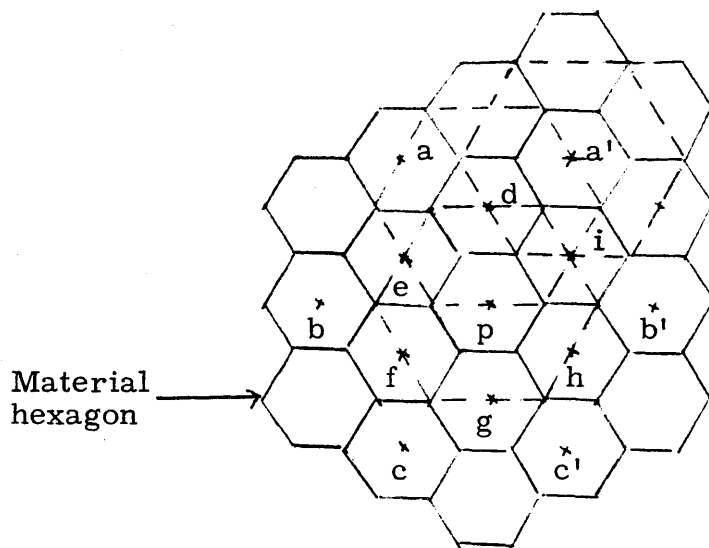
Fig. C.3. Standard superpatch configuration – physical mesh.

block relation. The block nature of the relation is due to the possibility

of having more than 1 function centered on a 'center'. Consider point p

in Fig. C.3. It can be seen that the surrounding centers which have

nonzero inner products with point p can be divided into two groups, an

outer ring $\{a, b, c, c', b', a'\}$ and an inner ring $\{d, e, f, g, h, i\}$. The inner

products (ψ_{ig}, ψ_{jg}) then fall into two classes typified by

$$(M\psi_{pg}^{\alpha}, \psi_{ag}^{\beta}) = (\Psi_{1g}^{1\alpha}, \Psi_{3g}^{1\beta}) M_d + (\Psi_{1g}^{1\beta}, \Psi_{3g}^{1\alpha}) M_e \quad \text{for the outer ring}$$

$$(C.1)$$

and

$$(M\psi_{pg}^{\alpha}, \psi_{eg}^{\beta}) = [(\Psi_{1g}^{1\alpha}, \Psi_{2g}^{1\beta}) + (\Psi_{1g}^{1\beta}, \Psi_{2g}^{1\alpha})](M_d + M_f)$$

$$+ [2(\Psi_{1g}^{1\alpha}, \Psi_{4g}^{1\beta}) + (\Psi_{2g}^{1\alpha}, \Psi_{4g}^{1\beta})] M_e$$

$$+ [2(\Psi_{1g}^{1\beta}, \Psi_{4g}^{1\alpha}) + (\Psi_{2g}^{1\beta}, \Psi_{4g}^{1\alpha})] M_p \quad \text{for the inner ring.}$$

(C.2)

where

M_i = material property of hexagonal block with center i.

For inner products of functions both centered on p we have that

$$^*(M\psi_{pg}^{\alpha}, \psi_{pg}^{\beta}) = (M_d + M_e + M_f + M_g + M_h + M_i)(\Psi_{4g}^{2\alpha}, \Psi_{4g}^{2\beta})$$

$$+ 6M_p(\Psi_{4g}^{1\alpha}, \Psi_{4g}^{1\beta}). \tag{C.3}$$

We now address ourselves to the mathematical mesh.

C.2.2 Mathematical Mesh

We first concentrate on the regular mesh and then discuss the distorted version.

(A) Regular Mesh

Our choice of mesh and our sets $\{\psi_{kg}^{\alpha}\}$ give us translational invariance of the inner products calculated over θ_j. This property reduces the required number of standard inner products to those over the triangles

---

*Throughout this appendix the formulas for the inner products involving the derivatives should be inferred by replacing ψ_{kg} with $\nabla\psi_{kg}$.

abc and adb of Fig. C.4. If the sets $\{\psi^{a}_{kg}\}$ have 60°-rotational symmetry, then we only have to concentrate on the triangle abc.
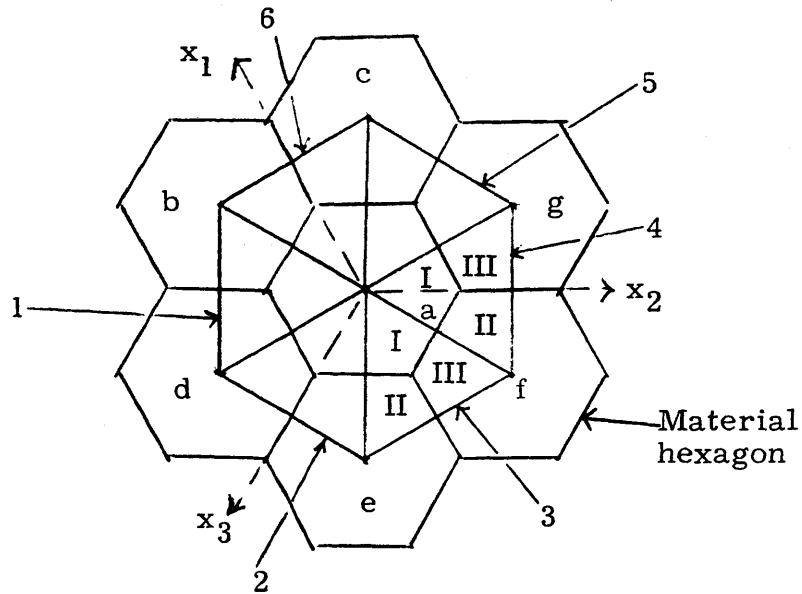
Fig. C.4. Standard superpatch configuration — mathematical mesh.

Let us begin by considering the sets which have 60°-rotational symmetry. The standard basic patch configuration, the triangle abc, is shown in more detail in Fig. C.5. We divide triangle abc into the three quadrilateral regions IV, V, and VI.
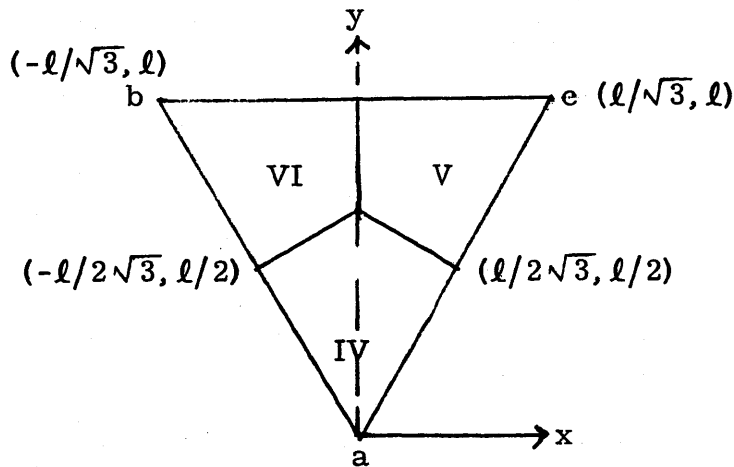
Fig. C.5.

Standard basic patch configuration — mathematical mesh.

The sets we consider are the 1-element and 2-element incomplete cubic sets and the two shell sets, C_1 and $\{C_1 + C_2\}$. These sets all have median symmetry. With these properties, the sets of sufficient standard inner products are those of Tables C.6-C.13. The definitions of the function sets can be found in sections 3.1 and 3.2. The notation (,

$)_\Gamma$ is to indicate that the inner product is taken over the region Γ.

For completeness we present in Tables C.14 and C.15 the corresponding results for the regular quadratic set. This set is discussed in section 3.2. It also has median symmetry.

We now use these standard inner products over the triangle abc to assemble the inner products $(\psi_{ig}^{\alpha}, \psi_{jg}^{\beta})$.
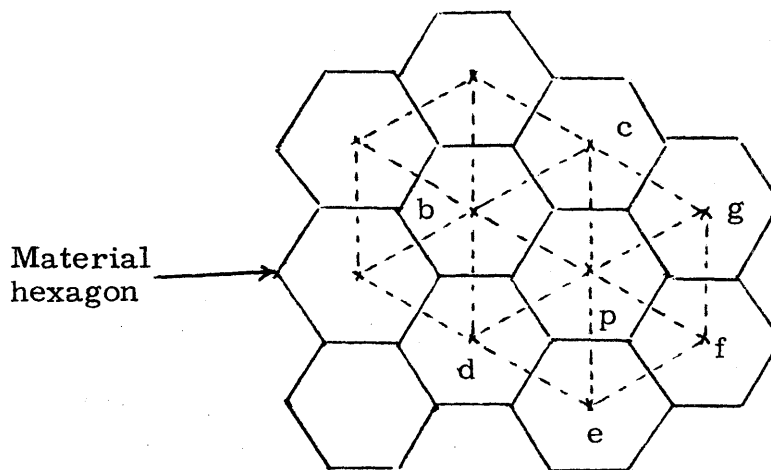
Fig. C.6. Coarse mesh.

Figure C.6 shows that the regular mathematical mesh leads to a 7-point block relation; the coupling between point p and its nearest neighbors the set $\{e, f, g, c, b, d\}$. As the set $\{\psi_{kg}^{\alpha}\}$ has 60°-rotational

Table C.6. Inner products — mathematical mesh. Standard basic patch configuration of Fig. C.5.

1-Element cubic incomplete set; $j = \Delta abc \equiv 1$

ℓ	k	$\left(\Psi^{jf}_{\ell g}, \Psi^{jf}_{kg}\right)_\Gamma \ell^{-2}$			$\left(\nabla\Psi^{jf}_{\ell g}, \nabla\Psi^{jf}_{kg}\right)_\Gamma$		
		$\Gamma = $ IV	$\Gamma = $ V	$\Gamma = $ VI	$\Gamma = $ IV	$\Gamma = $ V	$\Gamma = $ VI
a	a	0.98602611 E-1	0.9464698 E-2	0.9464698 E-2	0.2537489810	0.205101897	0.20510189
a	c	0.20861636 E-1	0.20861635 E-1	0.57019315 E-2	-0.1418428372	-0.141842837	-0.033856965

Table C.7. Flux integrals — mathematical mesh. Standard basic patch configuration of Fig. C.5.

1-Element cubic incomplete set ; $j = \Delta abc \equiv 1$.

ℓ	$\left(\Psi^{jf}_{\ell g}, 1\right)_\Gamma \ell^{-2}$		
	$\Gamma = $ IV	$\Gamma = $ V	$\Gamma = $ VI
a	0.13435866	0.033856958	0.033856958

Table C.8. Inner products — mathematical mesh. Standard basic patch configuration of Fig. C.5.
2-Element cubic incomplete set; j = Δabc ≡ 1.

ℓ	k	α	β	$\left(\Psi_{\ell g}^{j\alpha},\ \Psi_{kg}^{j\beta}\right)_\Gamma \ell^{-2}$			$\left(\nabla\Psi_{\ell g}^{j\alpha},\ \nabla\Psi_{kg}^{j\beta}\right)_\Gamma$		
				Γ = IV	Γ = V	Γ = VI	Γ = IV	Γ = V	Γ = VI
a	a	f	f	.72883793 E-1	.41100825 E-2	.41100827 E-2	.292595381	.123132407	.123132407
		f	c	-.20213393 E-1	-.35837781 E-2	-.35837782 E-2	.039043205	-.052854937	-.052854937
		c	c	.71352050 E-2	.36492750 E-2	.36492753 E-2	.018710423	.062813564	.062813570
a	c	f	f	.95313151 E-2	.95313155 E-2	.21297905 E-2	-.123444260	-.123444253	-.012919109
		f	c	-.12673102 E-1	-.42466847 E-2	-.23262464 E-2	.050385791	-.011188274	.010802469
		c	f	-.42466849 E-2	-.12673100 E-1	-.23262466 E-2	-.011188273	.050385802	.010802475
		c	c	.46850313 E-2	.46850306 E-2	.26580687 E-2	.012696357	.012696360	-.025392717

Table C.9. Flux integrals — mathematical mesh. Standard basic patch configuration of Fig. C.5.

2-Element cubic incomplete set; $j = \Delta abc \equiv 1$.

ℓ	α	$\left(\Psi_{\ell g}^{j\alpha}, \ 1 \right)_\Gamma \ \ell^{-2}$		
		$\Gamma = IV$	$\Gamma = V$	$\Gamma = VI$
a	f	0.11342080	0.20269626	0.20269626
	c	-0.36265428	-0.23533948	-0.23533950
		E-1	E-1	E-1

Table C.10. Inner products — mathematical mesh. Standard basic patch configuration of Fig. C.5.

C_1 shell set; $j = \Delta abc \equiv 1$

ℓ	k	$\left(\Psi_{\ell g}^{jc1}, \Psi_{kg}^{jc1}\right)_\Gamma \ell^{-2}/\sqrt{3}$			$\left(\nabla\Psi_{\ell g}^{jc1}, \nabla\Psi_{kg}^{jc1}\right)_\Gamma/\sqrt{3}$		
		$\Gamma = IV$	$\Gamma = V$	$\Gamma = VI$	$\Gamma = IV$	$\Gamma = V$	$\Gamma = VI$
a	a	0.437242 E-1	0.591563 E-2	0.591563 E-2	1/9	1/9	1/9
a	c	0.120884 E-1	0.120884 E-1	0.360097 E-2	-1/18	-1/18	-1/18

Table C.11. Flux integrals — mathematical mesh. Standard basic patch configuration of Fig. C.5.

C_1 shell set; $j = \Delta abc \equiv 1$

ℓ	$\left(\Psi_{\ell g}^{jc1}, 1\right)_\Gamma \ell^{-2}/\sqrt{3}$		
	$\Gamma = IV$	$\Gamma = V$	$\Gamma = VI$
a	0.679012 E-1	0.216049 E-1	0.216049 E-1

Table C.12. Inner products — mathematical mesh. Standard basic patch configuration of Fig. C.5.

$\{C_1 + C_2\}$ shell set; $j = \Delta abc \equiv 1$

ℓ	k	α	β	$\left(\Psi^{j\alpha}_{\ell g},\ \Psi^{j\beta}_{kg}\right)_\Gamma \ell^{-2}$			$\left(\nabla\Psi^{j\alpha}_{\ell g},\ \nabla\Psi^{j\beta}_{kg}\right)_\Gamma$		
				$\Gamma = IV$	$\Gamma = V$	$\Gamma = IV$	$\Gamma = IV$	$\Gamma = V$	$\Gamma = VI$
a	a	c1	c1	.75732665 E-1	.10246184 E-1	.10246185 E-1	.19245007	.19245007	.19245007
		c1	c2	-.21219133 E-1	-.60570981 E-2	-.60570981 E-2	.37037033 E-1	-.10185184	-.10185184
		c2	c2	.7135205 E-2	.3649275 E-2	.3649275 E-2	.18710423 E-1	.62813564 E-1	.62813564 E-1
a	c	c1	c1	.20937859 E-1	.20937859 E-1	.62368096 E-2	-.96225033 E-1	-.96225033 E-1	-.96225033 E-1
		c1	c2	-.13387347 E-1	-.75231472 E-2	-.40895068 E-2	.50925914 E-1	-.18518520 E-1	.50925919 E-1
		c2	c1	-.75231485 E-2	-.13387345 E-1	-.40895068 E-2	-.18518520 E-1	.50925920 E-1	.50925925 E-1
		c2	c2	.46850313 E-2	.46850313 E-2	.26580687 E-2	.12696357 E-1	.1269636 E-1	-.25392717 E-1

206

Table C.13. Flux integrals — mathematical mesh. Standard basic patch configuration of Fig. C.5.

$\{C_1 + C_2\}$ shell set; $j = \Delta abc \equiv 1$.

ℓ	α	$\left(\Psi_{\ell g}^{j\alpha},\ 1 \right)_{\Gamma} \ell^{-2}$		
		$\Gamma = IV$	$\Gamma = V$	$\Gamma = VI$
a	c1	0.11760837	0.37420846 E-1	0.37420849 E-1
	c2	-0.36265428 E-1	-0.23533948 E-1	-0.23533950 E-1

Table C.14. Inner products — mathematical mesh. Standard basic patch configuration of Fig. C.5.

Regular quadratic set; $j = \Delta abc \equiv 1$

ℓ	k	α	β	$\left(\Psi_{\ell g}^{j\alpha},\ \Psi_{kg}^{j\beta}\right)_\Gamma \ell^{-2}$			$\left(\nabla\Psi_{\ell g}^{j\alpha},\ \nabla\Psi_{kg}^{j\beta}\right)_\Gamma$		
				Γ = IV	Γ = V	Γ = VI	Γ = IV	Γ = V	Γ = VI
a	a	RQ	RQ	.36242783 E-1	.11236154 E-2	.11236154 E-2	.30293066	.40984736 E-1	.40984739 E-1
		RQ	c2	-.12980108 E-01	-.18432782 E-2	-.18432784 E-2	.58641968 E-1	-.29320984 E-1	-.29320487 E-1
		c2	c2	.71352050 E-2	.36492750 E-2	.36492753 E-2	.18710423 E-1	.62813564 E-1	.62813570 E-1
a	c	RQ	RQ	.30392071 E-2	.30392065 E-2	.33658976 E-3	-.41875717 E-1	-.41875711 E-1	-.12473619 E-1
		RQ	c2	-.797755384 E-2	-.21133399 E-2	-.10202334 E-2	.65586405 E-1	-.38580257 E-2	.21604935 E-1
		c2	RQ	-.21133404 E-2	-.79775374 E-2	-.10202334 E-2	-.38580255 E-2	.65586414 E-1	.21604941 E-1
		c2	c2	.46850313 E-2	.46850306 E-2	.26850687 E-2	.12696357 E-1	.12696360 E-1	-.25392717 E-1

Table C.15. Flux integrals — mathematical mesh. Standard basic patch configuration of Fig. C.5.

Regular quadratic set; $j = \Delta abc \equiv 1$

$$\left(\Psi_{\ell g}^{j\alpha}, \, 1 \right)_{\Gamma} \ell^{-2}$$

ℓ	α	$\Gamma = IV$	$\Gamma = V$	$\Gamma = VI$
a	RQ	0.75732665 E-1	0.10246185 E-1	0.10246185 E-1
	c2	-0.36265428 E-1	-0.23533948 E-1	-0.23533950 E-1

symmetry, that is, each θ_j of Θ_J can be rotated into each other about the 'center' of Θ_J without altering the form of the superelement, we have that

$$(M\psi_{pg}^{\alpha}, \psi_{fg}^{\beta}) = M_p\{(\Psi_{ag}^{1\beta}, \Psi_{cg}^{1\alpha})_V + (\Psi_{ag}^{1\alpha}, \Psi_{cg}^{1\beta})_{IV}\}$$

$$+ M_e(\Psi_{ag}^{1\beta}, \Psi_{cg}^{1\alpha})_{VI} + M_g(\Psi_{ag}^{1\alpha}, \Psi_{cg}^{1\beta})_{VI}$$

$$+ M_f\{(\Psi_{ag}^{1\alpha}, \Psi_{cg}^{1\beta})_V + (\Psi_{ag}^{1\beta}, \Psi_{cg}^{1\alpha})_{IV}\} \tag{C.4}$$

is the inner product pattern for point p with its nearest neighbors and

$$(M\psi_{pg}^{\alpha}, \psi_{pg}^{\beta}) = 6M_p(\Psi_{ag}^{1\alpha}, \Psi_{ag}^{1\beta})_{IV} + (M_e + M_f + M_g + M_c + M_b + M_d)$$

$$\cdot \{(\Psi_{ag}^{1\alpha}, \Psi_{ag}^{1\beta})_V + (\Psi_{ag}^{1\alpha}, \Psi_{ag}^{1\beta})_{VI}\} \tag{C.5}$$

is the pattern for both functions having the same Θ_J.

We now turn our attention to those sets which do not possess this property of 60°-rotational symmetry. These are the 3-element incomplete cubic set and the 3-element 9th-order incomplete set.

Let us consider the 3-element 9th-order incomplete set first. The standard geometrical configuration is the triangle abc of Fig. C.7.

To simplify matters here, we will think in terms of geometrical shapes. This was the approach advocated in section 3.2. We define the following shapes over the triangle abc,

$$\zeta_{ag}^{0}(x,y) = u_o^+(x_1)\, u_o^-(x_2)\, u_o^-(x_3) \tag{C.6}$$

$$\zeta_{ag}^{1}(x,y) = -u_o^+(x_1)\, u_o^-(x_2)\, u_1^-(x_3) \tag{C.7}$$
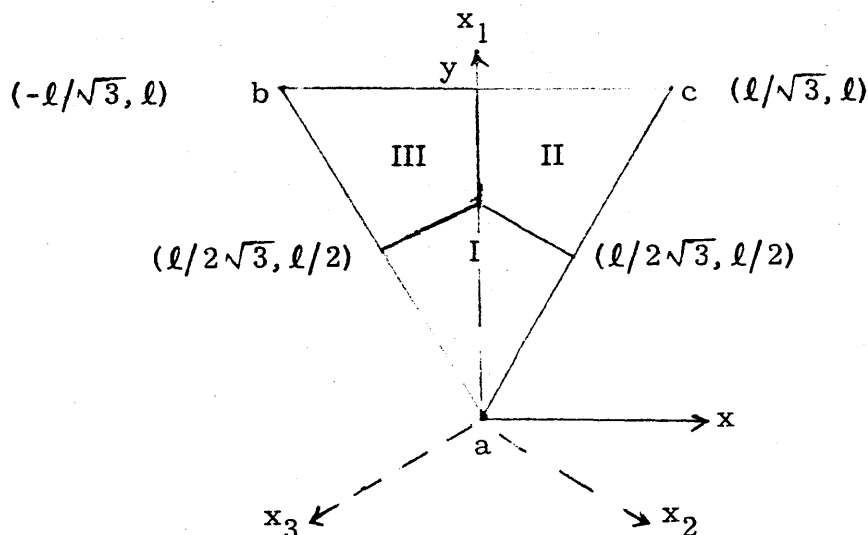
Fig. C.7. Standard basic patch configuration — mathematical
mesh (same as that of Fig. C.5 except that here,
axes (x_1, x_2, x_3) are also shown).

$$\zeta_{ag}^2(x, y) = u_1^+(x_1) \, u_0^-(x_2) \, u_0^-(x_3) \tag{C.8}$$

$$\zeta_{ag}^3(x, y) = u_0^+(x_1) \, u_1^-(x_2) \, u_0^-(x_3) \tag{C.9}$$

where the subscript a indicates that these shapes are 'centered' on

point a and are zero on the opposite side, bc.

The list of sufficient inner products is shown in Tables C.16 and

C.17. Let us call the triangle abc of Fig. C.7 the standard triangle

and denote it by the letter H. We now have to transform our results

with H to the $(\psi_{ig}^\alpha, \psi_{jg}^\beta)$ of Fig. C.6. In the case of 60°-rotational sym-

metry this was relatively simple. In the case under consideration

there are a few more steps involved. We have to relate the hexagon

cbdefg of Fig. C.4 to H. It was stated in the opening paragraph of

Table C.16. Inner products — mathematical mesh. Standard basic patch configuration of Fig. C.7.

3-Element 9th order incomplete set.

ℓ	k	α	β	$\left(\zeta^{\alpha}_{\ell g},\ \zeta^{\beta}_{kg}\right)_{\Gamma}\ell^{-4}$			$\left(\nabla\zeta^{\alpha}_{\ell g},\ \nabla\zeta^{\beta}_{kg}\right)_{\Gamma}\ell^{-2}$		
				$\Gamma = I$	$\Gamma = II$	$\Gamma = III$	$\Gamma = I$	$\Gamma = II$	$\Gamma = III$
a	a	0	0	$.60471726$ $E\text{-}1\ell^{-2}$	$.11813969$ $E\text{-}2\ell^{-2}$	$.11813969$ $E\text{-}2\ell^{-2}$	$.434358653$ ℓ^{-2}	$.595238755$ $E\text{-}1\ell^{-2}$	$.595238755$ $E\text{-}1\ell^{-2}$
		0	1	$.59524114$ $E\text{-}2\ell^{-1}$	$.28979538$ $E\text{-}3\ell^{-1}$	$.12022076$ $E\text{-}3\ell^{-1}$	$.794280552$ $E\text{-}1\ell^{-1}$	$-.396501555$ $E\text{-}2\ell^{-1}$	$.85274259$ $E\text{-}2\ell^{-1}$
		0	2	$.10172272$ $E\text{-}1\ell^{-1}$	$.32783217$ $E\text{-}3\ell^{-1}$	$.32783218$ $E\text{-}3\ell^{-1}$	$-.102668405$ $E\text{-}1\ell^{-1}$	$-.86436618$ $E\text{-}2\ell^{-1}$	$-.86436618$ $E\text{-}2\ell^{-1}$
		0	3	$-.59524114$ $E\text{-}2\ell^{-1}$	$-.12022876$ $E\text{-}3\ell^{-1}$	$-.28979539$ $E\text{-}3\ell^{-1}$	$-.794280552$ $E\text{-}1\ell^{-1}$	$-.85274259$ $E\text{-}2\ell^{-1}$	$.396501555$ $E\text{-}2\ell^{-1}$
		1	1	$.80574855$ $E\text{-}3$	$.71448051$ $E\text{-}4$	$.16083686$ $E\text{-}4$	$.35895786$ $E\text{-}1$	$.113899942$ $E\text{-}2$	$.212958212$ $E\text{-}2$
		1	2	$.11329617$ $E\text{-}2$	$.80408680$ $E\text{-}4$	$.33974351$ $E\text{-}4$	$-.138048810$ $E\text{-}2$	$.164548191$ $E\text{-}2$	$-.49547928$ $E\text{-}3$

ℓ	k	α	β	$\left(\zeta^\alpha_{\ell g},\ \zeta^\beta_{kg}\right)_\Gamma \ell^{-4}$			$\left(\nabla\zeta^\alpha_{\ell g},\ \nabla\zeta^\beta_{kg}\right)_\Gamma \ell^{-2}$		
				$\Gamma = I$	$\Gamma = II$	$\Gamma = III$	$\Gamma = I$	$\Gamma = II$	$\Gamma = III$
		1	3	-.54686221 E-3	-.28642338 E-4	-.28642338 E-4	.3481513 E-2	.27571529 E-3	.27571529 E-3
		2	2	.19095866 E-2	.91172935 E-4	.91172937 E-4	.559812640 E-2	.282539627 E-2	.282539627 E-2
		2	3	-.11329617 E-2	-.33974351 E-4	-.80408682 E-4	.138048810 E-2	.49547928 E-3	.164548191 E-2
		3	3	.80574855 E-3	.16083686 E-4	.71448053 E-4	.35895786 E-1	.212958212 E-2	.113899942 E-2
a	c	0	0	.33856690 E-2ℓ^{-2}	.33856691 E-2ℓ^{-2}	.39630243 E-3ℓ^{-2}	-.902619611 E-1ℓ^{-2}	-.902619611 E-1ℓ^{-2}	-.83021424 E-2ℓ^{-2}
		0	1	.34971346 E-3ℓ^{-1}	.34971347 E-3ℓ^{-1}	.93024782 E-4ℓ^{-1}	-.132836778 E-1ℓ^{-1}	-.105523864 E-1ℓ^{-1}	-.637948127 E-2ℓ^{-1}
		0	2	.97467719 E-3ℓ^{-1}	.80087349 E-3ℓ^{-1}	.11683658 E-3ℓ^{-1}	-.242494814 E-1ℓ^{-1}	-.146031382 E-1ℓ^{-1}	-.21649887 E-2ℓ^{-1}

ℓ	k	α	β	$\left(\zeta^{\alpha}_{\ell g}, \zeta^{\beta}_{kg}\right)_{\Gamma} \ell^{-4}$			$\left(\nabla\zeta^{\alpha}_{\ell g}, \nabla\zeta^{\beta}_{kg}\right)_{\Gamma} \ell^{-2}$		
				$\Gamma = I$	$\Gamma = II$	$\Gamma = III$	$\Gamma = I$	$\Gamma = II$	$\Gamma = III$
		0	3	$-.87294758$ $E\text{-}3\ell^{-1}$	$-.63923587$ $E\text{-}3\ell^{-1}$	$-.69120364$ $E\text{-}4\ell^{-1}$	$.319551435$ $E\text{-}1\ell^{-1}$	$.129497842$ $E\text{-}1\ell^{-1}$	$.264526616$ $E\text{-}1\ell^{-1}$
		1	0	$.63923584$ $E\text{-}3\ell^{-1}$	$.87294759$ $E\text{-}3\ell^{-1}$	$.69120364$ $E\text{-}4\ell^{-1}$	$-.26534404$ $E\text{-}2\ell^{-1}$	$.69937102$ $E\text{-}2\ell^{-1}$	$.14997946$ $E\text{-}2\ell^{-1}$
		1	1	$.62489345$ $E\text{-}4$	$.87693588$ $E\text{-}4$	$.16111997$ $E\text{-}4$	$-.96275509$ $E\text{-}3$	$.281964943$ $E\text{-}2$	$.2683367640$ $E\text{-}3$
		1	2	$.18200876$ $E\text{-}3$	$.20447427$ $E\text{-}3$	$.20196051$ $E\text{-}4$	$-.6995035$ $E\text{-}3$	$.75439563$ $E\text{-}3$	$.40314334$ $E\text{-}3$
		1	3	$-.16367283$ $E\text{-}3$	$-.16367283$ $E\text{-}3$	$-.11760043$ $E\text{-}4$	$.17947133$ $E\text{-}2$	$.115515197$ $E\text{-}2$	$-.5820606$ $E\text{-}4$
		2	0	$.80087347$ $E\text{-}3\ell^{-1}$	$.9746772$ $E\text{-}3\ell^{-1}$	$.11683685$ $E\text{-}3\ell^{-1}$	$.8797269$ $E\text{-}3\ell^{-1}$	$.102109641$ $E\text{-}1\ell^{-1}$	$.40527939$ $E\text{-}2\ell^{-1}$
		2	1	$.85660160$ $E\text{-}4$	$.10229351$ $E\text{-}3$	$.27462475$ $E\text{-}4$	$.110632465$ $E\text{-}2$	$.453541882$ $E\text{-}2$	$.214226491$ $E\text{-}2$

ℓ	k	α	β	$\left(\zeta^{\alpha}_{\ell g},\ \zeta^{\beta}_{kg}\right)_{\Gamma}\ \ell^{-4}$			$\left(\nabla\zeta^{\alpha}_{\ell g},\ \nabla\zeta^{\beta}_{kg}\right)_{\Gamma}\ \ell^{-2}$		
				$\Gamma = I$	$\Gamma = II$	$\Gamma = III$	$\Gamma = I$	$\Gamma = II$	$\Gamma = III$
		2	2	.22985505 E-3	.22985506 E-3	.34400149 E-4	.360992590 E-3	.135749671 E-2	.110937364 E-2
		2	3	-.20447426 E-3	-.18200876 E-3	-.20196051 E-4	-.50672868 E-3	.10021049 E-2	-.815868 E-3
		3	0	-.34971346 E-3ℓ^{-1}	-.34971347 E-3ℓ^{-1}	-.93024782 E-4ℓ^{-1}	.26141079 E-1ℓ^{-1}	.167835491 E-1ℓ^{-1}	-.145663557 E-2ℓ^{-1}
		3	1	-.47709926 E-4	-.47709928 E-4	-.21962795 E-4	.182712287 E-2	-.814944 E-5	-.974457665 E-3
		3	2	-.10229350 E-3	-.85660164 E-4	-.27462475 E-4	.69826981 E-2	.28118845 E-2	-.406477098 E-3
		3	3	.87693584 E-4	.62489348 E-4	.16111997 E-4	-.83508964 E-2	-.33561119 E-2	.258055885 E-3

Table C.17. Flux integrals — mathematical mesh. Standard basic patch configuration of Fig. C.7.

3-Element 9th order incomplete set.

ℓ	α	$\left(\zeta_{\ell g}^{\alpha},\ 1\right)_{\Gamma}\ell^{-3}$		
		$\Gamma = \mathrm{I}$	$\Gamma = \mathrm{II}$	$\Gamma = \mathrm{III}$
a	0	0.98860883	0.97229648	0.97229652
		$E\text{-}1\ell^{-1}$	$E\text{-}2\ell^{-1}$	$E\text{-}2\ell^{-1}$
	1	0.11107561	0.24336381	0.10966708
		$E\text{-}1$	$E\text{-}2$	$E\text{-}2$
	2	0.18622459	0.2773136	0.27731361
		$E\text{-}1$	$E\text{-}2$	$E\text{-}2$
	3	-0.11107561	-0.10966708	-0.24336383
		$E\text{-}1$	$E\text{-}2$	$E\text{-}2$

section C.2.2 that we would only have to consider triangles abc and abd of Fig. C.4. This is true but it is also true that we could equally well just consider triangles aef and afg. To avoid possible confusion with H and to correspond more closely with the algorithm of the computer programs we shall choose to use triangles aef and afg.

Tables C.18 and C.19 are lists of the required inner products. To obtain these from the inner products over H tabulated in Tables C.16 and C.17 we need the information presented below for the basic element function set $\{\Psi_{Jg}^{ja}\}$ of each of the superelement functions ψ_{Jg}^{a} centered at the points $\{a, g, f, e\}$ over the triangles aef and afg of Fig. C.4.

We arrange the relationships in the vector form $\begin{bmatrix} \Psi_{Jg}^{j0} \\ \Psi_{Jg}^{j1} \\ \Psi_{Jg}^{j2} \end{bmatrix}$ for convenience.

$$\begin{bmatrix} \Psi_{ag}^{40} \\ \Psi_{ag}^{41} \\ \Psi_{ag}^{42} \end{bmatrix} = \begin{bmatrix} \zeta_{ag}^{0} \\ -\zeta_{ag}^{1} \\ \frac{1}{\sqrt{3}} \{\zeta_{ag}^{2} - \zeta_{ag}^{3}\} \end{bmatrix} \tag{C.10}$$

$$\begin{bmatrix} \Psi_{ag}^{30} \\ \Psi_{ag}^{31} \\ \Psi_{ag}^{32} \end{bmatrix} = \begin{bmatrix} \zeta_{ag}^{0} \\ -\zeta_{ag}^{2} \\ \frac{1}{\sqrt{3}} \{-\zeta_{ag}^{3} - \zeta_{ag}^{1}\} \end{bmatrix} \tag{C.11}$$

Table C.18. Inner products — mathematical mesh. Standard super-patch configuration of Fig. C.4.

3-Element 9th order incomplete set; $\left(\Psi^{j\alpha}_{\ell g},\ \Psi^{j\beta}_{kg}\right)_\Gamma$ and $\left(\nabla\Psi^{j\alpha}_{\ell g},\ \nabla\Psi^{j\beta}_{kg}\right)_\Gamma$ required for the following combinations of $\{j,\ \alpha,\ \beta,\ \ell,\ k,\ \Gamma\}$.

(A)

$\Gamma = I - III\left[\alpha = 0 - 2\left[\beta = 0 - 2\right.\right.$

j	ℓ	k
$\Delta aef \equiv 3$	a	ℓ
		f
$\Delta afg \equiv 4$		f
		g

(B)

$\Gamma = I - III\left[j = 1 - 6\right.$

ℓ	k	α	β
a	a	0	0
			1
			2
		1	1
			2
		2	2

Table C.19. Flux integrals — mathematical mesh. Standard super-
patch configuration of Fig. C.4.

3-Element 9th order incomplete set; $\left(\Psi_{\ell g}^{j\alpha}, 1\right)_{\Gamma}$ required

for the following combinations of $\{j, \alpha, \ell, \Gamma\}$

ℓ	α
a	0
	1
	2

$\Gamma = I - III$ $\left\{\; j = 1 - 6\right.$

$$
\begin{bmatrix} \Psi_{gg}^{40} \\ \Psi_{gg}^{41} \\ \Psi_{gg}^{42} \end{bmatrix} = \begin{bmatrix} \zeta_{gg}^{0} \\ \zeta_{gg}^{3} \\ \frac{1}{\sqrt{3}} \{-\zeta_{gg}^{1} - \zeta_{gg}^{2}\} \end{bmatrix} \tag{C.12}
$$

$$
\begin{bmatrix} \Psi_{fg}^{30} \\ \Psi_{fg}^{31} \\ \Psi_{fg}^{32} \end{bmatrix} = \begin{bmatrix} \zeta_{fg}^{0} \\ \zeta_{fg}^{1} \\ \frac{1}{\sqrt{3}} \{-\zeta_{fg}^{2} + \zeta_{fg}^{3}\} \end{bmatrix} \tag{C.13}
$$

$$
\begin{bmatrix} \Psi_{fg}^{40} \\ \Psi_{fg}^{41} \\ \Psi_{fg}^{42} \end{bmatrix} = \begin{bmatrix} \zeta_{fg}^{0} \\ \zeta_{fg}^{2} \\ \frac{1}{\sqrt{3}} \{\zeta_{fg}^{3} + \zeta_{fg}^{1}\} \end{bmatrix} \tag{C.14}
$$

$$
\begin{bmatrix} \Psi_{eg}^{30} \\ \Psi_{eg}^{31} \\ \Psi_{eg}^{32} \end{bmatrix} = \begin{bmatrix} \zeta_{eg}^{0} \\ -\zeta_{eg}^{3} \\ \frac{1}{\sqrt{3}} \{\zeta_{eg}^{1} + \zeta_{eg}^{2}\} \end{bmatrix} \tag{C.15}
$$

and the superelement functions 'centered' at point a, $\{\psi_{ag}^{0}, \psi_{ag}^{1}, \psi_{ag}^{2}\}$ are composed of the following basic element functions:

$$
\begin{bmatrix} \Psi_{ag}^{10} \\ \Psi_{ag}^{11} \\ \Psi_{ag}^{12} \end{bmatrix} = \begin{bmatrix} \zeta_{ag}^{0} \\ \zeta_{ag}^{1} \\ \frac{1}{\sqrt{3}} (-\zeta_{a}^{2} + \zeta_{ag}^{3}) \end{bmatrix} \tag{C.16}
$$

$$
\begin{bmatrix} \Psi_{ag}^{20} \\ \Psi_{ag}^{21} \\ \Psi_{ag}^{22} \end{bmatrix} = \begin{bmatrix} \zeta_{ag}^{0} \\ \zeta_{ag}^{3} \\ \frac{1}{\sqrt{3}}(-\zeta_{ag}^{1} - \zeta_{ag}^{2}) \end{bmatrix}
\tag{C.17}
$$

$$
\begin{bmatrix} \Psi_{ag}^{30} \\ \Psi_{ag}^{31} \\ \Psi_{ag}^{32} \end{bmatrix} = \begin{bmatrix} \zeta_{ag}^{0} \\ -\zeta_{ag}^{2} \\ \frac{1}{\sqrt{3}}(-\zeta_{ag}^{3} - \zeta_{ag}^{1}) \end{bmatrix}
\tag{C.18}
$$

$$
\begin{bmatrix} \Psi_{ag}^{40} \\ \Psi_{ag}^{41} \\ \Psi_{ag}^{42} \end{bmatrix} = \begin{bmatrix} \zeta_{ag}^{0} \\ -\zeta_{ag}^{1} \\ \frac{1}{\sqrt{3}}(\zeta_{ag}^{2} - \zeta_{ag}^{3}) \end{bmatrix}
\tag{C.19}
$$

$$
\begin{bmatrix} \Psi_{ag}^{50} \\ \Psi_{ag}^{51} \\ \Psi_{ag}^{52} \end{bmatrix} = \begin{bmatrix} \zeta_{ag}^{0} \\ -\zeta_{ag}^{3} \\ \frac{1}{\sqrt{3}}(\zeta_{ag}^{2} + \zeta_{ag}^{1}) \end{bmatrix}
\tag{C.20}
$$

$$
\begin{bmatrix} \Psi_{ag}^{60} \\ \Psi_{ag}^{61} \\ \Psi_{ag}^{62} \end{bmatrix} = \begin{bmatrix} \zeta_{ag}^{0} \\ \zeta_{ag}^{2} \\ \frac{1}{\sqrt{3}}(\zeta_{ag}^{3} + \zeta_{ag}^{1}) \end{bmatrix}
\tag{C.21}
$$

We now have to relate these inner products over triangles aef and afg of Fig. C.4 with the general case shown in Fig. C.6.

The algorithm of the program is constructed so that $(M\psi^{\alpha}_{pg}, \psi^{\beta}_{pg})$, $(M\psi^{\alpha}_{pg}, \psi^{\beta}_{eg})$, $(M\psi^{\alpha}_{pg}, M\psi^{\beta}_{fg})$ and $(M\psi^{\alpha}_{pg}, \psi^{\beta}_{gg})$ are the only inner products required. We have that

$$(M\psi^{\alpha}_{pg}, \psi^{\beta}_{pg}) = M_p \sum_{j=1}^{6} (\Psi^{j\alpha}_{pg}, \Psi^{j\beta}_{pg})_I + \sum_{j=1}^{6} \overline{M}_j \sum_{\Gamma=II}^{III} (\Psi^{j\alpha}_{pg}, \Psi^{j\beta}_{pg})_\Gamma$$

$$(C.22)$$

where Table C.20 shows the convention to be used for the material properties M_j

$$(M\psi^{\alpha}_{pg}, \psi^{\beta}_{eg}) = \sum_{\Gamma=I}^{III} \left\{ (\Psi^{4\alpha}_{ag}, \Psi^{4\beta}_{gg})_\Gamma M^{e1}_\Gamma + (\Psi^{3\alpha}_{ag}, \Psi^{3\beta}_{eg}) M^{e2}_\Gamma \right\} \qquad (C.23)$$

$$(M\psi^{\alpha}_{pg}, \psi^{\beta}_{fg}) = \sum_{\Gamma=I}^{III} \left\{ (\Psi^{3\alpha}_{ag}, \Psi^{3\beta}_{fg})_\Gamma M^{f1}_\Gamma + (\Psi^{4\alpha}_{ag}, \Psi^{4\beta}_{fg}) M^{f2}_\Gamma \right\} \qquad (C.24)$$

$$(M\psi^{\alpha}_{pg}, \psi^{\beta}_{gg}) = \sum_{\Gamma=I}^{III} \left\{ (\Psi^{3\alpha}_{ag}, \Psi^{3\beta}_{eg})_\Gamma M^{g1}_\Gamma + (\Psi^{4\alpha}_{ag}, \Psi^{4\beta}_{gg}) M^{g2}_\Gamma \right\}. \qquad (C.25)$$

The corresponding table for the material properties is Table C.21 Equations (C.22)-(C.25) are more general than the equations derived previously, eqs. (C.4)-(C.5), for the case of 60°-rotational symmetry. Those equations are a subset of this system and this is the reason why the equations actually programmed are eqs. (C.22)-(C.25).

We now turn our attention to the 3-element incomplete cubic set. This is treated in exactly the same fashion as the 3-element 9th-order incomplete set was treated. Tables C.22-C.23 are the tables corresponding to Tables C.16-C.17 for this set. In terms of the notation of this chapter we have

Table C.20. Indexing scheme for material properties of eq. (C.22).

j	$\bar{M}_j$
1	M_d
2	M_e
3	M_f
4	M_g
5	M_c
6	M_b

Table C.21. Indexing scheme for material properties of eqs. (C.23)-(C.25).

Γ	M_Γ^{e1}	M_Γ^{e2}	M_Γ^{f1}	M_Γ^{f2}	M_Γ^{g1}	M_Γ^{g2}
I	M_a	M_a	M_a	M_a	M_a	M_a
II	M_d	M_e	M_e	M_f	M_g	M_f
III	M_e	M_f	M_f	M_g	M_c	M_g

Table C.22. Inner products — mathematical mesh. Standard basic patch configuration of Fig. C.5.
3-Element cubic incomplete set.

ℓ	k	α	β	$*\left(\zeta^{\alpha}_{\ell g}, \zeta^{\beta}_{kg}\right)_{\Gamma} \ell^{-4}$			$\left(\nabla\zeta^{\alpha}_{\ell g}, \nabla\zeta^{\beta}_{kg}\right)_{\Gamma} \ell^{-2}$		
				$\Gamma = \mathrm{I}$	$\Gamma = \mathrm{II}$	$\Gamma = \mathrm{III}$	$\Gamma = \mathrm{I}$	$\Gamma = \mathrm{II}$	$\Gamma = \mathrm{III}$
a	a	0	0	$.87355496$ $\mathrm{E}{-}1\ell^{-2}$	$.58094120$ $\mathrm{E}{-}2\ell^{-2}$	$.58094123$ $\mathrm{E}{-}2\ell^{-2}$	$.34248984$ ℓ^{-2}	$.1751652$ ℓ^{-2}	$.17516521$ ℓ^{-2}
		0	1	$-.10842022$ $\mathrm{E}{-}18\ell^{-1}$	$.57491018$ $\mathrm{E}{-}3\ell^{-1}$	$-.57491024$ $\mathrm{E}{-}3\ell^{-1}$	$.32526065$ $\mathrm{E}{-}18\ell^{-1}$	$.18724275$ $\mathrm{E}{-}1\ell^{-1}$	$-.18724278$ $\mathrm{E}{-}1\ell^{-1}$
		0	2	$.15985002$ $\mathrm{E}{-}1\ell^{-1}$	$.16300025$ $\mathrm{E}{-}2\ell^{-1}$	$.16300025$ $\mathrm{E}{-}2\ell^{-1}$	$.24234453$ $\mathrm{E}{-}1\ell^{-1}$	$.45617794$ $\mathrm{E}{-}1\ell^{-1}$	$.45617797$ $\mathrm{E}{-}1\ell^{-1}$
		0	3	$-.70398622$ $\mathrm{E}{-}2\ell^{-1}$	$-.19786429$ $\mathrm{E}{-}2\ell^{-1}$	$-.19786429$ $\mathrm{E}{-}2\ell^{-1}$	$.78405580$ $\mathrm{E}{-}1\ell^{-1}$	$-.71278572$ $\mathrm{E}{-}3\ell^{-1}$	$-.71278158$ $\mathrm{E}{-}3\ell^{-1}$
		1	1	$.32406761$ $\mathrm{E}{-}3$	$.67073363$ $\mathrm{E}{-}4$	$.67073372$ $\mathrm{E}{-}4$	$.397670735$ $\mathrm{E}{-}1$	$.36381373$ $\mathrm{E}{-}2$	$.36381373$ $\mathrm{E}{-}2$
		1	2	$-.10164395$ $\mathrm{E}{-}19$	$.16018113$ $\mathrm{E}{-}3$	$-.16018115$ $\mathrm{E}{-}3$	$.32526065$ $\mathrm{E}{-}18$	$.47839495$ $\mathrm{E}{-}2$	$-.47839501$ $\mathrm{E}{-}2$

ℓ	k	α	β	$^*\!\left(\zeta^\alpha_{\ell g},\ \zeta^\beta_{kg}\right)_\Gamma \ell^{-4}$			$\left(\nabla\zeta^\alpha_{\ell g},\ \nabla\zeta^\beta_{kg}\right)_\Gamma \ell^{-2}$		
				$\Gamma = \mathrm{I}$	$\Gamma = \mathrm{II}$	$\Gamma = \mathrm{III}$	$\Gamma = \mathrm{I}$	$\Gamma = \mathrm{II}$	$\Gamma = \mathrm{III}$
		1	3	.67762636 E-20	-.14292383 E-3	.14292383 E-3	-.102999206 E-16	.61213967 E-2	-.61213967 E-2
		2	2	.32068235 E-2	.45855327 E-3	.45855330 E-3	.14344658 E-1ℓ^2	.12072678 E-1	.12072679 E-1
		2	3	-.16017472 E-2	-.57376990 E-3	-.57376990 E-3	.30293063 E-2	-.15146554 E-2	-.15146543 E-2
		3	3	.12219053 E-2	.12219054 E-2	.12219054 E-2	.51320008 E-1	.51320001 E-1	.51320001 E-1
a	c	0	0	.13410436 E-1ℓ^{-2}	.13410434 E-1ℓ^{-2}	.20466448 E-2ℓ^{-2}	-.11244075 ℓ^{-2}	-.11244073 ℓ^{-2}	-.63793649 E-1ℓ^{-2}
		0	1	-.13978030 E-2ℓ^{-1}	-.68832079 E-3ℓ^{-1}	.10199609 E-3ℓ^{-1}	-.13631667 E-2ℓ^{-1}	-.43287032 E-1ℓ^{-1}	-.10905351 E-1ℓ^{-1}
		0	2	.38957076 E-2ℓ^{-1}	.30570612 E-2ℓ^{-1}	.60777077 E-3ℓ^{-1}	-.30159424 E-1ℓ^{-1}	-.98452443 E-2ℓ^{-1}	-.17730358 E-1ℓ^{-1}

ℓ	k	α	β	$*\left(\zeta_{\ell g}^{\alpha}, \zeta_{kg}^{\beta}\right)_{\Gamma} \ell^{-4}$			$\left(\nabla\zeta_{\ell g}^{\alpha}, \nabla\zeta_{kg}^{\beta}\right)_{\Gamma} \ell^{-2}$		
				$\Gamma = I$	$\Gamma = II$	$\Gamma = III$	$\Gamma = I$	$\Gamma = II$	$\Gamma = III$
		0	3	$-.70398605$ $E-2\ell^{-1}$	$-.19786422$ $E-2\ell^{-1}$	$-.19786432$ $E-2\ell^{-1}$	$.78405584$ $E-1\ell^{-1}$	$-.71276475$ $E-3\ell^{-1}$	$-.71278040$ $E-3\ell^{-1}$
		1	0	$.68832048$ $E-3\ell^{-1}$	$.13978022$ $E-2\ell^{-1}$	$-.10199614$ $E-3\ell^{-1}$	$.432870427$ $E-1\ell^{-1}$	$.1363170$ ℓ^{-1}	$.109053519$ ℓ^{-1}
		1	1	$-.92603412$ $E-4$	$-.92603414$ $E-4$	$-.57158957$ $E-5$	$-.73653758$ $E-2$	$-.73653758$ $E-2$	$-.83157437$ $E-3$
		1	2	$.19075785$ $E-3$	$.30340262$ $E-3$	$-.31197617$ $E-4$	$.12345681$ $E-1$	$.115740734$ $E-2$	$.31635808$ $E-2$
		1	3	$.18696760$ $E-9$	$-.14292374$ $E-3$	$.14292387$ $E-3$	$.204794128$ $E-7$	$.61214007$ $E-2$	$-.61214007$ $E-2$
		2	0	$.30570618$ $E-2\ell^{-1}$	$.38957069$ $E-2\ell^{-1}$	$.60777077$ $E-3\ell^{-1}$	$-.98452463$ $E-2\ell^{-1}$	$-.3015942$ $E-1\ell^{-1}$	$-.17730358$ $E-1\ell^{-1}$
		2	1	$-.30340278$ $E-3$	$-.19075795$ $E-3$	$.31197603$ $E-4$	$-.11574075$ $E-2$	$-.12345678$ $E-1$	$-.31635805$ $E-2$

ℓ	k	α	β	$*\left(\overset{\alpha}{\zeta}_{\ell g},\ \overset{\beta}{\zeta}_{kg}\right)_\Gamma \ell^{-4}$			$\left(\nabla\overset{\alpha}{\zeta}_{\ell g},\ \nabla\overset{\beta}{\zeta}_{kg}\right)_\Gamma \ell^{-2}$		
				$\Gamma = I$	$\Gamma = II$	$\Gamma = III$	$\Gamma = I$	$\Gamma = II$	$\Gamma = III$
		2	2	.88357741 E-3	.88357726 E-3	.18025701 E-3	-.23610770 E-2	-.23610766 E-2	-.4900350 E-2
		2	3	-.16017469 E-2	-.57376970 E-3	-.5737700 E-3	.30293081 E-2	-.15146497 E-2	-.15146539 E-2
		3	0	-.19786432 E-2ℓ^{-1}	-.70398632 E-2ℓ^{-1}	-.19786432 E-2ℓ^{-1}	-.712789 E-3ℓ^{-1}	.7840558 E-1ℓ^{-1}	-.712783 E-3ℓ^{-1}
		3	1	.14292390 E-3	.17933637 E-9	-.14292382 E-3	-.612139803 E-2	.5 E-8	.61213999 E-2
		3	2	-.57376998 E-3	-.16017473 E-2	-.57376998 E-3	-.15146566 E-2	.302930354 E-2	-.15146566 E-2
		3	3	.12219051 E-2	.12219052 E-2	.12219055 E-2	.51320013 E-1	.51320013 E-1	.51320013 E-1

$*$It should be noted that $\zeta^3_{ag}(x,\ y) = \zeta^3_{bg}(x,\ y) = \zeta^3_{cg}(x,\ y)$

Table C.23. Flux integrals — mathematical mesh. Standard basic patch configuration of Fig. C.5.

3-Element cubic incomplete set.

ℓ	α	$\left(\zeta^{\alpha}_{\ell g},\ 1\right)_{\Gamma}\ \ell^{-3}$		
		$\Gamma = I$	$\Gamma = II$	$\Gamma = III$
a	0	0.12473615 ℓ^{-1}	0.24234453 $E\text{-}1\ \ell^{-1}$	0.24234455 $E\text{-}1\ \ell^{-1}$
	1	-0.10842022 $E\text{-}18$	0.22890941 $E\text{-}2$	-0.22890944 $E\text{-}2$
	2	0.24501745 $E\text{-}1$	0.69941344 $E\text{-}2$	0.69941349 $E\text{-}2$
	3	-0.12830006 $E\text{-}1$	-0.12830006 $E\text{-}1$	-0.12830006 $E\text{-}1$

$$\zeta^{0}_{ag}(x, y) = \zeta^{3c}_{1}(x, y) \qquad \zeta^{2}_{ag}(x, y) = \zeta^{3c}_{3}(x, y)$$

$$\zeta^{1}_{ag}(x, y) = \zeta^{3c}_{2}(x, y) \qquad \zeta^{3}_{ag}(x, y) = \zeta^{3c}_{4}(x, y)$$

where the shapes are as defined by eqs. (3.7)-(3.10). The equations corresponding to the system, eqs. (C.10)-(C.21), are eqs. (3.13)-(3.15) of section 3.1.1. The remaining tables required for the algorithm are Tables C.18-C.21. These tables can be thought of as being common for all the sets used with the regular mathematical mesh.

(B) Distorted Mesh

This mesh introduces irregular polygons into the set of superpatches. Figure C.8 shows one of the possibilities.
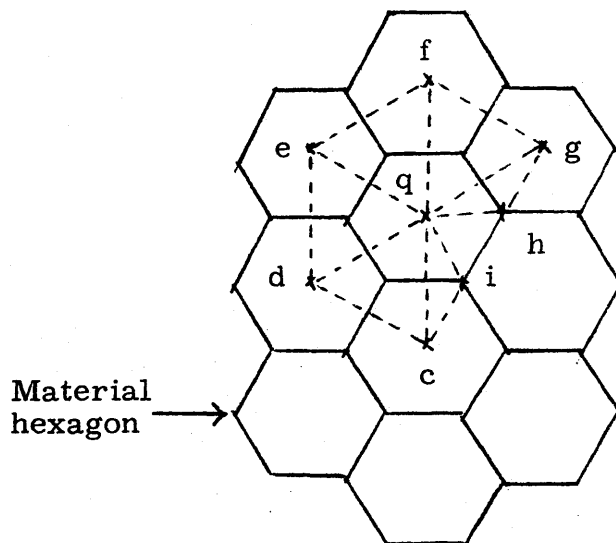
Fig. C.8. Distorted mesh.

With the introduction of irregular polygons it becomes imperative to look at the assemblage of inner products from the viewpoint of triangles.

There are basically three types of triangles involved: a large equilateral triangle such as triangle fqg, an isosceles triangle typified by triangle qhg, and a small equilateral triangle qhi.

The inner products over the large equilateral triangle are exactly those obtained earlier in the section for the standard geometrical configurations of Figs. C. 5 and C. 7. The inner products for the small equilateral triangle can be obtained from those results by the use of coordinate transformations.
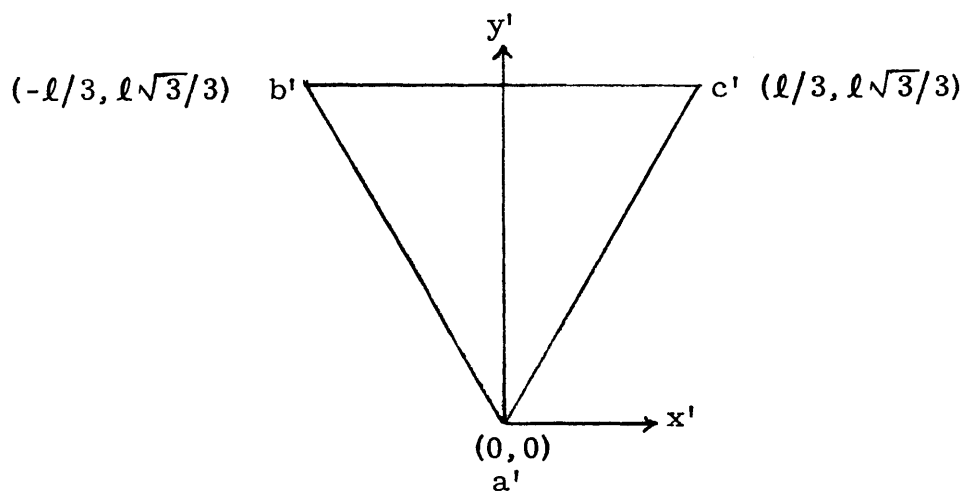
Fig. C. 9. Basic patch — small equilateral triangle — distorted mesh.

Figure C. 9 shows the small equilateral triangle. The required transformation between triangle abc of Fig. C. 5 and this triangle is

$$x' = \frac{x\sqrt{3}}{3}$$

$$y' = \frac{y\sqrt{3}}{3}.$$

(C. 26)

We then have that

$$\iint\limits_{\Delta a'b'c'} dx'dy'\ \Psi^{k\alpha}_{\theta g}(x',y')\ \Psi^{k\beta}_{\gamma g}(x',y') = \frac{1}{3}\ \iint\limits_{\Delta abc} dxdy\ \Psi^{j\alpha}_{\theta g}(x,y)\ \Psi^{j\alpha}_{\gamma g}(x,y)$$

(C.27)

where

$$\Psi^{k\alpha}_{\theta g}(x',y') = \Psi^{j\alpha}_{\theta g}(\sqrt{3}\,x',\sqrt{3}\,y') \qquad j \equiv \Delta abc \quad k \equiv \Delta a'b'c'.$$

(C.28)

Equation (C.28) is a logical extension of the discussion in section 3.2 where the sets $\{\psi_{kg}\}$ were constructed by rotating specific shapes and joining the corresponding $\{\theta_j\}$ to form Θ_J. We transform shapes and not interpolation conditions. The shell sets C_1 and $\{C_1+C_2\}$ were constructed by rotations of shapes and eqs. (C.27)-(C.28) will be applied in the use of these sets with the distorted mesh.

Continuing, we have that

$$\iint\limits_{\Delta a'b'c'} dx'dy' \cdot \nabla'\Psi^{k\alpha}_{\theta g}(x',y') \cdot \nabla'\Psi^{k}_{\gamma g}(x',y')$$

$$= \iint\limits_{\Delta abc} dxdy \cdot \nabla\Psi^{j\alpha}_{\theta g}(x,y) \cdot \nabla\Psi^{j\alpha}_{\gamma g}(x,y).$$

(C.29)
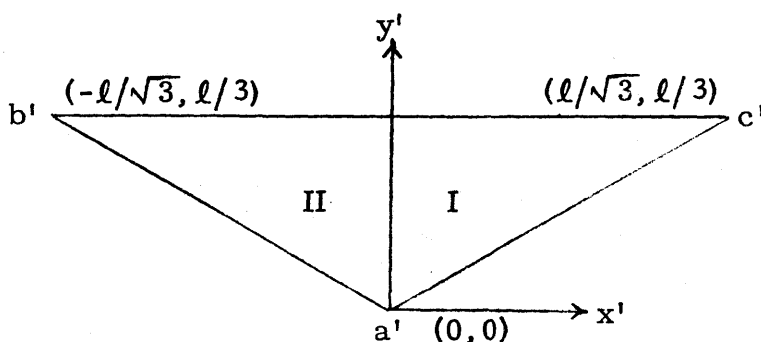
Fig. C.10.

Basic patch — isosceles triangle — distorted mesh.

The corresponding equations for the isosceles triangle a'b'c' of Fig. C.10 are

$$x' = x$$

$$y' = \frac{y}{3} \tag{C.30}$$

$$\iint\limits_{\Delta a'b'c'} dx'dy' = \Psi^{k\alpha}_{\theta g}(x',y')\,\Psi^{k\beta}_{\gamma g}(x',y')$$

$$= \frac{1}{3} \iint\limits_{\Delta abc} dxdy\;\Psi^{j\alpha}_{\theta g}(x,y)\,\Psi^{j\alpha}_{\gamma g}(x,y) \tag{C.31}$$

$$\Psi^{k\alpha}_{\theta g}(x',y') = \Psi^{j\alpha}_{\theta g}(x',y') \tag{C.32}$$

and

$$\iint\limits_{\Delta a'b'c'} dx'dy' \cdot \nabla'\Psi^{k\alpha}_{\theta g}(x',y') \cdot \nabla'\Psi^{k\beta}_{\gamma g}(x',y')$$

$$= \iint\limits_{\Delta abc} dxdy\left[\frac{1}{3}\frac{\partial}{\partial x}\Psi^{j\alpha}_{\theta g}(x,y)\frac{\partial}{\partial x}\Psi^{j\alpha}_{\gamma g}(x,y) + 3\frac{\partial}{\partial y}\Psi^{j\alpha}_{\theta g}(x,y)\frac{\partial}{\partial y}\Psi^{j\alpha}_{\gamma g}(x,y)\right]$$

$$\tag{C.33}$$

Tables C.24-C.25 list the inner products for the $\{C_1 + C_2\}$ shell set over the equilateral triangle a'b'c' of Fig. C.9. The C_1 shell set inner products are, by the design of the shell sets, obtainable from this table by simply deleting the entries where α or $\beta = 2$. Tables C.26-C.27 list the corresponding results for the isosceles triangle a'b'c' of Fig. C.10.

Table C.24. Inner products — distorted mesh. Basic patch of Fig. C.9.

$\{C_1+C_2\}$ shell set; j = equilateral triangle a'b'c' (Figure C.9).

ℓ	k	α	β	$\left(\Psi_{\ell g}^{j\alpha},\ \Psi_{kg}^{j\beta}\right)3\ell^{-2}$	$\left(\nabla\Psi_{\ell g}^{j\alpha},\ \nabla\Psi_{kg}^{j\beta}\right)$
a'	a'	1	1	0.09622503	0.57735021
		1	2	-0.0333333	-0.16666666
		2	2	0.01443375	0.14433755
a'	c'	1	1	0.048112509	-0.288675126
		1	2	-0.025	0.08333333
		2	1	-0.025	0.08333333
		2	2	0.01202813	0.0

Table C.25. Flux integrals — distorted mesh. Basic patch of Fig. C.9.

$\{C_1+C_2\}$ shell set; j = equilateral triangle a'b'c' (Figure C.9).

ℓ	α	$\left(\Psi_{\ell g}^{j\alpha},\ 1\right)3\ell^{-2}$
a'	1	0.19245005
	2	-0.0833333

Table C.26. Inner products — distorted mesh. Basic patch of Fig. C.10.

$\{C_1 + C_2\}$ shell set; j = isosceles triangle a'b'c' (Figure C.10).

ℓ	k	α	β	$\left(\Psi_{\ell g}^{j\alpha},\ \Psi_{kg}^{j\beta}\right)_\Gamma 3\ell^{-2}$		$\left(\nabla\Psi_{\ell g}^{j\alpha},\ \nabla\Psi_{kg}^{j\beta}\right)_\Gamma/3$	
				$\Gamma = \mathrm{I}$	$\Gamma = \mathrm{II}$	$\Gamma = \mathrm{I}$	$\Gamma = \mathrm{II}$
a'	a'	1	1	.48112516 E-1	.48112516 E-1	.288675105	.288675105
		1	2	-.166666 E-1	-.1666666 E-1	-.8333333 E-1	-.833333 E-1
		2	2	.7216877 E-1	.7216877 E-2	.7216877 E-1	.7216877 E-1
c'	c'	1	1	.841968319 E-1	.12028133 E-1	.9622506 E-1	.9622506 E-1
		1	2	-.260416509 E-1	-.72916707 E-2	.0	-.555555 E-1
		2	2	.99232 E-2	.45105515 E-2	.120281247 E-1	.360843943 E-1
b'	b'	1	1	.12028133 E-1	.841968319 E-1	.9622506 E-1	.9622506 E-1
		1	2	-.72916707 E-2	-.260416509 E-1	-.555555 E-1	.0
		2	2	.45105515 E-2	.99232 E-2	.360843943 E-1	.120281247 E-1
b'	a'	1	1	.12021 E-1	.360843 E-1	-.144337	-.144337

ℓ	k	α	β	$\left(\Psi^{j\alpha}_{\ell g}, \Psi^{j\beta}_{kg}\right)_\Gamma 3\ell^{-2}$		$\left(\nabla\Psi^{j\alpha}_{\ell g}, \nabla\Psi^{j\beta}_{kg}\right)_\Gamma /3$	
				$\Gamma = I$	$\Gamma = II$	$\Gamma = I$	$\Gamma = II$
		1	2	-.624999 E-2	-.187496 E-1	.416666 E-1	.416666 E-1
		2	1	-.83333 E-2	-.166666 E-1	.833333 E-1	.0
		2	2	.4209838 E-2	.781828 E-2	-.180421 E-1	.180421 E-1
c'	a'	1	1	.360843 E-1	.12021 E-1	-.144337	-.144337
		1	2	-.187496 E-1	-.624999 E-2	.416666 E-1	.416666 E-1
		2	1	-.166666 E-1	-.83333 E-2	.0	.833333 E-1
		2	2	.781828 E-2	.4209838 E-2	.180421 E-1	-.180421 E-1
c'	b'	1	1	.24056256 E-1	.24056256 E-1	.481124 E-1	.481124 E-1
		1	2	-.15624997 E-1	-.93750039 E-2	-.27778 E-1	.0
		2	1	-.9374996 E-2	-.156250043 E-1	.0	-.27778 E-1
		2	2	.60140627 E-2	.60140627 E-2	.0	.0

Table C.27. Flux integrals — distorted mesh. Basic patch of Fig. C.10.

$\{C_1+C_2\}$ shell set; j = isosceles triangle a'b'c' (Figure C.10).

ℓ	α	$\left(\Psi^{j\alpha}_{\ell g},\ 1\right)_{\Gamma}\ \ell^{-2}\ 3$	
		$\Gamma = \mathrm{I}$	$\Gamma = \mathrm{II}$
a'	1	0.96224 E-1	0.96224 E-1
	2	-0.416666 E-1	-0.416666 E-1
b'	1	0.48111336 E-1	0.14433872
	2	-0.312500144 E-1	-0.520833116 E-1
c'	1	0.14433872	0.48111336 E-1
	2	-0.520833116 E-1	-0.312500144 E-1

Appendix D

IMPOSITION OF CONDITIONS AT SINGULAR POINTS

We consider in this appendix the implications of applying the conditions of flux continuity and current continuity at a singular point. It is an example of an examination of how the various conditions applied relate to each other in terms of the equations they give rise to. The results obtained have a direct bearing on the case where function continuity and derivative continuity are simultaneously applied across intersecting patch boundaries and this aspect of the problem is also included in the discussion.

Consider Fig. D.1. Regions 1, 2, ..., K are regions containing
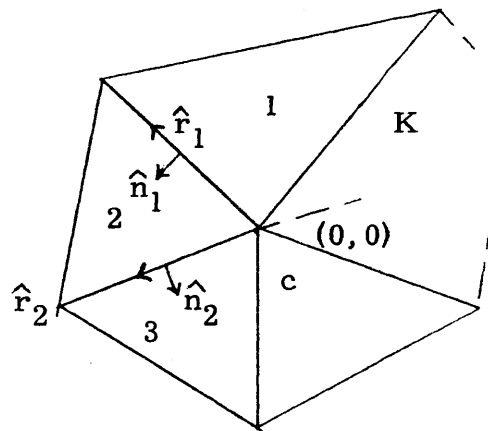
Fig. D.1. Singular point configuration.

different material with the corresponding diffusion coefficients $D_1, \ldots,$ D_K. Point c, (0,0), is the intersection point of all the material interfaces. The unit normal to these interfaces is denoted by $\hat{n}_k$ and the unit vector parallel to the interface is $\hat{r}_k$. We have

$$\widehat{n}_k = a_k \underline{i} + b_k \underline{j}$$

$$\widehat{r}_k = -b_k \underline{i} + a_k \underline{j}. \tag{D.1}$$

Normal current continuity across each interface gives

$$D_k[a_{kx}a_k + a_{ky}b_k] = [a_{k+1x}a_k + a_{k+1y}b_k] D_{k+1} \tag{D.2}$$

where

$$a_{kx} = \frac{\partial}{\partial x} \Psi^{k\beta}_{ig}(\underline{r})$$

$$a_{ky} = \frac{\partial}{\partial y} \Psi^{k\beta}_{ig}(\underline{r})$$

and region (K+1) is understood to be region 1. With function continuity

we have that $\lim\limits_{|\epsilon| \to 0} \widehat{r}_k \cdot \nabla\psi_{ig}(\underline{r}_c + |\epsilon|\widehat{r}_k)^*$ is continuous across material

interfaces. This means

$$-a_{kx}b_k + a_{ky}a_k = -a_{k+1x}b_k + a_{k+1y}a_k. \tag{D.3}$$

Equations (D.2) and (D.3) lead to the following system of homogeneous

equations.

$^*\underline{r}_c \equiv$ point c.

$$
\begin{bmatrix}
D_1a_1 & D_1b_1 & -D_2a_1 & -D_2b_1 & 0 & \\
-b_1 & a_1 & b_1 & -a_1 & 0 & 0 \\
0 & 0 & D_2a_2 & D_2b_2 & -D_3a_2 & -D_3b_2 \\
& 0 & -b_2 & a_2 & b_2 & -a_2 \\
& & & & & \\
& & & & & \\
-D_1a_K & -D_1b_K & 0 & & & \\
b_K & -a_K & 0 & & &
\end{bmatrix}
\begin{bmatrix}
a_{1x} \\ a_{1y} \\ a_{2x} \\ a_{2y} \\ \\ \\ a_{kx} \\ a_{ky}
\end{bmatrix}
=
\begin{bmatrix}
0 \\ \\ \\ \\ \\ \\ \\ 0
\end{bmatrix}
$$

(D.4)

In block form this becomes

$$
\begin{bmatrix}
A_1 & B_1 & 0 & & 0 \\
0 & A_2 & B_2 & 0 & \\
\vdots & & & & 0 \\
& 0 & & & B_{K-1} \\
B_K & 0 & & & A_K
\end{bmatrix}
\underline{a} = \underline{0}
$$

(D.5)

where

$$
A_k = \begin{bmatrix} D_k a_k & D_k b_k \\ -b_k & a_k \end{bmatrix} \quad \text{and} \quad B_k = \begin{bmatrix} -D_{k+1}a_k & -D_{k+1}b_k \\ b_k & -a_k \end{bmatrix}
$$

For the case where all the regions contain the same material, that is, the homogeneous case we have

$$
A_k = -B_k
$$

(D.6)

Equation (D.5) then reduces to

$$\begin{bmatrix} A_1 & -A_1 & & & & 0 \\ & A_2 & -A_2 & 0 & & \\ & & & & & \\ 0 & & & & -A_{K-1} \\ -A_K & 0 & & & A_K \end{bmatrix} \underline{a} = \underline{0} \qquad (D.7)$$

By adding columns we can reduce the coefficient matrix to

$$C = \begin{bmatrix} A_1 & & 0 \\ 0 & A_2 & 0 \\ & & 0 \\ & & 0 \\ -A_K & -A_K & 0 \end{bmatrix} \qquad (D.8)$$

As $|C| = 0$ this means that the constraints of function continuity and normal derivative continuity across interfaces lead to redundant equations and consequently a nonunique solution.

Now let us examine the general inhomogeneous case, eq. (D.4). If we add to the $(2k+1)^{\text{th}}$ column the $(2k)^{\text{th}}$ column multiplied by b_k/a_k; set $b_K = 0$ and $a_K = 1$, and transpose the resulting coefficient matrix, we obtain

$$C = \begin{bmatrix} D_1 a_1 + D_1 b_1^2/a_1 & & 0 & -D_1 & -b_1/a_1 \\ & a_1 & & 0 & -1 \\ & & & & 0 \\ & & & & \\ & & & D_K & 0 \\ & & & & 1 \end{bmatrix} \qquad \text{(D. 9)}$$

If we choose $K = 3$, $(a_1, b_1) = (-1/2, \sqrt{3}/2)$ and $(a_2, b_2) = (-1/2, -\sqrt{3}/2)$, it can be shown, by expanding the resulting determinant, that

$$|C| \neq 0 \qquad \text{in general.} \qquad \text{(D. 10)}$$

This means that $|C|$ is not identically zero with the consequence that the only solution of $\underline{a}$ is the trivial solution $\underline{0}$. In other words, the imposition of normal current continuity and function continuity can lead to zero gradients at point c. As flux continuity is an essential condition, this means that normal current continuity should not be imposed at singular points.

Appendix E

COMPUTER PROGRAMS

It should be emphasized at the start that the programs written during the course of this thesis were not meant to be 'Production' versions. They were designed solely as research tools with definite limitations as far as the range of problems is concerned and should be so regarded. Modifications were made as objectives changed and the logic of many of the codes reflect this hybridizing process. This introduction should serve as a note of caution against further modification of the programs as they now stand. If modifications are strongly desired it is recommended that the codes be rewritten using modules of algorithms taken from the current versions.

The programs are the computer implementation of the finite element method to solve the multigroup static neutron diffusion problem, eqs. (1.17) - (1.19); that is to say they assemble and solve the Galerkin system of equations, eq. (1.18). All the programs are limited to two group calculations with the assumptions that,

   (i) There is no upscattering

   (ii) No fission neutrons are born in the thermal group.
The equations actually programmed are those of eqs. (1.24) - (1.25). The orthodox power iteration scheme, eq. (1.26),

is used to solve the eigenvalue problem for the system multiplication constant, the eigenvalue λ. We shall divide the codes into two sets on the basis of the number of spatial dimensions treated. For the 1-D set we have the following programs

(a)   1-D FLOAT

(b)   1-D SECTION.

In 2-D we further subdivide the set into groups of programs using the physical mesh shown in Fig. 3.6 and those utilizing the mathematical coarse mesh of Fig. 2.6(b). The physical mesh group consists of

(a)   2-D PHYMESH

while the mathematical coarse mesh group is composed of

(a)   2-D MATHFIT

(b)   2-D MATHNO

We now present a short description of each code together with the corresponding input for a sample problem. The 1-D codes are discussed in section E.1 and the presentation on the 2-D codes follows in sections E.2 and E.3. All the programs are written in FORTRAN IV for the IBM 370/168 computer system. The source listings are presented in Appendix F.

E.1 1-D Programs

We first discuss 1-D FLOAT and then 1-D SECTION.

E.1.1 1-D FLOAT

(a) Description

1-D FLOAT was written to investigate the question of the condition of join in 1-D. The problem simulated is the one of Fig. 4.2. For convenience we repeat that Fig. here
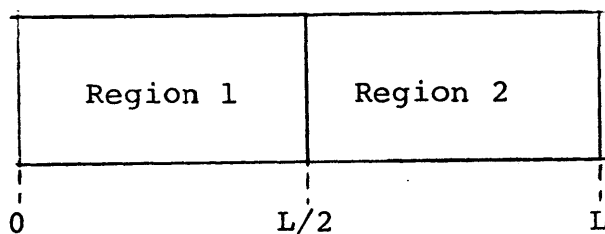
Fig. E.1. 1-D 2 Region Problem.

The version listed in Appendix F has the following restrictions

(i) The superelement set used is Kang's cubic Hermite set.[1]

(ii) Only five superelement functions ψ_{kg} can be used. These are the ones shown in Fig. E.2.
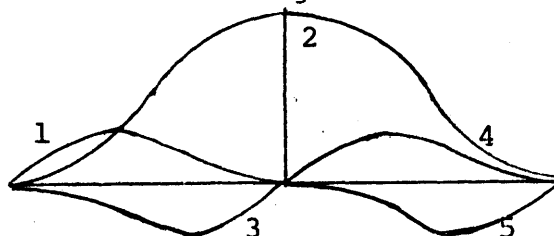
Fig. E.2. Superelement function set used. Kang's cubic Hermite.[1]

The numbers on the fig. are the indices of the super-element functions as used in the program. The program is set up for the flux continuity-current float case. The places where modifications are required for the other cases are indicated in the source listing in Appendix F.

We present next a summary of the subroutines involved

MAIN: - This forms the Galerkin coefficient matrices and uses the power iteration technique to solve the resulting matrix equation. The solution is then normalized to the input fission rate.

HPOLY: - This subroutine returns the value of the power of the mesh spacing H, for the inner product involved.

D: - Table of coefficients for the inner products $(\nabla\psi_{ig}, \nabla\psi_{jg})$.

E: - Table of coefficients for the inner products (ψ_{ig}, ψ_{jg}).

XIMQ: - Standard IBM subroutine for solving a linear system of equations.

Figure E.3 shows the general code logic. We now present the input preparation .
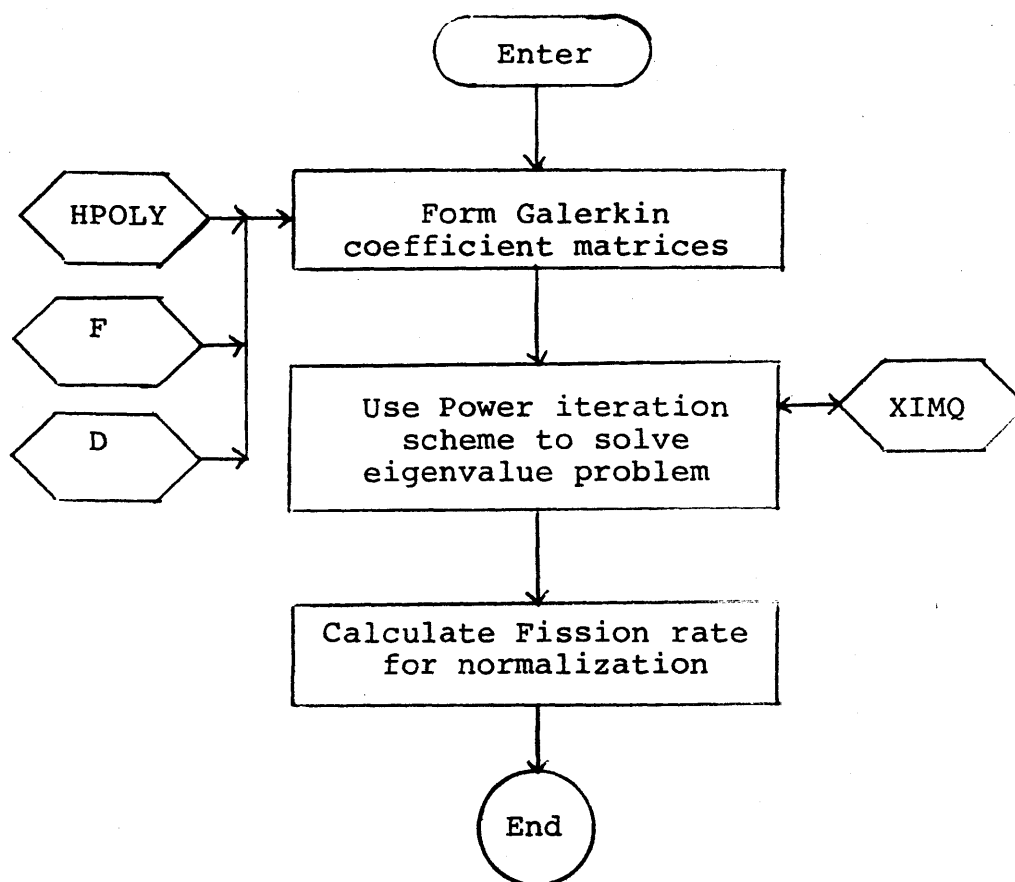
Fig. E.3. Flow chart for 1-D FLOAT.

(b)   Input Preparation

Card 1 - I5

MAXITR - Maximum number of outer iterations

Card 2 - E10.8

H - Mesh spacing (superelement function center-
center)

Card 3 - 2E10.8

>   ERMOD - Solution convergence criterion

>   EREIG - Eigenvalue convergence criterion

Card 4 - I5, E10.8, 2I5

>   NUMVAR - Number of unknowns per group

>   POWIN - Fission rate for normalization

>   NIMAX - Number of non-zero entries in lower
>   triangular part of the Galerkin
>   coefficient matrix

>   NREGIN - Number of different material compositions

Card 5 - I5, 7E10.8

>   IREGIN - Material composition index (beginning
>   with 1 and ending with NREGIN)

>   S1GR1(IREGIN) - Group 1 removal cross section

>   S1GR2(IREGIN) - Group 2 removal cross section

>   DIFF1(IREGIN) - Group 1 diffusion coefficient

>   DIFF2(IREGIN) - Group 2 diffusion coefficient

>   SIFNU1(IREGIN) - $\nu\Sigma_{f1}$

>   SIFNU2(IREGIN) - $\nu\Sigma_{f2}$

>   S1GS21(IREGIN) - Outscattering cross section;
>   Group 1 to Group 2.

Card 5 has to be repeated NREGIN times

Card 6 - 7I5

IREGIN - Material composition of the region over
which the inner product   specified by
the information on this card is formed.

I - $\left.\right\}$ Indices required to specify the Ith row and

J - $\left.\right\}$ J^{th} column entry of the Galerkin coeffi-
cient matrix

N - Pointer passed to subroutine F to determine
the coefficient of the inner produce
(ψ_{ig}, ψ_{jg}).

IRDFUN - Order of mesh spacing of (ψ_{ig}, ψ_{jg})

II - Pointer passed to subroutine D to determine
the coefficient of the inner product
$(\nabla\psi_{ig}, \nabla\psi_{jg})$

IRDDER - Order of mesh spacing of $(\nabla\psi_{ig}, \nabla\psi_{jg})$.

Card 6 is repeated for all the non-zero entries in
the lower triangular part of the Galerkin coefficient
matrix; i.e. NIMAX times.

A list of input cards is presented on the next page for
the sample problem illustrated by Figs. E.1 - E.2 .

```
C      THIS IS THE SAMPLE INPUT FOR 1-D FLOAT                                    1DFL0001
   50                                                                            1DFL0002
5.      E01                                                                      1DFL0003
0.1    E-03 .1      E-3                                                          1DFL0004
    5 .1     E 3    11      2                                                    1DFL0005
    15.7682 E-310.43    E-31.683502E 1.297017E0 8.8200E-5 1.4600E-3 1.8300E-3   1DFL0006
    2 2.7555E-3 2.49    E-31.658375E 1.297017E  9.1500E-5 1.4900E-3 2.07  E-3   1DFL0007
    1    1    1    11     3    1     1                                           1DFL0008
    1    1    2    12     2    2                                                 1DFL0009
    1    1    3    13     3    3     1                                           1DFL0010
    1    2    2    14     1    4    -1                                           1DFL0011
    1    2    3    15     2    2                                                 1DFL0012
    1    3    3    11     3    1     1                                           1DFL0013
    2    2    4    17     2    6                                                 1DFL0014
    2    2    5    18     2    6                                                 1DFL0015
    2    4    4    11     3    1     1                                           1DFL0016
    2    4    5    13     3    3     1                                           1DFL0017
    2    5    5    11     3    1     1                                           1DFL0018
```

E.1.2 1-D SECTION

(a) Description

This program was designed to simulate the 1-D section problems discussed in section 4.1.1(2) and shown in Figs. 4.6 and 4.8 . The version listed in Appendix F uses the 1-D Hybrid Quadratic superelement set and is set up for the current continuity cases. The changes necessary for the derivative continuity cases are indicated in the listing.

We present below a summary of the subroutines

MAIN: This sets up the Galerkin coefficient matrices and uses the power iteration scheme to solve the eigenvalue problem. It also initiates the logic to compute the power to normalize the solution.

FISRT: This is where the calculation of the power is actually carried out.

SINGD: SINGD calculates the parameter α of the 1-D Hybrid Quadratic set for inner products of superelement functions centered on the same mesh point.

DIFFD: This subroutine computes the parameter α of the 1-D Hybrid Quadratic set for inner products of superelement functions centered on different points.

XIMQ: The function of this standard IBM subroutine is to solve a system of linear algebraic equations.

The remaining subroutines are tables of inner products and flux integrals. Subroutine F is the table of the function inner products (ψ_{ig}, ψ_{jg}) while D is the table of the derivative inner products $(\nabla\psi_{ig}, \nabla\psi_{jg})$. As the logic of the two subroutines are identical we shall only discuss F and the subroutine RINTEG which is the table of flux integrals.

E: The indexing scheme for the superelement functions is to refer to each function by a number ab where,

$$a = \begin{cases} 1 & .. \text{ Left side of centering point} \\ 2 & .. \text{ Right side of centering point} \end{cases}$$

and

b = 1 - 4 .. indicating the type of basic element function.

The option ab = 5 is the null function.

The general flow diagram to determine the value of (ab,cd) is shown in Fig. E.4.

RINTEG: The flow diagram for determining the value of (ab,1) is shown in Fig. E.5.

This completes the description of the program. Fig. E.6 shows the general flow of logic. We now present the data preparation.
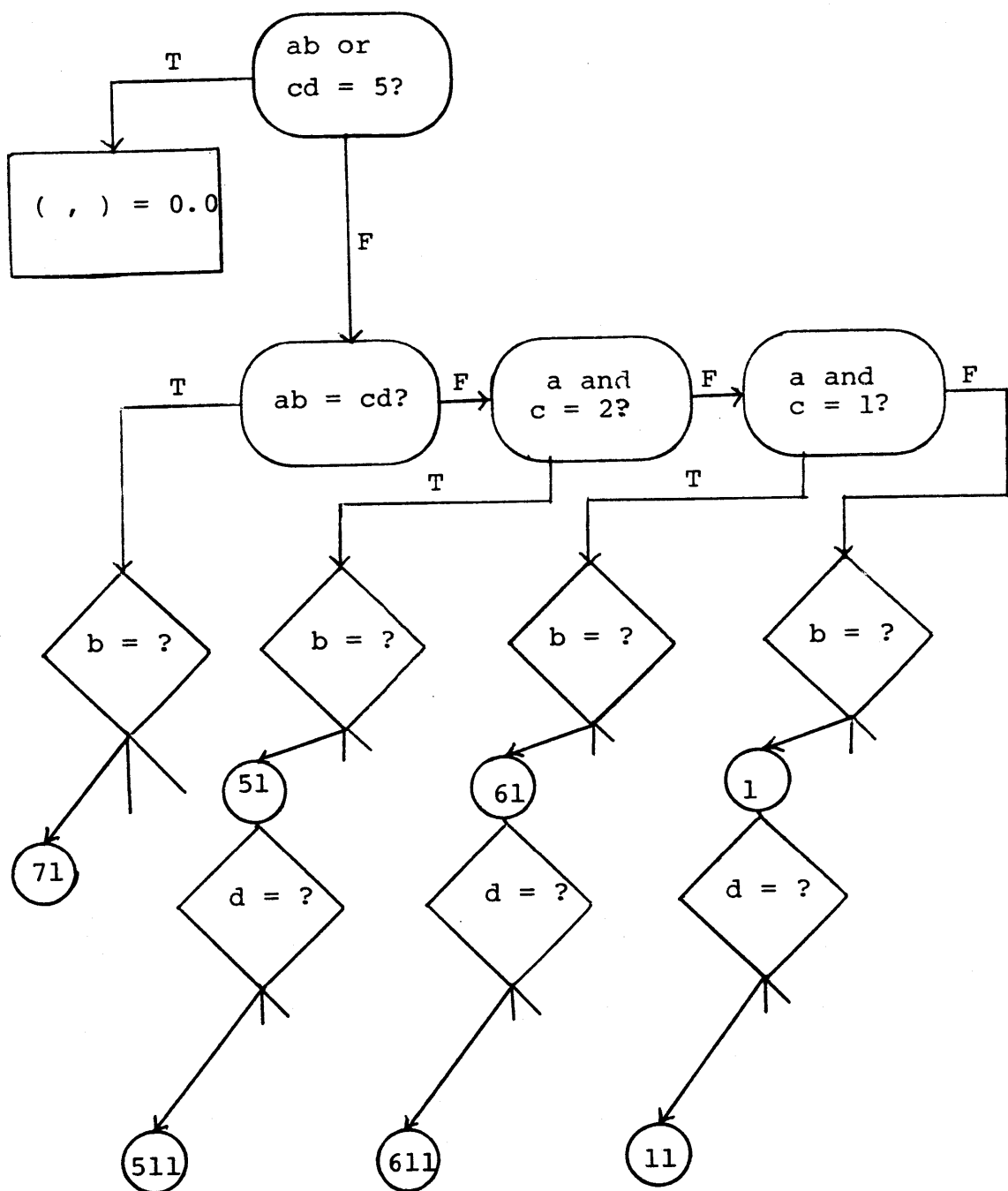
Fig. E.4.   Logic for subroutine F.
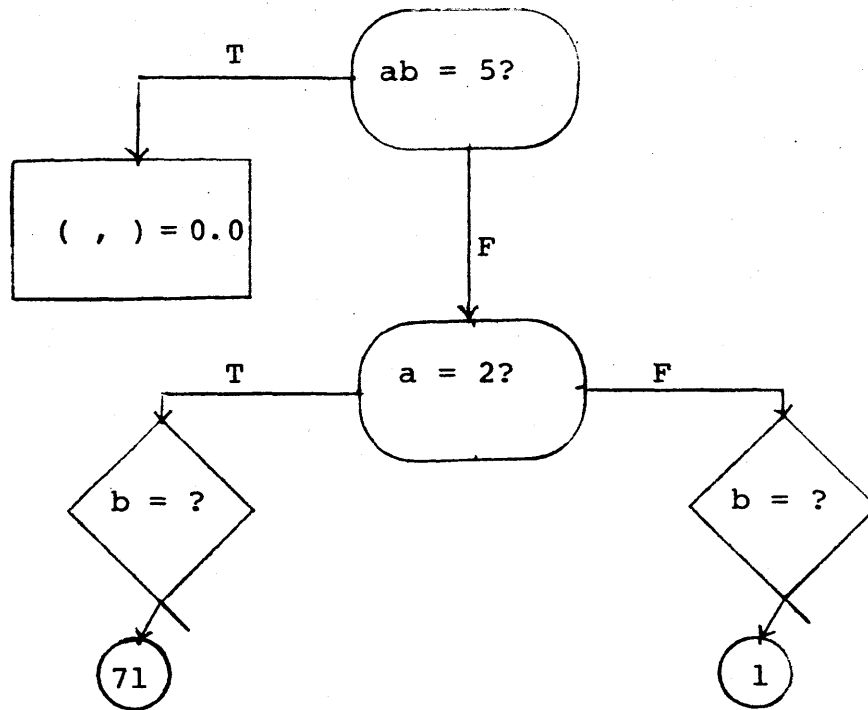
Fig. E.5.   Logic for subroutine RINTEG.
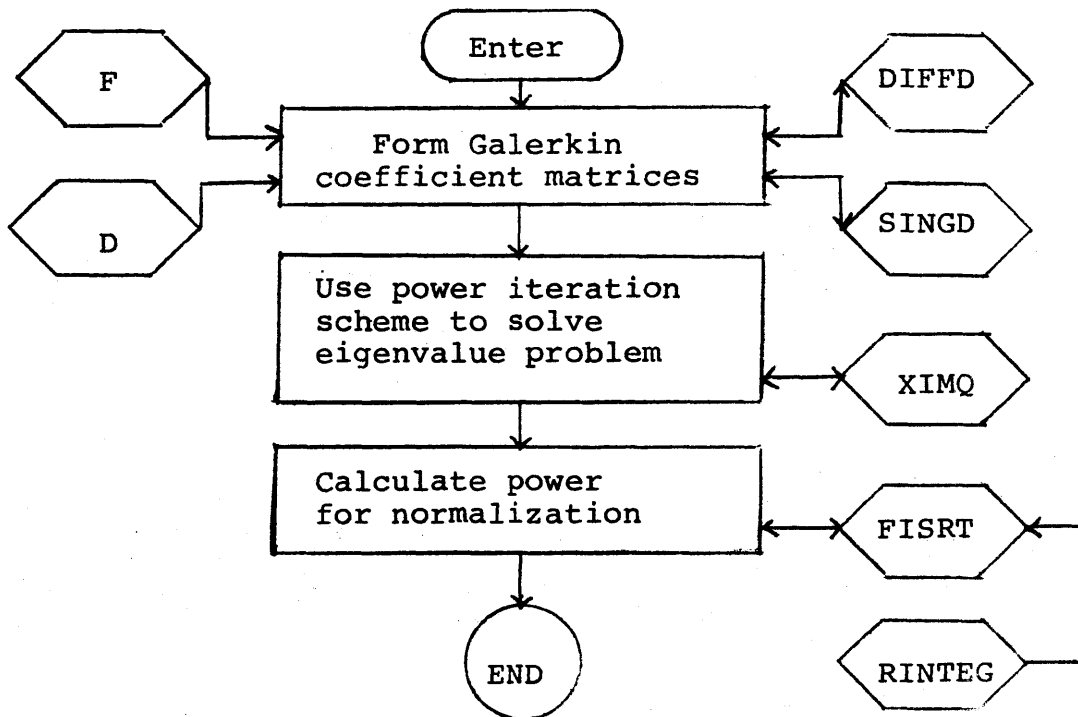
Fig. E.6.   Flow chart for 1-D SECTION.

(b) Input Preparation

Card 1 - I5

MAXITR - Maximum number of power iterations.

Card 2 - 2E10.8

ERMOD - Convergence criterion for solution

EREIG - Convergence criterion for eigenvalue.

Card 3 - 2E10.8

POWIN - Power for normalization

RNU - ν.

Card 4 - I5

NUMLAP - Number of basic patches per superpatch.

Card 5 - I5

IHMAX - Number of sets of different H problems

The cards below are to be repeated IHMAX times.

Card 6 - E10.8

H - The h of the 1-D Hybrid Quadratic set. Refer to
    eqs. (3.40) - (3.41).

Card 7 - 3I5

NUMVAR - Total number of unknowns per group

NIMAX - Number of non-zero entries in lower triangular
        part of the Galerkin coefficient matrix.

NREGIN - Total number of different material
        compositions.

The set of Cards 8 - 9 are to be repeated NUMVAR
times.

Card 8 - 2I5

    I - Superelement function index (from 1 to NUMVAR).

    MESHPT - Mesh point on which I^{th} superelement function
        is centered.

Card 9 is to be repeated NUMLAP times.

Card 9 - 2I5

    ITYPE - Index for type of basic element function of
        I^{th} superelement function over the basic patch.
        (Basic patches indexed from 1 to NUMLAP. Type
        index from 1 - 4.)

    MREGIN - Material composition number of material in
        this basic patch.

Card 10 - I5

    IMATMX - Number of sets of different material problems.

The cards below have to be repeated IMATMX times.

Card 11 - Same as Card 5 of 1-D FLOAT.

Card 12 - 2I5

I -⎫ Indices required to specify the Ith row and J^{th}

J -⎭ column non-zero entry of the lower triangular

part of the Galerkin coefficient matrix.

Card 12 is to be repeated NIMAX times.

We present on the next page a listing of the input

cards required for the sample problem shown in Fig. 4.6.

The mesh used is the one for the h ≖ 8.333 cms results.

We now turn our attention to the 2-D codes beginning

with the mathematical mesh group in Section E.2 and con-

cluding with the physical mesh group in Section E.3.

E.2   2-D Mathematical Mesh Programs

There are two programs to be discussed, 2-D MATHFIT

and 2-D MATHNO. We shall discuss 2-D MATHFIT first and in

detail as the other 2-D programs are quite similar to it.

Reference will be continually made to Appendix C as the

inner products and flux integrals used in these codes are

presented there along with the definitions of the conventions

adhered to.

We should make one comment here about the problem

solved in the 2-D programs. This problem is the 60° sector

of the small HTGR shown in Fig. 4.9. The conditions applied

along the edges of the sector are those of rotational

```
C       THIS IS THE SAMPLE INPUT FOR 1-D SECTION          1DSC0001
    50                                                     1DSC0002
0.1     E-03 .1      E-3                                   1DSC0003
0.1      E032.43                                           1DSC0004
    4                                                      1DSC0005
    1                                                      1DSC0006
8.3333                                                     1DSC0007
    12     37      2                                       1DSC0008
     1      1                                              1DSC0009
     5      1                                              1DSC0010
     5      1                                              1DSC0011
    24      1                                              1DSC0012
    23      1                                              1DSC0013
     2      2                                              1DSC0014
    11      1                                              1DSC0015
    12      1                                              1DSC0016
    22      1                                              1DSC0017
    21      2                                              1DSC0018
     3      2                                              1DSC0019
    13      1                                              1DSC0020
    14      1                                              1DSC0021
    24      1                                              1DSC0022
    23      2                                              1DSC0023
     4      3                                              1DSC0024
    11      1                                              1DSC0025
    12      2                                              1DSC0026
    22      2                                              1DSC0027
    21      2                                              1DSC0028
     5      3                                              1DSC0029
    13      1                                              1DSC0030
    14      2                                              1DSC0031
    24      2                                              1DSC0032
    23      2                                              1DSC0033
     6      4                                              1DSC0034
    11      2                                              1DSC0035
    12      2                                              1DSC0036
```

```
22      2                                                                           1DSC0037
21      2                                                                           1DSC0038
 7      4                                                                           1DSC0039
13      2                                                                           1DSC0040
14      2                                                                           1DSC0041
24      2                                                                           1DSC0042
23      2                                                                           1DSC0043
 8      5                                                                           1DSC0044
11      2                                                                           1DSC0045
12      2                                                                           1DSC0046
22      2                                                                           1DSCC047
21      1                                                                           1DSC0048
 9      5                                                                           1DSC0049
13      2                                                                           1DSC0050
14      2                                                                           1DSC0051
24      2                                                                           1DSC0052
23      1                                                                           1DSC0053
10      6                                                                           1DSC0054
11      2                                                                           1DSCC055
12      1                                                                           1DSC0056
22      1                                                                           1DSC0057
21      1                                                                           1DSC0058
11      6                                                                           1DSC0059
13      2                                                                           1DSC0060
14      1                                                                           1DSC0061
24      1                                                                           1DSC0062
23      1                                                                           1DSC0063
12      7                                                                           1DSC0064
13      1                                                                           1DSC0065
14      1                                                                           1DSC0066
 5      1                                                                           1DSC0067
 5      1                                                                           1DSC0068
 1                                                                                  1DSC0069
   15.7682 E-310.43    E-31.683502E 1.297017E021.4326E-5 3.5478E-3 1.8300E-3       1DSC0070
   25.7682 E-310.43    E-30.3367   E 1.297017E021.4326E-5 3.5478E-3 1.8300E-3       1DSC0071
    1      1                                                                        1DSC0072
```

1	2	1DSC0073
1	3	1DSC0074
2	2	1DSC0075
2	3	1DSC0076
2	4	1DSC0077
2	5	1DSC0078
3	3	1DSC0079
3	4	1DSC0080
3	5	1DSC0081
4	4	1DSC0082
4	5	1DSC0083
4	6	1DSC0084
4	7	1DSC0085
5	5	1DSC0086
5	6	1DSC0087
5	7	1DSC0088
6	6	1DSC0089
6	7	1DSC0090
6	8	1DSC0091
6	9	1DSC0092
7	7	1DSC0093
7	8	1DSC0094
7	9	1DSC0095
8	8	1DSC0096
8	9	1DSC0097
8	10	1DSC0098
8	11	1DSC0099
9	9	1DSC0100
9	10	1DSC0101
9	11	1DSC0102
10	10	1DSC0103
10	11	1DSC0104
10	12	1DSC0105
11	11	1DSC0106
11	12	1DSC0107
12	12	1DSC0108

symmetry. To set up those conditions in the programs, data about the neighbouring sectors must be input and they must reflect this 60° rotational symmetry. Material compositions, superelement function indices, etc., must all have this symmetry. The minimum region of the neighboring sectors for which this data must be input is the region which falls within the superpatches of the benchmark problem.

We will now discuss 2-D MATHFIT.

E.2.1 2-D MATHFIT

(a) Description

This program was written to solve a 60° sector of the small HTGR; that is the benchmark problem of Fig. 4.9. It should be noted that the conditions on the straight edges of the sector are conditions of rotational symmetry. The mesh used is the coarse mesh of Fig. 4.15. The boundary has been fitted exactly and interface distortion is also included. A known error was deliberately made in this code with the result that the power is not calculated correctly for the boundary row of material hexagons. As far as our results are concerned this is of no consequence as the benchmark problem has only reflector material in that particular area.

The version listed in Appendix F cannot be used to throw out the interface distortion. The superelement set

used is the Perturbation Quadratic one.

We now summarize the function of each subroutine.

MAIN: This can be divided into three parts. In the first
part sweeps are made through the mesh to form the
Galerkin matrices. The mesh is divided into two
groups of superpatches, the regular hexagons and the
irregular polygons. We first sweep through all the
regular hexagons, center by center, collecting
together all the inner products formed by the
superelement functions 'centered' at these centers.
We then concern ourselves with the irregular polygons.
These superpatches are decomposed into their consti-
tuent basic patches which are discussed in Section
C.2.2 (b). The basic patches are the large equila-
teral triangle of Fig. C.5, the small equilateral
triangle of Fig. C.9 and the isosceles triangle of
Fig. C.10. The sweep through the large equilateral
triangle is made in the same loop with the sweep
through the regular hexagons. After this sweep we
concern ourselves first with the small equilateral
triangles and then with the isosceles triangle. We
start with the outer boundary on the first iteration
through the loop and end with the core-reflector
interface.

The second phase of MAIN is the implementation
of the power iteration technique to solve the eigen-
value problem. The final portion of MAIN initiates
the calculation of the material hexagon powers
normalized to the core power input on the data cards.

FISR: This subroutine performs in essense the same function
as the first part of MAIN. It sweeps through the
mesh to collect the terms for the material hexagon
powers. The logic is essentially that of the first
part of MAIN. We first sweep through the regular
hexagon superpatches, center by center, and then
concern ourselves with the irregular polygons treat-
ing first the large equilateral triangles, then the
small equilateral triangles and finally the isosceles
triangles.

RINPOW: This is where the powers are actually summed for
each material hexagon. There are three different
branches in this subroutine. The first branch is
to compute the powers for the regular hexagon super-
patches and the large equilateral triangles. The
second branch is for the small equilateral tri-
angle. The final alternative calculates the power
contribution of the isosceles triangles.

RINPRD: The summation of the inner products over the regular hexagon superpatches and the large equilateral triangles are actually carried out in this subroutine. There are four branches involved. The first one leads to the equations patterned after eq. (C.23). The second alternative is the implementation of the equation (C.24). The third branch are the equations patterned after eq. (C.25). All these branches are involved with calculating the 'cross' inner products, that is inner products of superelement functions 'centered' on different centers. The 'self' inner products are computed in the fourth and final branch. This is the implementation of the equation (C.22).

RINEQT: This is the small equilateral triangle equivalent of RINPRD. It sums the inner products over the small equilateral triangle. In this case matters are simpler as there is only one possible 'cross' inner product and only one possible 'self' inner product.

RINIST: This is actually an entry point to the subroutine RINEQT but for convenience we shall examine it here as though it had a seperate entity of its own. There are three types of 'cross' inner products and

three types of 'self' inner products dictated by
the geometry of the triangle. This can be seen
from Table C.26 by examining the indices ℓ and k
which are related to the geometry. The relation-
ship between these indices and the branches pro-
grammed into the subroutine will become clearer
when we examine the subroutines CSxyβF and CSxyβD.

XIMQ: This is the standard IBM subroutine for solving a
set of linear algebraic equations.

The remaining subroutines to be discussed are all
tables of either inner products or flux integrals. We
divide the inner product tables into three groups. Those
concerned with the small equilateral triangle have names of
the form EQT$\alpha\beta$. The tables for the isosceles triangle are
denoted as CSxyCβ. The remaining tables are concerned with
the large equilateral triangle and therefore by implication
with the regular hexagon superpatch. They have names of the
form $\beta\theta z$. The option β = F are the tables of the 'function'
inner products, $(\Psi_{\ell g}^{j\alpha}, \Psi_{kg}^{j\gamma})_\Gamma$ while β = D are those of the
'derivative' inner products, $(\nabla\Psi_{\ell g}^{j\alpha}, \nabla\Psi_{kg}^{j\gamma})_\Gamma$. Within this
division we have the finer subdivision of 'cross' or 'self'
inner products. Here α = S, y = S and θ = S indicates
'self' tables while α = C, y $\neq$ S and $\theta \neq$ S indicates 'cross'
tables. Table E.1 is a tabulation of the subroutines

Table E.1. Subroutines for table data used in 2-D MATHFIT.

| Basic Patch | Inner Products | | | | Flux Integrals |
| | Function | | Derivative | | |
	Cross	Self	Cross	Self	
Small Equilateral Triangle	EQTCF	EQTSF	EQTCD	EQTSD	EQTPW
Isosceles Triangle	CS12CF, CS13CF, CS23CF	CS1SCF, CS2SCF, CS3SCF	CS12CD, CS13CD, CS23CD	CS1SCD, CS2SCD, CS3SCD	CSPOW 1, CSPOW 2,
Large Equilateral Triangle	FE1, FE2 FF1, FF2 FG1, FG2	FS1, FS2 FS3	DE1, DE2 DF1, DF2 DG1, DG2	DS1, DS2 DS3	RPOW 1, RPOW 2 RPOW 3

according to these subdivisions. For completeness the flux integral subroutines are also included. We now discuss one subroutine from each category as the logic for subroutines of the same category is common. We start with the small equilateral triangle.

(i) <u>Small equilateral triangle</u>: In the case of the 'cross' tables the ordering scheme is ITYP1 = 1 - 3 -[ITYP2 = 1- 3

where ITYP1 = Index of superelement function centered

on a' (Fig. C.9)

ITYP2 = Index of superelement function centered

on c' (Fig. C.9).

In the case of the 'self' tables the scheme is,

ITYP1 = 1 - 3 -[ITYP2 = ITYP1 - 3.

In the case of the flux integral tables,

ITYP1 = 1 - 3.

(ii) <u>Isosceles triangle</u>: For the 'cross' tables we have,

INDEX = 1 - 2 -[ITYP1 = 1 - 3 -[ITYP2 = 1 - 3

where INDEX = Area indicator (Fig. C.10),

ITYP1 = Index of superlement function centered

on point x,

ITYP2 = Index of superelement function centered

on point y,

and {x,y} are given by the form of the subroutine name, CSxyCβ. For these tables the numerals {1,2,3} represent the points {c',b',a'} of Fig. C.10.

For the 'self' tables we have,

IROT = 1 - 2 -[ITYP1 = 1 - 3 -[ITYP2 = ITYP1 - 3

where now

IROT = Area index (Fig. C.10).

Finally, for the flux integral tables,

IROT = 1 - 3 -[ITYP1 = 1 - 3

with a change in definition of the programming variables. We now have that

IROT = Triangle corner index

ITYP1 = Index of superelement function centered
on point IROT

and x of the subroutine name CSPOWx is now the area indicator.

(iii) <u>Large equilateral triangle</u>: For the 'cross' tables we have,

INDEX = 1 - 3 -[ITYP1 = 1 - 3 -[ITYP2 = 1 - 3

where

INDEX = Area indicator

ITYP1 = Index of superelement function

centered on point a,

ITYP2 = Index of superelement function

centered on point θ,

and θ is given by the subroutine name Fθz or Dθz. The
character z refers to the particular triangle concerned
in accordance with the convention shown in Fig. E.7.
Reference should be made to eqs. (C.23) - (C.25) and Fig. C.6.
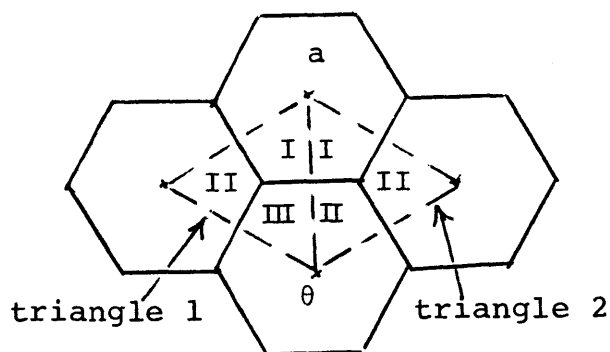
Fig. E.7. Convention for labelling triangles used in
           Fθz and Dθz.

The ordering scheme for the 'self' tables is

IROT = 1 - 6 ─[ITYP1 = 1 - 3 ─[ITYP2 = ITYP1 - 3

IROT = Triangle index (Fig. C.4).

Finally, we have for the flux integral tables,

IROT = 1 - 6 ─[ITYP1 = 1 - 3

and the area indicator is now z, part of the subroutine name
RPOWz.

This concludes the discussion on the subroutines. Fig. E.8 shows the general logic of the program. We now turn our attention to the preparation of the input data.

(b)   Input Preparation

Card 1 - I5

>   MAXITR - Maximum number of iterations for power
>   iteration.

Card 2 - 2E10.8

>   ERMOD - Solution convergence criterion
>
>   EREIG - Eigenvalue convergence criterion.

Card 3 - 2E10.8

>   POWIN - Core power for normalization
>
>   RNU - ν.

Card 4 - I5

>   NUMTYP - Maximum number of superelement functions per
>   group 'centered' on a mesh center.

Card 5 - I5

>   IHMAX - Maximum number of different H cases.
>
>   The cards below have to be repeated IHMAX times.

Card 6 - E10.8

>   H - Material hexagon center to material hexagon center
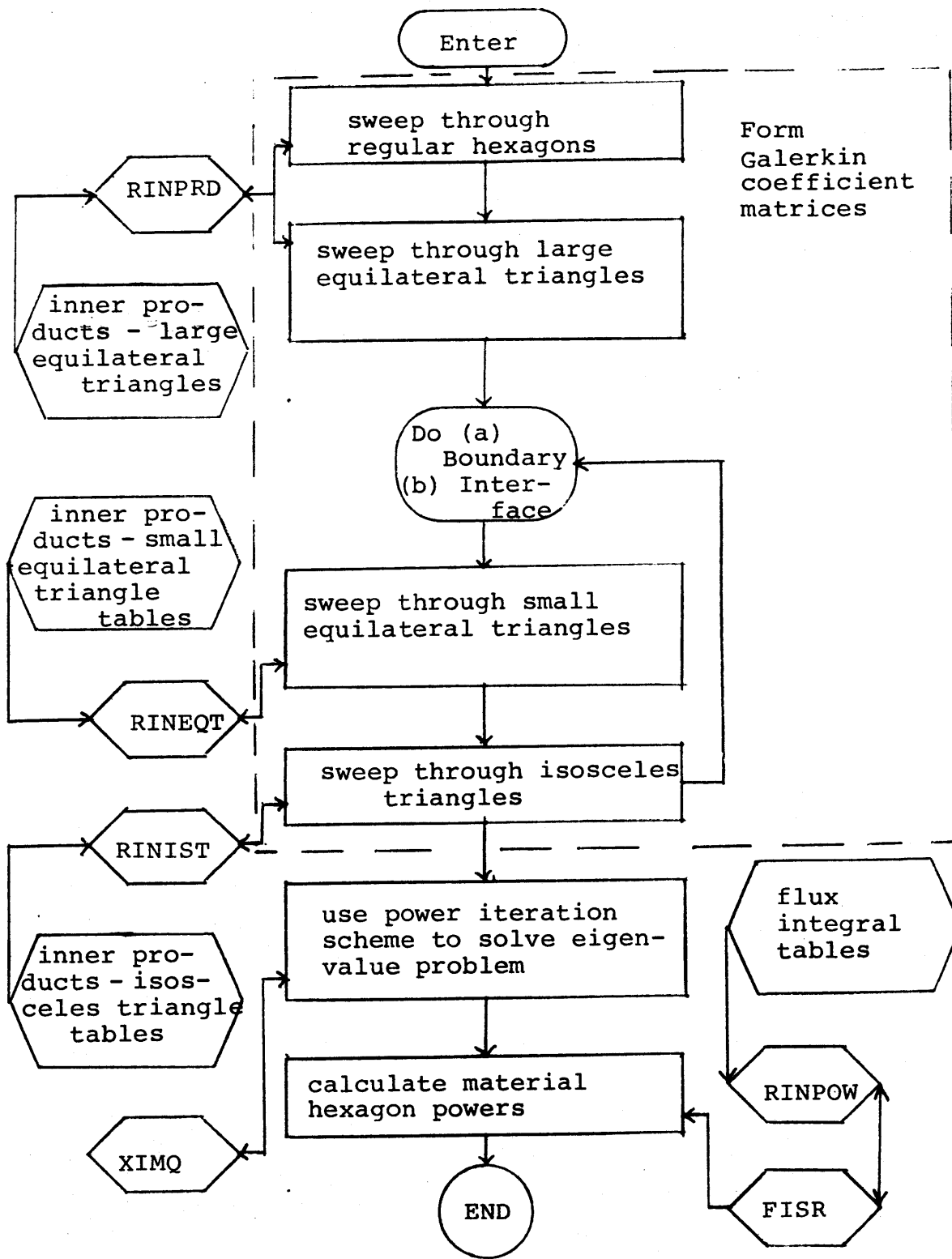
Fig. E.8.   Flow chart for 2-D MATHFIT.

length. (A word of caution is necessary here.
Some tables use a different length to measure
mesh size. Have to check that tables are
consistent with input H.)

Card 7 - 3I5

NUMVAR - Total number of unknowns per group

MAXBLK - Total number of material hexagons. All
material hexagons used in the formation of
the inner products have to be included in
this count.

NREGIN - Total number of different material compositions.

Card 8 - I5

IMATMX - Total number of cases with different sets of
materials.

The cards below have to be repeated IMATMX times.

Card 9 - I5, 7E10.8

IREGIN - Material composition index. Must run from 1
to NREGIN

SIGR1 - Group 1 Removal cross section

SIGR2 - Group 2 Removal cross section

DIFF1 - Group 1 Diffusion coefficient

DIFF2 - Group 2 Diffusion coefficient

SIFNU1 $\nu\Sigma_{f1}$

SIFNU2 $\nu\Sigma_{f2}$

SIGS21 - Outscattering cross section group 1 to

      group 2.

Card 10 - 2E10.8

BSQ1 - Group 1 transverse buckling

BSQ2 - Group 2 transverse buckling.

Cards 9 and 10 have to be repeated NREGIN times.

A word is in order here, before we list the remaining
data cards, about the indexing scheme used. Each material
hexagon is assigned a number, called the block number and
there are arrays which relate the block numbers to material
compositions and to a set of coordinates (m,n). Block
numbers cannot be assigned on an arbitrary basis. They
must conform to the following sequence. Reference should be
made to Fig. E.9. The central material hexagon is block
number 1. Then the non-boundary non-interface hexagons are
to be labelled, IBLK1 - IBLK2 where IBLK1 has to be 2.
Next, the boundary hexagons are to be numbered in sequence,
IBLK1L - IBLK2L. We then turn to the hexagons on the L side
of the interface, IBLK5L - IBLK6L and after that the
hexagons on the R side of the interface, IBLK7R - IBLK8R.
Finally the hexagons which are bisected by the line ac,
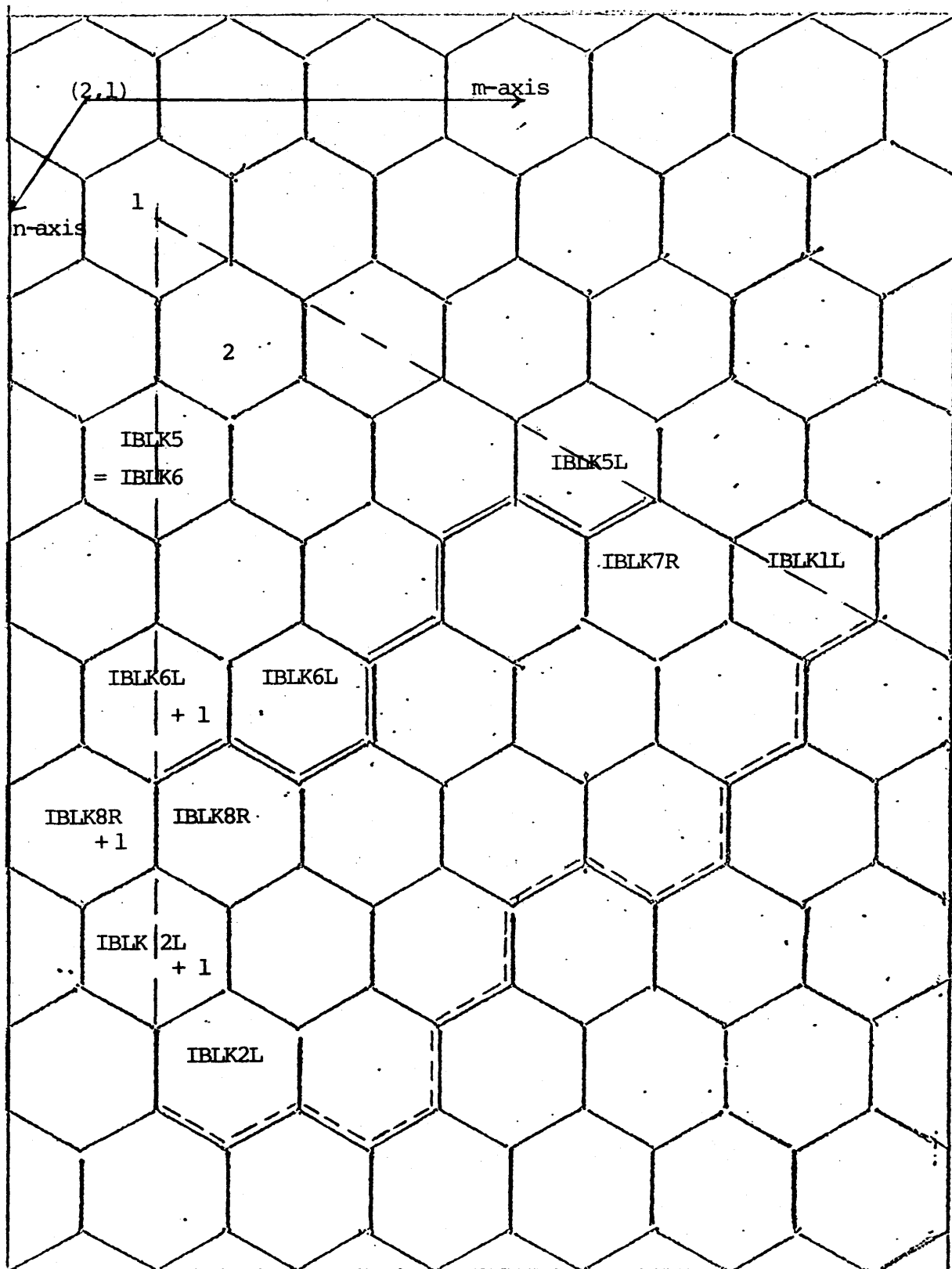
Fig. E.9.   Block numbering sequence and (m,n) axes for 2-D
            MATHFIT.

IBLK5 - IBLK6, are to be numbered in sequence. All remaining material hexagons can be labelled in an arbitrary manner. We now present the remaining data cards. The triangular problem refers to the Triangular Neumann problem of Fig. 4.12.

Card 11 - 2I5

    IBLK1 = 2

    IBLK2

Card 12 - 2I5

    IBLK3 = 0   For triangular problem $\left.\begin{array}{l}\\ \\ \end{array}\right\}$ = block s

    IBLK4 = 0   = block s

Card 13 - 2I5

    IBLK5

    IBLK6

Card 14 - 2I5

    IBLK7 = 0   For triangular problem $\left.\begin{array}{l}\\ \\ \end{array}\right\}$ = block f

    IBLK8 = 0   = block f

Card 15 - 2I5

    IBLK9 = 0   For triangular problem $\left.\begin{array}{l}\\ \\ \end{array}\right\}$ = block r

    IBLK10 = 0   = block r

Card 16 - I5

    IBLK11 = 0   For triangular problem = block h

Card 17 - 2I5

    IBLK1L

    IBLK2L

Card 18 - 2I5

    IBLK3R

    IBLK4R

Card 19 - 2I5

    IBLK5L

    IBLK6L

Card 20 - 2I5

    IBLK7R

    IBLK8R

    Cards 21 - 22 are to be repeated MAXBLK times.

Card 21 - 4I5

    IBLK - Material hexagon block number.

    IPROP - Material composition index of material

        contained in this hexagon.

  M - m-coordinate of this material hexagon.

  N - n-coordinate of this material hexagon.

Card 22 - 10I5

(IFUNCT (IBLK, ITYP), ITYP = 1, NUMTYP) - Index of

superelement function 'centered' on material

hexagon numbered IBLK and of type ITYP (must be

between 1 and NUMVAR).

The cards below contain information regarding the
irregular polygons.

Card 23 - 16I5

NEQTR1 -   - type 1

NEQTR2 -   - type 2

NEQTR3 -   - type 3

NEQTR4 -   Number of large equilateral triangle   - type 4

NEQTR5 -   - type 5

NEQTR6 -   - type 6

Refer to Fig. E.10 for the definition of the different
types.
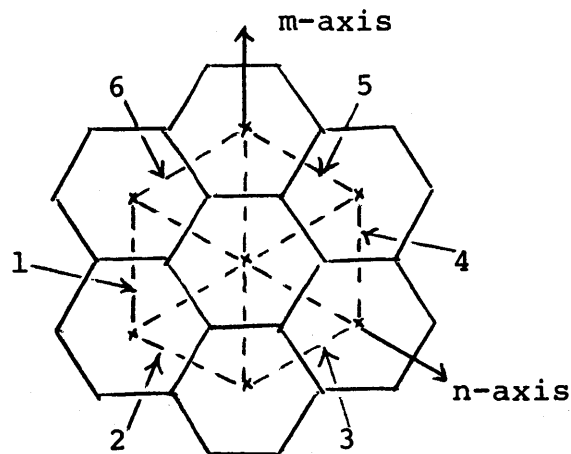
Fig. E.10.   Convention for large equilateral triangles.

Card 24 - 16I5

> (IEQTR1 (J) J = 1, NEQTR1) - Block number of material
> hexagon in which the Jth large equilateral triangle
> of type 1 falls.

Card 25 - 16I5

> (IEQTR2 (J), J = 1, NEQTR2) - Equivalent of Card 24
> for type 2.

Card 26 - 16I5

> (IEQTR3 (J), J = 1, NEQTR3) - Equivalent of Card 24
> for type 3.

Card 27 - 16I5

> (IEQTR4 (J), J = 1, NEQTR4) - Equivalent of Card 24
> for type 4.

Card 28 - 16I5

> (IEQTR5 (J), J = 1, NEQTR5) - Equivalent of Card 24
> for type 5.

Card 29 - 16I5

> (IEQTR6 (J), J = 1, NEQTR6) - Equivalent of Card 24
> for type 6.

If NEQTRx is zero then the corresponding data card of
the set 24 - 29 should be dropped from the input.

The remaining cards are data for the small equilateral triangles and for the isosceles triangles. They should be repeated twice. The first set is for the boundary. The second is for the interface.

Card 30 - 16I5

NCORN - Number of corner points on

(a) Boundary - First set of data cards

(b) Interface - Second set of data cards.

The corner points are indexed 1 - NCORN.

Card 31 - 16I5

((ICFUNC (I, ITYP), I = 1, NCORNP), ITYP = 1, (NUMTYP) -

Index of superelement function of type ITYP

centered on the corner point I where

NCORNP = NCORN + 1 (index must be between 1 and

NUMVAR).

Card 32 - 16I5

((ICLFBK (ISIDE, I), I = 1, NCORN), ISIDE = 1,2) -

Block number of the material hexagons to the L

side and R side of the corner point I. ISIDE = 1

is the L side.

Fig. E.11 illustrates this point.
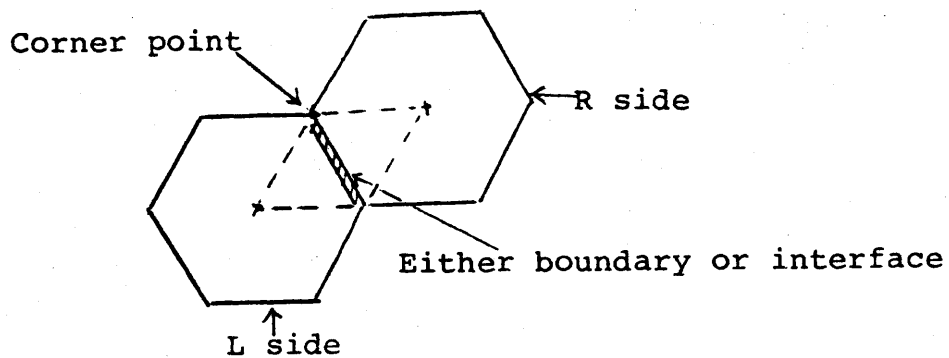
Fig. E.11. Convention for small equilateral triangle.

Card 33 - 1615

((I3RDPT (ISIDE, I), I = 1, IBLKED), ISIDE = 1,2) -

Index of corner point which forms the third corner

of the Ith isosceles triangle on the ISIDE side

of

(a) Boundary - First set of data cards

(b) Interface - Second set of data cards.

The isosceles triangles on the ISIDE side are

indexed starting with the numeral 1.

Fig. E.12 is an illustration of the convention used.
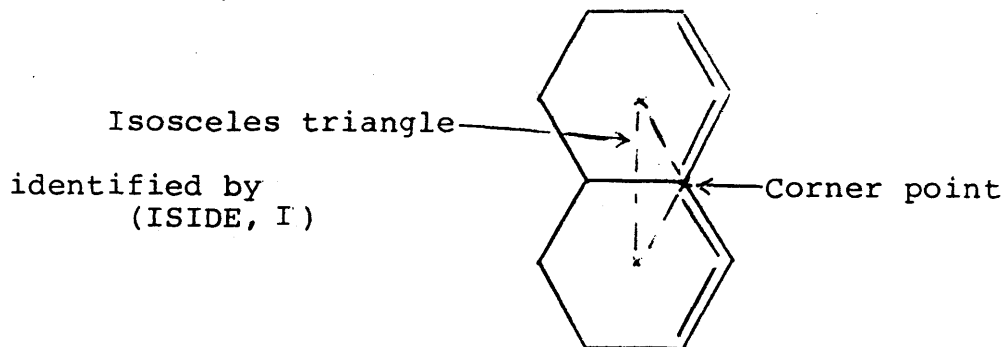
Fig. E.12.   Convention for isosceles triangle.

It must be noted that IBLKED is the larger of the following two numbers: the number of isosceles triangles on the R side and the number of isosceles triangles on the L side.   This means that 0 will have to be input for some of the array elements of I3RDPT (ISIDE, I).

In concluding this section on the input preparation we should make the following comments.

(i)   In the case of the interface the last material hexagon on the L side should be such that the edge ac bisects it as in Fig. E.13.
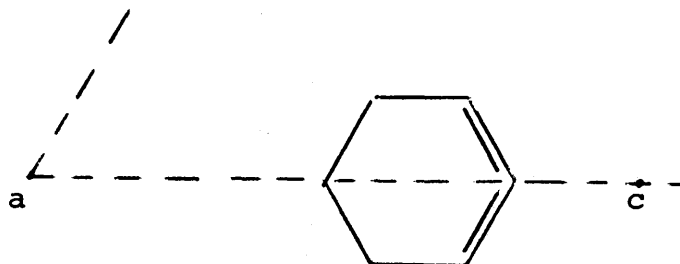
Fig. E.13.   Last material hexagon on interface.

(ii)   If the number of superelement functions centered
on a certain mesh center is less than NUMTYP then the value
0 should be input for the indices of the missing superelement
functions.

(iii) To ensure 60° rotational symmetry conditions on
the edges of the sector, the material compositions and the
indices of the superelement functions in the neighbouring
sectors must reflect this symmetry.

This completes the description of the data preparation.
We present on the next page a list of input cards for the
sample problem shown in Figs. E.14 - E.15 .

We now turn our attention to the second mathematical
mesh program.

E.2.2   2-D MATHNO

(a)   Description

2-D MATHNO solves the same 60° sector small HTGR
problem which 2-D MATHFIT does but it does not fit the
boundary exactly. The mesh used is the one of Fig. 4.10;
that is to say the only superpatch used is the regular
hexagon. This is the program used for the 'initial' phase
calculations referred to in Section 3.3 (6). As can be
inferred much of the logic is similar to that of 2-D MATHFIT
and we will draw upon the presentation of Section E.2.1 in
our description.

```
C     THIS IS THE SAMPLE INPUT FOR 2-D MATHFII                    2DMF0001
     50                                                           2DMF0002
0.1     E-05 0.1    E-05                                          2DMF0003
3.7037      2.43                                                  2DMF0004
      2                                                           2DMF0005
      1                                                           2DMF0006
34.64  500                                                        2DMF0007
     64    55      4                                              2DMF0008
     1                                                            2DMF0009
     15.93655D-31.03003D-21.6835 D0 1.29702D0 2.14326D-43.54780D-31.83     D-3   2DMF0010
0.0        0.0                                                    2DMF0011
     23.58649D-34.07584D-31.47493D0 1.14155D0 3.86370D-46.17220D-32.25000D-3   2DMF0012
0.0        0.0                                                    2DMF0013
     34.98523D-32.96000D-40.96899D0 0.78988D0  0.0   D0 0.0    D0 4.98000D-3   2DMF0014
0.0        0.0                                                    2DMF0015
     4 0.0    D0  0.0   DC  0.0   D0  0.0   D0  0.0   D0  0.0   D0  0.    D0    2DMF0016
0.0        0.0                                                    2DMF0017
      2     7                                                     2DMF0018
      0     0                                                     2DMF0019
     27    27                                                     2DMF0020
      0     0                                                     2DMF0021
      0     0                                                     2DMF0022
      0                                                           2DMF0023
      8    14                                                     2DMF0024
      0     0                                                     2DMF0025
     16    19                                                     2DMF0026
     21    25                                                     2DMF0027
      1     1     3     2                                         2DMF0028
      1     2                                                     2DMF0029
      2     2     4     3                                         2DMF0030
      3     4                                                     2DMF0031
      3     2     5     3                                         2DMF0032
      5     6                                                     2DMF0033
      4     2     5     4                                         2DMF0034
      7     8                                                     2DMF0035
      5     1     5     5                                         2DMF0036
```

282

9	10			2DMF0037
6	3	7	8	2DMF0038
19	20			2DMF0039
7	3	8	6	2DMF0040
24	25			2DMF0041
8	3	9	5	2DMF0042
32	33			2DMF0043
9	3	9	6	2DMF0044
34	35			2DMF0045
10	3	9	7	2DMF0046
36	37			2DMF0047
11	3	3	7	2DMF0048
26	27			2DMF0049
12	3	8	8	2DMF0050
28	29			2DMF0051
13	3	8	9	2DMF0052
30	31			2DMF0053
14	3	7	9	2DMF0054
21	22			2DMF0055
15	3	6	8	2DMF0056
32	33			2DMF0057
16	2	7	4	2DMF0058
15	47			2DMF0059
17	2	5	4	2DMF0060
11	48			2DMF0061
18	2	6	5	2DMF0062
12	49			2DMF0063
19	2	6	6	2DMF0064
13	50			2DMF0065
20	2	5	6	2DMF0066
15	47			2DMF0067
21	3	8	5	2DMF0068
23	51			2DMF0069
22	3	7	5	2DMF0070
16	52			2DMF0071
23	3	7	6	2DMF0072

											Ref
42	2	2	2								2DMF0109
3	4										2DMF0110
43	2	3	4								2DMF0111
7	8										2DMF0112
44	3	4	6								2DMF0113
16	52										2DMF0114
45	3	5	8								2DMF0115
34	35										2DMF0116
46	4	6	10								2DMF0118
											2DMF0119
47	2	2	1								2DMF0120
3	4										2DMF0121
48	2	4	2								2DMF0122
3	4										2DMF0123
49	1	6	3								2DMF0124
9	10										2DMF0125
50	3	8	4								2DMF0126
14	55										2DMF0127
51	3	10	5								2DMF0128
21	22										2DMF0129
52	2	3	1								2DMF0130
3	4										2DMF0131
53	2	5	2								2DMF0132
7	8										2DMF0133
54	2	7	3								2DMF0134
13	50										2DMF0135
55	3	9	4								2DMF0136
19	20										2DMF0137
11	10	9	5	5	7						2DMF0138
16	17	18	19	8	9	10	11	12	13	14	2DMF0139
16	17	18	19	8	9	10	11	12	13		2DMF0140
17	18	21	24	25	8	9	11	12			2DMF0141
21	22	23	24	25							2DMF0142
21	22	23	24	25							2DMF0143
17	21	23	24	8	11	14					2DMF0144

```
15                                                                                    2DMF0145
                                                                                      2DMF0146
                                                                                      2DMF0147
 8    9    9   1C   10   10   11   12   12   13   13   13   14   14   14   28 2DMF0148
28   29   29   30   32   32   32   33   33   34   35   35   37   40            2DMF0149
 2    4    7    8   10   13   16                                               2DMF0150
 9                                                                            2DMF0151
38   39   40   41   42   43   44   45   46   38   56   57   58   59   60   61 2DMF0152
62   63   64   56                                                             2DMF0153
16   16   17   18   18   19   19   19   20   21   22   22   22   23   23   24 2DMF0154
25   25                                                                       2DMF0155
 3    4    6    9    0    2    5    7    8   10                                2DMF0156
```
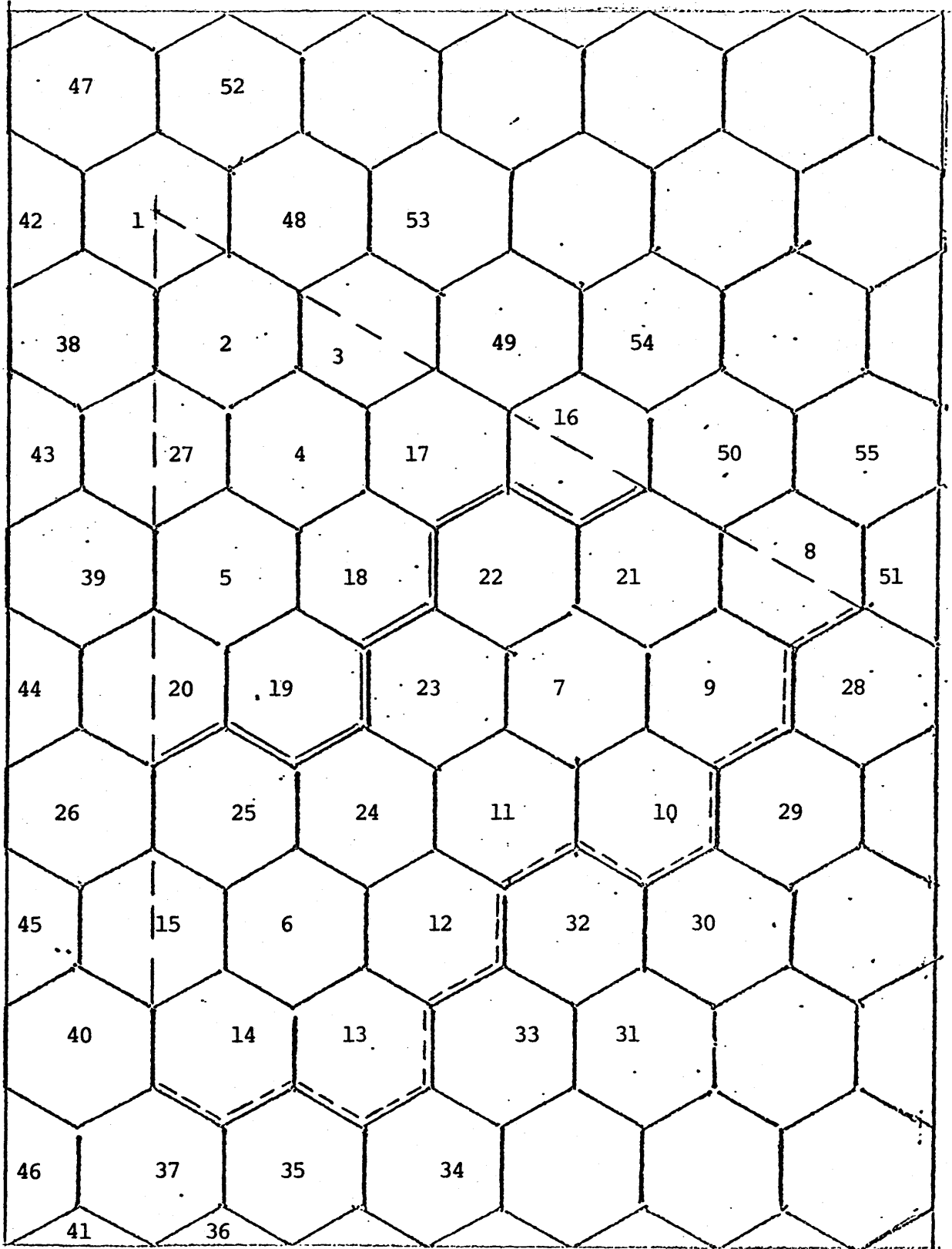
Fig. E.14. 2-D MATHFIT sample problem. Block numbers.
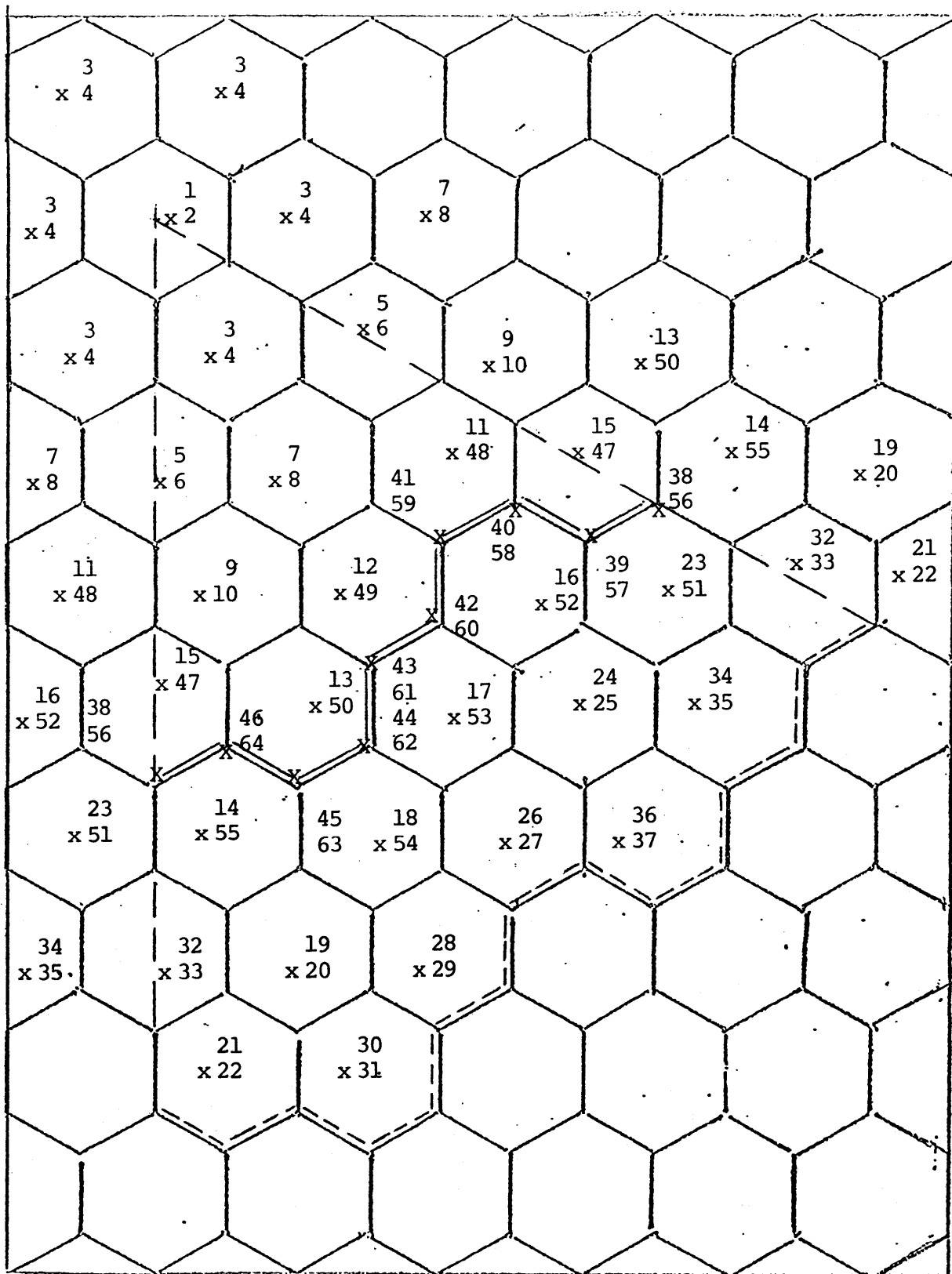
Fig. E.15. 2-D MATHFIT sample problem. Superelement function
indices.

The version listed in Appendix F uses the Perturbation Quadratic set for the superelement functions.

We now describe the subroutines.

MAIN: As with 2-D MATHFIT this subroutine can be divided into three parts. The difference in the first part, the formation of the Galerkin matrices, is that we only have to sweep through regular hexagons. The second parts are identical. In the final section the difference is that the material hexagon powers are not stored.

FISR: Its function here is identical to its function in 2-D MATHFIT, the difference in logic being that it only has to sweep through regular hexagons. In addition no allowance is made for the storage of material hexagon powers.

RINPOW: This can be considered as the RINPOW of 2-D MATHFIT minus the branches for the small equilateral triangles and the isosceles triangles and also minus the logic for the storage of the material hexagon powers.

RINPRD: RINPRD of 2-D MATHFIT was obtained from this subroutine by adding the option to sum inner products over the large equilateral triangles.

XIMQ: This is the standard IBM subroutine for solving a set of linear algebraic equations.

The remaining subroutines are tables. These are the tables for the regular hexagon superpatches and reference should be made to the description presented in Section E.2.1. The tables used in this program are the ones in the 'large equilateral triangles' row of Table E.1.

This concludes the description of the subroutines. We present in Fig. E.16 a general flow diagram for the program. The next section lists the input data required.

(b) Input Preparation

Card 1 - Card 22 same as that for 2-D MATHFIT. We present on the next page a list of input cards for the sample problem shown in Figs. E.17 - E.18 . The next section discusses the physical mesh codes.

E.3 2-D Physical Mesh Programs

As stated in the introduction there is only one code in this group, the code 2-D PHYMESH.

E.3.1 2-D PHYMESH

(a) Description

2-D PHYMESH is the physical mesh counterpart of 2-D MATHNO. It solves the same 60° sector small HTGR problem

```
C     THIS IS THE SAMPLE INPUT FOR 2-D MATHNO                              2DMN0001
    50                                                                     2DMN0002
C.1     E-05 C.1    E-05                                                   2DMN0003
3.7037      2.43                                                          2DMN0004
    2                                                                     2DMN0005
    1                                                                     2DMN0006
34.64    E00                                                             2DMN0007
    46    55    4                                                        2DMN0008
    1                                                                     2DMN0009
    15.93655D-31.03003D-21.6835 D0 1.29702D0 2.14326D-43.54780D-31.8      D-3  2DMN0010
1.0      E-4-1.0    E-4                                                   2DMN0011
    23.58649D-34.07584D-31.47493D0 1.14155D0 3.86370D-46.17220D-32.25000D-3   2DMN0012
1.0      E-4-1.0    E-4                                                   2DMN0013
    34.98523D-32.96000D-40.96899D0 0.78988D0 0.0    D0 0.0    D0 4.98000D-3   2DMN0014
0.0         0.0                                                          2DMN0015
    44.98523D-32.96000D-40.96899D0 0.78988D0 0.0    D0 0.0    D0 4.98000D-3   2DMN0016
0.0         0.0                                                          2DMN0017
    2    23                                                              2DMN0018
    0    0                                                              2DMN0019
   34    36                                                             2DMN0020
    0    0                                                              2DMN0021
    0    0                                                              2DMN0022
    0                                                                    2DMN0023
    1    1    3    2                                                    2DMN0024
    1    2                                                              2DMN0025
    2    2    4    3                                                    2DMN0026
    3    4                                                              2DMN0027
    3    2    5    3                                                    2DMN0028
    5    6                                                              2DMN0029
    4    2    7    4                                                    2DMN0030
   19   20                                                              2DMN0031
    5    3    9    5                                                    2DMN0032
   41   42                                                              2DMN0033
    6    2    6    4                                                    2DMN0034
   11   12                                                              2DMN0035
    7    3    8    5                                                    2DMN0036
```

31	32			2DMN0037
8	1	5	5	2DMN0038
9	10			2DMN0039
9	3	6	7	2DMN0040
17	18			2DMN0041
10	3	7	9	2DMN0042
29	30			2DMN0043
11	2	5	4	2DMN0044
7	8			2DMN0045
12	2	6	5	2DMN0046
13	14			2DMN0047
13	2	6	6	2DMN0048
15	16			2DMN0049
14	3	7	5	2DMN0050
21	22			2DMN0051
15	3	7	6	2DMN0052
23	24			2DMN0053
16	3	7	7	2DMN0054
25	26			2DMN0055
17	3	7	8	2DMN0056
27	28			2DMN0057
18	3	8	6	2DMN0058
33	34			2DMN0059
19	3	8	7	2DMN0060
35	36			2DMN0061
20	3	8	8	2DMN0062
37	38			2DMN0063
21	3	8	9	2DMN0064
39	40			2DMN0065
22	3	9	6	2DMN0066
43	44			2DMN0067
23	3	9	7	2DMN0068
45	46			2DMN0069
24	4	10	6	2DMN0070
				2DMN0071
25	4	10	7	2DMN0072

26	4	10	8
27	4	10	9
28	4	9	8
29	4	9	9
30	4	9	10
31	4	9	11
32	4	3	10
33	4	8	11
34	2	4	4
5	6		
35	2	5	6
19	20		
36	3	6	8
41	42		
37	4	7	1C
38	2	2	1
3	4		
39	2	3	3
3	4		
40	2	4	5
11	12		
41	3	5	7
31	32		
42	4	6	9
43	2	2	2

3	4			2DMN0109
44	2	3	4	2DMN0110
7	8			2DMN0111
45	3	4	6	2DMN0112
21	22			2DMN0113
46	3	5	8	2DMN0114
43	44			2DMN0115
47	4	6	10	2DMN0116
				2DMN0117
48	2	4	2	2DMN0118
3	4			2DMN0119
49	1	6	3	2DMN0120
9	10			2DMN0121
50	3	8	4	2DMN0122
17	18			2DMN0123
51	3	10	5	2DMN0124
29	30			2DMN0125
52	2	3	1	2DMN0126
3	4			2DMN0127
53	2	5	2	2DMN0128
7	8			2DMN0129
54	2	7	3	2DMN0130
15	16			2DMN0131
55	3	9	4	2DMN0132
27	28			2DMN0133

Fig. E.16.   Flow chart for 2-D MATHNO and 2-D PHYMESH.
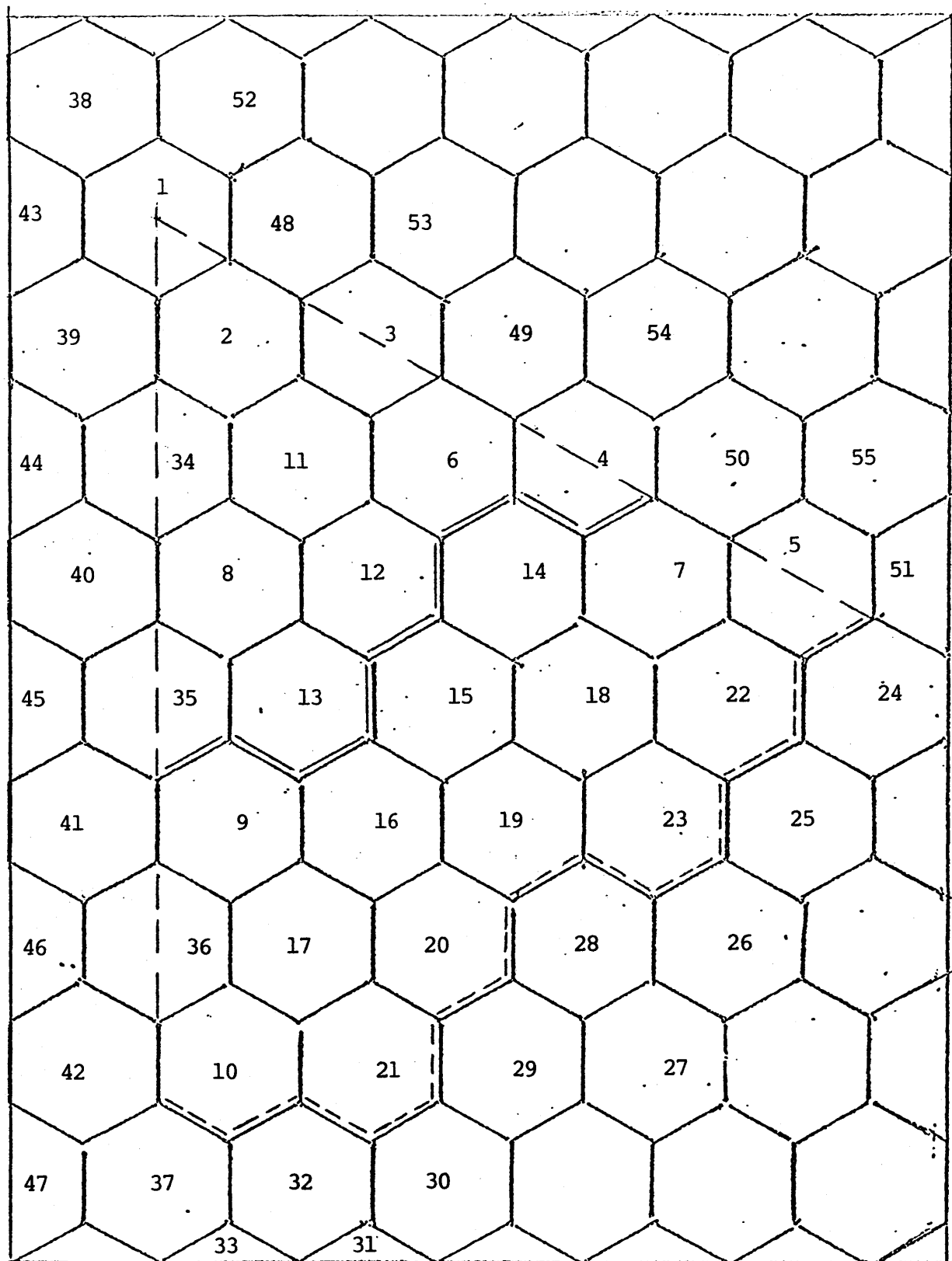
Fig. E.17. 2-D MATHNO sample problem. Block numbers.
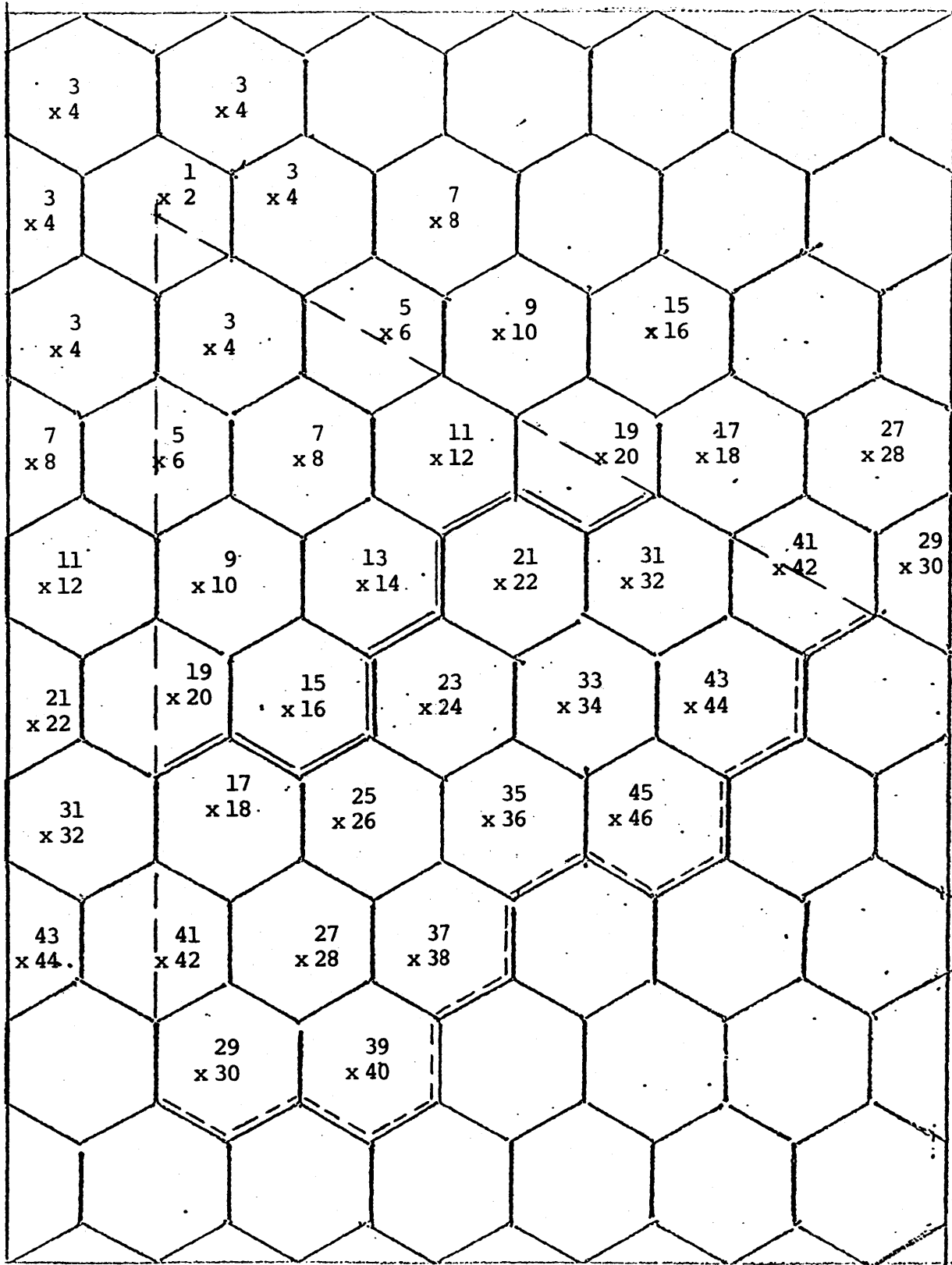
Fig. E.18. 2-D MATHNO sample problem. Superelement function indices.

without fitting the boundary exactly. The mesh used is the
one discussed in Section 3.3 (1) and shown in Fig. 3.6.
There is only one superpatch, the regular hexagon. The
logic of the program is quite similar to that of 2-D
MATHNO and we shall refer to Section E.2.2 in this
presentation.

The superelement function set used in the version
listed in Appendix F is the Perturbation Quadratic set. It
should be noted that this is not the version used to solve
the Triangular Neumann problem discussed in Section 4.1.1
(3). The Appendix F version is also restricted to two
superelement functions per mesh center.

We now describe the subroutines of the program.

MAIN: This performs the same function as the MAIN of
      2-D MATHNO and the logic is quite similar. The main
      difference is that the individual material hexagon
      powers are not printed.

FISR: It sweeps through the regular hexagon superpatches
      to collect the terms for the material hexagon powers;
      in other words, it carries out the same function as
      FISR in 2-D MATHNO.

RINPOW: As with the RINPOW of 2-D MATHNO this is where
      the material hexagon powers are actually computed
      and summed.

RINPRD: This subroutine computes the inner products. It
has three branches. Two branches are for 'cross'
products and the remaining one is for 'self'
product. One of the 'cross' product branches is
concerned with the outer ring discussed in Section
C.2.1. It implements eq. (C.1). The other branch
leads to eq. (C.2), that is, it calculates the
inner products for the inner ring. The 'self'
branch implements eq. (C.3).

XIMQ: This is a standard IBM subroutine to solve a set of
linear algebraic equations.

The remaining subroutines are tables of inner products
and flux integrals. Subroutines F and D are tables of
'cross' inner products. FS and DS are tables of 'self'
inner products while POW is a table of flux integrals.
In our presentation below we do not examine the tables for
the derivative inner products $(\nabla\psi_{ig},\nabla\psi_{jg})$, D and DS as the
tables F and FS for the function inner products (ψ_{ig},ψ_{jg})
are logically quite similar to their derivative counter-
parts.

E: The ordering scheme is,

$I1 = 1 - 2$ -[$II2 = 1 - 3$ -[$ITYP1 = 1 - 2$ -[$ITYP2 = 1 - 2$

where ITYP1 is the type of the superelement function centered on point I1 and ITYP2 is the type of the superelement function centered on the point (II2 + 1). Reference should be made to Fig. C.2 for the geometrical relationship between the points.

FS: For this subroutine the ordering used is

INDEX = 1 - 2 -[ITYP1 = 1 - 2   -[ITYP2 = 1 - 2

where ITYP1 and ITYP2 are the respective types of the superelement functions centered on point 4 in Fig. C.2 and,

INDEX = 1   refers to triangle 4ex

INDEX = 2   refers to quadrilateral estf.

POW: We use the following ordering,

ITYP1 = 1 - 2   -[INDEX = 1 - 2

where ITYP1 is the type of the superelement function centered on point 4 in Fig. C.2 and INDEX has the meaning it has in subroutine FS.

We conclude the description of the program with Fig. E.16 which is a general logic diagram for the code. The next section is concerned with the data preparation.

(b) Input Preparation

Card 1 - Card 10 same as that for 2-D MATHFIT.

As in the case of 2-D MATHFIT each material hexagon
has a block number associated with it. These block numbers
cannot be assigned on an arbitrary basis but should conform
to the following sequence. Reference should be made to Fig.
E.19. The central hexagon is IBLK1 and should be assigned
the number 1. The hexagon contiguous to it is IBLK2 and
should be numbered 2. The next sequence to be numbered is
the sequence IBLK3-IBLK4, the hexagons bisected by the edges
ab. The sequence IBLK15 - IBLK16, the hexagons which 'fill
the gaps' between the hexagons IBLK3 - IBLK4 are then to be
labelled. After this the hexagons which 'fill the gaps'
for the edge ac, IBLK17 - IBLK18 are to be labelled. The
remaining material hexagons, IBLK21 - IBLK22 are then to be
numbered. Sweeps are to be made parallel to the n-axis.
The remaining hexagons to be numbered, IBLK23 - IBLK24, can
be labelled in any sequence with the exception of the hexa-
gons bisected by the edge ac. These also appear in the
input as IBLK5 - IBLK6 and must be labelled in sequence.

Card 11 - 2I5

    IBLK1 = 1

    IBLK2 = 2
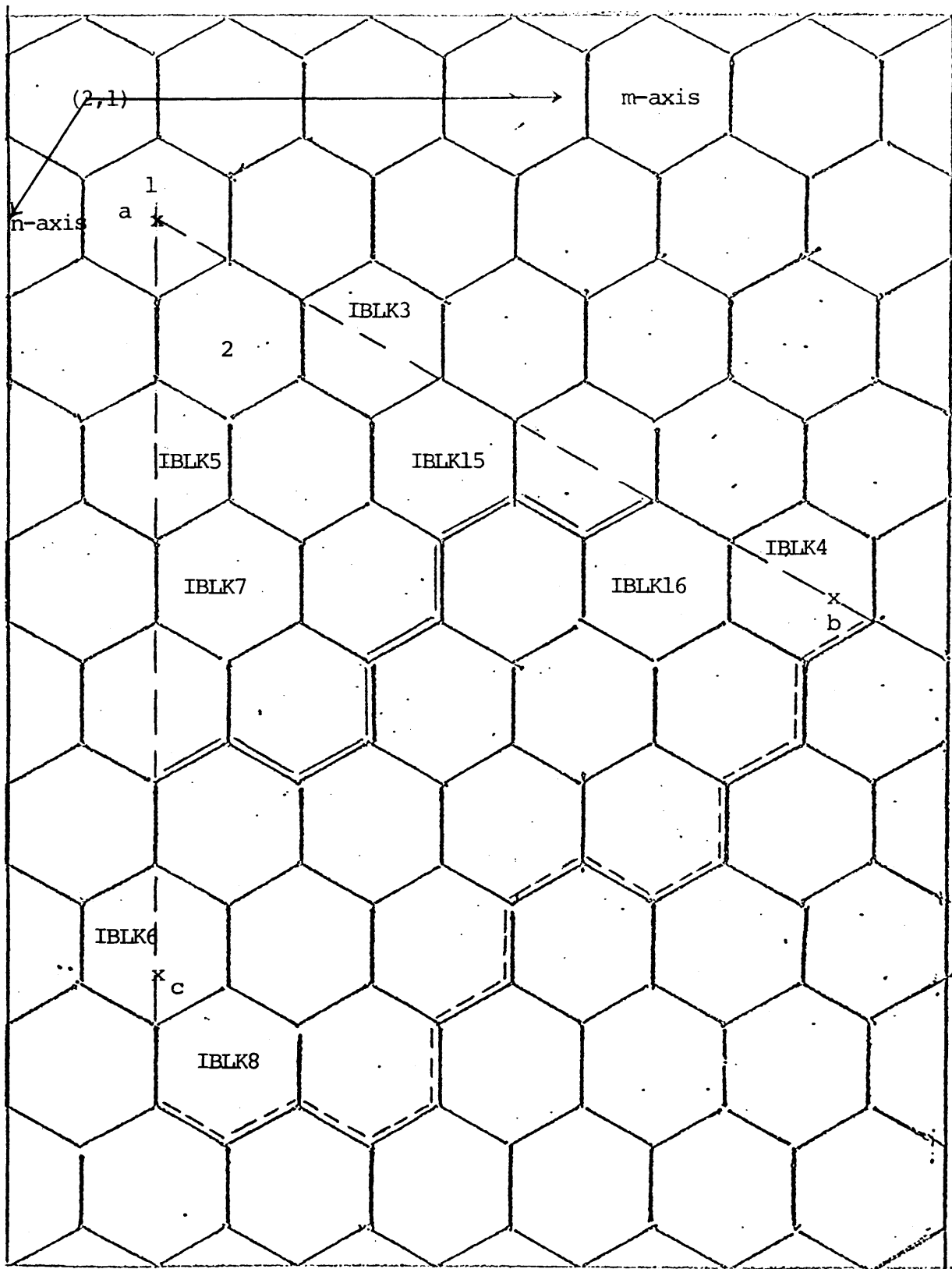
Fig. E.19. Block numbering sequence and (m,n) axis for 2-D PHYMESH.

Card 12 - 2I5

    IBLK3

    IBLK4

Card 13 - 2I5

    IBLK5

    IBLK6

Card 14 - 2I5

    IBLK7 = 0

    IBLK8 = 0

Card 15 - 2I5

    IBLK9 = 0

    IBLK10 = 10

Card 16 - 2I5

    IBLK11 = 0

    IBLK12 = 0

Card 17 - 2I5

    IBLK13 = 0

    IBLK14 = 0

Card 18 - 2I5

    IBLK15

    IBLK16

Card 19 - 2I5

IBLK17

IBLK18

Card 20 - 2I5

IBLK19 = 0

IBLK20 = 0

Card 21 - 2I5

IBLK21

IBLK22

Card 22 - 2I5

IBLK23

INLK24

The cards below are to be repeated MAXBLK times.

Card 23 - Same as Card 21 of 2-D MATHFIT.

Card 24 - Same as Card 22 of 2-D MATHFIT.

The list of input cards for the sample problem shown in Figs. (E.17) and (E.20) is on the next page. The block numbers are the same as the ones for the 2-D MATHNO sample problem. It should be noted that for the version listed in Appendix F, the superelement functions centered on block

```
C      THIS IS THE SAMPLE INPUT FOR 2-D PHYMESH                              2DPH0001
    50                                                                        2DPH0002
0.1    E-05 0.1   E-05                                                        2DPH0003
0.1    E 03 2.43                                                              2DPH0004
     2                                                                        2DPH0005
     1                                                                        2DPH0006
40.00                                                                         2DPH0007
    46    55    4                                                             2DPH0008
     1                                                                        2DPH0009
    15.93655D-31.03003D-21.6835 D0 1.29702D0 2.14326D-43.54780D-31.83    D-3  2DPH0010
1.0     E-4-1.0    E-4                                                        2DPH0011
    23.58649D-34.07584D-31.47493D0 1.14155D0 3.86370D-46.17220D-32.25000D-3   2DPH0012
1.0     E-4-1.0    E-4                                                        2DPH0013
    34.98523D-32.96000D-40.96899D0 0.78988D0  0.0    D0 0.0    D0 4.98000D-3  2DPH0014
0.0         0.0                                                               2DPH0015
     4 0.0    D0  0.0    D0  0.0    D0  0.0    D0  0.0    D0  0.0    D0  0.0    D0   2DPH0016
0.0         0.0                                                               2DPH0017
     1     2                                                                  2DPH0018
     3     5                                                                  2DPH0019
    34    36                                                                  2DPH0020
                                                                             2DPH0021
                                                                             2DPH0022
                                                                             2DPH0023
                                                                             2DPH0024
     6     7                                                                  2DPH0025
     8    10                                                                  2DPH0026
                                                                             2DPH0027
    11    23                                                                  2DPH0028
    24    55                                                                  2DPH0029
     1     1     3     2                                                      2DPH0030
     1     2                                                                  2DPH0031
     2     2     4     3                                                      2DPH0032
     3     4                                                                  2DPH0033
     3     2     5     3                                                      2DPH0034
     5     6                                                                  2DPH0035
     4     2     7     4                                                      2DPH0036
```

19	20			2DPH0037
5	3	9	5	2DPH0038
41	42			2DPH0039
6	2	6	4	2DPH0040
11	12			2DPH0041
7	3	8	5	2DPH0042
31	32			2DPH0043
8	1	5	5	2DPH0044
9	10			2DPH0045
9	3	6	7	2DPH0046
17	18			2DPH0047
10	3	7	9	2DPH0048
29	30			2DPH0049
11	2	5	4	2DPH0050
7	8			2DPH0051
12	2	6	5	2DPH0052
13	14			2DPH0053
13	2	6	6	2DPH0054
15	16			2DPH0055
14	3	7	5	2DPH0056
21	22			2DPH0057
15	3	7	6	2DPH0058
23	24			2DPH0059
16	3	7	7	2DPH0060
25	26			2DPH0061
17	3	7	8	2DPH0062
27	28			2DPH0063
18	3	8	6	2DPH0064
33	34			2DPH0065
19	3	8	7	2DPH0066
35	36			2DPH0067
20	3	8	8	2DPH0068
37	38			2DPH0069
21	3	8	9	2DPH0070
39	40			2DPH0071
22	3	9	6	2DPH0072

43	44			2DPH0073
23	3	9	7	2DPH0074
45	46			2DPH0075
24	4	10	6	2DPH0076
				2DPH0077
25	4	10	7	2DPH0078
				2DPH0079
26	4	10	8	2DPH0080
				2DPH0081
27	4	10	9	2DPH0082
				2DPH0083
28	4	9	8	2DPH0084
				2DPH0085
29	4	9	9	2DPH0086
				2DPH0087
30	4	9	10	2DPH0088
				2DPH0089
31	4	9	11	2DPH0090
				2DPH0091
32	4	8	10	2DPH0092
				2DPH0093
33	4	8	11	2DPH0094
				2DPH0095
34	2	4	4	2DPH0096
5	6			2DPH0097
35	2	5	6	2DPH0098
19	20			2DPH0099
36	3	6	8	2DPH0100
41	42			2DPH0101
37	4	7	10	2DPH0102
				2DPH0103
38	2	2	1	2DPH0104
				2DPH0105
39	2	3	3	2DPH0106
3	4			2DPH0107
40	2	4	5	2DPH0108

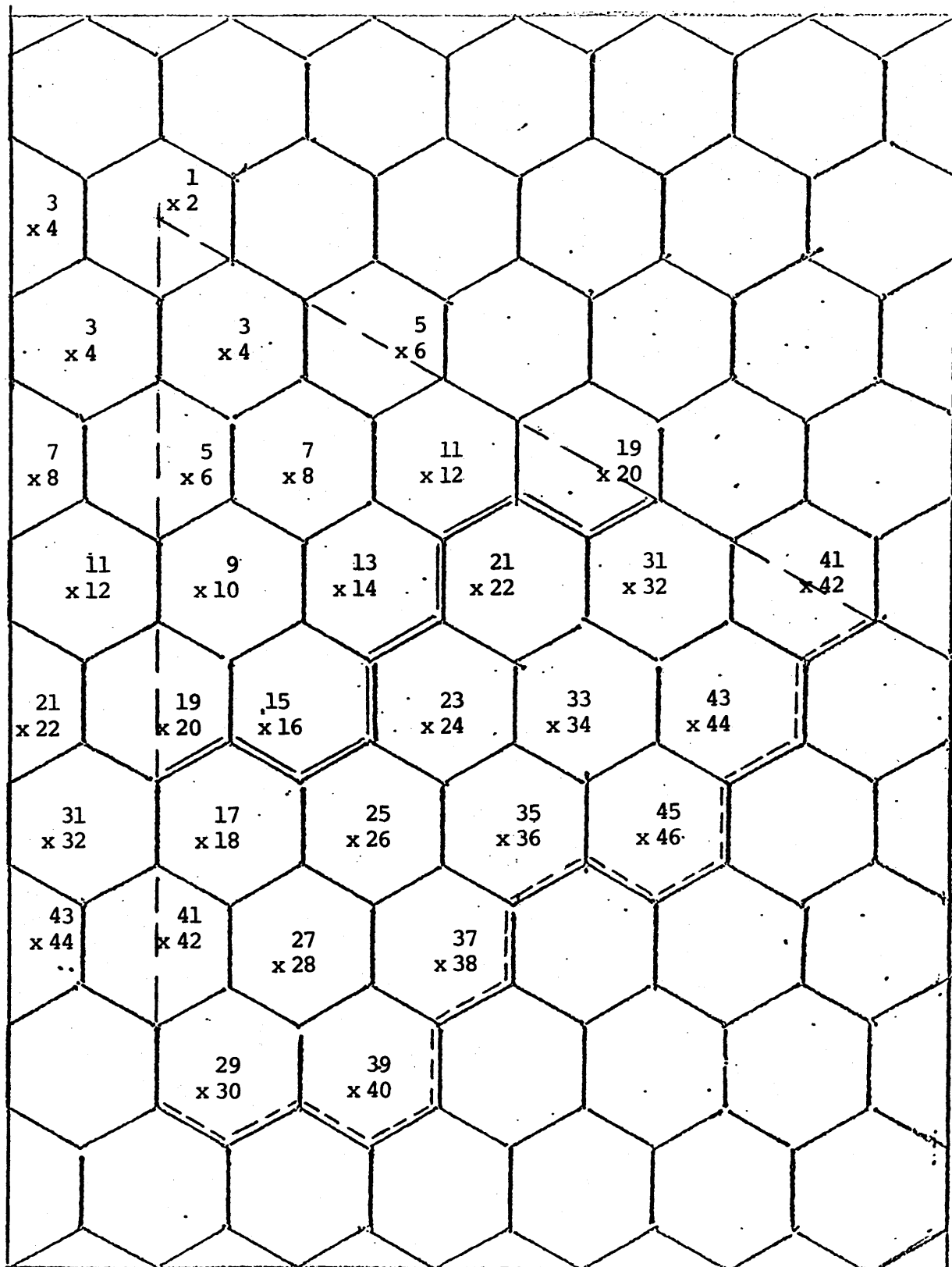|				
11	12			2DPH0109
41	3	5	7	2DPH0110
31	32			2DPH0111
42	4	6	9	2DPH0112
				2DPH0113
43	2	2	2	2DPH0114
3	4			2DPH0115
44	2	3	4	2DPH0116
7	8			2DPH0117
45	3	4	6	2DPH0118
21	22			2DPH0119
46	3	5	8	2DPH0120
43	44			2DPH0121
47	4	6	10	2DPH0122
				2DPH0123
48	2	4	2	2DPH0124
				2DPH0125
49	1	6	3	2DPH0126
				2DPH0127
50	3	8	4	2DPH0128
				2DPH0129
51	3	10	5	2DPH0130
				2DPH0131
52	2	3	1	2DPH0132
				2DPH0133
53	2	5	2	2DPH0134
				2DPH0135
54	2	7	3	2DPH0136
				2DPH0137
55	3	9	4	2DPH0138
				2DPH0139

Fig. E.20. 2-D PHYMESH sample problem. Superelement function
indices.

number 1 must be indexed 1 and 2. The ones centered on

block 2 have to be numbered 3 and 4 while those centered

on IBLK5 must be numbered 5 and 6.

Appendix F

SOURCE LISTING OF COMPUTER PROGRAMS

(M.I.T. Library copies only)